School of Civil Engineering

SHEAR STRENGTH OF HIGH PERFORMANCE
CONCRETE BEAMS

Paul KONG Yeow Liong

This thesis is presented as part of the requirements for

the award of the Degree of Doctor of Philosophy

of the

Curtin University of Technology

November 1996

Abstract

An analytical and experimental investigation on the shear strength of High Performance Concrete (HPC) beams with vertical shear reinforcement or stirrups was carried out. The analytical work involved developing a theory based on the truss analogy, capable of predicting the response and shear strength of such beams subjected to combined bending moment and shear force.

The experimental work comprised forty-eight beam specimens in eight series of tests. Most of the beams were 250 mm wide, 350 mm deep and had a clear span of approximately 2 metres. The largest beam was 250 mm wide, 600 mm deep and had a clear span of 3.1 metres. Test parameters included the concrete cover to the shear reinforcement cage, shear reinforcement ratio, longitudinal tensile steel ratio, overall beam depth, shear span-to-depth ratio and concrete compressive strength. The loading configurations included using one, two or four symmetrically placed concentrated loads on simply supported spans.

The theory predicted the shear strength of the beams in the present study well. When beams from previous investigations were included, the theory also gave good prediction of the shear strength. Apart from this, comparisons of shear strength were also made with the predictions by the shear design provisions contained in the Australian Standard AS 3600 (1994), American Concrete Institute Building Code ACI 318-95, Eurocode EC2 Part 1 and Canadian Standard CSA A23.3-94. The AS 3600 method was found to give the best correlation with the test results among all the code methods.

Acknowledgments

Table of Contents

Content   **Page**

Notation

The following is a list of symbols used in this work and the definition of each symbol.

a shear span of a beam (Theory)

a maximum aggregate size (General Method of CSA A23.3-94)

A_g gross cross-sectional area of a beam (Theory)

A_s cross-sectional area of longitudinal tensile steel (CSA A23.3-94)

$A_{s\ell}$ total cross-sectional area of longitudinal tensile steel (Theory)

$A_{s\ell M}$ cross-sectional area of longitudinal tensile steel attributed to flexure (Theory)

$A_{s\ell V}$ cross-sectional area of longitudinal tensile steel attributed to shear (Theory)

A_{st} cross-sectional area of transverse steel (Theory)

A_{st} cross-sectional area of longitudinal tensile steel (AS 3600)

A_{sv} cross-sectional area of shear reinforcement (Theory and AS 3600)

$A_{sv.min}$ cross-sectional area of minimum shear reinforcement (AS 3600)

A_{sw} cross-sectional area of shear reinforcement (EC2 Part 1)

A_v cross-sectional area of shear reinforcement (ACI 318-95 and CSA A23.3-94)

b_v effective width of a beam for shear (Theory and AS 3600)

b_w effective width of a beam for shear (ACI 318-95, EC2 Part 1 and CSA A23.3-94)

d nominal effective depth of a beam taken from the extreme compression fibre to the centroid of the tensile force of the longitudinal tensile reinforcement

d_{max} vertical midspan deflection (Theory)

d_o distance from the extreme compression fibre to the centroid of the outermost layer of tensile reinforcement (AS 3600)

d_v effective depth of a beam for shear taken as $0.9d_o$ (Theory)

d_v effective depth of a beam for shear taken as $0.9d$ (General Method of CSA A23.3-94)

D overall depth of a beam

E_c modulus of elasticity of concrete

E_s modulus of elasticity of steel

f'_c characteristic concrete compressive cylinder strength (Theory, AS 3600, ACI 318-95 and CSA A23.3-94)

f_{cd} characteristic concrete compressive cylinder strength (EC2 Part 1)

f_{cm} concrete compressive strength at the relevant age (AS 3600)

f_{cr} concrete cracking stress (Theory)

$f_{s\ell}$ longitudinal steel stress (Theory)

$f_{s\ell y}$ longitudinal steel yield stress (Theory)

f_{st} transverse steel stress (Theory)

f_{sty} transverse steel yield stress (Theory)

$f_{sy.f}$ yield stress of shear reinforcement (AS 3600)

f_{tm} concrete tensile strength at the relevant age (AS 3600)

f_y yield stress of shear reinforcement (ACI 318-95 and CSA A23.3-94)

f_{ywd} yield stress of shear reinforcement (EC2 Part 1)

f_2 principal concrete compressive stress (CSA A23.3-94)

L total length of a beam

L_e clear span of a beam

M moment at the critical section of a beam (Theory)

M_u moment at a section of a beam (ACI 318-95 and CSA A23.3-94)

N axial force in a beam (Theory)

s spacing of stirrups

s_z	spacing of longitudinal cracks in the web of a beam (General Method of CSA A23.3-94)
v	shear stress in concrete (General Method of CSA A23.3-94)
$v_{\ell t}$	shear stress in concrete (Theory)
V	shear force at the critical section of a beam (Theory)
V_c	concrete contribution to shear (ACI 318-95 and Simplified Method of CSA A23.3-94)
V_{cd}	concrete contribution to shear (EC2 Part 1)
V_{cg}	concrete contribution to shear (General Method of CSA A23.3-94)
V_e	test shear strength of a beam
V_n	predicted shear strength of a beam (ACI 318-95)
V_p	predicted shear strength of a beam
V_r	predicted shear strength of a beam (Simplified Method of CSA A23.3-94)
V_{rg}	predicted shear strength of a beam (General Method of CSA A23.3-94)
V_{Rd1}	predicted shear strength of a beam without shear reinforcement (EC2 Part 1)
V_{Rd2}	maximum shear strength limited by web crushing (EC2 Part 1)
V_{Rd3}	predicted shear strength of a beam with shear reinforcement (EC2 Part 1)
V_s	steel contribution to shear (ACI 318-95 and Simplified Method of CSA A23.3-94)
V_{sg}	steel contribution to shear (General Method of CSA A23.3-94)
V_u	predicted shear strength of a beam (Theory and AS 3600)
V_u	shear force at a section of a beam (ACI 318-95 and CSA A23.3-94)
V_{uc}	concrete contribution to shear (AS 3600)
$V_{u.max}$	maximum shear strength limited by web crushing (AS 3600)
V_{us}	steel contribution to shear (AS 3600)
V_{wd}	steel contribution to shear (EC2 Part 1)
w	crack width (General Method of CSA A23.3-94)

β	enhancement factor for concrete contribution due to the effect of a concentrated load near a support (EC2 Part 1)
β	factor for concrete contribution (General Method of CSA A23.3-94)
β_1	coefficient to account for the effect of depth (AS 3600)
β_2	coefficient to account for the effect of axial force (AS 3600)
β_3	coefficient to account for the effect of a concentrated load near a support (AS 3600)
ε_{cr}	concrete cracking strain (Theory)
ε_d	principal concrete compressive strain (Theory)
ε_ℓ	average concrete strain in the longitudinal direction (Theory)
ε_o	strain corresponding to the peak concrete compressive stress (Theory)
ε_r	principal concrete tensile strain (Theory)
$\varepsilon_{s\ell}$	strain in smeared longitudinal tensile steel (Theory)
ε_{st}	strain in transverse steel (Theory)
ε_t	average concrete strain in the transverse direction (Theory)
ε_x	longitudinal strain at the level of the tensile steel reinforcement in a beam (CSA A23.3-94)
ε_1	principal tensile strain in concrete (General Method of CSA A23.3-94)
$\gamma_{\ell t}$	average concrete shear strain in the ℓ-t coordinate system (Theory)
ν	efficiency factor according to the Plasticity Theory
θ	angle of inclination of the principal compressive stress direction with respect to the longitudinal axis of a beam (Theory and CSA A23.3-94)
θ_v	angle of inclination of the concrete compressive strut (AS 3600)
ρ_ℓ	longitudinal steel reinforcement ratio $A_{s\ell V}/(0.9b_v d_o)$ (Theory)
ρ_ℓ	nominal longitudinal tensile steel reinforcement ratio $A_{s\ell}/b_w d$ (EC2 Part 1)
ρ_ℓ	nominal longitudinal tensile steel reinforcement ratio $A_{s\ell}/b_v d_o$
ρ_t	transverse steel reinforcement ratio (Theory)
ρ_w	nominal longitudinal tensile steel reinforcement ratio (ACI 318-95)
σ_d	principal concrete compressive stress (Theory)

σ_ℓ average concrete stress in the direction of the longitudinal axis of a beam
                    (Theory)

σ_r principal concrete tensile stress (Theory)

σ_t average concrete stress in the direction transverse to the longitudinal axis of
                    a beam (Theory)

ζ stress and strain softening factor (Theory)

List of Figures

List of Tables

Introduction

1.1 Definition Of HPC

Conventional concrete contains the basic elements of coarse aggregate, fine aggregate, cement and water. With additions such as silica fume and superplasticiser, the strength and performance of this concrete can be improved. This has brought about the terminologies "high strength concrete" (HSC) and "high performance concrete" (HPC), which are used to describe this superior brand of concrete.

High performance concrete has properties or attributes which satisfy certain performance criteria. These properties have been defined by the Strategic Highway Research Program SHRP-C-205 (Zia, Leming and Ahmad (1991)) as follows:

    (i)   it shall have one of the following strength characteristics:

4-hour compressive strength $\geq$ 18 MPa termed as very early strength concrete (VES), or

24-hour compressive strength $\geq$ 35 MPa termed as high early strength concrete (HES), or

28-day compressive strength $\geq$ 70 MPa termed as very high strength concrete (VHS).

(ii)   it shall have a durability factor > 80% after 300 cycles of freezing and thawing.

(iii) it shall have a water-to-cementitious materials ratio ≤ 0.35.

HSC can be considered as HPC if it satisfies the above requirements for its intended application. In most practical cases, HPC actually leads to HSC. In this study, there is no clear distinction between these two terms and HPC is used to adequately represent HSC as well.

Concrete of higher strengths have been produced with the progression of time since its early history. Commercial concrete with compressive strength of 30 MPa was available in the 1950s and during recent times, concrete with compressive strength greater than 100 MPa is available (Lloyd and Rangan (1993)).

However, there is strictly no absolute strength value which distinctively separates low strength and high strength concretes. A concrete is considered to be high strength according to geographical location and the state-of-the-art concrete technology. At present in Australia, concrete with strength greater than 50 MPa is considered to be in the *high strength concrete* category. The Australian Standard AS 3600 (1994) is intended to apply to concrete with a compressive strength in the range of 20 to 50 MPa.

1.2   Aims Of The Work

Much research has been carried out with respect to shear in concrete beams but only recent tests have focused on HPC. HPC has been accepted as a new material and is notably different from conventional concrete which has been used extensively over the past few decades.

The shear design provisions contained in current codes such as AS 3600 (1994) are mainly semi-empirical and are based on test data from concrete with compressive strength less than 50 MPa. The significant difference in behaviour between high and low strength concretes lies in the fact that crack surfaces in HPC are relatively smoother compared to those in lower strength concrete and this may affect contributions to shear due to aggregate interlock action. Furthermore, bond action between reinforcing bar and HPC may be different. Therefore, there is a need to examine the shear behaviour of HPC beams and the design formulae in the current codes should be updated accordingly. However, there is only limited number of test data on shear strength of HPC beams compared to those for conventional concrete.

The aims of this research therefore are:

    (i)   to study the behaviour of reinforced HPC beams with vertical stirrups subjected to combined bending moment and shear force.

    (ii)   to develop a rational model for determining the shear strength of reinforced HPC beams.

    (iii)   to evaluate the adequacy of the shear provisions in the current Australian Standard AS 3600 and in other codes, and to study the correlation with test results.

1.3 Scope Of The Work

The experimental work involved the testing of reinforced HPC beams with vertical stirrups. Only simply supported solid rectangular beams were tested. The test programme comprising 48 beams covered a number of parameters including concrete cover to shear reinforcement cage, shear reinforcement ratio, longitudinal tensile steel ratio, overall beam depth, shear span-to-depth ratio and concrete compressive strength. The loading configuration was also varied.

As far as the analytical work was concerned, a theory based on truss analogy was developed to predict the response and shear strength of reinforced concrete beams. In addition, the shear design provisions in several codes of practice (AS 3600 (1994), ACI 318-95, EC2 Part1 and CSA A23.3-94) were examined in the light of the test results.

1.4 Organisation Of Thesis

Chapter 2 describes previous research work related to the topic. Both analytical and experimental components of past research are described.

The theory of the present work is detailed in Chapter 3.

Chapter 4 describes the experimental work. Materials and equipment used in the test programme, the specimen details and the test procedure used are reported here.

The presentation and analyses of test data are given in Chapter 5. In this chapter, test results from the present study together with other test results available in the literature are compared with analytical predictions. The test shear strengths are also compared with code predictions.

Chapter 6 summarises the findings of this investigation and presents a set of conclusions. Recommendations for further work are also given in this chapter.

Complete test data are given in the Appendices.

Background

2.1 Introduction

The literature on shear behaviour of reinforced concrete beams is very extensive as it extends back to the turn of the twentieth century. As such, it is beyond the scope of this study to encompass all preceding works related to this topic. A comprehensive review is available in journal articles such as that by the ASCE-ACI Task Committee 426 (1973).

This chapter focuses on two recent theoretical concepts for shear in reinforced concrete. Recent tests conducted on high strength/high performance concrete beams are also described.

A brief review of the shear provisions in the Australian Standard AS 3600 (1994) is given together with a modification to the minimum shear reinforcement requirement. Other codes of practice such as the American Concrete Institute Building Code ACI 318-95, Eurocode EC2 Part 1 and Canadian Standard CSA A23.3-94 are also discussed.

2.2 Theories For Shear

The prediction of the shear response of a reinforced concrete beam is complex. Two of the more recent theoretical concepts are:

(i)   Theories based on Truss Analogy.

(ii)   Shear-Friction Theory.

These theories are briefly described below.

2.2.1 Theories based on Truss Analogy

Early shear design for reinforced concrete beams was based on a truss analogy developed by Ritter in 1899 and Mörsch in 1902. Postulation of this theory was based on the assumption that a concrete panel, reinforced with longitudinal and transverse steel bars, would develop diagonal inclined cracks when subjected to shear (Figure 2.1). These shear cracks were assumed to be straight and at an angle of inclination of θ to the horizontal direction. The concrete struts between these cracks carried a compressive stress σ_d induced by shear.

Considering only shear action on the beam panel, the web region within the effective depth d_v is assumed to resist shear. Figure 2.1(b) shows axial force N induced by the shear force and this is shared equally between the top and bottom stringers.

From vertical equilibrium (Figure 2.1(c)), the shear contribution from the stirrups at a spacing of s with a yield force of $A_{sv}f_{sy.f}$ in each stirrup can be evaluated from:

$$V_{us} = \frac{A_{sv}\, f_{sy.f}\, d_v\, \cot\theta}{s} \tag{2.1}$$

Ritter and Mörsch proposed that θ may be taken as 45°. However, research in the past three decades has shown that θ is not always 45° once cracking occurs.

6

(a) Truss Analogy

(b) Equilibrium for Shear

(c) Vertical Equilibrium
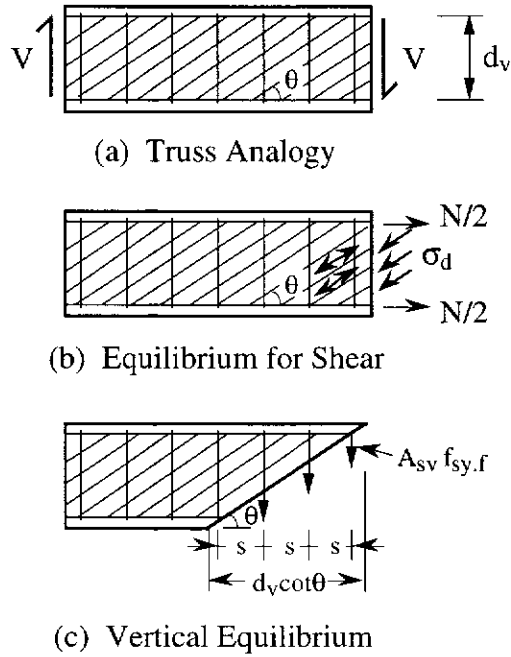
Figure 2.1 Truss Model for Shear in A Beam Panel

Collins (1972) introduced compatibility equations to the truss model in order to determine the angle of inclination of the concrete strut. This theory was referred to as the "Compression Field Theory (CFT)". In 1978, Collins proposed that the principal strain directions in the concrete coincided with the corresponding principal stress directions.

Based on compatibility, equilibrium and constitutive material relationships, the CFT was able to predict the behavioural response of a reinforced concrete member subjected to shear. However, the CFT was based on the uniaxial compressive stress-strain curve of concrete and was found to be inaccurate in predicting the strength and deformation of reinforced concrete members.

Further tests by Vecchio and Collins (1981 and 1982) found that it was necessary to take into account the reduction of the concrete compressive capacity due to the

principal tensile strain in cracked concrete. This improvement led to what is now known as the *"Modified Compression Field Theory"* or *MCFT* (Vecchio and Collins (1986 and 1988)).

Hsu (1988 and 1993) documented independent research which resulted in a theory equivalent to the MCFT called the Softened Truss Model Theory.

Quite distinct from the CFT, MCFT and Softened Truss Model Theory is the more traditional Plasticity Theory (Nielsen (1984)) which considers a truss model in a rigid-plastic analysis. Such an analysis uses the assumption that concrete and steel are perfectly plastic materials. As long as a stress field acting on a member does not cause the material(s) to reach yield, no deformation is considered to occur. The load can be increased until yielding is reached and the member collapses.

The theory presented in Chapter 3 is based on the truss analogy concept.

2.2.2 Shear-Friction Theory

The Shear-Friction Theory is based on the action of shear reinforcement crossing a crack plane. As the shear interfaces on both sides of the crack separate and slip due to loading applied to the concrete member, the reinforcement crossing the crack will be "subjected to dowel action . . . and to tension, which presses the concrete interfaces against each other" (Krauthammer (1992)).

Kriski and Loov (1996) proposed that the shear resistance (v_r) transferred across a crack is limited by the stress that can be sustained by bond and anchorage:

$$v_r \quad = \quad k \sqrt{\sigma f'_c} \qquad\qquad (2.2)$$

8

where

k	=	shear-friction factor
σ	=	normal stress on the plane

Kriski and Loov (1996) asserted that the Shear-Friction Theory could predict the shear strength of beams which had major shear cracks where slip could occur. Theoretical equations were derived from a free-body diagram shown in Figure 2.2.
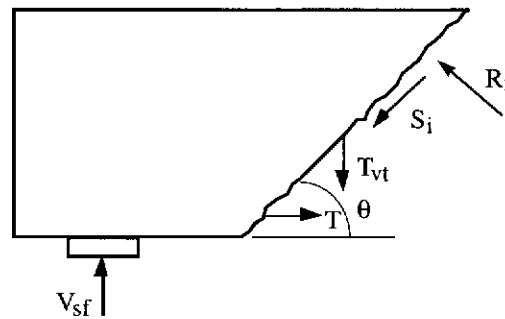
Figure 2.2   Shear-Friction Model (after Kriski and Loov (1996))

The total normal force acting on the inclined plane was designated as R_i whereas the total shear force acting across the same plane was designated as S_i. The tension force in the longitudinal reinforcement was represented by T and the sum of the vertical stirrup forces crossing the inclined crack was given by T_{vt}. The vertical shear force which acted on the free body was V_{sf}. In satisfying equilibrium for the free-body diagram parallel and perpendicular to the shear plane, the following equations were obtained:

$$R_i = T \sin\theta + T_{vt} \cos\theta - V_{sf} \cos\theta \qquad (2.3)$$

$$S_i = T \cos\theta - T_{vt} \sin\theta + V_{sf} \sin\theta \qquad (2.4)$$

Equation 2.2 was re-stated as follows:

$$\frac{S_i}{A} = k\sqrt{\frac{R_i}{A}f'_c}$$

(2.5)

where   A   =   area of the inclined plane

Hence, solving for V_{sf}, the following equation was derived for determining the shear strength of a beam:

$$V_{sf} = b_1\left[\sqrt{1 - c_1/b_1{}^2} - 1\right]$$

(2.6)

where b_1 = $\dfrac{(T\cos\theta - T_{vt}\sin\theta)\sin\theta + 0.5k^2f'_cA\cos\theta}{\sin^2\theta}$

c_1 = $\dfrac{(T\cos\theta - T_{vt}\sin\theta)^2 - k^2f'_cA(T\sin\theta + T_{vt}\cos\theta)}{\sin^2\theta}$

The determination of the shear strength is by trial and error since "all possible failure planes between the inside edge of the support plate and the inside edge of the load plate to a maximum angle of 90° should be checked" (Kriski and Loov (1996)). The plane with the lowest calculated V_{sf} value gives the governing shear strength of the beam.

Kriski and Loov (1996) performed shear-friction analyses on beams tested by Clark (1951), Kani, Huggins and Wittkopp (1979), Sarsam and Al-Musawi (1992) and themselves in order to substantiate the accuracy of this theory.

2.3 Experimental Studies On Shear Strength Of HPC/NSC Beams
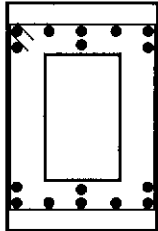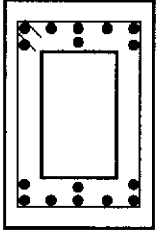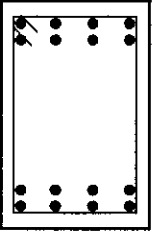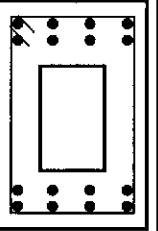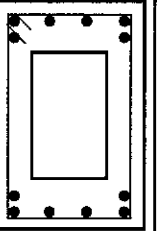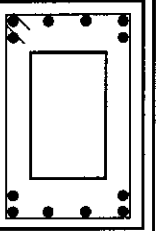
Beams with shear reinforcement tested recently by other researchers are considered here. The details and shear capacities of these beams are given in the following subsections. The M/Vd_0 ratios for the test beams were determined consistent with the theory in Chapter 3. Refer to the Notation for the meaning of symbols used.

2.3.1 Vecchio and Collins (1982)

Various beam specimens were tested at the University of Toronto by Kani, Morawski, Saddler and Arbesman (Vecchio and Collins (1982)). The cross-sections for the non-prestressed reinforced concrete beams are shown in Table 2.1. Full details of these beams are given in Table 2.2.

Exact details of the spans of these beams were not given and further information could not be obtained to determine the M/Vd_0 ratio. However, since Vecchio and Collins considered these beams to have a critical section at approximately the zero bending moment location, they are analysed as such in this study.

Table 2.1 Cross-Sections of Reinforced Concrete Beams Tested at the University of Toronto (Vecchio and Collins (1982))

	SA3	SA4	SK3	SK4	SP0	SM1
Dimensions (mm)	305 x 610	305 x 610	305 x 610	305 x 610	305 x 610	305 x 610
Void (mm)	152 x 406	152 x 406	-	121 x 381	152 x 406	152 x 406
Top Cover (mm)	25	25	16	16	12	12
Bottom Cov.(mm)	12	12	16	16	12	12
Side Cover (mm)	0	41	5	5	12	12
Concrete Strength (MPa)	40.0	40.0	28.2	28.2	25.0	29.0
Stirrups	#3	#3	#3	#3	#3	#3
Spacing (mm)	72.4	72.4	100	100	150	175
Yield Stress (MPa)	373	373	400	400	373	424
Long. Steel	12-#9; 4-#7	12-#9; 4-#7	16-#8	16-#8	12-#7	12-#7
Yield Stress (MPa)	345; 462	345; 462	442	442	421	452

Note: #3: 10 mm (3/8 inch) diameter bar.   #7: 22 mm (7/8 inch) diameter bar.

#8: 25 mm (1 inch) diameter bar.   #9: 29 mm (1.125 inches) diameter bar.

Table 2.2 Details of Reinforced Concrete Beams Tested at the University of Toronto (Vecchio and Collins (1982))

Beam Mark	f_c (MPa)	b_v (mm)	D (mm)	d (mm)	d_o (mm)	$A_{s\ell}$ (mm^2)	$f_{s\ell y}$ (MPa)	ρ_t	s (mm)	f_{sty} (MPa)	V_e (Exp) (kN)
SK3	28.2	305	610	540	572	4080	442	0.00515	100	400	725.0
SK4*	28.2	305	610	540	572	4080	442	0.00854	100	400	601.0
SM1°	29.0	305	610	560	576	2328	452	0.00587	175	424	427.0
SP0°	25.0	305	610	560	576	2328	421	0.00684	150	373	436.0
SA3°	40.0	305	610	548	576	4644	365	0.0142	72.4	373	730.0
SA4°	40.0	305	610	548	576	4644	365	0.0142	72.4	373	534.0

Note: * beams with centrally located void of 121 mm x 381 mm.

° beams with centrally located void of 152 mm x 406 mm.

$A_{s\ell}$ is one-half the total longitudinal steel area.

In these tests,

- beams were tested in reverse bending with the centre of the test regions subjected to a zero bending moment and a large shear force.

- the effect of concrete cover on shear strength was studied. Beams SA3 and SA4 were similar except beam SA3 did not have any side concrete cover but beam SA4 had a side clear cover of 41 mm.

- beams with rectangular solid and hollow cross-sections were tested.

The shear strength of beam SA4 was much lower than that for beam SA3. Vecchio and Collins attributed the lower shear strength to the 41 mm side cover. However, it is noted that the clear cover to the inside wall surface was only 25 mm. This small cover and the large void in the middle of the beam may have affected the confinement of the concrete within the stirrup cage, and caused the lower shear strength. Therefore, this anomalous result was excluded from analyses in Chapter 5.

From this study, the following conclusions were drawn:

- the experimental response curves compared well with the analytical curves predicted by the Modified Compression Field Theory developed by these investigators.

- a spalled web thickness within the confinement of the stirrups was considered to be effective for shear.

12

- a uniform shear flow distribution could be used for analysing concrete beams.

- concrete softening was significant in predicting the behaviour of concrete.

- normal compressive stresses increased the shear resistance of reinforced concrete but normal tensile stresses had the opposite effect.

- the MCFT smeared approach was suitable for reinforced concrete which had well distributed cracking.

2.3.2 Mphonde (1984)
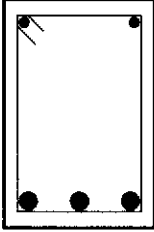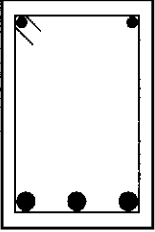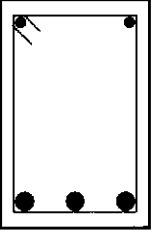
Twelve reinforced normal and high strength concrete beams were tested with a constant M/Vd_o ratio of 2.58. All the beams had a clear span of 2134 mm and were loaded by a concentrated load at midspan. The cross-section was the same for all the beams but the shear reinforcement varied as shown in Table 2.3. Other details for these beams are given in Table 2.4. It is noted that eight other beams with preformed cracks tested by Mphonde (1984) are not included here.

In beams B150-3-3, B150-7-3, B150-11-3 and B150-15-3, stirrups with 3.2 and 4.8 mm diameter were bundled at each spacing location. A mean value of 280 MPa was used to represent the yield stresses of these two types of stirrups (Table 2.4).

The following is a summary of the objectives of this study:

- to determine the cracking strengths and the ultimate shear capacities of reinforced concrete beams.

- to examine the adequacy of the ACI shear design method for beams with concrete compressive strength greater than 41 MPa.

- to determine the effect of concrete compressive strength (which varied from 22 to 83 MPa) on shear strength.

- to determine the effect of the amount of shear reinforcement on shear strength.

Table 2.3 Cross-Sections of Reinforced Concrete Beams Tested by Mphonde (1984)

	B50 Series	B100 Series	B150 Series
Dimensions (mm)	152 x 337	152 x 337	152 x 337
Conc. Cover (mm) to Long. Steel	25	25	25
Stirrups Spacing (mm) Yield Stress (MPa)	3.2 mmØ 90 303	4.8 mmØ 90 269	3.2 & 4.8 mmØ 90 303 & 269
Long. Steel Yield Stress (MPa)	2-#3(T); 3-#8(B) 448(B)	2-#3(T); 3-#8(B) 448(B)	2-#3(T); 3-#8(B) 448(B)

Note: Yield stress for the top longitudinal steel bars is not known.

#3:   10 mm (3/8 inch) diameter bar.

#8:   25 mm (1 inch) diameter bar.

Table 2.4 Details of Reinforced Concrete Beams Tested by Mphonde (1984)

Beam Mark	f'_c (MPa)	b_v (mm)	D (mm)	d (mm)	d_o (mm)	a (mm)	a/d_o	$\dfrac{M}{Vd_o}$	$A_{s\ell}$ (mm^2)	$f_{s\ell y}$ (MPa)	ρ_t	s (mm)	f_{sty} (MPa)	V_e (Exp) (kN)
B50-3-3	22.1	152	337	298	298	1067	3.58	2.58	1470	448	0.001176	90	303	76.3
B50-7-3	39.8	152	337	298	298	1067	3.58	2.58	1470	448	0.001176	90	303	94.1
B50-11-3	59.7	152	337	298	298	1067	3.58	2.58	1470	448	0.001176	90	303	98.1
B50-15-3	83.0	152	337	298	298	1067	3.58	2.58	1470	448	0.001176	90	303	111.5
B100-3-3	27.9	152	337	298	298	1067	3.58	2.58	1470	448	0.002646	90	269	95.4
B100-7-3	47.1	152	337	298	298	1067	3.58	2.58	1470	448	0.002646	90	269	120.8
B100-11-3	68.6	152	337	298	298	1067	3.58	2.58	1470	448	0.002646	90	269	152.1
B100-15-3	81.9	152	337	298	298	1067	3.58	2.58	1470	448	0.002646	90	269	115.9
B150-3-3	28.7	152	337	298	298	1067	3.58	2.58	1470	448	0.003821	90	280	139.3
B150-7-3	46.6	152	337	298	298	1067	3.58	2.58	1470	448	0.003821	90	280	133.8
B150-11-3	69.5	152	337	298	298	1067	3.58	2.58	1470	448	0.003821	90	280	161.9
B150-15-3	82.7	152	337	298	298	1067	3.58	2.58	1470	448	0.003821	90	280	150.3

The values of 50, 100 and 150 in the first term of the beam marks (Table 2.4) referred to the web reinforcement (for example, the number 50 referred to $\rho_t f_{sty} = 50$ lb/in^2 = 0.34 MPa). The subsequent numbers of 3, 7, 11 and 15 referred to four grades of concrete (nominal target strengths were 3000, 7000, 11000 and 15000 psi or 21, 48, 76 and 103 MPa respectively). The number 3 behind indicated an a/d ratio of 3.6.

There was significant scatter in these results. For example, the shear strength decreased from 152.1 to 115.9 kN when the concrete compressive strength increased from 68.6 to 81.9 MPa in beams B100-11-3 and B100-15-3 respectively. Therefore, the shear strength was not directly dependent on the concrete compressive strength.

Findings which transpired from these tests were as follows:

- the ACI code provisions for shear in these slender beams were conservative.

- scatter in the shear strength tended to increase with greater amount of shear reinforcement.

- shear reinforcement carried negligible shear prior to the occurrence of diagonal cracking. It did not have an influence on the diagonal cracking shear force.

- as the amount of shear reinforcement increased, the beams failed in a more ductile manner.

- beams provided with a reasonable amount of shear reinforcement generally failed in shear compression. Sudden diagonal tension failures occurred if the amount of shear reinforcement was very small.

- beams with shear reinforcement had greater ductility in diagonal tension failures compared to beams without shear reinforcement. The failures were not as sudden or explosive.
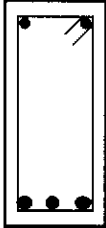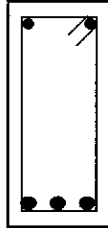
2.3.3 Elzanaty, Nilson and Slate (1986)

Three beams with shear reinforcement of 6.4 mm diameter smooth round bars were tested by these investigators. The beams were 178 mm x 305 mm in cross-section

(Table 2.5). Two symmetrically placed point loads were applied on the beams. The M/Vd_0 ratio and shear reinforcement ratio were kept constant at 3.00 and 0.00171 respectively. Other details for these beams are summarised in Table 2.6.

Beams G4, G5 and G6 were part of eighteen beams tested by Elzanaty, Nilson and Slate (the other fifteen beams were without shear reinforcement). The main objective of testing these three beams was to determine the influence of the concrete compressive strength on the shear strength. It was noted that the cross-sectional area of the longitudinal tensile steel for beam G4 was slightly greater than those for beams G5 and G6 although the concrete compressive strength was the main parameter.

Table 2.5   Cross-Sections of Reinforced Concrete Beams Tested by Elzanaty, Nilson and Slate (1986)

	Beam G4	Beam G5	Beam G6
Dimensions (mm)	178 x 305	178 x 305	178 x 305
Conc. Cover (mm) to Long. Steel	25	25	25
Stirrups Yield Stress (MPa)	6.4 mmØ 379	6.4 mmØ 379	6.4 mmØ 379
Long. Steel Yield Stress (MPa)	2-6.4mmØ(T); 4-#7(B) 379(T); 434(B)	2-6.4mmØ(T); 3-#7(B) 379(T); 434(B)	2-6.4mmØ(T); 3-#7(B) 379(T); 434(B)

Note: #7:   22 mm (7/8 inch) diameter bar.

16

Table 2.6 Details of Reinforced Concrete Beams Tested by Elzanaty, Nilson and Slate (1986)

Beam Mark	f'_c (MPa)	b_v (mm)	D (mm)	d (mm)	d_o (mm)	a (mm)	a/d_o	$\dfrac{M}{Vd_o}$	ρ_ℓ	$f_{s\ell y}$ (MPa)	ρ_t	s (mm)	f_{sty} (MPa)	V_e (Exp) (kN)
G4	62.8	178	305	268	268	1072	4.00	3.00	0.033	434	0.00171	210	379	150.0
G5	40.0	178	305	268	268	1072	4.00	3.00	0.025	434	0.00171	210	379	112.0
G6	20.7	178	305	268	268	1072	4.00	3.00	0.025	434	0.00171	210	379	78.0
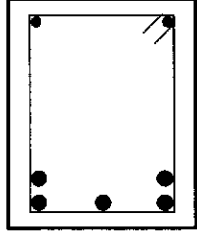
From this study, the following conclusions were drawn:

- the ACI code was conservative for concrete compressive strength ranging from 20.7 to 62.8 MPa. The code was more conservative at greater concrete compressive strength.

- shear strength of beams increased with greater concrete compressive strength.

- stirrup strains monitored during the tests indicated negligible strain values up to the diagonal cracking of the beams. This implied that the stirrups had little or no influence on the diagonal cracking of the beams.

- shear failure was more sudden and the cracked surfaces were smoother for higher concrete compressive strength.

2.3.4 Johnson and Ramirez (1989)

Seven beams with shear reinforcement of 6.4 mm diameter deformed bars were tested by Johnson and Ramirez (1989). The beams had a cross-section of 305 mm x 610 mm (Table 2.7). Two symmetrically placed concentrated loads were applied on each beam which had a clear span of 4254 mm. The M/Vd_o ratio was kept constant at 1.97. The longitudinal steel reinforcement was also maintained the same for all the beams. Other details of these beams are given in Table 2.8.

17

Table 2.7 Cross-Sections of Reinforced Concrete Beams Tested by

Johnson and Ramirez (1989)

Dimensions (mm)	305 x 610
Conc. Cover (mm) to Stirrup	38 (sides); 25 (top and bottom)
Stirrups Yield Stress (MPa)	6.4 mmØ 479
Long. Steel Yield Stress (MPa)	2-#9(T); 5-#10(B) 540 (T); 525 (B)

Note: #9:   29 mm (1.125 inches) diameter bar.

#10:   32 mm (1.25 inches) diameter bar.

Table 2.8 Details of Reinforced Concrete Beams Tested by Johnson

and Ramirez (1989)

Beam Mark	f_c (MPa)	b_v (mm)	D (mm)	d (mm)	d_o (mm)	a (mm)	a/d_o	$\dfrac{M}{Vd_o}$	$A_{s\ell}$ (mm^2)	$f_{s\ell y}$ (MPa)	ρ_t	s (mm)	f_{sty} (MPa)	V_e (Exp) (kN)
1	36.4	305	610	539	562	1670	2.97	1.97	3960	525	0.00156	133	479	338.5
2	36.4	305	610	539	562	1670	2.97	1.97	3960	525	0.00078	267	479	221.9
3	72.3	305	610	539	562	1670	2.97	1.97	3960	525	0.00078	267	479	262.7
4	72.3	305	610	539	562	1670	2.97	1.97	3960	525	0.00078	267	479	315.9
5	55.8	305	610	539	562	1670	2.97	1.97	3960	525	0.00156	133	479	382.7
7	51.3	305	610	539	562	1670	2.97	1.97	3960	525	0.00078	267	479	280.8
8	51.3	305	610	539	562	1670	2.97	1.97	3960	525	0.00078	267	479	258.1

The primary objective of this study was to evaluate the adequacy of the minimum amount of shear reinforcement in beams with relatively high concrete compressive strength according to the ACI 318-83 code provisions.

The main conclusions from this study were:
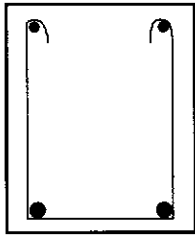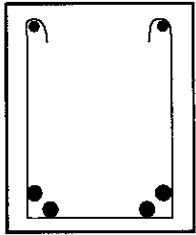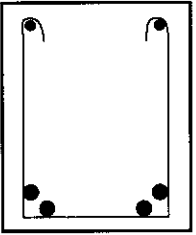
- the reserve capacity provided by shear reinforcement increased significantly as the amount of shear reinforcement was increased from the minimum amount required to twice this amount.

- the number of inclined cracks increased with an increase in the amount of shear reinforcement which indicated greater redistribution of internal forces.

- the shear force transferred to the stirrups during diagonal tension cracking was greater for higher concrete compressive strength and caused stirrups to yield and rupture, thus arresting the redistribution of internal forces and the ability to carry greater shear force. This was evident when beam 3 failed after one of its stirrups fractured.

- the shear contribution from the shear reinforcement was found to decrease with increasing concrete compressive strength for beams with the minimum amount of shear reinforcement. Therefore, it was proposed that the minimum amount of shear reinforcement be increased for greater concrete compressive strength.

2.3.5   Ganwei and Nielsen (1990)

Five beams with a concrete compressive strength of 83.2 MPa tested by Bernhardt and Fynboe were reported in Ganwei and Nielsen (1990). The beams had a cross-section of 150 mm x 200 mm as given in Table 2.9. The M/Vd_0 ratios were 1.40 and 2.29.

The tests were carried out to study the shear behaviour of high strength concrete beams reinforced with open stirrups. Further details of these five beams are provided in Table 2.10. Beams S-7-A and S-7-B, and S-8-A and S-8-B were identical pairs.

19

Table 2.9 Cross-Sections of Reinforced Concrete Beams in Ganwei and Nielsen (1990)

	Beam S-5-A	Beams S-7-A & B	Beams S-8-A & B
Dimensions (mm)	150 x 200	150 x 200	150 x 200
Conc. Clear Cover (mm)	15	15	15
Stirrups Spacing (mm) Yield Stress (MPa)	8 mmØ 150 427	8 mmØ 100 427	8 mmØ 150 427
Long. Steel Yield Stress (MPa)	2-8mmØ(T); 2-20mmØ(B) 510(B)	2-8mmØ(T); 4-20mmØ(B) 510(B)	2-8mmØ(T); 4-20mmØ(B) 510(B)

Note: Yield stress for the top longitudinal steel bars is not known.

Table 2.10   Details of Reinforced Concrete Beams in Ganwei and Nielsen (1990)

Beam Mark	f'_c (MPa)	b_v (mm)	D (mm)	d (mm)	d_o (mm)	a (mm)	a/d_o	$\dfrac{M}{Vd_o}$	$A_{s\ell}$ (mm²)	$f_{s\ell y}$ (MPa)	ρ_t	s (mm)	f_{sty} (MPa)	V_e (Exp) (kN)
S-5-A	83.2	150	200	167	167	400	2.40	1.40	628	510	0.00447	150	427	110.0
S-7-A	83.2	150	200	160	167	550	3.29	2.29	1256	510	0.00673	100	427	140.0
S-7-B	83.2	150	200	160	167	550	3.29	2.29	1256	510	0.00673	100	427	150.0
S-8-A	83.2	150	200	160	167	550	3.29	2.29	1256	510	0.00447	150	427	125.0
S-8-B	83.2	150	200	160	167	550	3.29	2.29	1256	510	0.00447	150	427	135.0

20

The main conclusions from these tests were as follows:

- the experimental shear capacities of the beams were only 60% - 70% of the predictions from the Plasticity Theory.

- the low test shear capacities were attributed to the open stirrups used. However, there were no independent tests to confirm if better stirrup cage constructions would have produced beams with greater shear strengths.

2.3.6 Roller and Russell (1990)
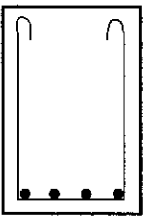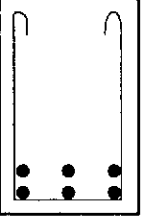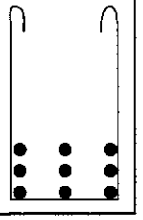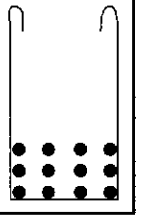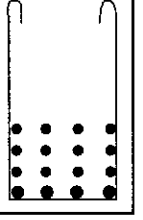
A total of ten beams were tested with concrete compressive strength ranging from 72.4 to 125.3 MPa. These beams had rectangular cross-sections of 356 mm x 635 mm to 356 mm x 743 mm (beams 1 to 5) in the first series, and 457 mm x 870 mm (beams 6 to 10) in the second series as shown in Table 2.11. Except for the shear reinforcement in beam 1, all the steel bars conformed to ASTM A615 (Grade 60). Swedish 6 mm stirrups were used in beam 1 only. No top steel was used in any of the beams.

All the beams were loaded with a central point load in a simply supported span. The shear spans were 1397 mm in the first series and 2286 mm in the second series. Full details of these beams are provided in Table 2.12.
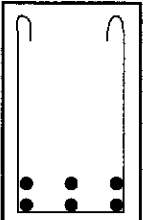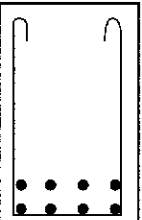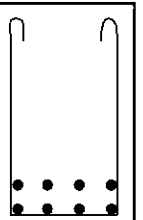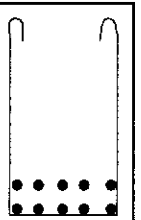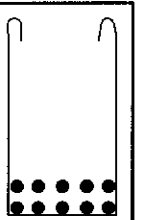
The main objectives of these tests were as follows:

- to study the effect of the concrete compressive strength on the shear strength of the beams.

- to study the effect of the shear reinforcement ratio on the shear strength of the beams.

- to consider the adequacy of the ACI 318-83 code requirement for the minimum amount of shear reinforcement extended to HSC beams.

21

Table 2.11   Cross-Sections of Reinforced Concrete Beams Tested by

Roller and Russell (1990)

	Beam 1	Beam 2	Beam 3	Beam 4	Beam 5
Dimensions (mm)	356 x 635	356 x 679	356 x 718	356 x 718	356 x 743
Stirrups	6.4 mmØ	12.7 mmØ	15.9 mmØ	15.9 mmØ	15.9 mmØ
Spacing (mm)	216	165	127	89	64
Yield Stress (MPa)	407	448	458	458	458
Long. Steel	4-31.8mmØ	3-34.9mmØ; 3-34.9mmØ	3-34.9mmØ; 3-34.9mmØ; 3-34.9mmØ	4-34.9mmØ; 4-34.9mmØ; 4-34.9mmØ	4-31.8mmØ; 4-31.8mmØ; 4-31.8mmØ; 4-34.9mmØ
Yield Stress (MPa)	472	431	431	431	472; 431

(a)   First Test Series

	Beam 6	Beam 7	Beam 8	Beam 9	Beam 10
Dimensions (mm)	457 x 870	457 x 870	457 x 870	457 x 870	457 x 870
Stirrups	9.5 mmØ	9.5 mmØ	9.5 mmØ	9.5 mmØ	9.5 mmØ
Spacing (mm)	381	197	381	197	133
Yield Stress (MPa)	445	445	445	445	445
Long. Steel	3-34.9mmØ; 3-34.9mmØ	4-31.8mmØ; 4-31.8mmØ	4-31.8mmØ; 4-31.8mmØ	5-31.8mmØ; 5-31.8mmØ	5-34.9mmØ; 5-34.9mmØ
Yield Stress (MPa)	464	483	483	483	464

(b)   Second Test Series

22

Beam Mark	f'_c (MPa)	b_v (mm)	D (mm)	d (mm)	d_o (mm)	a (mm)	a/d_o	$\dfrac{M}{Vd_o}$	$A_{s\ell}$ (mm²)	$f_{s\ell y}$ (MPa)	ρ_t	s (mm)	f_{sty} (MPa)	V_e (Exp) (kN)
1	120.1	356	635	559	559	1397	2.50	1.50	3180	472	0.00074	216	407	297.8
2	120.1	356	679	559	599	1397	2.33	1.33	5740	431	0.00431	165	448	1099.1
3	120.1	356	718	559	635	1397	2.20	1.20	8610	431	0.00878	127	458	1657.5
4	120.1	356	718	559	635	1397	2.20	1.20	11490	431	0.01255	89	458	1942.9
5	120.1	356	743	559	660	1397	2.12	1.12	13370	460*	0.01757	64	458	2237.9
6	72.4	457	870	762	793	2286	2.88	1.88	5740	464	0.00081	381	445	665.1
7	72.4	457	870	762	795	2286	2.88	1.88	6360	483	0.00157	197	445	787.6
8	125.3	457	870	762	795	2286	2.88	1.88	6360	483	0.00081	381	445	482.6
9	125.3	457	870	762	795	2286	2.88	1.88	7940	483	0.00157	197	445	749.1
10	125.3	457	870	762	793	2286	2.88	1.88	9560	464	0.00233	133	445	1171.7

Note: * refers to average yield stress representative of 12 - 31.8 mmØ bars (472 MPa) and
4 - 34.9 mmØ bars (431 MPa).

From their study, Roller and Russell concluded that:

• the ACI 318-83 code provisions mainly over-predicted the shear strengths of the beams.

• the minimum amount of shear reinforcement in the ACI code of $0.35b_w s/f_y$ should be increased for higher strength concrete.

The beams were tested with open stirrups which may have resulted in the lower than predicted shear strengths in beams 1, 8 and 9, due to poor anchorage of the stirrups.

2.3.7 Sarsam and Al-Musawi (1992)
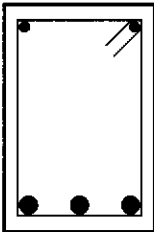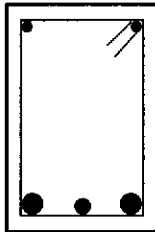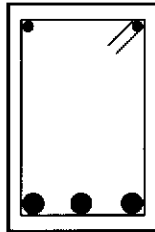
Sarsam and Al-Musawi (1992) tested fourteen beams reinforced with 4 mm diameter high yield cold-drawn smooth wire stirrups. The concrete compressive strength ranged from 39.0 to 80.1 MPa. Overall dimensions of the beams were 180 mm x 270 mm as shown in Table 2.13. The shear spans varied from 580 to 940 mm with M/Vd_o ratios of 1.50 and 3.00, and the specimens were loaded with two symmetrically placed point loads 400 mm apart.

The three beam series of A, B and C corresponded to members with longitudinal steel reinforcement of 3 - 20 mm, 2 - 25 mm and 1 - 16 mm, and 3 - 25 mm diameter deformed bars respectively. The complete details of these beams are given in Table 2.14 (beams with M/Vd_o ratio of 3.00 are shown in *italics* while all other beams have a M/Vd_o ratio of 1.50).

The primary objectives of this study were as follows:

- to examine the shear strength of concrete beams made from HSC and conventional concrete (including 107 specimens from literature).

- to study the influences of variables such as the concrete compressive strength, shear reinforcement ratio, longitudinal steel reinforcement ratio and a/d ratio on the shear strength.

- to compare test shear strengths with predictions from the ACI, Canadian, New Zealand and British codes of practice, and also from Zsutty's (1968) equation.

Table 2.13   Cross-Sections of Reinforced Concrete Beams Tested by Sarsam and Al-Musawi (1992)

	Series A	Series B	Series C
Dimensions (mm)	180 x 270	180 x 270	180 x 270
Conc. Cover (mm) to Long. Steel	25	25	25
Stirrups Yield Stress (MPa)	4 mmØ 820	4 mmØ 820	4 mmØ 820
Long. Steel Yield Stress (MPa)	2-10mmØ(T); 3-20mmØ(B) 450(T); 495(B)	2-10mmØ(T); 2-25mmØ+1-16mmØ(B) 450(T); 543,525(B)	2-10mmØ(T); 3-25mmØ(B) 450(T); 543(B)

24

Table 2.14 Details of Reinforced Concrete Beams Tested by Sarsam

and Al-Musawi (1992)

Beam Mark	f_c (MPa)	b_v (mm)	D (mm)	d (mm)	d_o (mm)	a (mm)	a/d_o	$\dfrac{M}{Vd_o}$	A_{sf} (mm²)	$f_{s\ell y}$ (MPa)	ρ_t	s (mm)	f_{sty} (MPa)	V_e (Exp) (kN)
AL2-N	*40.4*	*180*	*270*	*235*	*235*	*940*	*4.00*	*3.00*	*943*	*495*	*0.00093*	*150*	*820*	*114.7*
AL2-H	*75.3*	*180*	*270*	*235*	*235*	*940*	*4.00*	*3.00*	*943*	*495*	*0.00093*	*150*	*820*	*122.6*
AS2-N	39.0	180	270	235	235	588	2.50	1.50	943	495	0.00093	150	820	189.3
AS2-H	75.5	180	270	232	232	580	2.50	1.50	943	495	0.00093	150	820	201.0
AS3-N	40.2	180	270	235	235	588	2.50	1.50	943	495	0.00140	100	820	199.1
AS3-H	71.8	180	270	235	235	588	2.50	1.50	943	495	0.00140	100	820	199.1
BL2-H	*75.7*	*180*	*270*	*233*	*233*	*932*	*4.00*	*3.00*	*1181*	*540**	*0.00093*	*150*	*820*	*138.3*
BS2-H	73.9	180	270	233	233	583	2.50	1.50	1181	540*	0.00093	150	820	223.5
BS3-H	73.4	180	270	233	233	583	2.50	1.50	1181	540*	0.00140	100	820	228.1
BS4-H	80.1	180	270	233	233	583	2.50	1.50	1181	540*	0.00186	75	820	206.9
CL2-H	*70.1*	*180*	*270*	*233*	*233*	*932*	*4.00*	*3.00*	*1470*	*543*	*0.00093*	*150*	*820*	*147.2*
CS2-H	70.2	180	270	233	233	583	2.50	1.50	1470	543	0.00093	150	820	247.2
CS3-H	74.2	180	270	233	233	583	2.50	1.50	1470	543	0.00140	100	820	247.2
CS4-H	75.7	180	270	233	233	583	2.50	1.50	1470	543	0.00186	75	820	220.7

Note: *   refers to an average yield stress representative of 2 - 25 mmØ bars (543 MPa) and

1 - 16 mmØ bar (525 MPa).

Beams with M/Vd_o ratio of 3.00 or a/d_o ratio of 4.00 are given in *italics*.

From this research, Sarsam and Al-Musawi were able to conclude that:

- both the ACI and Canadian codes were conservative.

- the results suggested that size or depth factor did not have a significant effect on the shear strength of beams with shear reinforcement.

- increasing the concrete compressive strength up to about 80 MPa did not reduce the safety factor (i.e., ratio of test shear strength to predicted shear strength) for the ACI code predictions.
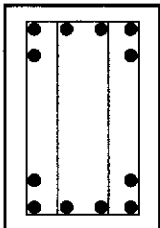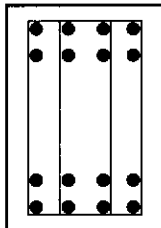
2.3.8 Watanabe (1993)

Ten beams with HSC in the range of 50.7 to 111.0 MPa was used in this investigation. Each specimen had a central test region which was 1100 mm long and two end anchorage regions of 550 mm long effective for the bending moment. The

specimen was loaded in reverse bending to give an anti-symmetric bending moment diagram. This set-up can be visualised as being made up of two identical and symmetrical simply supported bending moment diagrams, each due to a concentrated load at midspan; connected to each other but on opposite sides of the beam. The critical section of a beam was taken at d_0 from the location of maximum bending moment in the direction of decreasing bending moment. The M/Vd_0 ratio was 1.04 for all the beams.

All the test regions of the beams were 150 mm x 300 mm. Cross-sections for Series B and PB are shown in Table 2.15. Full details of the beams are provided in Table 2.16. Equal top and bottom longitudinal steel reinforcement were used in all beams.

Table 2.15   Cross-Sections of Reinforced Concrete Beams Tested by Watanabe (1993)

	Series B	Series PB
Dimensions (mm)	150 x 300	150 x 300
Conc. Cover (mm) to Long. Steel	22	22
Stirrups Yield Stress (MPa)	6 or 8 mmØ 297 - 902	6 or 8 mmØ 290 - 784
Long. Steel Yield Stress (MPa)	6-D16(T); 6-D16(B) 953(T); 953(B)	8-D16(T); 8-D16(B) 996(T); 996(B)

Note: Beams B-1, B-4 and B-6 had 2-legged stirrups; other beams had 4-legged stirrups.

D16:   16 mm diameter deformed bar.

Table 2.16 Details of Reinforced Concrete Beams Tested by Watanabe (1993)

Beam Mark	f'_c (MPa)	b_v (mm)	D (mm)	d (mm)	d_o (mm)	$\dfrac{M}{Vd_o}$	$A_{s\ell}$ (mm²)	$f_{s\ell y}$ (MPa)	ρ_t	s (mm)	f_{sty} (MPa)	V_e (Exp) (kN)
PB-1	111.0	150	300	255	270	1.04	1600	996	0.00850	100	419	352.0
PB-2	111.0	150	300	255	270	1.04	1600	996	0.02640	50	290	563.0
PB-3	111.0	150	300	255	270	1.04	1600	996	0.00850	100	784	516.0
PB-4	111.0	150	300	255	270	1.04	1600	996	0.02640	50	727	730.0
B-1	50.7	150	300	260	270	1.04	1200	953	0.00500	75	297	161.0
B-4	50.7	150	300	260	270	1.04	1200	953	0.00660	100	902	338.0
B-5	50.7	150	300	260	270	1.04	1200	953	0.01710	50	846	478.0
B-6	73.5	150	300	260	270	1.04	1200	953	0.00570	75	411	291.0
B-7	73.5	150	300	260	270	1.04	1200	953	0.00850	100	846	435.0
B-8	73.5	150	300	260	270	1.04	1200	953	0.01760	75	902	471.0

Note: $A_{s\ell}$ is one-half the total longitudinal steel area.

Serial spiral or welded closed loop stirrups were used for shear reinforcement. Beams B-1, B-4 and B-6 had sets of stirrups with two legs across the beam width whereas all the other beams had sets of four legs across the beam width.

These beams contained large amount of longitudinal reinforcement which is not common in most practical reinforced concrete beams.

The main objectives of this research were:

● to investigate the shear design methods for beams with HSC.

● to determine the effects of concrete compressive strength, amount of shear reinforcement and amount of longitudinal steel on the shear strength of beams.

The following were the conclusions drawn from the tests:

● for beams with concrete compressive strength up to 110 MPa, Nielsen's truss or the AIJ (Japanese) code method could be used to predict the shear strength provided that the effective concrete strength was taken as $vf'_c = 1.7f'^{0.667}_c$.

● the ACI code gave over-conservative predictions of shear strength for beams with large amount of shear reinforcement.

2.3.9   Gabrielsson (1993)

Six reinforced HPC beams with shear reinforcement and overall depth in the range of 200 to 300 mm, out of fourteen beams tested by Gabrielsson (1993b), are given in Table 2.17 (also described in Gabrielsson (1993a)). Five beams which did not contain shear reinforcement (i.e., beams HB1, SAR3, HP1, HP3 and HP5) are not included here.

Two other beams, S4 and HS2, considered to have failed in shear by Gabrielsson, appeared to have failed in flexure instead when their photographs taken after failure (given in Gabrielsson (1993a)) were examined. In addition, beam HB3 was reported to have suffered flexure failure. These three beams are also not included here.

The beams given in Table 2.17 are heavily reinforced with high strength steels.

Table 2.17   Details of Reinforced Concrete Beams Tested by Gabrielsson (1993)

Beam Mark	f_c (MPa)	b_v (mm)	d (mm)	d_o (mm)	a (mm)	a/d_o	$\dfrac{M}{Vd_o}$	$A_{s\ell}$ (mm²)	$f_{s\ell y}$ (MPa)	ρ_t	s (mm)	f_{sty} (MPa)	V_e (Exp) (kN)
S2	72.8	200	152	152	500	3.29	2.29	1000	664	0.00242	208	521	172.5
S3	90.4	200	152	152	500	3.29	2.29	1000	664	0.00322	156	521	210.0
HS1	81.6	200	260	260	800	3.08	2.08	1600	664	0.00296	170	521	250.5
HPS1	98.4	200	225	225	550	2.44	1.44	1600	664	0.00335	150	521	324.0
HPS2	103.2	200	225	225	550	2.44	1.44	1600	664	0.00335	150	521	305.0
HB2	86.4	200	223	223	500	2.16	1.16	2000	475	0.00405	124	521	322.0

The concrete compressive strength for these specimens were derived from 100 mm and 150 mm cubes. A conversion factor of 0.8 was used to establish the equivalent cylinder strengths given in Table 2.17.

The aims of this research were as follows:

- to check the applicability of the Swedish design rules for HPC beams where a concrete contribution is added to a steel contribution for a 45° truss model.

28

- to compare Swedish shear design predictions to the predictions from the Modified Compression Field Theory (Vecchio and Collins (1986)).

Based on fourteen beams tested, Gabrielsson made the following conclusions:
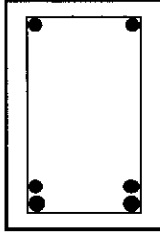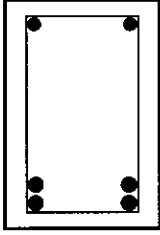
- the Swedish design rules based on traditional truss theory overestimated the shear strengths of beams with a/d ratio of 4.0 to 4.2 (not given in Table 2.17).

- the MCFT described the failure reasonably well but it underestimated the shear strengths of all the test beams.

- for HPC beams, cracking began at a higher percentage of the ultimate strength compared to conventional concrete beams. The compressive stress-strain curve for HPC was quite different from that for Normal Strength Concrete (NSC).

- it was suggested that a shear analysis be performed on a section within the shear span and not where the maximum bending moment occurred since shear failure occurred inside the shear span where the bending moment was considerably smaller.

2.3.10   Xie, Ahmad, Yu, Hino and Chung (1994)

Nine beams reinforced with 6.4 mm diameter smooth bars were part of a testing programme by Xie et al. (1994). All the beams were 127 mm x 254 mm in cross-section as shown in Table 2.18. These beams were loaded by a concentrated load at midspan. The concrete compressive strength ranged from 42.4 to 108.7 MPa.

The experimental investigation was conducted to study the ductility of normal and high strength concrete beams. Variables such as concrete compressive strength, shear span-to-depth ratio and amount of shear reinforcement were considered in these tests. Details of the beams are given in Table 2.19.

Table 2.18 Cross-Sections of Reinforced Concrete Beams Tested by Xie et al. (1994)

	Series NNW	Series NHW
Dimensions (mm)	127 x 254	127 x 254
Stirrups Yield Stress (MPa)	6.4 mmØ 324	6.4 mmØ 324
Long. Steel Yield Stress (MPa)	2-#4(T); 2-#4+2-#6(B) 421	2-#4(T); 4-#6(B) 421

Note: #4:   13 mm (1/2 inch) diameter bar.

#6:   19 mm (3/4 inch) diameter bar.

Table 2.19 Details of Reinforced Concrete Beams Tested by Xie et al. (1994)

Beam Mark	f'_c (MPa)	b_v (mm)	D (mm)	d (mm)	d_o (mm)	a (mm)	a/d_o	$\dfrac{M}{Vd_o}$	$A_{s\ell}$ (mm^2)	$f_{s\ell y}$ (MPa)	ρ_t	s (mm)	f_{sty} (MPa)	V_e (Exp) (kN)
NNW-1	42.4	127	254	203	213	200	0.9	-	826	421	0.00490	102	324	239.6
NNW-2	43.4	127	254	203	213	400	1.9	0.9	826	421	0.00490	102	324	123.3
NNW-3	42.9	127	254	203	213	600	2.8	1.8	826	421	0.00490	102	324	87.2
NHW-1	97.7	127	254	198	213	200	0.9	-	1135	421	0.00510	99	324	324.1
NHW-2	99.7	127	254	198	213	400	1.9	0.9	1135	421	0.00510	99	324	178.6
NHW-3	103.4	127	254	198	213	600	2.8	1.8	1135	421	0.00510	99	324	102.6
NHW-3a	94.7	127	254	198	213	600	2.8	1.8	1135	421	0.00650	76	324	108.5
NHW-3b	108.7	127	254	198	213	600	2.8	1.8	1135	421	0.00780	64	324	122.8
NHW-4	104.0	127	254	198	213	800	3.8	2.8	1135	421	0.00510	99	324	94.0

Note: Clear concrete cover of 25 mm (1 inch) was assumed at the bottom of the beams.

A summary of the findings attained by Xie et al. from their tests is as follows:

- beams with shear reinforcement gave stable and reproducible post-peak load versus midspan deflection characteristics when tested in an energy-absorbing stiff testing machine.

30

- for beams with a/d ratio of 3 (i.e., NNW-3, NHW-3, NHW-3a and NHW-3b), the shear ductility index (area under the load-deflection curve) was not significantly influenced by an increase in concrete compressive strength.
- high strength concrete beams with a/d ratio of 3 (i.e., NHW-3, NHW-3a and NHW-3b) demonstrated near plastic post-peak response when twice the minimum amount of shear reinforcement according to ACI 318-89 was used.
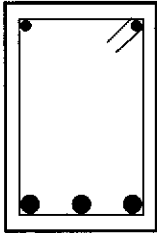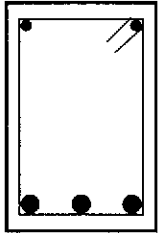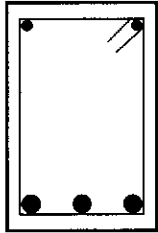
2.3.11 Thirugnanasundralingam, Sanjayan and Hollins (1995)

These investigators tested nine beams altogether; three of which had shear reinforcement. The three beams with shear reinforcement were 150 mm wide, 350 mm deep and 2000 mm long. The clear span in each beam was 1800 mm with a constant shear span of 750 mm. Smooth 8 mm diameter mild steel round bar was used for shear reinforcement. The cross-sections of these beams are shown in Table 2.20. Further details of the beams are provided in Table 2.21. Test yield stresses of the stirrup and longitudinal steel bars were not available and nominal values were used according to Thirugnanasundralingam (1996). Beams 7, 8 and 9 were tested to study the effect of the amount of shear reinforcement on the shear strength of reinforced high strength concrete beams. However, the test trend was not clear from these results. The shear strength of beam 8 was almost double that of beam 7, but the reason for this inconsistency is not known.

The conclusions from these tests with regard to beams with shear reinforcement were:

- the diagonal cracking shear force was not influenced by the stirrup spacing. All the three beams had a cracking shear force of 70 kN.
- the ACI 318-89 code predictions were conservative for these beams.
- crack widths were smaller in beams with shear reinforcement compared to those in beams without shear reinforcement. In addition, the crack widths in the beams with shear reinforcement did not grow until close to failure.
- shear reinforcement contributed to enhanced dowel action and aggregate interlock which increased the post-cracking shear strength of the beams.

Table 2.20 Cross-Sections of Reinforced Concrete Beams Tested by Thirugnanasundralingam et al. (1995)

	Beam 7	Beam 8	Beam 9
Dimensions (mm)	150 x 350	150 x 350	150 x 350
Conc. Cover (mm) to Stirrup	10	10	10
Stirrups Spacing (mm) Yield Stress (MPa)	8 mmØ 200 250	8 mmØ 250 250	8 mmØ 300 250
Long. Steel Yield Stress (MPa)	2Y12(T); 3Y24(B) 400	2Y12(T); 3Y24(B) 400	2Y12(T); 3Y24(B) 400

Note: Y12: 12 mm diameter deformed bar.

Y24: 24 mm diameter deformed bar.

A nominal yield stress of 400 MPa was assumed for all longitudinal steel bars.

A nominal yield stress of 250 MPa was assumed for the stirrups.

Table 2.21 Details of Reinforced Concrete Beams Tested by Thirugnanasundralingam et al. (1995)
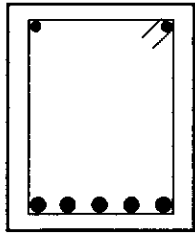
Beam Mark	f'_c (MPa)	b_v (mm)	D (mm)	d (mm)	d_o (mm)	a (mm)	a/d_o	$\dfrac{M}{Vd_o}$	A_{st} (mm^2)	f_{sty} (MPa)	p_t	s (mm)	f_{sty} (MPa)	V_e (Exp) (kN)
7	84.0	150	350	320	320	750	2.34	1.34	1357	400	0.00335	200	250	111.0
8	84.0	150	350	320	320	750	2.34	1.34	1357	400	0.00268	250	250	206.0
9	84.0	150	350	320	320	750	2.34	1.34	1357	400	0.00223	300	250	113.0

2.3.12   Kriski and Loov (1996)

Kriski and Loov (1996) tested twelve beams in their investigation. The cross-section of these specimens are given in Table 2.22. All of the beams were 360 mm wide and 400 mm deep with an effective depth of 345 mm. The simply supported beams were loaded at midspan by a concentrated load. Complete details of the beams are given in Table 2.23.

Kriski and Loov concluded that the inclined cracks from the tests were steeper than those predicted by the Shear-Friction Theory. It was argued that a steeper crack would give a higher shear strength because the longitudinal steel which had a much larger cross-sectional area than the shear reinforcement, was more perpendicular to the crack and provided a larger clamping force (Kriski and Loov (1996)).

Table 2.22   Cross-Section of Reinforced Concrete Beams Tested by Kriski and Loov (1996)

Dimensions (mm)	360 x 400
Conc. Cover (mm) to Long. Steel	43
Stirrups Spacing (mm) Yield Stress (MPa)	5.68 mmØ 150 600
Long. Steel Yield Stress (MPa)	2-10mmØ(T); 5-25mmØ(B) 433(B)

Note: Yield stress for the top longitudinal steel bars is not known.

Table 2.23 Details of Reinforced Concrete Beams Tested by Kriski and Loov (1996)

Beam Mark	f'_c (MPa)	b_v (mm)	D (mm)	d (mm)	d_o (mm)	a (mm)	a/d_o	$\dfrac{M}{Vd_o}$	A_{sf} (mm^2)	f_{sfy} (MPa)	ρ_t	s (mm)	f_{sty} (MPa)	V_e (Exp) (kN)
1	28.9	360	400	345	345	1052	3.05	2.05	2500	433	0.00094	150	600	249.0
2	28.6	360	400	345	345	900	2.61	1.61	2500	433	0.00094	150	600	383.5
3	28.9	360	400	345	345	1052	3.05	2.05	2500	433	0.00094	150	600	224.5
4	28.9	360	400	345	345	749	2.17	1.17	2500	433	0.00094	150	600	444.5
5	30.1	360	400	345	345	900	2.61	1.61	2500	433	0.00094	150	600	293.0
6	33.6	360	400	345	345	749	2.17	1.17	2500	433	0.00094	150	600	331.0
7	74.3	360	400	345	345	1052	3.05	2.05	2500	433	0.00094	150	600	304.5
8	77.8	360	400	345	345	900	2.61	1.61	2500	433	0.00094	150	600	391.0
9	77.0	360	400	345	345	1052	3.05	2.05	2500	433	0.00094	150	600	242.0
10	76.3	360	400	345	345	900	2.61	1.61	2500	433	0.00094	150	600	390.5
11	81.5	360	400	345	345	749	2.17	1.17	2500	433	0.00094	150	600	512.0
12	77.7	360	400	345	345	749	2.17	1.17	2500	433	0.00094	150	600	594.5

Kriski and Loov also suggested that the shear strength of a beam with concrete compressive strength up to about 80 MPa could be assumed to vary with $\sqrt{f'_c}$. However, they also proposed that more work be carried out to evaluate the applicability of the Shear-Friction Theory for determining the shear strength of rectangular reinforced concrete beams with shear reinforcement.

2.3.13 Tests at Curtin University of Technology (1993)

Thirty two beams were tested with varying concrete compressive strength and amount of shear reinforcement. These tests were part of a research project carried out by Ilyas (1993) to study the shear capacities of reinforced HPC beams. Details of these specimens are given in Table 2.24.

These tests were performed to study the effects of the longitudinal steel ratio, transverse steel ratio and shear span-to-depth ratio on the shear strength. Three of the beams (B11, C12 and D11) did not fail in a diagonal cracking failure mode as other beams. Instead, concrete cracking along the level of the longitudinal tensile steel propagated to the anchorage region which initiated the failure of the beams. Hence, these three results are not considered in correlation analyses given in Chapter 5.

The test results given in Table 2.24 have not been published before. The longitudinal reinforcement ratio and shear reinforcement ratio were two of the main parameters of the tests. The shear strength did not increase with the shear reinforcement ratio for beams with M/Vd_o of 1.16 or 1.17. However, for beams with M/Vd_o of 2.66 to 2.68, the shear strength generally increased with the shear reinforcement ratio when the longitudinal reinforcement ratio was kept constant. The scatter in the results for the shorter beams may have been due to arch action effect in those beams.

Table 2.24 Details of Reinforced HPC Beams Tested at Curtin University of Technology (1993)

Beam Mark	f'_c (MPa)	b_v (mm)	D (mm)	d (mm)	d_o (mm)	a (mm)	a/d_o	$\dfrac{M}{Vd_o}$	$A_{s\ell}$ (mm²)	$f_{s\ell y}$ (MPa)	ρ_t	s (mm)	f_{sty} (MPa)	V_e (Exp) (kN)
A11	55.4	200	350	317	317	684	2.16	1.16	1240	450	0.000784	160	516	270.0
A12	55.4	200	350	317	317	684	2.16	1.16	1240	450	0.001255	100	516	313.0
A13	55.4	200	350	317	317	684	2.16	1.16	1240	450	0.001673	75	516	292.0
A14	55.4	200	350	316	316	684	2.16	1.16	1240	450	0.001227	160	510	262.0
A15	55.4	200	350	315	315	684	2.17	1.17	1240	450	0.001948	160	496	270.0
B11	*56.1*	*200*	*350*	*317*	*317*	*684*	*2.16*	*1.16*	*1860*	*450*	*0.000784*	*160*	*516*	*534.0*
B12	56.1	200	350	317	317	684	2.16	1.16	1860	450	0.001255	100	516	496.0
B13	56.1	200	350	317	317	684	2.16	1.16	1860	450	0.001673	75	516	401.0
B14	56.1	200	350	316	316	684	2.16	1.16	1860	450	0.001227	160	510	385.0
B15	56.1	200	350	315	315	684	2.17	1.17	1860	450	0.001948	160	496	403.0
C11	56.8	200	350	292	317	684	2.16	1.16	2480	450	0.000784	160	516	459.0
C12	*56.8*	*200*	*350*	*292*	*317*	*684*	*2.16*	*1.16*	*2480*	*450*	*0.001255*	*100*	*516*	*601.0*
C13	56.8	200	350	292	317	684	2.16	1.16	2480	450	0.001673	75	516	447.0
C14	56.8	200	350	291	316	684	2.16	1.16	2480	450	0.001227	160	510	364.0
C15	56.8	200	350	290	315	684	2.17	1.17	2480	450	0.001948	160	496	416.0
D11	*48.0*	*200*	*350*	*297*	*317*	*684*	*2.16*	*1.16*	*3100*	*450*	*0.000784*	*160*	*516*	*448.0*
D12	48.0	200	350	297	317	684	2.16	1.16	3100	450	0.001255	100	516	443.0
D13	48.0	200	350	297	317	684	2.16	1.16	3100	450	0.001673	75	516	505.0
D14	48.0	200	350	296	316	684	2.16	1.16	3100	450	0.001227	160	510	499.0
D15	48.0	200	350	295	315	684	2.17	1.17	3100	450	0.001948	160	496	508.0
B21	63.2	200	350	317	317	1160	3.66	2.66	1860	450	0.000784	160	516	221.0
B22	63.2	200	350	317	317	1160	3.66	2.66	1860	450	0.001255	100	516	237.0
B24	63.2	200	350	316	316	1160	3.67	2.67	1860	450	0.001227	160	510	255.0
C21	63.2	200	350	292	317	1160	3.66	2.66	2480	450	0.000784	160	516	256.0
C22	63.2	200	350	292	317	1160	3.66	2.66	2480	450	0.001255	100	516	311.0
C23	61.4	200	350	292	317	1160	3.66	2.66	2480	450	0.001673	75	516	379.0
C24	63.2	200	350	291	316	1160	3.67	2.67	2480	450	0.001227	160	510	301.0
D21	61.4	200	350	297	317	1160	3.66	2.66	3100	450	0.000784	160	516	256.0
D22	61.4	200	350	297	317	1160	3.66	2.66	3100	450	0.001255	100	516	290.0
D23	61.4	200	350	297	317	1160	3.66	2.66	3100	450	0.001673	75	516	344.0
D24	61.4	200	350	296	316	1160	3.67	2.67	3100	450	0.001227	160	510	295.0
D25	61.4	200	350	295	315	1160	3.68	2.68	3100	450	0.001948	160	496	404.0

Note: Beams given in *italics* failed at the supports.

2.4 Shear Design Provisions In Codes

Four national codes of practice are considered for comparisons of test to predicted shear strengths of reinforced concrete beams: Australian Standard AS 3600 (1994), Eurocode EC2 Part 1, American Concrete Institute Building Code AC1 318-95 and Canadian Standard CSA A23.3-94.

2.4.1 Australian Standard AS 3600 (1994)

The Australian Standard AS 3600 (1994) shear design equations are based on a variable angle truss model. Shear resistance is made up of concrete and steel contributions:

$$V_u = V_{uc} + V_{us} \qquad (2.7)$$

where

$$V_{uc} = \beta_1\beta_2\beta_3 b_v d_o \left(\frac{A_{st}f'_c}{b_v d_o}\right)^{\frac{1}{3}} \qquad (2.8)$$

b_v = effective web width

d_o = distance from the extreme compression fibre to the centroid of the outermost layer of longitudinal tensile reinforcement, and

A_{st} = cross-sectional area of longitudinal tensile steel reinforcement.

The formula for the concrete contribution is similar to a statistically derived expression by Zsutty (1968). The factors for determining V_{uc} according to AS 3600 (1994) are:

(i) β_1 accounts for the size factor of a section. Deeper sections are considered to carry lower shear stress at failure.

$$\beta_1 = 1.1\left(1.6 - \frac{d_o}{1000}\right) \geq 1.1 \quad (d_o \text{ in mm}) \quad (2.9)$$

(ii) β_2 accounts for axial force effects.

$$\beta_2 = 1.0 \quad \text{(when no axial force exists)}$$

(iii) β_3 accounts for the presence of a large concentrated load near a

support.

$$\beta_3 \quad = \quad \frac{2\,d_o}{a} \quad (1.0 \le \beta_3 \le 2.0) \tag{2.10}$$

where a is the distance of the concentrated load from the support.

For vertical shear reinforcement, AS 3600 gives the stirrup contribution as:

$$V_{us} \quad = \quad \frac{A_{sv}\,f_{sy.f}\,d_o\,\cot\theta_v}{s} \quad = \quad \rho_t\,f_{sy.f}\,b_v\,d_o\,\cot\theta_v \tag{2.11}$$

where

A_{sv}	$=$	cross-sectional area of shear reinforcement
$f_{sy.f}$	$=$	yield stress of shear reinforcement
θ_v	$=$	angle of inclination of the concrete compression strut
ρ_t	$=$	shear reinforcement ratio, and
s	$=$	spacing of the stirrup cages.

In order to avoid web crushing failure when a large amount of shear reinforcement is used, AS 3600 limits the shear capacity to:

$$V_{u.max} = \quad 0.2\ f'_c\ b_v\ d_o \tag{2.12}$$

AS 3600 (1994) also stipulates that a minimum amount of shear reinforcement be used before it is effective for shear contribution:

$$A_{sv.min} \quad = \quad \frac{0.35\ b_v\ s}{f_{sy.f}} \tag{2.13}$$

The angle of inclination θ_v is "the angle between the axis of the concrete compression strut and the longitudinal axis of the member" (AS 3600). It is assumed to vary linearly between 30° when the minimum amount of shear reinforcement is used and 45° when the limiting amount of shear reinforcement corresponding to web crushing is used.

It is proposed to modify Equation 2.13 by:

$$A_{sv.min} = \frac{0.06 \sqrt{f_c} \, b_v \, s}{f_{sy.f}}$$ (2.14)

so that the shear design method may be applied to concretes with compressive strength up to 100 MPa instead of the 50 MPa upper limit currently imposed by AS 3600. In the present study, Equation 2.14 is adopted as part of the AS 3600 method. This modification is consistent with the minimum requirement proposed in the Canadian Code CSA A23.3-94 (Section 2.4.4).

For most practical beams with relatively small amount of shear reinforcement, the angle θ_v remains close to 30° as the limiting amount of shear reinforcement corresponding to web crushing is much greater than $A_{sv.min}$. Therefore, the steel contribution V_{us} will have negligible difference when determined using either Equation 2.13 or Equation 2.14.

2.4.2 American Code ACI 318-95

The ACI code adopts the 45° truss model with an additional term for concrete contribution.

$$V_n = V_c + V_s$$ (2.15)

where

$$V_c = \left(0.16\sqrt{f_c} + 17.2\rho_w \frac{V_u d}{M_u} \right) b_w d \qquad (\leq 0.3 \sqrt{f_c} \, b_w d)$$ (2.16)

and

ρ_w = longitudinal tensile steel reinforcement ratio

V_u, M_u = shear force and moment at the critical section

b_w = effective web width, and

d = effective depth.

The $V_u d/M_u$ term is generally small. Therefore, ACI 318-95 allows the following simplified equation to be used:

$$V_c = 0.17 \sqrt{f_c} \, b_w \, d$$ (2.17)

38

The ACI code allows for arch action by applying a multiplier to V_c for deep flexural beams. For beams with ℓ_n/d (clear span/depth ratio) of less than 5, the multiplier can be applied to Equation 2.17:

$$V_c = \left(3.5 - 2.5 \frac{M_u}{V_u d}\right) 0.17 \sqrt{f'_c} \; b_w \, d \qquad (2.18)$$

where the multiplier is in the range of 1.0 to 2.5.

For the stirrup contribution to shear, the conservative 45° truss solution is used:

$$V_s = \frac{A_v \, f_y \, d}{s} \qquad (2.19)$$

where

A_v =   cross-sectional area of shear reinforcement, and

f_y =   yield stress of shear reinforcement.

2.4.3   Eurocode EC2 Part 1

The Eurocode EC2 Part 1 does not encourage the use of concrete with compressive strength less than 12 MPa or greater than 50 MPa for structural purposes. It is partly based on the Plasticity Theory by Nielsen (1984). Two methods of design are given:

(i)   the Standard Method, which combines a concrete contribution and a stirrup contribution based on the 45° truss model.

(ii)   the Variable Strut Inclination Method.

Shear design centres on three values of shear resistances stated as V_{Rd1}, V_{Rd2} and V_{Rd3}. V_{Rd1} refers to the shear capacity of a concrete member without shear reinforcement determined from an empirical formula:

$$V_{Rd1} = \tau_{rd} \, k \, (1.2 + 40\rho_\ell) \, b_w \, d \qquad (2.20)$$

where

τ_{rd} =   basic design shear strength   = $0.25 \, f_{ctk0.05}$

$f_{ctk0.05}$ =   the lower 5% fractile characteristic tensile strength   = $0.7 \, f_{ctm}$

f_{ctm} =   mean value of the tensile concrete strength   = $0.30 \, (f_{ck})^{2/3}$

f_{ck} = characteristic cylinder compressive strength of concrete

k = 1.0 for members where more than 50% of the bottom reinforcement is curtailed; or otherwise,

k = $(1.6 - d) \geq 1.0$ (d in metres), and

ρ_{ℓ} = $\dfrac{A_{s\ell}}{b_w\, d} \leq 0.02$.

It is noted that although ρ_{ℓ} in Equation 2.20 is limited to 2%, most of the beams in this study have steel ratios greater than 2%. The large amount of longitudinal steel in the beams is to ensure shear failure instead of flexural failure.

The above equation can be simplified to the following equation:

$$V_{Rd1} = 0.0525\, k\, (f_{ck})^{2/3}\, (1.2 + 40\rho_{\ell})\ b_w\, d \qquad (2.21)$$

When determining V_{Rd1}, an enhancement factor can be applied if the member is loaded by a concentrated load situated at a distance $x \leq 2.5d$ from the face of the support. The multiplier is given as:

$$\beta = \frac{2.5d}{x} \quad (1.0 \leq \beta \leq 5.0) \qquad (2.22)$$

The resistance V_{Rd2} is the shear capacity of a beam when web crushing occurs according to the Plasticity Theory (Nielsen (1984)). The maximum V_{Rd2} value that can be attained is limited by the effective stress in the compressive strut such that:

$$V_{Rd2}\,(\text{max}) = 0.5\, v\, f_{cd}\, b_w\, (0.9d) \qquad (2.23)$$

where

f_{cd} = design value of concrete cylinder compressive strength, which equals the characteristic cylinder strength at 28 days, and

v = the efficiency factor = $0.7 - \dfrac{f_{ck}}{200} \geq 0.5$.

For the purpose of analysis, f_{cd} is assumed to be equal to f_{ck}.

The consideration for minimum shear reinforcement is given in Table 5.5 of EC2 Part 1. For concrete grade of 50 MPa and steel class of 400 MPa, the minimum shear

reinforcement ratio is given as 0.0016. This requirement differs from that of the ACI 318-95 and AS 3600 (1994) codes, and is almost twice the amount calculated from $\left(\dfrac{0.35}{f_{sy.f}}\right) = 0.00088$. According to Equation 2.14, the minimum shear reinforcement ratio is $\left(\dfrac{0.06 \sqrt{f_c}}{f_{sy.f}}\right) = 0.0011$.

The difference between the Standard Method and the Variable Strut Inclination Method is in the determination of the resistance V_{Rd3}. The alternative methods of calculating V_{Rd3} are discussed below.

2.4.3.1   Standard Method

The Standard Method is similar to the provisions of ACI 318-95 with the total shear resistance given as:

$$V_{Rd3} \quad = \quad V_{cd} + V_{wd} \tag{2.24}$$

where

$$V_{cd} \quad = \quad \text{concrete contribution and is taken as equal to } V_{Rd1}$$

$$V_{wd} \quad = \quad \frac{A_{sw}\, f_{ywd}}{s}\, (0.9d) \tag{2.25}$$

$$A_{sw} \quad = \quad \text{cross-sectional area of shear reinforcement, and}$$

$$f_{ywd} \quad = \quad \text{yield stress of shear reinforcement.}$$

The formula for V_{Rd3} can be written as:

$$V_{Rd3} \quad = \quad \beta\,[0.0525\, k\, (f_{ck})^{2/3}\,(1.2+40\rho_\ell)\, b_w d] + \frac{A_{sw}\, f_{ywd}}{s}\, (0.9d)$$

$$\leq V_{Rd2}\,(\text{max})$$

$$\tag{2.26}$$

For analysis, the limits on ρ_ℓ, β and v were adhered to when calculating V_{Rd3}.

41

2.4.3.2 Variable Strut Inclination Method

The Variable Strut Inclination Method is based on a truss with an angle θ chosen within the ranges of:

(i) $0.4 < \cot\theta < 2.5$ - for beams with constant longitudinal reinforcement, or

(ii) $0.5 < \cot\theta < 2.0$ - for beams with curtailed longitudinal reinforcement.

The shear resistance based on the crushing of the compressive strut is:

$$V_{Rd2} = \frac{b_w(0.9d)\,vf_{cd}}{(\cot\theta + \tan\theta)} \qquad (2.27)$$

The shear resistance based on a truss model with stirrups yielding is:

$$V_{Rd3} = \frac{A_{sw}\,f_{ywd}}{s}\,(0.9d)\cot\theta \qquad (2.28)$$

A limitation based on the Plasticity Theory is placed on the effectiveness of the shear reinforcement such that:

$$\frac{A_{sw}\,f_{ywd}}{b_w\,s} \leq 0.5\,v\,f_{cd} \qquad (2.29)$$

In design, the applied shear force is equated to V_{Rd2} to obtain the largest value of $\cot\theta$, which corresponds to the smallest amount of shear reinforcement. The amount of shear reinforcement is then found from the equation for V_{Rd3}. For analysis, a solution can only be found by equating V_{Rd3} to V_{Rd2}. The solution for θ can be found from:

$$\tan\theta \geq \frac{1}{\sqrt{\left(\dfrac{vf_{cd}}{\rho_{sw}f_{ywd}} - 1\right)}} \qquad (2.30)$$

$$\text{or} \quad \cot\theta \leq \sqrt{\left(\dfrac{vf_{cd}}{\rho_{sw}f_{ywd}} - 1\right)} \qquad (2.31)$$

The solution for $\tan\theta$ should also include the consideration of limiting $\rho_{sw}f_{ywd}$ as stated in Equation 2.29 and restricting $\cot\theta$ as described at the beginning of this sub-section. After solving for $\tan\theta$, the shear resistance V_{Rd3} may be calculated.

2.4.4 Canadian Standard CSA A23.3-94

The Canadian Standard CSA A23.3-94 permits two alternative methods of shear design for reinforced concrete beams: namely, the Simplified Method and General Method. The former is based on the traditional "concrete plus steel contributions" approach whereas the latter revolves around the Modified Compression Field Theory.

The Simplified Method is based on the 45° truss model with an effective depth of d. However, the General Method has a variable angle truss. Although the General Method is based on the MCFT, it is also formulated in the form of a concrete contribution plus steel contribution approach.

The minimum shear reinforcement area is given by Equation 2.14.

2.4.4.1 Simplified Method

The shear resistance V_r can be stated as follows:

$$V_r = V_c + V_s \tag{2.32}$$

The concrete contribution is given by:

$$V_c = 0.2 \sqrt{f'_c} \, b_w d \quad \text{when } A_v \geq \frac{0.06\sqrt{f'_c} b_w s}{f_y} \text{ or } d \leq 300 \text{ mm} \tag{2.33a}$$

$$\text{or} \quad V_c = \left(\frac{260}{1000+d}\right)\sqrt{f'_c} \, b_w d \geq 0.1\sqrt{f'_c} \, b_w d \quad \text{when } A_v < \frac{0.06\sqrt{f'_c} b_w s}{f_y} \text{ and } d > 300 \text{ mm} \tag{2.33b}$$

The steel contribution is given by:

$$V_s = \frac{A_v \, f_y \, d}{s} \leq 0.8 \sqrt{f'_c} \, b_w d \tag{2.34}$$

2.4.4.2   General Method

Designing or analysing using the General Method requires the determination of the effective shear depth (d_v), which is assumed in the Canadian Standard as being not less than 0.9d.

The nominal shear strength of a beam can be stated as:

$$V_{rg} \quad = \quad V_{cg} + V_{sg} \quad \leq \quad 0.25 \, f'_c b_w d_v \tag{2.35a}$$

where

$$V_{cg} \quad = \quad \beta \sqrt{f'_c} \, b_w d_v \tag{2.35b}$$

$$V_{sg} \quad = \quad \frac{A_v f_y}{s} \, d_v \cot\theta \tag{2.35c}$$

$$\beta \quad = \quad \frac{0.33 \cot\theta}{1 + \sqrt{500\varepsilon_1}} \quad \leq \quad \frac{0.18}{\left(0.3 + \frac{24w}{a+16} \right)} \tag{2.35d}$$

θ =   angle of inclination of the principal compressive stress direction with respect to the longitudinal axis of the beam

ε_1 =   principal tensile strain in cracked concrete

w   =   crack width (mm), and

a   =   maximum aggregate size (mm).

Using the Mohr's strain circle, the principal tensile strain can be expressed in terms of the longitudinal strain ε_x and the principal compressive strain ε_2 in concrete:

$$\varepsilon_1 \quad = \quad \varepsilon_x + (\varepsilon_x - \varepsilon_2) \cot^2\theta \tag{2.36}$$

The principal compressive strain ε_2, can be found from the pre-peak branch of a parabolic concrete compressive stress-strain curve (Collins, Mitchell, Adebar and Vecchio (1996)):

$$\varepsilon_2 \quad = \quad -0.002 \left(1 - \sqrt{1 - \frac{f_2}{f_{2max}}} \, \right) \tag{2.37}$$

where

f_2 =   principal compressive stress in concrete, and

f_{2max} =   crushing strength of cracked concrete.

The principal compressive stress can be determined from a Mohr's stress circle as:

$$f_2 \quad = \quad v\,(\tan\theta + \cot\theta) \tag{2.38}$$

where

$$v \quad = \quad \text{shear stress} \quad = \quad \frac{V_u}{b_w d_v} \text{ , and}$$

V_u =   shear force at the critical section.

When softening is considered, the crushing strength of cracked concrete can be factored from the cylinder compressive strength f'_c as:

$$f_{2max} \quad = \quad \frac{f'_c}{(0.8+170\varepsilon_1)} \quad \leq f'_c \tag{2.39}$$

Substituting Equations 2.37, 2.38 and 2.39 into Equation 2.36, the principal tensile strain can be re-stated as:

$$\varepsilon_1 \quad = \quad \varepsilon_x + \left[\varepsilon_x + 0.002\left(1 - \sqrt{1 - \frac{v}{f'_c}(\tan\theta + \cot\theta)(0.8+170\varepsilon_1)}\,\right)\right]\cot^2\theta$$

$$\tag{2.40}$$

The strain ε_x is taken as the strain at the level of the tensile reinforcement based on an assumed linear strain gradient across the depth of a beam. Due to the effects of a bending moment and a shear force, ε_x can be estimated as:

$$\varepsilon_x \quad = \quad \frac{M_u/d_v + 0.5V_u\cot\theta}{E_s\,A_s} \tag{2.41}$$

where

M_u =   moment at the critical section, and

A_s =   cross-sectional area of longitudinal steel in the flexural tension side of a beam.

The determination of ε_x is dependent on the location of the critical section which dictates the values of M_u and V_u. Visualising the beam as a variable angle truss, the yielding of shear reinforcement occurs over a length of $d_v\cot\theta$ (Collins, Mitchell, Adebar and Vecchio (1996)). It is reasonable to consider the section in the middle of this length as being critical. Therefore, the critical section may be taken at a distance of $0.5d_v\cot\theta$ from a concentrated load or support. In simplifying, the distance of $0.5d_v\cot\theta$ is taken as approximately equal to d_v.

There can be several θ values which will give satisfactory solution to the above equations. However, values of θ and β were given by Collins, Mitchell, Adebar and Vecchio (1996) to ensure that the transverse stirrup strain (ε_t) was at least equal to 0.002 and the principal compressive stress in the concrete strut did not exceed the softened concrete crushing strength (Table 2.25).

Table 2.25   Values of θ and β for Beams With At Least the Minimum Shear Reinforcement

$\dfrac{V_{rg}}{b_wd_vf'_c}$		Longitudinal Strain, ε_x ($\times10^{-3}$)						
		≤ 0	≤ 0.25	≤ 0.50	≤ 0.75	≤ 1.00	≤ 1.50	≤ 2.00
≤ 0.050	θ°	27.0°	28.5°	29.0°	33.0°	36.0°	41.0°	43.0°
	β	0.405	0.290	0.208	0.197	0.185	0.162	0.143
≤ 0.075	θ°	27.0°	27.5°	30.0°	33.5°	36.0°	40.0°	42.0°
	β	0.405	0.250	0.205	0.194	0.179	0.158	0.137
≤ 0.100	θ°	23.5°	26.5°	30.5°	34.0°	36.0°	38.0°	39.0°
	β	0.271	0.211	0.200	0.189	0.174	0.143	0.120
≤ 0.125	θ°	23.5°	28.0°	31.5°	34.0°	36.0°	37.0°	38.0°
	β	0.216	0.208	0.197	0.181	0.167	0.133	0.112
≤ 0.150	θ°	25.0°	29.0°	32.0°	34.0°	36.0°	36.5°	37.0°
	β	0.212	0.203	0.189	0.171	0.160	0.125	0.103
≤ 0.200	θ°	27.5°	31.0°	33.0°	34.0°	34.5°	35.0°	36.0°
	β	0.203	0.194	0.174	0.151	0.131	0.100	0.083
≤ 0.250	θ°	30.0°	32.0°	33.0°	34.0°	35.5°	38.5°	41.5°
	β	0.191	0.167	0.136	0.126	0.116	0.108	0.104

The values of θ and β given in Table 2.25 were based on an assumed diagonal crack spacing of 305 mm and a maximum aggregate size of 19 mm. Collins, Mitchell,

Adebar and Vecchio (1996) considered these values to hold for "the full range of beams containing stirrups".

There is no direct solution to find the shear strength of a beam. The shear strength V_{rg} is dependent on θ and β, β in turn is dependent ε_1 and θ, ε_1 in turn is dependent on ε_x and ε_x in turn is dependent on V_{rg} (V_{rg} replaces V_u in Equation 2.41). The simplest way to obtain a solution using Table 2.25 is to assume that the beam being analysed is lightly shear reinforced with $\left(\dfrac{V_{rg}}{b_w d_v f'_c}\right) \leq 0.050$ and an initial trial value of ε_x is assumed. Then a set of θ and β values can be found from Table 2.25 and V_{rg} can be calculated. The longitudinal strain ε_x can then be calculated and checked. This process is iterated until ε_x converges and the final V_{rg} value is accepted as the predicted shear strength. Linear interpolation can be used between values given in Table 2.25.

In analysing the test data, some beams were out of the range of the tabulated values. For $\varepsilon_x > 2.0 \times 10^{-3}$ and/or $\left(\dfrac{V_{rg}}{b_w d_v f'_c}\right) > 0.25$, the conservative assumptions of $\theta = 45°$ and $\beta = 0.100$ were adopted in Chapter 5.

However, not all the beams from the previous investigations have at least the minimum amount of shear reinforcement as given by Equation 2.14. For beams with less than the minimum shear reinforcement, the θ and β values were determined from Table 2.26.

The θ and β values are dependent on the spacing of the longitudinal cracks in the web of a beam s_z. This spacing is a function of the maximum distance between longitudinal bars or between longitudinal bars and the flexural compression zone. For beams with less than the minimum shear reinforcement and no intermediate layers of longitudinal crack control reinforcement, the crack spacing parameter s_z may be taken as d_v (or 0.9d).

Table 2.26 Values of θ and β for Beams With Less Than the Minimum Shear Reinforcement

s_z (mm)		Longitudinal Strain, ε_x ($\times 10^{-3}$)					
		≤ 0	≤ 0.25	≤ 0.50	≤ 1.00	≤ 1.50	≤ 2.00
≤ 125	θ°	27.0°	29.0°	32.0°	34.0°	36.0°	38.0°
	β	0.406	0.309	0.263	0.214	0.183	0.161
≤ 250	θ°	30.0°	34.0°	37.0°	41.0°	43.0°	45.0°
	β	0.384	0.283	0.235	0.183	0.156	0.138
≤ 500	θ°	34.0°	39.0°	43.0°	48.0°	51.0°	54.0°
	β	0.359	0.248	0.201	0.153	0.127	0.108
≤ 1000	θ°	37.0°	45.0°	51.0°	56.0°	60.0°	63.0°
	β	0.335	0.212	0.163	0.118	0.095	0.080
≤ 2000	θ°	41.0°	53.0°	59.0°	66.0°	69.0°	72.0°
	β	0.306	0.171	0.126	0.084	0.064	0.052

2.4.5 Comparisons of Code Methods

The Australian Standard AS 3600 (1994) adopts a concrete plus steel contribution approach which is easy to apply. This code assumes a variable angle truss with a minimum angle of inclination of the principal compressive strut of 30° to give an increased contribution to shear compared to a 45° truss. However, the minimum shear reinforcement requirement and the limiting amount of shear reinforcement for web crushing should be reviewed for HPC.

The American code ACI 318-95 is the easiest method to use but from previous work, it has been found to be quite conservative, particularly for conventional concrete.

The Eurocode EC2 Part 1 methods provide generally conservative predictions, particularly the Variable Strut Inclination Method. The applicability of the efficiency factor ν in Equation 2.23 to HPC is still debatable.

The Simplified Method of the Canadian code CSA A23.3-94 is comparable to the ACI code method. In contrast, the General Method of CSA A23.3-94 is quite complex to solve. The solution can be tedious and an iterative solution is required.

Theory

This chapter presents a theory developed to predict the shear response and the shear strength of reinforced concrete beams with vertical stirrups. The theory is based on the stress analysis of the web portion of a beam and adopted from previous work by Hsu (1988 and 1993) and Vecchio and Collins (1982 and 1993).

3.1 Analytical Model

Figure 3.1 shows a region of a reinforced concrete beam subjected to bending moment M, shear force V and axial force N. The region is sufficiently away from the disturbances caused by concentrated loads, supports and openings.

Figure 3.1(a) is the beam cross-section where $A_{s\ell}$ is the total area of longitudinal steel in the tension zone, b_v is the width of the web and d_0 is the distance from the extreme compression fibre to the centroid of the outermost layer of tensile steel. The actions acting on the beam are shown in Figure 3.1(b) and the internal forces are illustrated in Figures 3.1(c), (d) and (e). The bending moment is resisted by the compressive force C and the tensile force T. The force C is provided by the concrete and the

longitudinal steel in the compression zone of the beam and T is given by that part of $A_{s\ell}$ designated as $A_{s\ell M}$.

d_o

$A_{s\ell}$

$\leftarrow b_v \rightarrow$

Cross-Section

(a)

M

N

V

Actions

(b)

σ_ℓ

$v_{\ell t}$

C

T

$d_v (=0.9d_o)$

Internal Forces due to:-

(M) (N) (V)

(c) (d) (e)
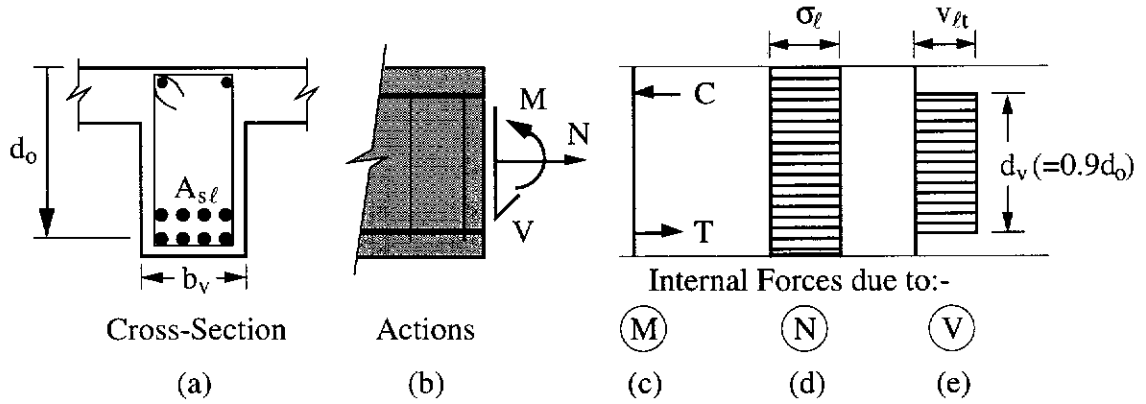
Figure 3.1   Segment of a Reinforced Concrete Beam

The resultant of the axial force is represented by a uniform stress σ_ℓ (Figure 3.1(d)). The shear force V is assumed to be uniformly distributed within a shear effective depth d_v taken equal to $0.9d_o$ (Figure 3.1(e)). This assumption implies that V is primarily resisted by the web of the cross-section. It satisfies the boundary conditions of zero shear stress at the top and bottom of the beam and is considered to be reasonable.

The shear response and the shear strength of a region of a beam can be evaluated by performing a stress analysis of a cracked concrete element within the depth d_v.

The cracked concrete element may be represented in the form of a truss comprising a concrete strut, tied together by reinforcing bars in the longitudinal and transverse directions as shown in Figure 3.2.

Unlike an element in a structural wall which usually contains uniform reinforcement (i.e., bars of the same diameter at equal spacing) in both longitudinal and transverse

50

directions, reinforcement in the web portion of a beam is discrete. Some intuition, therefore, is needed to visualise the truss model illustrated in Figure 3.2. It is assumed that the part of the longitudinal tensile steel not utilised to resist the bending moment, designated as $A_{s\ell V}$, is available to resist the shear force, i.e., $A_{s\ell V} = A_{s\ell} - A_{s\ell M}$. The vertical stirrups in the region of the beam constitute the transverse steel. Both these reinforcement are considered to be smeared in the web of the beam in order to perform the analysis of the truss. The reinforcement carry only axial stresses.
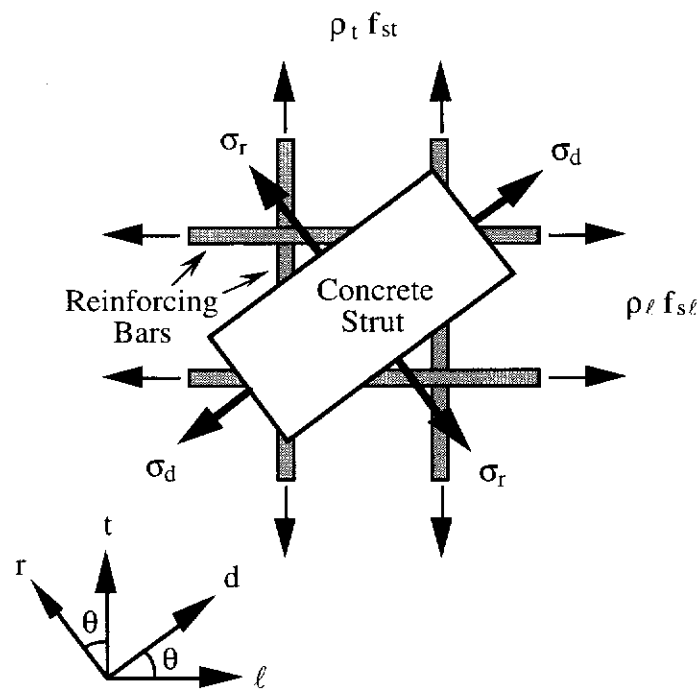
Figure 3.2   Reinforced Concrete Element for Stress Analysis

The "stress analysis" of the truss can proceed by considering equilibrium, strain compatibility and stress-strain relationships of concrete and steel.

3.2 Stress Analysis

3.2.1 Equilibrium

In the truss model (Figure 3.2), the concrete strut which is inclined at an angle θ to the longitudinal direction (i.e., ℓ-direction) develops a compressive stress σ_d along its axis (i.e., d-direction) and a tensile stress σ_r in the orthogonal direction (i.e., r-direction). Both σ_d and σ_r are taken as principal stresses. A convenient way to deal with these principal stresses is to transform them in the ℓ- and t-directions using a Mohr's stress circle. These may then be superposed on the stresses in the reinforcement as shown in Figure 3.3.
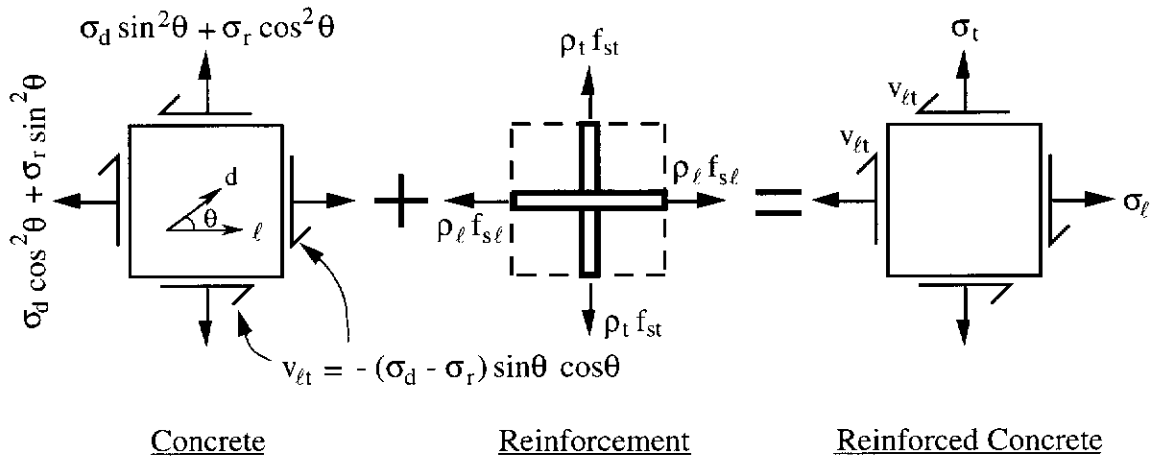
Figure 3.3   Superposition of Stresses

For equilibrium, the equations are:

$$\sigma_\ell = \sigma_d \cos^2\theta + \sigma_r \sin^2\theta + \rho_\ell f_{s\ell} \qquad (3.1)$$

$$\sigma_t = \sigma_d \sin^2\theta + \sigma_r \cos^2\theta + \rho_t f_{st} \qquad (3.2)$$

$$v_{\ell t} = -(\sigma_d - \sigma_r)\sin\theta \cos\theta \qquad (3.3)$$

where

σ_ℓ, σ_t = normal stresses in ℓ- and t-directions respectively and are positive for tension

$v_{\ell t}$ = average shear stress in the ℓ- and t-coordinate system, is positive as shown in Figure 3.3 and is taken as $\left(\dfrac{V}{b_v(0.9d_o)}\right)$

ρ_ℓ = $\left(\dfrac{A_{s\ell}V}{b_v(0.9d_o)}\right)$

ρ_t = $\left(\dfrac{A_{sv}}{b_v s}\right)$

A_{sv} = total area of all legs of vertical stirrup(s) across the width of a beam

s = spacing of stirrups along the longitudinal axis of a beam, and

$f_{s\ell}, f_{st}$ = stresses in longitudinal and transverse reinforcement respectively.

3.2.2 Strain Compatibility

The principal strain directions are assumed to coincide with the corresponding principal stress directions. The average strains in the ℓ- and t-directions may be related to principal strains by means of a Mohr's strain circle as follows:

$$\varepsilon_\ell = \varepsilon_d \cos^2\theta + \varepsilon_r \sin^2\theta \qquad (3.4)$$

$$\varepsilon_t = \varepsilon_d \sin^2\theta + \varepsilon_r \cos^2\theta \qquad (3.5)$$

$$\gamma_{\ell t} = -2 (\varepsilon_d - \varepsilon_r) \sin\theta \cos\theta \qquad (3.6)$$

where

$\varepsilon_\ell, \varepsilon_t$ = average strains in the element in ℓ- and t-directions respectively and are positive for tension

$\varepsilon_d, \varepsilon_r$ = average principal strains in the element in d- and r-directions respectively and are positive for tension, and

$\gamma_{\ell t}$ = average shear strain in the element in the ℓ- and t-coordinate system.

3.2.3 Stress-Strain Relationships of Concrete and Steel

3.2.3.1 Softened Concrete in Compression

The ascending and descending branches of the stress-strain curve for high strength concrete are steeper than those for normal strength concrete. A well-known stress-strain relationship with a pronounced post-peak decay which satisfactorily modelled high strength concrete was introduced by Thorenfeldt, Tomaszewicz and Jensen (1987). However, Vecchio and Collins (1993) recognised that the effective compressive strength of a strut in a reinforced concrete element was less than the uniaxial concrete compressive strength due to the presence of tensile strains in the perpendicular direction. This effect may be taken into account by means of a *softening factor*. Figure 3.4 shows a softened concrete compressive stress-strain curve, where ζ is the softening factor.
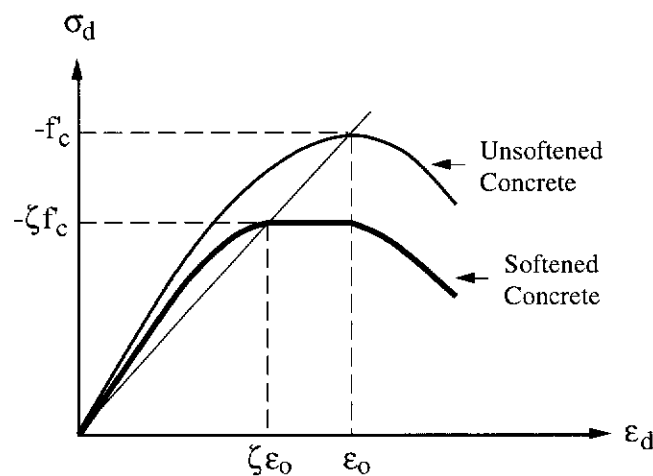
Figure 3.4   Softened Concrete in Compression

The stress-strain curve of softened concrete in compression may be described as follows:

- $\zeta \varepsilon_o \leq \varepsilon_d \leq 0$ (the initial part of the curve where both stress and strain softening are applied) -

$$\sigma_d = -\zeta f_c \left(\frac{\varepsilon_d}{\zeta \varepsilon_o}\right)\left(\frac{n'}{n' - 1 + \left(\frac{\varepsilon_d}{\zeta \varepsilon_o}\right)^{n'k'}}\right) \qquad (3.7a)$$

- $\varepsilon_o \leq \varepsilon_d < \zeta \varepsilon_o$ (the middle part where Vecchio and Collins (1993) proposed a flat region throughout this range of ε_d) -

$$\sigma_d = -\zeta f_c \qquad (3.7b)$$

- $\varepsilon_d < \varepsilon_o$ (the post-peak branch where only stress softening is applied) -

$$\sigma_d = -\zeta f_c \left(\frac{\varepsilon_d}{\varepsilon_o}\right)\left(\frac{n'}{n' - 1 + \left(\frac{\varepsilon_d}{\varepsilon_o}\right)^{n'k'}}\right) \qquad (3.7c)$$

where

f'_c = concrete compressive cylinder strength

n' = $0.8 + \dfrac{f_c}{17}$

k' = 1.0 when $\varepsilon_d/\varepsilon_o \leq 1.0$

    = $0.67 + \dfrac{f_c}{62}$ when $\varepsilon_d/\varepsilon_o > 1.0$, and

ε_o = $-\dfrac{f_c}{E_c}\left(\dfrac{n'}{n' - 1}\right).$

The modulus of elasticity of concrete E_c is taken as (Carrasquillo, Nilson and Slate (1981)):

$$E_c = 3320\sqrt{f'_c} + 6900 \qquad (3.7d)$$

Vecchio and Collins (1993) proposed a softening factor applicable to high strength concrete as well as normal strength concrete. Based on the results of 116 test specimens, the following softening factor was established:

$$\zeta \quad = \quad \frac{1}{1.0 + K_f K_c} \qquad\qquad (3.7e)$$

where

$$K_f \quad = \quad 0.1825 \sqrt{f'_c} \geq 1.0, \text{ and}$$

$$K_c \quad = \quad 0.35 \left(-\frac{\varepsilon_r}{\varepsilon_d} - 0.28 \right)^{0.8} \geq 1.0.$$

3.2.3.2 Concrete in Tension

The stress-strain relationship of concrete in tension is given by the following (Collins, Mitchell, Adebar and Vecchio (1996)):

- $\varepsilon_r < \varepsilon_{cr}$ (ascending branch) -

$$\sigma_r \quad = \quad E_c \varepsilon_r \qquad\qquad (3.8a)$$

- $\varepsilon_r \geq \varepsilon_{cr}$ (descending branch) -

$$\sigma_r \quad = \quad \frac{f_{cr}}{\left(1 + \sqrt{500\varepsilon_r} \right)} \qquad\qquad (3.8b)$$

where

ε_{cr} = concrete cracking strain = $\dfrac{f_{cr}}{E_c}$

f_{cr} = concrete cracking stress = $0.33 \sqrt{f'_c}$, and

E_c = modulus of elasticity of concrete as given in Equation 3.7d.

Figure 3.5 illustrates these equations.
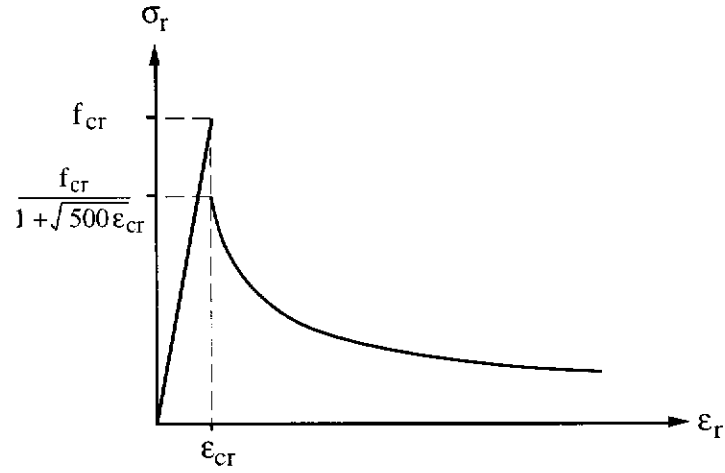
Figure 3.5   Concrete Tensile Stress-Strain Curve

3.2.3.3   Reinforcing Steel

In this study, the stress-strain relationships of longitudinal and transverse steel reinforcement are represented by elasto-plastic curves as follows:

$$f_{s\ell} = E_s \, \varepsilon_\ell \qquad \text{when } \varepsilon_\ell \leq f_{s\ell y}/E_s \qquad (3.9a)$$

$$= f_{s\ell y} \qquad \text{when } \varepsilon_\ell > f_{s\ell y}/E_s \qquad (3.9b)$$

$$f_{st} = E_s \, \varepsilon_t \qquad \text{when } \varepsilon_t \leq f_{sty}/E_s \qquad (3.10a)$$

$$= f_{sty} \qquad \text{when } \varepsilon_t > f_{sty}/E_s \qquad (3.10b)$$

where

$f_{s\ell y}$ =   yield stress of longitudinal steel

f_{sty} =   yield stress of transverse steel, and

E_s =   modulus of elasticity of steel taken as 200×10^3 MPa.

57

3.2.4 Solution

The stress analysis of the truss involves thirteen unknowns, viz., σ_ℓ, σ_t, σ_d, σ_r, $v_{\ell t}$, ε_ℓ, ε_t, ε_d, ε_r, $\gamma_{\ell t}$, θ, $f_{s\ell}$ and f_{st}. There are ten equations given by equilibrium, strain compatibility and stress-strain relationships of concrete and steel, i.e., Equations 3.1 to 3.10. Still three more equations are needed for a solution.

At a certain region of a beam the axial force N (see Figure 3.1) is known. Assuming that the force N produces a uniform stress on the beam cross-section, the intensity of this stress in the web of the beam in the ℓ-direction is equal to N/A_g, where A_g is the gross concrete area of the beam cross-section. This assumption is not entirely true as the stress distribution is non-uniform due to flexural cracks. However, this is only an estimate of the nominal average axial stress of the cross-section. For the case of a reinforced concrete beam, N/A_g will be zero and the accuracy of this assumption does not affect the stress analysis of the beam. Therefore,

$$\sigma_\ell = \frac{N}{A_g} \tag{3.11}$$

Note that N is positive when it is tension and negative when it is compression.

As the beam region is not subjected to any axial force in the transverse direction (see Figure 3.1), it is assumed that the resultant tensile stress in that direction is zero, i.e.,

$$\sigma_t = 0 \tag{3.12}$$

In order to trace the load-deformation response of the beam region in terms of $v_{\ell t}$ and $\gamma_{\ell t}$, the strain ε_d can be specified for each load stage. This condition and Equations 3.11 and 3.12 provide the additional three equations required to complete the stress analysis of the truss. However, the area of longitudinal tensile steel $A_{s\ell v}$ that resists the shear force must be defined.

As mentioned earlier,

$$A_{s\ell V} = A_{s\ell} - A_{s\ell M} \qquad (3.13)$$

where $A_{s\ell}$ is the total longitudinal steel in the tension zone and $A_{s\ell M}$ is that part of $A_{s\ell}$ required to resist the bending moment. Note that $A_{s\ell V}$ is always positive and taken as greater than zero. The value of $A_{s\ell M}$ may approximately be calculated by:

$$A_{s\ell M} \approx \frac{M}{(0.9d_o)\, f_{s\ell y}} \qquad (3.14)$$

where M is the bending moment co-existing with the shear force V (see Figure 3.1).

For a constant moment-to-shear ratio, the magnitudes of M and V, and hence the values of $A_{s\ell M}$ and $A_{s\ell V}$ vary for each stage of loading. This makes the calculation of $A_{s\ell V}$ extremely tedious. For simplicity, the value of $A_{s\ell M}$ is calculated at the load stage corresponding to the peak of the $v_{\ell t}$-$\gamma_{\ell t}$ curve, which represents the shear strength V_u of the region. Since V_u is unknown in the beginning, some iteration is required. Initially, a trial value of V_u is selected and $A_{s\ell V}$ is calculated by Equations 3.14 and 3.13 for a known value of M/V. The stress analysis of the truss is then performed to establish the peak of the $v_{\ell t}$-$\gamma_{\ell t}$ curve and hence V_u. Using this new value of V_u, $A_{s\ell V}$ is calculated by Equations 3.14 and 3.13 and the stress analysis is repeated. The entire process is continued until the trial value of V_u converges to the value obtained from the stress analysis of the truss. Calculations have shown that convergence usually occurs after five or six iterations.

3.3   Solution Algorithm

The solution process is simplified by combining and re-arranging some of the equations.

59

3.3.1 Longitudinal Strain ε_ℓ

Equation 3.1 is expressed as:

$$\sigma_\ell = \sigma_d\cos^2\theta + \sigma_r(1-\cos^2\theta) + \rho_\ell f_{s\ell} \qquad (3.15)$$

$$\text{or} \quad \cos^2\theta = \left(\frac{\sigma_\ell - \sigma_r - \rho_\ell f_{s\ell}}{\sigma_d - \sigma_r}\right) \qquad (3.16)$$

Similarly, Equation 3.4 is expressed as:

$$\varepsilon_\ell = \varepsilon_d\cos^2\theta + \varepsilon_r(1-\cos^2\theta) \qquad (3.17)$$

$$\text{or} \quad \cos^2\theta = \left(\frac{\varepsilon_\ell - \varepsilon_r}{\varepsilon_d - \varepsilon_r}\right) \qquad (3.18)$$

Combine Equations 3.16 and 3.18 to eliminate θ and obtain:

$$\left(\frac{\varepsilon_\ell - \varepsilon_r}{\varepsilon_d - \varepsilon_r}\right) = \left(\frac{\sigma_\ell - \sigma_r - \rho_\ell f_{s\ell}}{\sigma_d - \sigma_r}\right) \qquad (3.19)$$

The value of $f_{s\ell}$ in Equation 3.19 is given by Equation 3.9a or 3.9b.

When the smeared longitudinal steel has not reached yield,

$$f_{s\ell} = E_s \varepsilon_\ell \qquad (3.9a)$$

Substitution of Equation 3.9a in Equation 3.19 and re-arrangement gives:

$$\varepsilon_\ell = \frac{\varepsilon_r(\sigma_d-\sigma_r) + (\sigma_\ell - \sigma_r)(\varepsilon_d-\varepsilon_r)}{\sigma_d - \sigma_r + \rho_\ell E_s(\varepsilon_d-\varepsilon_r)} \quad \text{when } \varepsilon_\ell \le f_{s\ell y}/E_s \qquad (3.20)$$

When the smeared longitudinal steel has reached yield,

$$f_{s\ell} = f_{s\ell y} \qquad (3.9b)$$

Substitution of Equation 3.9b in Equation 3.19 and re-arrangement gives:

$$\varepsilon_\ell = \left(\frac{\sigma_\ell - \sigma_r - \rho_\ell f_{s\ell y}}{\sigma_d - \sigma_r}\right)(\varepsilon_d - \varepsilon_r) + \varepsilon_r \quad \text{when } \varepsilon_\ell > f_{s\ell y}/E_s \qquad (3.21)$$

3.3.2 Transverse Strain ε_t

Equation 3.2 is expressed as:

$$\sigma_t = \sigma_d \sin^2\theta + \sigma_r(1-\sin^2\theta) + \rho_t f_{st} \qquad (3.22)$$

or

$$\sin^2\theta = \left(\frac{\sigma_t - \sigma_r - \rho_t f_{st}}{\sigma_d - \sigma_r}\right) \qquad (3.23)$$

Similarly, Equation 3.5 is expressed as:

$$\varepsilon_t = \varepsilon_d \sin^2\theta + \varepsilon_r(1-\sin^2\theta) \qquad (3.24)$$

or

$$\sin^2\theta = \left(\frac{\varepsilon_t - \varepsilon_r}{\varepsilon_d - \varepsilon_r}\right) \qquad (3.25)$$

Combine Equations 3.23 and 3.25 to eliminate θ and substituting $\sigma_t = 0$ (Equation 3.12), the following equation is obtained:

$$\left(\frac{\varepsilon_t - \varepsilon_r}{\varepsilon_d - \varepsilon_r}\right) = \left(\frac{-\sigma_r - \rho_t f_{st}}{\sigma_d - \sigma_r}\right) \qquad (3.26)$$

The value of f_{st} in Equation 3.26 is given by Equation 3.10a or 3.10b.

When the transverse steel has not reached yield,

$$f_{st} = E_s \varepsilon_t \qquad (3.10a)$$

Substitution of Equation 3.10a in Equation 3.26 and re-arrangement gives:

$$\varepsilon_t = \frac{\varepsilon_r(\sigma_d-\sigma_r) - \sigma_r(\varepsilon_d-\varepsilon_r)}{\sigma_d - \sigma_r + \rho_t E_s(\varepsilon_d-\varepsilon_r)} \qquad \text{when } \varepsilon_t \leq f_{sty}/E_s \qquad (3.27)$$

When the transverse steel has reached yield,

$$f_{st} = f_{sty} \qquad (3.10b)$$

Substitution of Equation 3.10b in Equation 3.26 and re-arrangement gives:

$$\varepsilon_t = \left(\frac{-\sigma_r - \rho_t f_{sty}}{\sigma_d - \sigma_r}\right)(\varepsilon_d - \varepsilon_r) + \varepsilon_r \qquad \text{when } \varepsilon_t > f_{sty}/E_s \qquad (3.28)$$

61

3.3.3 Principal Concrete Tensile Strain ε_r

Combining Equations 3.4 and 3.5, the following equation is obtained:

$$\varepsilon_\ell + \varepsilon_t \;=\; \varepsilon_d + \varepsilon_r \tag{3.29}$$

or

$$\varepsilon_r \;=\; \varepsilon_\ell + \varepsilon_t - \varepsilon_d \tag{3.30}$$

3.3.4 Angle of Inclination of the Concrete Compressive Strut θ

From Equations 3.18 and 3.25,

$$\tan^2\theta \;=\; \left(\frac{\varepsilon_t - \varepsilon_r}{\varepsilon_\ell - \varepsilon_r}\right) \tag{3.31}$$

Equation 3.29 may be written as:

$$\varepsilon_t - \varepsilon_r \;=\; \varepsilon_d - \varepsilon_\ell \tag{3.32}$$

$$\varepsilon_\ell - \varepsilon_r \;=\; \varepsilon_d - \varepsilon_t \tag{3.33}$$

Substitution of Equations 3.32 and 3.33 in Equation 3.31 and re-arrangement gives:

$$\theta \;=\; \tan^{-1}\left(\sqrt{\frac{\varepsilon_\ell - \varepsilon_d}{\varepsilon_t - \varepsilon_d}}\right) \tag{3.34}$$

3.3.5 Calculation Steps

For a given beam, the calculation steps are as follows:

Step 1:   Input beam data, including geometrical, sectional and material properties, and the M/V ratio.

Step 2:   Assume a value of V_u.

Step 3:   Select a value of ε_d.

Step 4:   Assume a value of ε_r.

Step 5:   Determine σ_ℓ by Equation 3.11.

Step 6:   Calculate σ_d by Equation 3.7.

Step 7:   Calculate σ_r by Equation 3.8.

Step 8:   Take $M = V_u(M/V)$ and calculate $A_{s\ell M}$ and $A_{s\ell V}$ by Equations 3.14 and 3.13 respectively. Use $A_{s\ell V}$ to calculate ρ_ℓ.

Step 9:   Calculate ε_ℓ by Equation 3.20 or 3.21.

Step 10:   Calculate ε_t by Equation 3.27 or 3.28.

Step 11:   Calculate ε_r by Equation 3.30. Compare the calculated ε_r value with the assumed value in *Step 4*. If there is convergence, proceed to *Step 12*; otherwise, return to *Step 4* and iterate.

Step 12:   Calculate θ by Equation 3.34. Hence, calculate $v_{\ell t}$ and $\gamma_{\ell t}$ by Equations 3.3 and 3.6 respectively. Calculate $V = v_{\ell t}(b_v d_v)$.

Step 13:   Repeat *Steps 3* to *12* for other values of ε_d in the range of $-0.0035 < \varepsilon_d < 0$. Plot the $v_{\ell t}$-$\gamma_{\ell t}$ (or V-$\gamma_{\ell t}$) curve. The peak of this curve gives the ultimate shear strength V_u.

Step 14:   Compare the calculated V_u value in *Step 13* with the assumed value in *Step 2*. If there is convergence, the solution is accepted; otherwise, return to *Step 2* and iterate.

3.4   Example

The solution algorithm is illustrated below for the beam S1-1 tested in this study.

Step 1: Input Beam Data

The beam cross-section is shown in Figure 3.6.
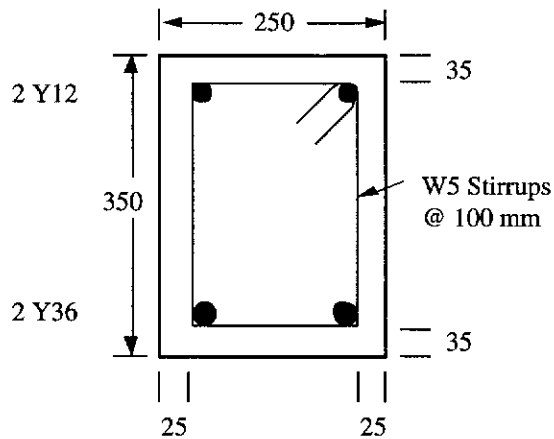
Figure 3.6   Cross-Section of Beam S1-1

The following data apply:

$$f'_c \quad = \quad 63.6 \text{ MPa}$$

$$A_{sv} \quad = \quad 2\left(\frac{\pi \times 5^2}{4}\right) \quad = \quad 39.2 \text{ mm}^2$$

$$\rho_t \quad = \quad \frac{A_{sv}}{b_v s} \quad = \quad \frac{39.2}{250 \times 100} \quad = \quad 1.57\text{x}10^{-3}$$

$$f_{sty} \quad = \quad 569 \text{ MPa}$$

$$E_s \quad = \quad 200\text{x}10^3 \text{ MPa}$$

$$b_v \quad = \quad 250 \text{ mm}$$

$$D \quad = \quad 350 \text{ mm}$$

$$d_o \quad = \quad 292 \text{ mm}$$

$$d_v \quad = \quad 0.9 d_o \quad = \quad 262.8 \text{ mm}$$

$$N \quad = \quad 0$$

$$A_{s\ell} \quad = \quad 2046 \text{ mm}^2$$

$$f_{s\ell y} \quad = \quad 452 \text{ MPa}$$

The beam was subjected to two equal concentrated loads placed symmetrically on the span. The shear span was 730 mm. For the calculation of shear strength, the critical section is assumed to be at a distance d_o from the concentrated load. Therefore, the M/V ratio is taken as $(a-d_o) = (730-292) = 438$ mm.

Step 2:   Assume V_u

After several cycles of iteration, take:

$$V_u \quad = \quad 237.9 \text{ kN}$$

The selection of V_u actually occurs after performing an initial stress analysis where ε_d is varied from 0 to -0.0035. The approximate peak shear force from this preliminary analysis is then taken as the initial guess of V_u for the refined iterative solution given in this example. Otherwise, an initial value can be estimated using the AS 3600 method (Equation 2.7), but assuming a 45° truss.

Step 3: Select ε_d

The value of ε_d selected for this example is the strain at the peak shear capacity V_u:

$$\varepsilon_d \quad = \quad -1.024 \times 10^{-3}$$

A reasonable starting value for ε_d is -1.0×10^{-5}.

Step 4: Assume ε_r

After several cycles of iteration, take:

$$\varepsilon_r \quad = \quad 21.06 \times 10^{-3}$$

A reasonable starting value for ε_r is 1.0×10^{-5}. As ε_d varies from 0 to -0.0035, the first guess of ε_r for the next ε_d value is taken from the previous solution for ε_d.

Step 5: Determine σ_ℓ

Because $N = 0$, $\sigma_\ell = 0$.

Step 6: Calculate σ_d

$$n' \quad = \quad 0.8 + \frac{63.6}{17} \quad = \quad 4.541$$

Eq. 3.7d: $\quad E_c \quad = \quad 3320\sqrt{63.6} + 6900 = 33.38 \times 10^3 \text{ MPa}$

$$\varepsilon_o \quad = \quad -\frac{63.6}{33.38 \times 10^3}\left(\frac{4.541}{4.541 - 1}\right) \quad = \quad -2.444 \times 10^{-3}$$

$$K_f \quad = \quad 0.1825\sqrt{63.6} \quad = \quad 1.455 \ (> 1.0)$$

$$K_c \quad = \quad 0.35\left(\frac{21.06 \times 10^{-3}}{1.024 \times 10^{-3}} - 0.28\right)^{0.8} \quad = \quad 3.889 \ (> 1.0)$$

Eq. 3.7e: $\quad \zeta \quad = \quad \frac{1}{1.0 + 1.455 \times 3.889} \quad = \quad 0.1502$

$$\zeta \varepsilon_o \quad = \quad 0.1502 \times -2.444 \times 10^{-3} = -0.3671 \times 10^{-3} \ (\varepsilon_o < \varepsilon_d < \zeta \varepsilon_o)$$

Eq. 3.7b: $\quad \sigma_d \quad = \quad -0.1502 \times 63.6 \quad = \quad -9.553 \text{ MPa}$

65

Step 7: *Calculate* σ_r

$$f_{cr} = 0.33\sqrt{63.6} = 2.632 \text{ MPa}$$

$$\varepsilon_{cr} = \frac{2.632}{33.38 \times 10^3} = 0.079 \times 10^{-3}$$

Since $\varepsilon_r > \varepsilon_{cr}$, the following applies:

Eq. 3.8b: $\qquad \sigma_r = \dfrac{2.632}{\left(1 + \sqrt{500 \times 21.06 \times 10^{-3}}\right)} = 0.620 \text{ MPa}$

Step 8: *Calculate* $A_{s\ell M}$, $A_{s\ell V}$ *and* ρ_ℓ

$$M = V_u(M/V) = 237.9 \times 10^3 \times 438.0 \text{ Nmm}$$

Eq. 3.14: $\qquad A_{s\ell M} = \dfrac{237900 \times 438.0}{262.8 \times 452.0} = 877.2 \text{ mm}^2$

Eq. 3.13: $\qquad A_{s\ell V} = 2046.0 - 877.2 = 1168.8 \text{ mm}^2$

Therefore,

$$\rho_\ell = \left(\frac{A_{s\ell V}}{b_v d_v}\right) = \left(\frac{1168.8}{250 \times 262.8}\right) = 1.779 \times 10^{-2}$$

Step 9: *Calculate* ε_ℓ

Assume $\varepsilon_\ell \leq f_{s\ell y}/E_s$:

Eq. 3.20: $\quad \varepsilon_\ell = \dfrac{21.06 \times 10^{-3}(-9.553-0.620) + (0.0-0.620)(-1.024 \times 10^{-3}-21.06 \times 10^{-3})}{-9.553 - 0.620 + 1.779 \times 10^{-2} \times 200 \times 10^3(-1.024 \times 10^{-3}-21.06 \times 10^{-3})}$

$$= 2.260 \times 10^{-3}$$

$$f_{s\ell y}/E_s = 452/200 \times 10^3 = 2.260 \times 10^{-3}$$

Since $\varepsilon_\ell = f_{s\ell y}/E_s$, $A_{s\ell V}$ just yields and the assumption is satisfactory.

Step 10: *Calculate* ε_t

Assume $\varepsilon_t > f_{sty}/E_s$:

Eq. 3.28: $\quad \varepsilon_t = \left(\dfrac{-0.620-1.57 \times 10^{-3} \times 569}{-9.553 - 0.620}\right)(-1.024 \times 10^{-3}-21.06 \times 10^{-3}) + 21.06 \times 10^{-3}$

$$= 17.77 \times 10^{-3}$$

$$f_{sty}/E_s = 569/200 \times 10^3 = 2.845 \times 10^{-3}$$

Since $\varepsilon_t > f_{sty}/E_s$, the assumption is satisfactory.

Step 11: Calculate ε_r

The principal concrete tensile strain is calculated as:

Eq. 3.30: ε_r = $2.260 \times 10^{-3} + 17.77 \times 10^{-3} + 1.024 \times 10^{-3}$

  = 21.05×10^{-3}

This value of ε_r is close enough to the assumed value in *Step 4*. Therefore, accept the value.

Step 12: Calculate θ, $v_{\ell t}$, $\gamma_{\ell t}$ and V

The remaining quantities are calculated as follows:

Eq. 3.34: θ = $\tan^{-1}\left(\sqrt{\dfrac{2.260 \times 10^{-3} + 1.024 \times 10^{-3}}{1.777 \times 10^{-2} + 1.024 \times 10^{-3}}}\right) = 22.69°$

Eq. 3.3: $v_{\ell t}$ = $-(-9.553 - 0.620) \sin 22.69° \cos 22.69° = 3.6204$ MPa

Eq. 3.6: $\gamma_{\ell t}$ = $-2(-1.024 \times 10^{-3} - 21.06 \times 10^{-3}) \sin 22.69° \cos 22.69°$

  = 15.72×10^{-3}

Therefore,

  V = $v_{\ell t}(b_v d_v)$ = $3.6204 \times 250 \times 262.8$ = 237.9×10^3 N

  = 237.9 kN

Step 13: Other Values of ε_d

Repeat calculations for other values of ε_d. The results are plotted in Figure 3.7.
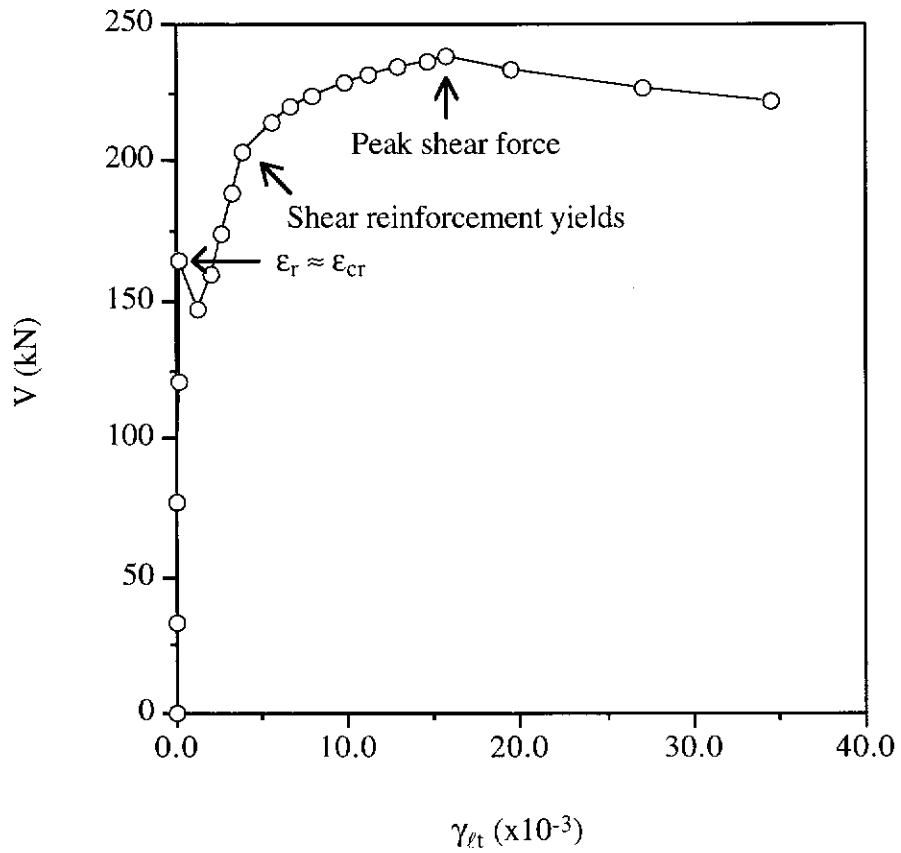
Figure 3.7 Predicted Response of Beam S1-1

Step 14: Check V_u

The peak of the V-$\gamma_{\ell t}$ curve is 237.9 kN, which is the calculated V_u. This value agrees with the V_u value assumed in *Step 2*. Therefore, the solution is acceptable.

Manufacture And Testing Of HPC Beams

4.1   Introduction

This chapter describes the experimental work. Details of the test beams, the materials and equipment used and the manufacture of these beams are elaborated. The test set-up, the instrumentation and the testing procedure are also presented.

The test program was established to study the behaviour of reinforced HPC beams subjected to combined bending moment and shear force. The following is a list of beam series and the parameter that varied within each series. Most beams were loaded by two point loads placed symmetrically on the span.

(i)   Series 1 - concrete cover to shear reinforcement cage.

(ii)   Series 2 - amount of shear reinforcement.

(iii)   Series 3 - amount of longitudinal reinforcement.

(iv)   Series 4 - overall beam depth.

(v)   Series 5 - shear span-to-depth ratio.

(vi)   Series 6 - same as Series 3 but with four point loads.

(vii)   Series 7 - single point load at midspan with stirrups at various spacings.

(viii)   Series 8 - similar to Series 2.

4.2 Test Specimens

Six beams were manufactured and tested in each series. All beams were rectangular in cross-section, with a constant width of 250 mm.

4.2.1 Beam Details

The cross-sections of beams are shown in Figures 4.1(a) to 4.1(f). Complete details are given in Tables 4.1 and 4.2. The longitudinal bars were provided with 90° cogs at each end as shown in Figure 4.2. The two-legged vertical stirrups were anchored in the compression zone by 135° hooks (Figures 4.1(a)-4.1(f)).

4.2.2 Concrete

The concrete was supplied by a ready-mix plant in Perth, Western Australia. Three grades of HPC mixes were used, S65, S80 and S100, with nominal 28-day compressive strengths of 65, 80 and 100 MPa respectively. The mixes contained about 5% silica fume. Superplasticiser was included to increase the workability of the mixes. The maximum size of aggregate was 7 mm. Slump of 150 mm was prescribed for all the mixes. Other details of the mixes were not released by the supplier.

In each beam series, 100 x 200 mm cylinders were tested in compression at various ages and at the time of beam test. At early ages, two or three cylinders were tested each time. During the period of beam test, which lasted up to four days, five to nine cylinders were tested. The results of the concrete compressive strength tests are given in Table 4.3. The compressive strength development of concrete for each beam series is shown in Figure 4.3.

70
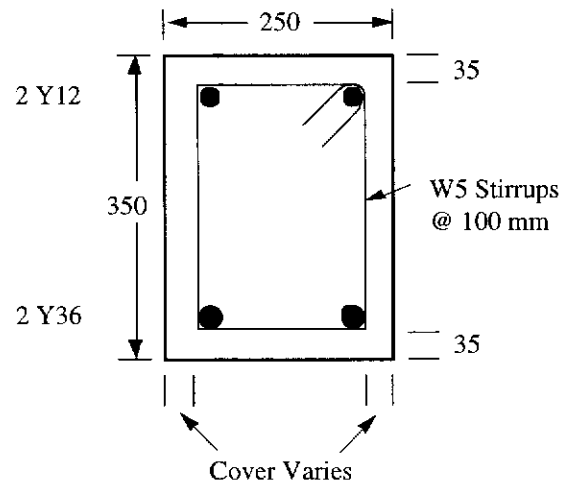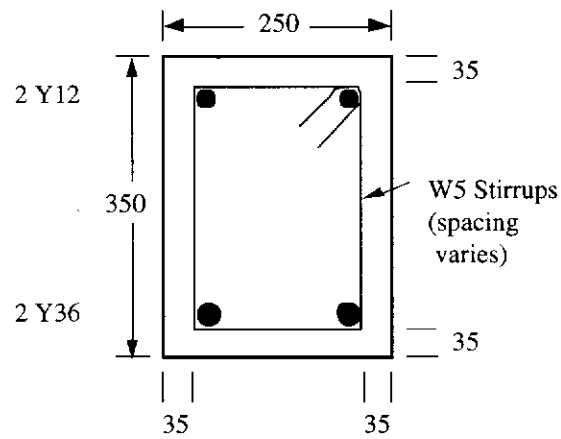
(a) Series 1

(b) Series 2 and 8

Note: All dimensions are in millimetres.

Figure 4.1 Beam Cross-Sections

71
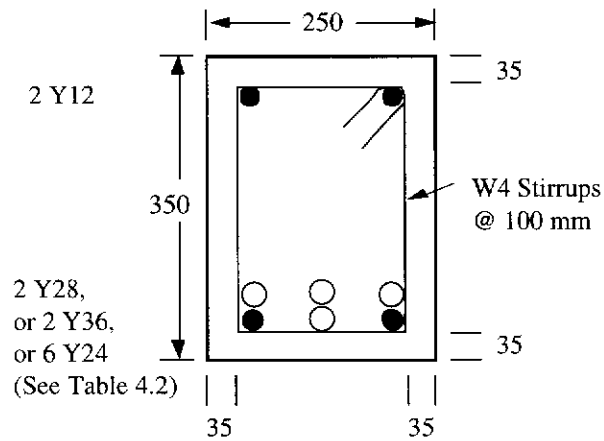
(c) Series 3 and 6
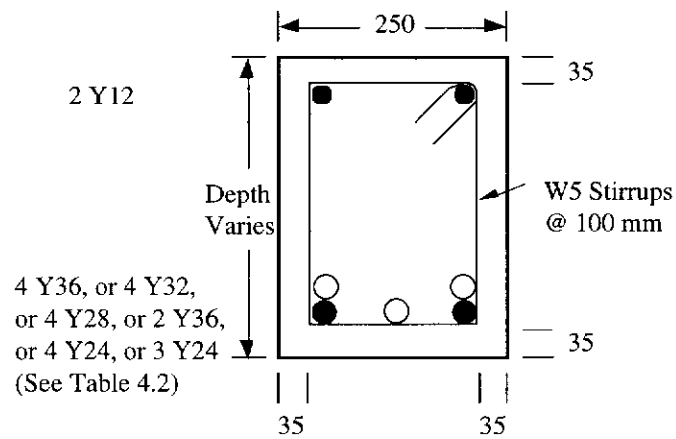
(d) Series 4

Note: All dimensions are in millimetres.

Figure 4.1 Beam Cross-Sections (*Continued*)
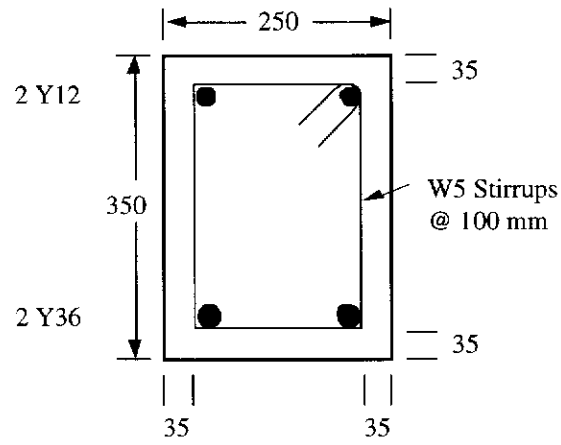
(e) Series 5
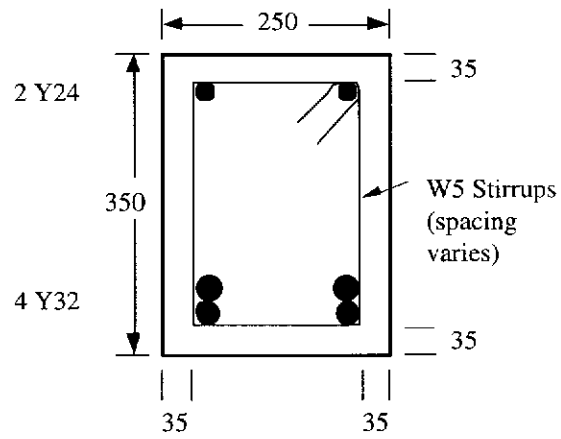
(f) Series 7

Note: All dimensions are in millimetres.

Figure 4.1 Beam Cross-Sections (*Continued*)

Table 4.1 Beam Details

Beam Mark	D (mm)	d (mm)	d_o (mm)	Total Length (mm)	Span L_e (mm)	Over-hang (mm)	a (mm)	a/d_o	Concrete Cover (mm) top	bottom	sides
S1-1	350	292	292	2700	1960	370	730	2.50	35	35	25
S1-2	350	292	292	2700	1960	370	730	2.50	35	35	25
S1-3	350	292	292	2700	1960	370	730	2.50	35	35	35
S1-4	350	292	292	2700	1960	370	730	2.50	35	35	35
S1-5	350	292	292	2700	1960	370	730	2.50	35	35	50
S1-6	350	292	292	2700	1960	370	730	2.50	35	35	50
S2-1	350	292	292	2700	1960	370	730	2.50	35	35	35
S2-2	350	292	292	2700	1960	370	730	2.50	35	35	35
S2-3	350	292	292	2700	1960	370	730	2.50	35	35	35
S2-4	350	292	292	2700	1960	370	730	2.50	35	35	35
S2-5	350	292	292	2700	1960	370	730	2.50	35	35	35
S2-6	350	292	292	2700	1960	370	730	2.50	35	35	35
S3-1	350	297	297	2700	1980	360	740	2.49	35	35	35
S3-2	350	297	297	2700	1980	360	740	2.49	35	35	35
S3-3	350	293	293	2700	1960	370	730	2.49	35	35	35
S3-4	350	293	293	2700	1960	370	730	2.49	35	35	35
S3-5	350	287	299	2700	1940	380	720	2.41	35	35	35
S3-6	350	287	299	2700	1940	380	720	2.41	35	35	35
S4-1	600	524	542	3800	3100	350	1300	2.40	35	35	35
S4-2	500	428	444	3800	2640	580	1070	2.41	35	35	35
S4-3	400	332	346	2900	2160	370	830	2.40	35	35	35
S4-4	350	292	292	2900	1960	470	730	2.50	35	35	35
S4-5	300	236	248	2400	1680	360	590	2.38	35	35	35
S4-6	250	198	198	2400	1500	450	500	2.53	35	35	35
S5-1	350	292	292	2900	2260	320	880	3.01	35	35	35
S5-2	350	292	292	2900	2100	400	800	2.74	35	35	35
S5-3	350	292	292	2700	1960	370	730	2.50	35	35	35
S5-4	350	292	292	2400	1660	370	580	1.99	35	35	35
S5-5	350	292	292	2400	1520	440	510	1.75	35	35	35
S5-6	350	292	292	2100	1380	360	440	1.51	35	35	35
S6-1	350	297	297	2700	1980	360	810	2.73	35	35	35
S6-2	350	297	297	2700	1980	360	810	2.73	35	35	35
S6-3	350	293	293	2700	1960	370	800	2.73	35	35	35
S6-4	350	293	293	2700	1960	370	800	2.73	35	35	35
S6-5	350	287	299	2700	1940	380	790	2.64	35	35	35
S6-6	350	287	299	2700	1940	380	790	2.64	35	35	35
S7-1	350	278	294	2700	1940	380	970	3.30	35	35	35
S7-2	350	278	294	2700	1940	380	970	3.30	35	35	35
S7-3	350	278	294	2700	1940	380	970	3.30	35	35	35
S7-4	350	278	294	2700	1940	380	970	3.30	35	35	35
S7-5	350	278	294	2700	1940	380	970	3.30	35	35	35
S7-6	350	278	294	2700	1940	380	970	3.30	35	35	35
S8-1	350	292	292	2700	1960	370	730	2.50	35	35	35
S8-2	350	292	292	2700	1960	370	730	2.50	35	35	35
S8-3	350	292	292	2700	1960	370	730	2.50	35	35	35
S8-4	350	292	292	2700	1960	370	730	2.50	35	35	35
S8-5	350	292	292	2700	1960	370	730	2.50	35	35	35
S8-6	350	292	292	2700	1960	370	730	2.50	35	35	35

Note: For all beams, width b_v = 250 mm.

For meaning of symbols, see Notation.

Table 4.2 Reinforcement Details

Beam Mark	Shear Reinforcement				Longitudinal Reinforcement		
	Diameter (mm)	Spacing, s (mm)	ρ_t	f_{sty} (MPa)	Top Steel	Bottom Steel	f_{sty} (MPa) (Bottom Steel)
S1-1	5	100	0.00157	569	2Y12	2Y36	452
S1-2	5	100	0.00157	569	2Y12	2Y36	452
S1-3	5	100	0.00157	569	2Y12	2Y36	452
S1-4	5	100	0.00157	569	2Y12	2Y36	452
S1-5	5	100	0.00157	569	2Y12	2Y36	452
S1-6	5	100	0.00157	569	2Y12	2Y36	452
S2-1	5	150	0.00105	569	2Y12	2Y36	452
S2-2	5	125	0.00126	569	2Y12	2Y36	452
S2-3	5	100	0.00157	569	2Y12	2Y36	452
S2-4	5	100	0.00157	569	2Y12	2Y36	452
S2-5	5	75	0.00209	569	2Y12	2Y36	452
S2-6	5	60	0.00262	569	2Y12	2Y36	452
S3-1	4	100	0.00101	632	2Y12	2Y28	450
S3-2	4	100	0.00101	632	2Y12	2Y28	450
S3-3	4	100	0.00101	632	2Y12	2Y36	452
S3-4	4	100	0.00101	632	2Y12	2Y36	452
S3-5	4	100	0.00101	632	2Y12	*6Y24*	442
S3-6	4	100	0.00101	632	2Y12	*6Y24*	442
S4-1	5	100	0.00157	569	2Y12	*4Y36*	452
S4-2	5	100	0.00157	569	2Y12	*4Y32*	433
S4-3	5	100	0.00157	569	2Y12	*4Y28*	450
S4-4	5	100	0.00157	569	2Y12	2Y36	452
S4-5	5	100	0.00157	569	2Y12	*4Y24*	442
S4-6	5	100	0.00157	569	2Y12	3Y24	442
S5-1	5	100	0.00157	569	2Y12	2Y36	452
S5-2	5	100	0.00157	569	2Y12	2Y36	452
S5-3	5	100	0.00157	569	2Y12	2Y36	452
S5-4	5	100	0.00157	569	2Y12	2Y36	452
S5-5	5	100	0.00157	569	2Y12	2Y36	452
S5-6	5	100	0.00157	569	2Y12	2Y36	452
S6-1	4	100	0.00101	632	2Y12	2Y28	450
S6-2	4	100	0.00101	632	2Y12	2Y28	450
S6-3	4	100	0.00101	632	2Y12	2Y36	452
S6-4	4	100	0.00101	632	2Y12	2Y36	452
S6-5	4	100	0.00101	632	2Y12	*6Y24*	442
S6-6	4	100	0.00101	632	2Y12	*6Y24*	442
S7-1	5	150	0.00105	569	2Y24	*4Y32*	433
S7-2	5	125	0.00126	569	2Y24	*4Y32*	433
S7-3	5	100	0.00157	569	2Y24	*4Y32*	433
S7-4	5	80	0.00196	569	2Y24	*4Y32*	433
S7-5	5	70	0.00224	569	2Y24	*4Y32*	433
S7-6	5	60	0.00262	569	2Y24	*4Y32*	433
S8-1	5	150	0.00105	569	2Y12	2Y36	452
S8-2	5	125	0.00126	569	2Y12	2Y36	452
S8-3	5	100	0.00157	569	2Y12	2Y36	452
S8-4	5	100	0.00157	569	2Y12	2Y36	452
S8-5	5	80	0.00196	569	2Y12	2Y36	452
S8-6	5	70	0.00224	569	2Y12	2Y36	452

Note: The longitudinal tensile reinforcement shown in *italics* in Table 4.2 indicate bundled bars (see Figure 4.1).

r = 5 d_b

100

overhang
(See Table 4.1)

Support Bearing Plate
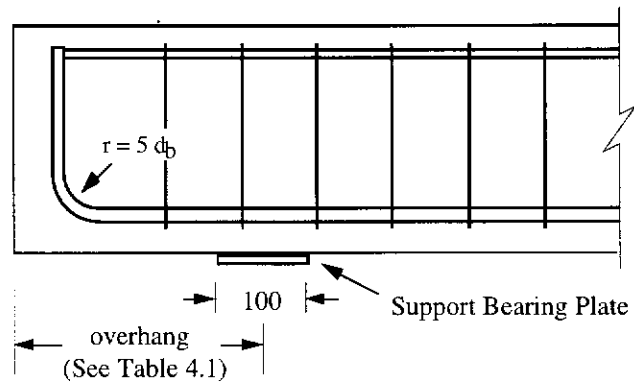
Figure 4.2 Anchorage of Longitudinal Tensile Bars

Table 4.3 Concrete Compressive Strength

Beam Series	Age (days) Early Age	Age (days) Beam Test Period	Cylinder No. (MPa) 1	2	3	4	5	6	Average Strength (MPa)	Average Strength at the time of Beam Test (MPa)
1	7		44.6	44.2	48.7				45.8	
	14		60.5	57.2					58.9	
	36		65.2	61.1					63.2	
		47	64.2	62.3					63.2	
		50	60.7	63.9	66.7				63.8	**63.6**
2	7		54.1	52.5	56.0				54.2	
	14		59.6	65.3	60.1				61.7	
		28	74.5	74.0	68.7				72.4	
		29	68.6	73.9	73.6				72.0	
		31	72.7	74.0					73.4	**72.5**
3	7		49.8	48.8	48.6				49.1	
	15		61.2	55.1	62.4				59.6	
		27	70.7	66.8					68.8	
		28	72.2	64.8	64.7	64.7	67.7	67.9	67.0	**67.4**
4	7		58.2	56.6	61.7				58.8	
	14		76.9	77.5	82.0				78.8	
		28	88.1	85.1	85.5	88.9	86.0	87.8	86.9	
		29	87.7	90.1	86.3				88.0	**87.3**
5	7		59.2	67.4	61.1				62.6	
	14		64.3	65.3	59.9				63.2	
	26		79.5	81.4	81.2				80.7	
		48	86.6	87.9	90.9				88.5	
		50	91.7	87.4	91.6				90.2	**89.4**
6	9		53.2	58.0	53.3				54.8	
	15		60.5	65.6	63.6				63.2	
		28	71.2	68.3					69.8	
		29	67.4	66.4	67.2				67.0	
		30	70.3	71.7	69.6	68.1			69.9	**68.9**
7	7		52.4	53.0	51.0				52.1	
	13		64.5	62.8	63.9				63.7	
		27	74.6	75.5					75.0	
		28	74.2	73.0	73.3				73.5	
		29	75.9	77.3					76.6	**74.8**
8	7		46.9	50.2	49.4				48.8	
	14		64.3	65.3	59.9				63.2	
		27	75.2	73.1	72.2				73.5	
		28	75.5	74.6	75.5	75.8			75.4	**74.6**

76
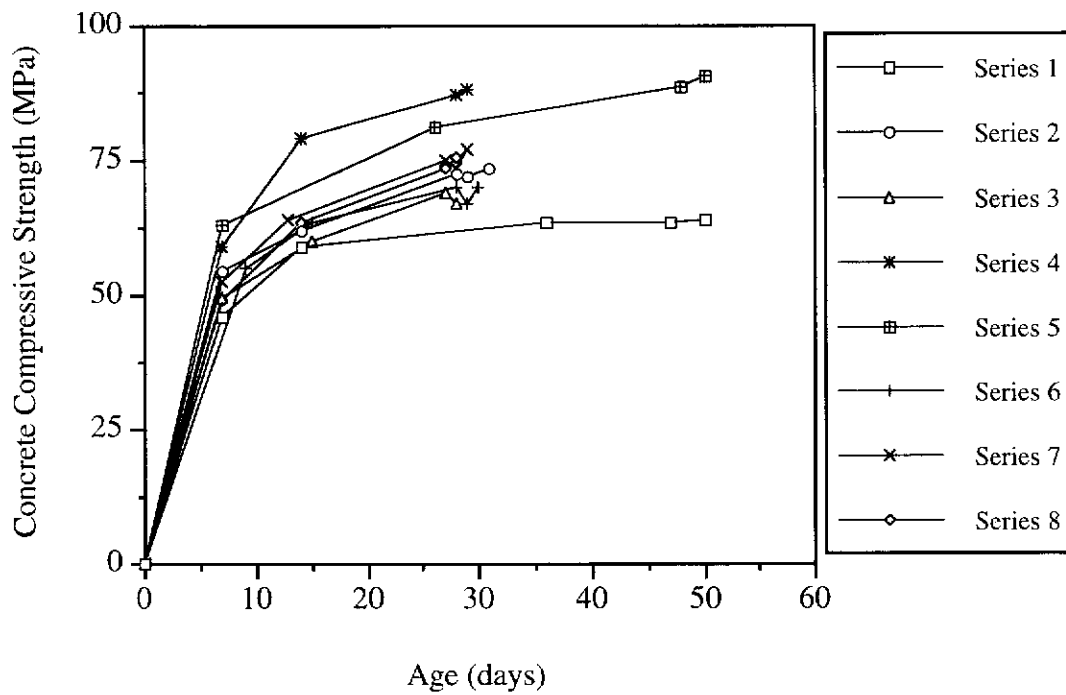
Figure 4.3 Concrete Compressive Strength Development

Splitting tensile tests were carried out on 150 x 300 mm cylinders. These cylinders were tested at the time of beam test. The results are given in Table 4.4. No tensile tests were done for Series 1.

Table 4.4 Concrete Tensile Strength (Split Cylinder Test)

Beam Series	Age (days)	Cylinder No. (MPa)			Average Strength (MPa)
		1	2	3	
2	28	3.79	3.91	3.13	**3.61**
3	28	3.91	3.49	3.51	**3.64**
4	28	4.48	3.95	3.95	**4.13**
5	48	4.63	5.85	5.51	**5.33**
6	28	3.77	3.55	3.53	**3.62**
7	28	4.13	4.07	4.06	**4.09**
8	28	3.63	4.01	3.65	**3.76**

Compression tests were also carried out on two 100 x 200 mm cylinders in each series to determine the modulus of elasticity of concrete. The modulus of elasticity was taken as the secant modulus measured at 45% of the compressive strength of the cylinder. The results of these tests are given in Table 4.5.

Table 4.5   Modulus of Elasticity of Concrete

Beam Series	Age (days)	Cylinder No. ($\times 10^3$ MPa)		Average Modulus of Elasticity ($\times 10^3$ MPa)
		1	2	
1	47	30.2	31.9	**31.0**
2	28	31.4	31.4	**31.4**
3	28	29.5	30.0	**29.8**
4	28	32.5	33.4	**33.0**
5	48	33.9	32.8	**33.4**
6	28	30.7	30.9	**30.8**
7	28	32.6	33.6	**33.1**
8	28	29.3	29.2	**29.2**

4.2.3   Longitudinal Reinforcement

All beams were provided with both top and bottom longitudinal bars (Figure 4.1). All bars were deformed bars (designated as Y-bars) used in the Australian practice. Y12 bars were used as top steel in all beams except for the beams in Series 7, where larger Y24 bars were used. For bottom steel, Y24, Y28, Y32 and Y36 bars were used.

Large amount of longitudinal reinforcement was necessary to ensure shear failure in the beams instead of flexural failure. In some cases, the bottom bars were bundled (Figures 4.1 and 4.4). No space was allowed between the bundled bars. The bundling of bars did not entail anchorage or bond failure in any of the beams.

Tensile tests were performed on samples of bars. The stress-strain curves for the bars are shown in Figure 4.5 and the tensile test results are given in Table 4.6.
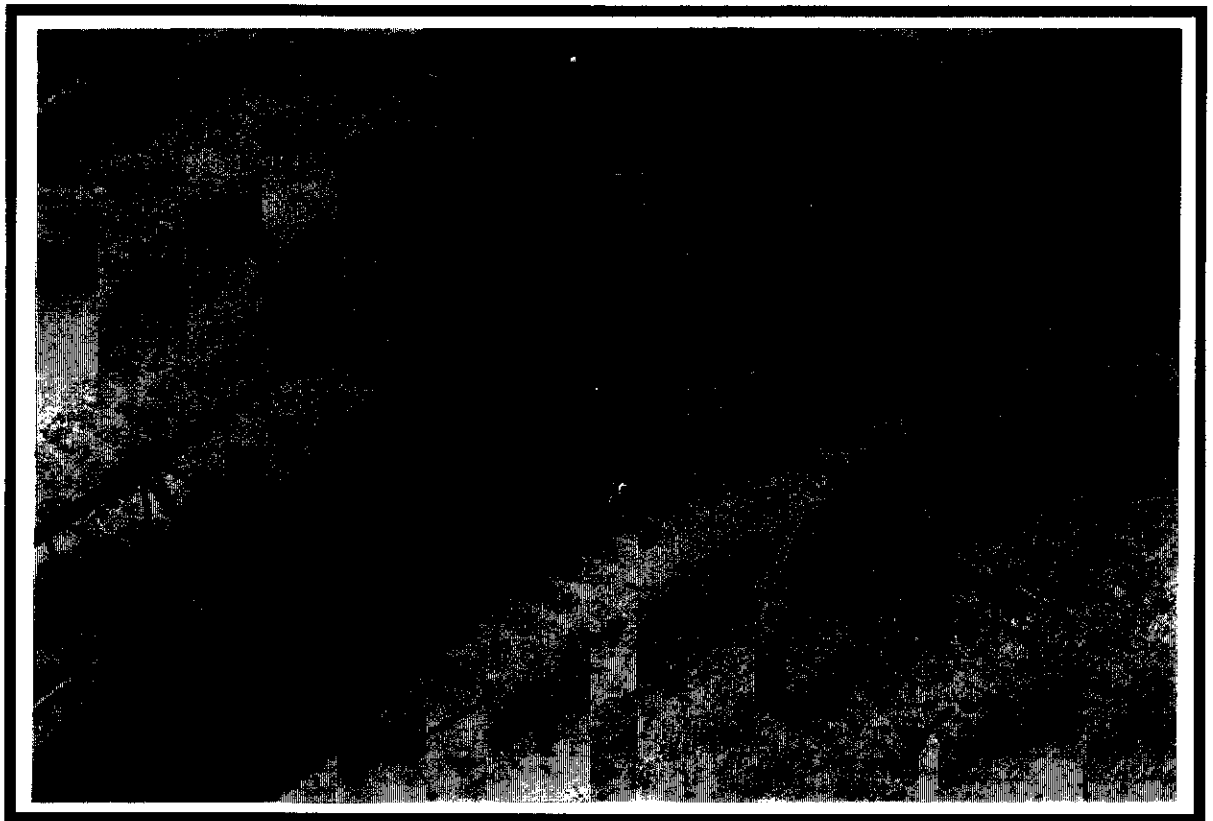
Figure 4.4   Steel Cage with Bundled Bars (Series 3)
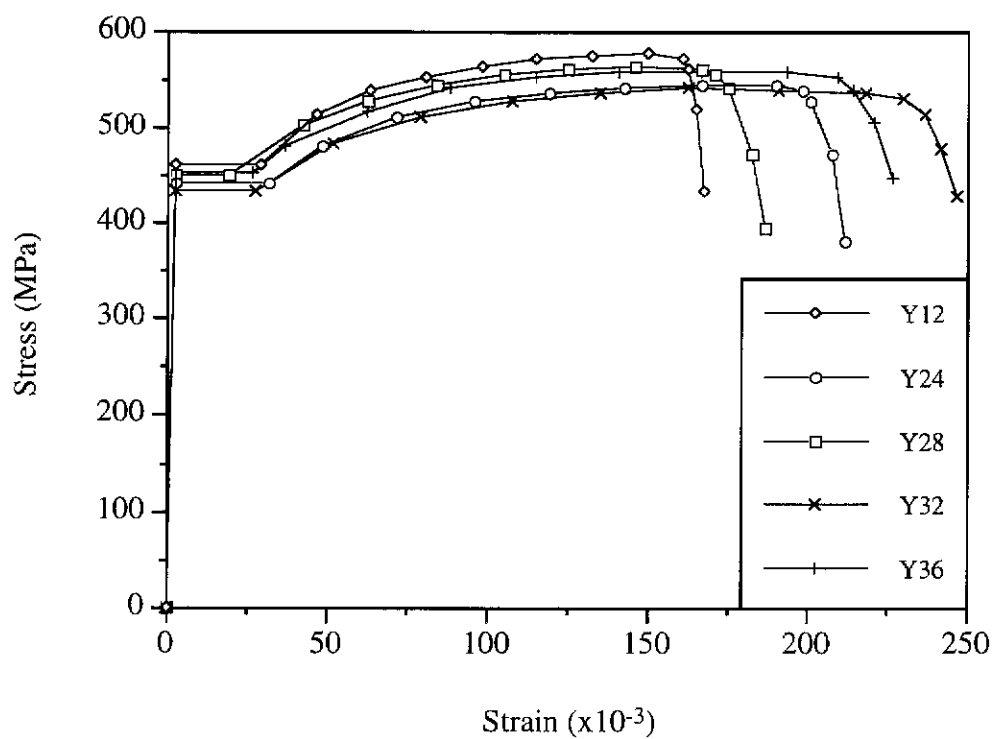
Figure 4.5   Stress-Strain Curves of Longitudinal Reinforcement

Table 4.6   Tensile Test Results of Longitudinal Reinforcement

Bar Mark	Y12	Y24	Y28	Y32	Y36
Cross-Sectional Area (mm^2)	112	460	616	821	1023
Yield Strength (MPa)	462	442	450	433	452
Ultimate Strength (MPa)	577	544	562	541	559

4.2.4   Transverse Reinforcement

For shear reinforcement, 4 and 5 mm diameter smooth hard-drawn high tensile wires (designated as W4 and W5) were used. The stirrups were vertical rectangular closed ties with 135° hooks for good anchorage.

For the beams in Series 1, 2, 4, 5, 7 and 8, W5 was used as shear reinforcement and for the beams in Series 3 and 6, W4 was used.

Tensile tests were carried out on samples of W4 and W5 wires. The stress-strain curves are shown in Figure 4.6 and the results are given in Table 4.7.

4.2.5   Manufacture of Test Specimens

Six beams were manufactured during each casting, with three beams each in two separate timber moulds. Steel cages were secured to the sides of the timber moulds by using bar chairs and welding sacrificial steel bars to the steel cages. Figure 4.7 shows the cages set in place in the moulds.
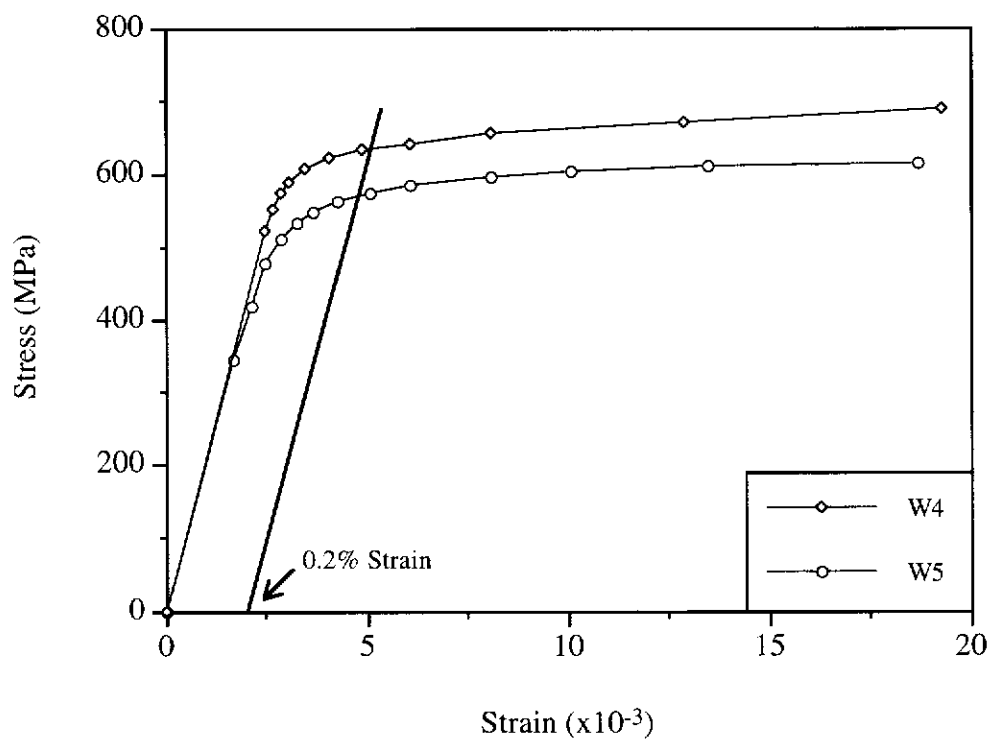
Figure 4.6   Stress-Strain Curves of Shear Reinforcement

Table 4.7   Tensile Test Results of Shear Reinforcement

Wire Mark	W4	W5
Diameter of Wire (mm)	3.96	4.94
0.2% Proof Stress (MPa)	632	569
Ultimate Strength (MPa)	687	614

Figure 4.7   Reinforcement Cage in Timber Moulds

Concrete was placed in layers into the moulds. Hand-held mechanical vibrators were used to compact the fresh concrete. Control cylinders were compacted in layers on a vibrating table.

Both the beam specimens and control cylinders were covered in hessian and plastic sheets to minimise the loss of moisture after initial setting of the concrete. They were kept moist and undercover for the first seven days after casting. After that period, the beams and cylinders were left to air dry in the laboratory until the time of testing.

4.3   Test Set-Up

The test set-up used for different beam series is illustrated in Figure 4.8. The beams were loaded to failure in a 2500 kN capacity Avery testing machine. The load from the test machine was transferred through spherical seats to a steel spreader beam which in turn distributed the load as concentrated loads on the concrete beams. The spreader beam transferred the load to a test beam through 255 mm long x 50 mm diameter steel rollers. To ensure a good dispersion of force, 100 mm wide x 250 mm long x 20 mm thick distribution plates were placed under the rollers. These plates in turn rested on rubber pads or plywood strips which absorbed the irregularities of the top surface of the concrete beam. Figure 4.9 shows a typical test set-up.

In the case of Series 6 with four concentrated loads, two smaller spreader beams were used in between the main spreader beam and the test beam.

4.4   Instrumentation

4.4.1   Measurement of Vertical Deflection

The vertical deflections of test beams were measured using Linear Variable Differential Transformers (LVDTs). In Series 1, 50 mm plunger travel LVDTs were located at midspan and at each loading point as shown in Figure 4.10.

There were only small differences in the vertical deflections at these three locations (Figure 4.10). Therefore, for Series 2 to 8, vertical deflections were measured only at midspan, but at the bottom of both the front and back faces of a beam.
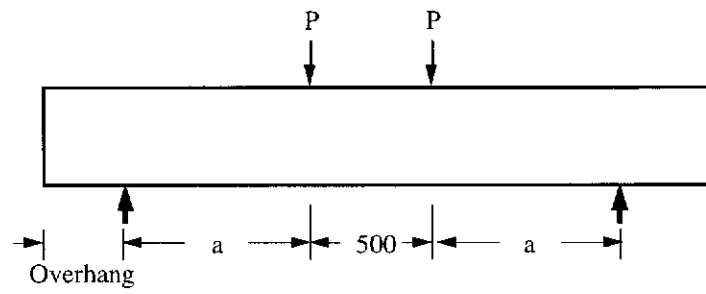
(a) Series 1, 2, 3, 4, 5 and 8
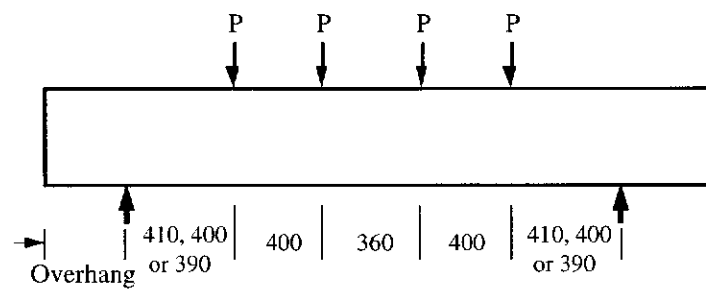
(b) Series 6
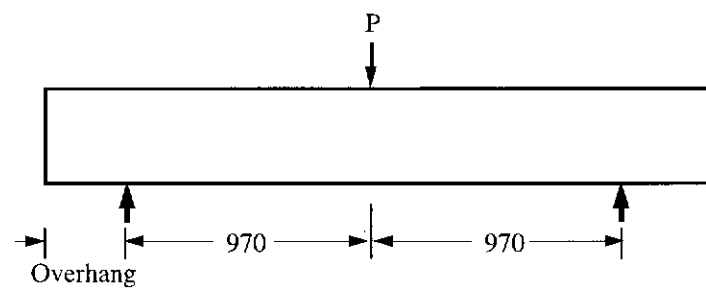
(c) Series 7

Figure 4.8   Test Set-Up
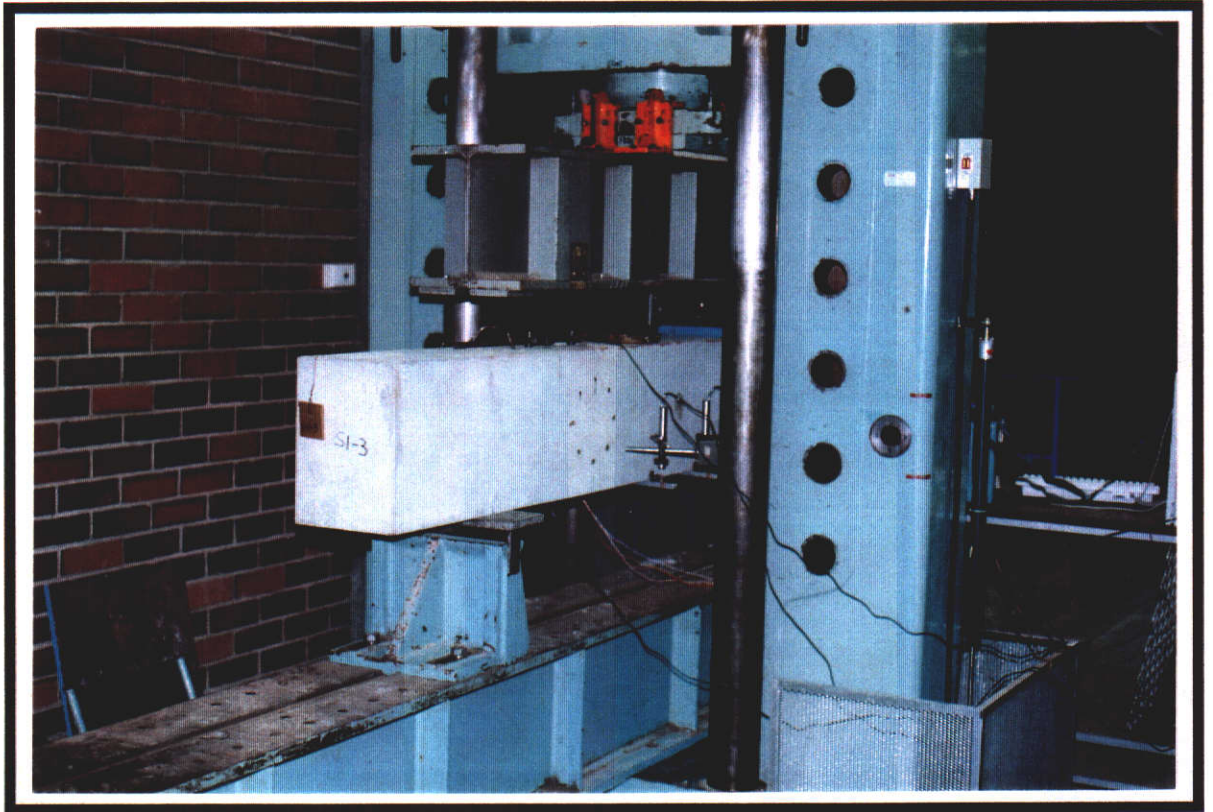
Figure 4.9   Typical Test Set-Up
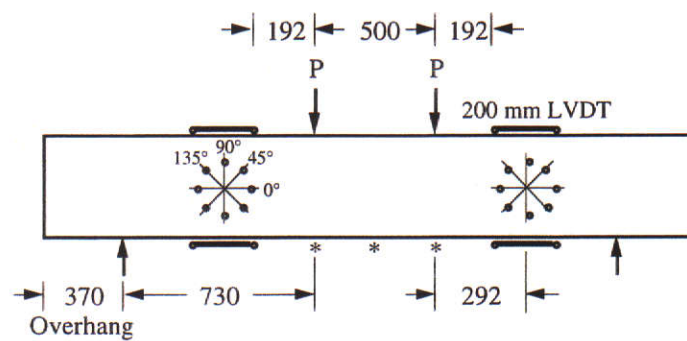
Note: * position of LVDT for measuring vertical deflection.
All dimensions are in millimetres.

Figure 4.10   Instrumentation for Series 1

4.4.2 Measurement of Curvature

To estimate the curvature of test beams, four LVDTs were placed on the top and bottom as shown in Figure 4.10. Each LVDT had a 5 mm plunger travel. A pair of steel pins were fixed into drillholes set at 200-350 mm apart. The pins were attached to the drillholes using a high grade epoxy.

4.4.3 Measurement of Steel Strains

Electrical resistance strain gauges were used to measure the strains in the longitudinal tensile bars. The strain gauges had a resistance of 120 Ohm and a strain limit of 5% of the gauge length.

The ribs on reinforcing bars were removed through a process of angle grinding, filing and surface smoothing using emery paper. Just prior to the installation of a strain gauge, the surface receiving the strain gauge was cleaned with a wetted emery paper. The surface was then cleaned with a degreaser, methylated spirit, a conditioner and a neutraliser.

For the attachment of the strain gauges, an epoxy gluing system was adopted. The gauge and the terminal were coated with an air drying polyurethane before applying a waterproofing system. The system involved priming vinyl-insulated lead wires connected to the terminals with a layer of air drying nitrile rubber, covering the gauge with a layer of teflon film, waterproofing with a layer of butyl rubber sealant, mechanically protecting the gauge with a layer of neoprene rubber and then encapsulating all these with a tough aluminium tape.

The strain gauges were located at various positions along the lengths of the beams. The strain gauge locations used in Series 1 to 7 are shown in Figures 4.11 to 4.17. No strain gauge was used in Series 8.

Strain gauges were attached to longitudinal tensile bars in the following beams: S1-3 and S1-4 in Series 1; S2-3 and S2-4 in Series 2; S3-3 and S3-4 in Series 3; S4-1, S4-4 and S4-6 in Series 4; S5-1, S5-3 and S5-6 in Series 5; S6-3 and S6-4 in Series 6; and S7-3 and S7-4 in Series 7.

In Series 1, some of the strain gauges were located at a distance of $d = 292$ mm from the load positions. From this series, it was found that the main shear cracks reached the level of the tensile reinforcement at a distance of about 1.6d to 2.0d from the point loads within the shear spans. A distance of 1.8d from the load point was chosen as being a reasonable estimation of the horizontal projection of the shear crack at the level of the tensile steel. Therefore, strain gauges were located at distances of (d+0.5×width of loading plate) and 1.8d from the load positions in Series 2, 3, 4, 5 and 7.

The locations for S6-3 and S6-4 were slightly different. The distances of d and 1.8d given in Figure 4.16 were measured from the centroid of the combined load of 2P on one-half of the beam.

4.4.4 Measurement of Concrete Strains

Concrete surface strains were measured in Series 1 and 2 using Demec gauges. These gauges were located in a rosette format as illustrated in Figure 4.10. An analyses of these test measurements indicated that the readings were influenced by the development of cracks and the results were inconclusive. Therefore, these data are not reported in this work. No concrete surface strains were measured in other series.
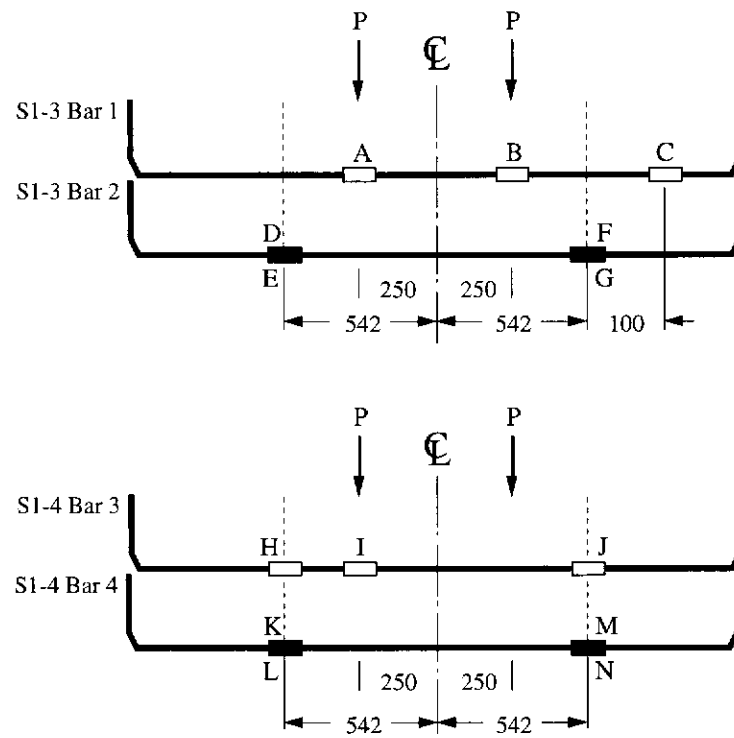
Note: ----- indicates section at distance (d) from the load.
        ▢ indicates strain gauge on one side.
        ▬ indicates strain gauges on both sides.

Figure 4.11   Strain Gauges in Beams S1-3 and S1-4 (Series 1)
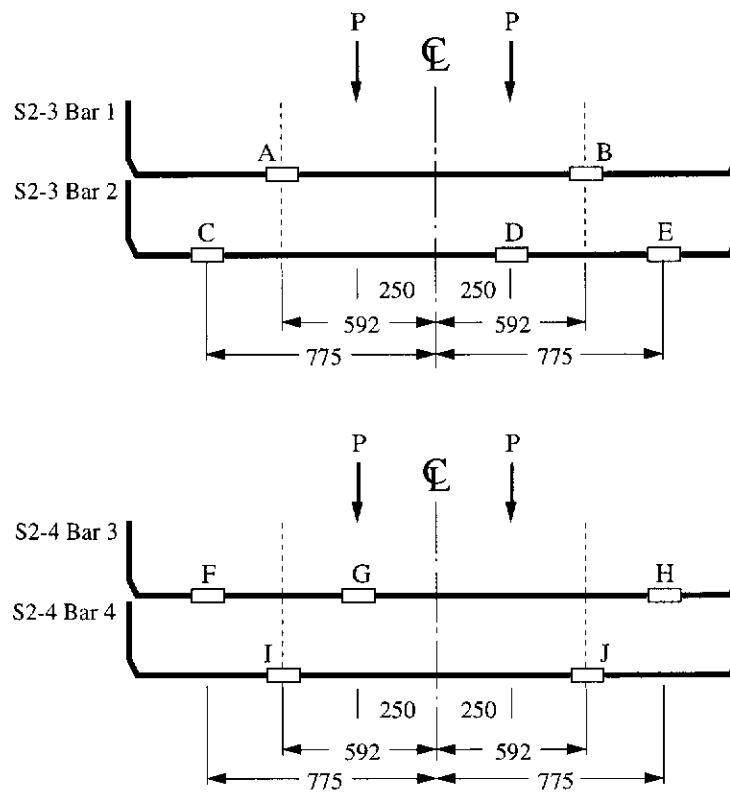
88

Note: ----- indicates section at distance (d+0.5×width of loading plate) from load.
        ☐ indicates strain gauge on one side.

Figure 4.12   Strain Gauges in Beams S2-3 and S2-4 (Series 2)
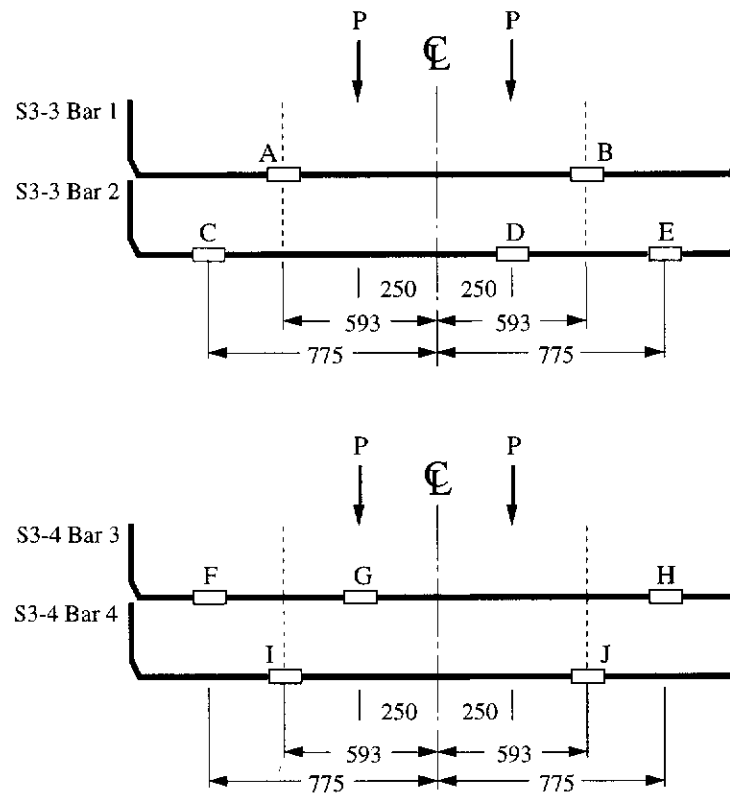
Note: ----- indicates section at distance (d+0.5×width of loading plate) from load.
⊏⊐ indicates strain gauge on one side.

Figure 4.13   Strain Gauges in Beams S3-3 and S3-4 (Series 3)
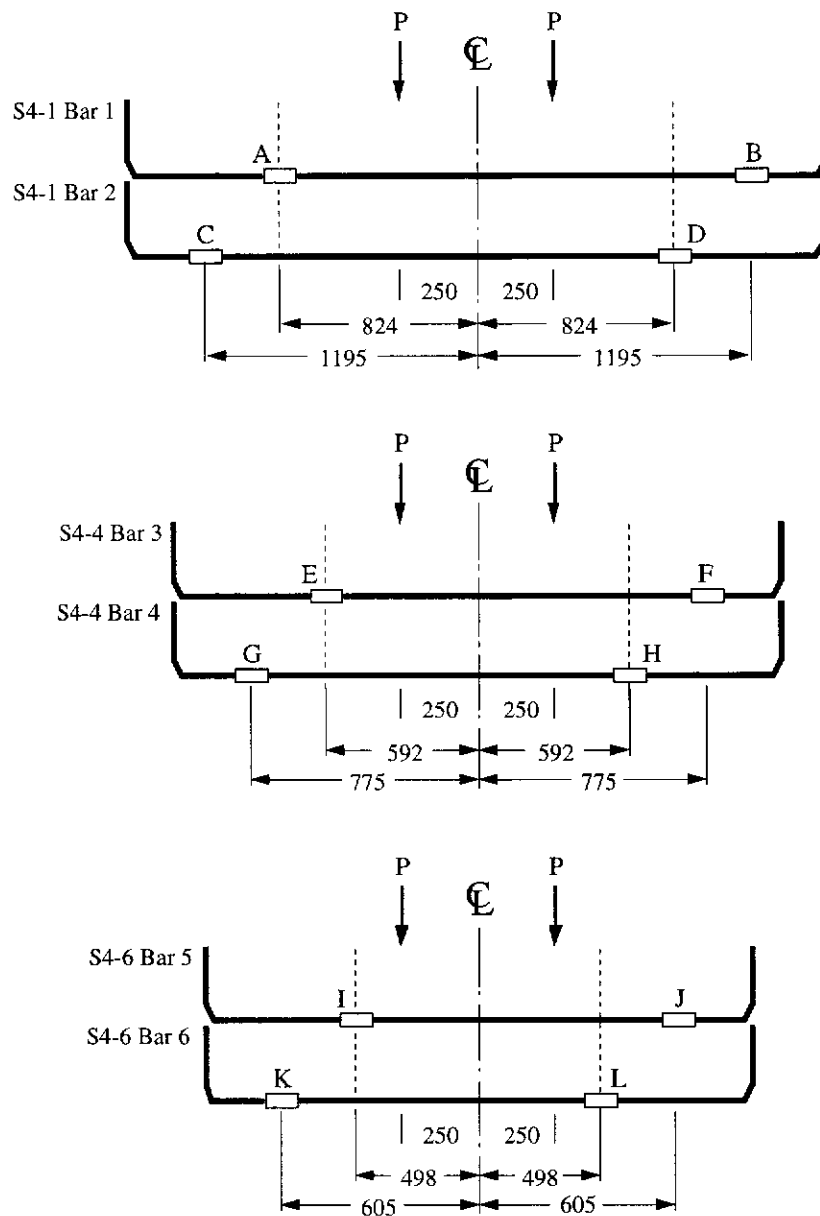
Note: ----- indicates section at distance (d+0.5×width of loading plate) from load.
          ⬜ indicates strain gauge on one side.
          Bars 1 and 2 are the bottom-most bars in the bundled bars construction.

Figure 4.14   Strain Gauges in Beams S4-1, S4-4 and S4-6 (Series 4)
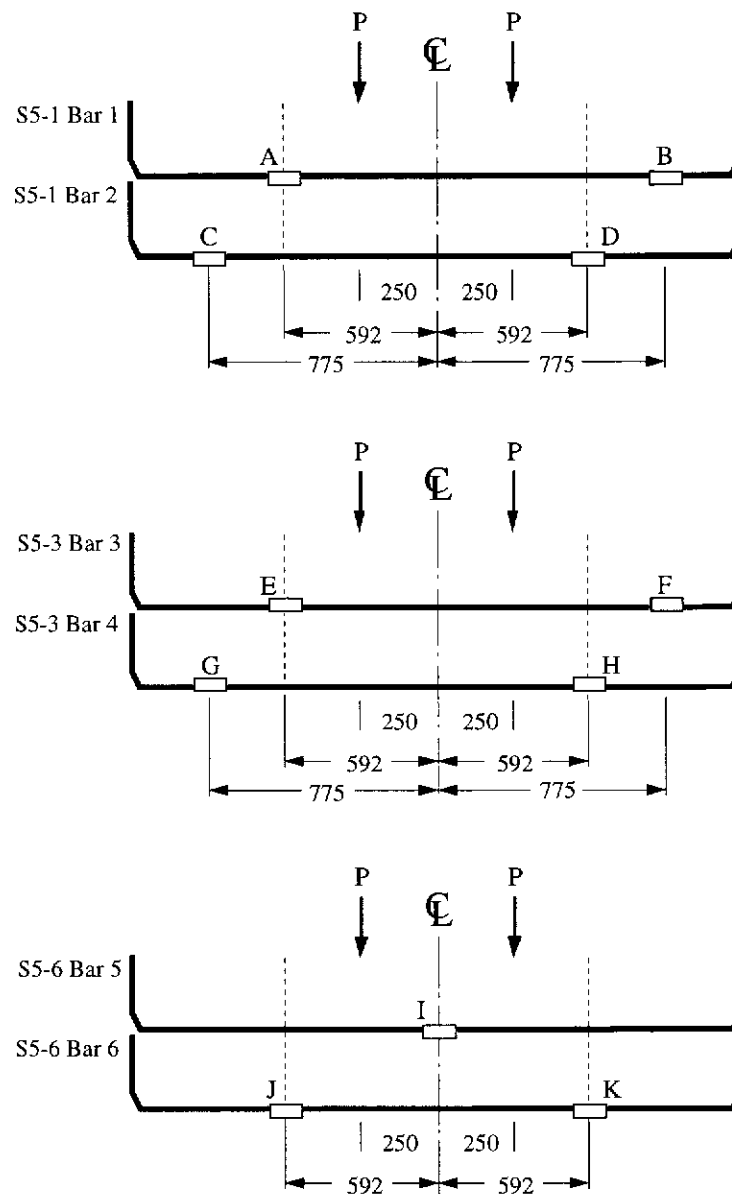
91

Note: ----- indicates section at distance (d+0.5×width of loading plate) from load.
⬜ indicates strain gauge on one side.

Figure 4.15 Strain Gauges in Beams S5-1, S5-3 and S5-6 (Series 5)
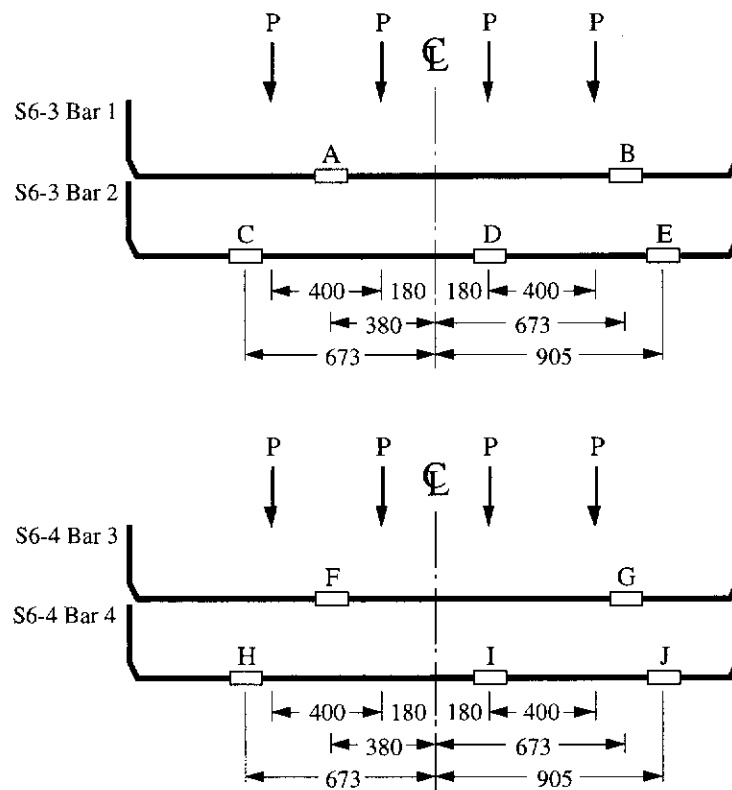
Figure 4.16 Strain Gauges in Beams S6-3 and S6-4 (Series 6)
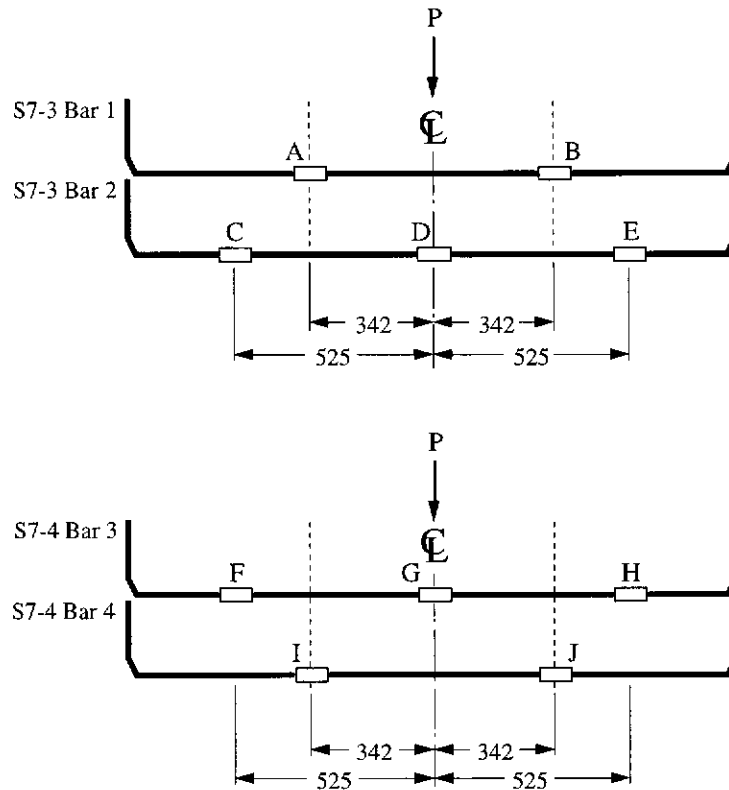
Note: ☐ indicates strain gauge on one side.

All the bars shown are the bottom-most bars in the bundled bars construction.

Figure 4.17   Strain Gauges in Beams S7-3 and S7-4 (Series 7)

4.4.5   Data Acquisition

Two semi-automated data acquisition systems were used. One data logger system was used to record the data from the test machine and the LVDTs. A second data logger system was used to record the data from the strain gauges. Each system was connected to a separate computer but both systems were triggered from a single switch. All test data are given in Appendix A.

4.5 Test Procedure

All beams were loaded to failure. Each beam was initially "exercised" by applying a small load to ensure that the test set-up and the instrumentation worked properly. The beam was then unloaded and datum readings were taken.

Initially, the beam was loaded in increments of 50 kN until the load reached 350 kN. The rate of load increment was set in the range of 0.8 to 1.0 kN/sec. At higher loads, a ram rate of 2.0 mm/min was used. Close to failure, the load increments were approximately 10-25 kN.

After failure, each beam was photographed to show the crack pattern and the mode of failure. Appendix B contains photographs of all the beams after failure.

The test results are presented in the next chapter.

Presentation And Discussion Of Results

5.1 Introduction

The test results are presented in this chapter. The behaviour of the test beams are discussed and the shear strengths are tabulated.

The effects of various parameters on the shear strength of the test beams are elaborated in this chapter.

The test results are compared with predictions from the theory. Comparisons of available test results from previous investigations with predictions from the theory are also given.

All the test data from the present and previous investigations are compared with code predictions. The codes which are considered here are AS 3600 (1994), ACI 318-95, EC2 Part 1 and CSA A23.3-94.

5.2 Test Results

5.2.1 Behaviour of Test Beams

All the beams failed in shear except for beams S2-6, S4-5, S5-6, S6-1 and S6-2, which failed in flexure. A summary of experimental results are given in Table 5.1. Complete details are given in Appendix A.

The behaviour of all test beams was similar. Small flexure cracks occurred first. Subsequently, the flexure cracks extended as flexure-shear cracks. A main shear crack developed suddenly and persisted in opening up with increasing load until the failure of the beam. Figure 5.1 shows the typical progressive propagation of cracks in beam S5-1 at increments of 50 kN of load (25 kN shear) up to 350 kN. The last photograph in this figure shows the beam after failure. Photographs showing the crack patterns and failure modes of other beams are given in Appendix B.

5.2.2 Effects of Test Parameters

The effect of each test parameter on the shear strength is discussed below. The shear capacity of the test beams (V_e) was divided by ($b_v d_o$) to give the nominal shear stress $V_e/b_v d_o$ at failure.

5.2.2.1 Cover to Shear Reinforcement Cage

Vecchio and Collins (1982) reported that the concrete cover to the shear reinforcement spalls at the time of failure and that the effective width of a beam in shear is equal to the total beam width less the clear cover on both sides of a beam. Therefore, Series 1

Table 5.1 Summary of Test Results

Beam Mark	f'_c (MPa)	b (mm)	Side Clear Cover (mm)	D (mm)	d_o (mm)	a (mm)	$\dfrac{a}{d_o}$	$\dfrac{M}{Vd_o}$	$A_{s\ell}$ (mm²)	$f_{s\ell y}$ (MPa)	ρ_t	f_{sty} (MPa)	V_e (Exp) (kN)
S1-1	63.6	250	*2 5*	350	292	730	2.50	1.50	2046	452	0.00157	569	228.3
S1-2	63.6	250	*2 5*	350	292	730	2.50	1.50	2046	452	0.00157	569	208.3
S1-3	63.6	250	*3 5*	350	292	730	2.50	1.50	2046	452	0.00157	569	206.1
S1-4	63.6	250	*3 5*	350	292	730	2.50	1.50	2046	452	0.00157	569	277.9
S1-5	63.6	250	*5 0*	350	292	730	2.50	1.50	2046	452	0.00157	569	253.3
S1-6	63.6	250	*5 0*	350	292	730	2.50	1.50	2046	452	0.00157	569	224.1
S2-1	72.5	250	35	350	292	730	2.50	1.50	2046	452	*0.00105*	569	260.3
S2-2	72.5	250	35	350	292	730	2.50	1.50	2046	452	*0.00126*	569	232.5
S2-3	72.5	250	35	350	292	730	2.50	1.50	2046	452	*0.00157*	569	253.3
S2-4	72.5	250	35	350	292	730	2.50	1.50	2046	452	*0.00157*	569	219.4
S2-5	72.5	250	35	350	292	730	2.50	1.50	2046	452	*0.00209*	569	282.1
S2-6	72.5	250	35	350	292	730	2.50	1.50	2046	452	*0.00262*	569	359.0[#]
S3-1	67.4	250	35	350	297	740	2.49	1.49	*1232*	450	0.00101	632	209.2
S3-2	67.4	250	35	350	297	740	2.49	1.49	*1232*	450	0.00101	632	178.0
S3-3	67.4	250	35	350	293	730	2.49	1.49	*2046*	452	0.00101	632	228.6
S3-4	67.4	250	35	350	293	730	2.49	1.49	*2046*	452	0.00101	632	174.9
S3-5	67.4	250	35	350	299	720	2.41	1.41	*2760*	442	0.00101	632	296.6
S3-6	67.4	250	35	350	299	720	2.41	1.41	*2760*	442	0.00101	632	282.9
S4-1	87.3	250	35	*600*	542	1300	2.40	1.40	4092	452	0.00157	569	354.0
S4-2	87.3	250	35	*500*	444	1070	2.41	1.41	3284	433	0.00157	569	572.8
S4-3	87.3	250	35	*400*	346	830	2.40	1.40	2464	450	0.00157	569	243.4
S4-4	87.3	250	35	*350*	292	730	2.50	1.50	2046	452	0.00157	569	258.1
S4-5	87.3	250	35	*300*	248	590	2.38	1.38	1840	442	0.00157	569	321.1[#]
S4-6	87.3	250	35	*250*	198	500	2.53	1.53	1380	442	0.00157	569	202.9
S5-1	89.4	250	35	350	292	880	*3.01*	*2.01*	2046	452	0.00157	569	241.7
S5-2	89.4	250	35	350	292	800	*2.74*	*1.74*	2046	452	0.00157	569	259.9
S5-3	89.4	250	35	350	292	730	*2.50*	*1.50*	2046	452	0.00157	569	243.8
S5-4	89.4	250	35	350	292	580	*1.99*	*0.99*	2046	452	0.00157	569	476.7
S5-5	89.4	250	35	350	292	510	*1.75*	*0.75*	2046	452	0.00157	569	573.4
S5-6	89.4	250	35	350	292	440	*1.51*	*0.51*	2046	452	0.00157	569	647.7[#]
S6-1	68.9	250	35	350	297	810	2.73	1.73	*1232*	450	0.00101	632	155.4[#]
S6-2	68.9	250	35	350	297	810	2.73	1.73	*1232*	450	0.00101	632	155.1[#]
S6-3	68.9	250	35	350	293	800	2.73	1.73	*2046*	452	0.00101	632	178.4
S6-4	68.9	250	35	350	293	800	2.73	1.73	*2046*	452	0.00101	632	214.4
S6-5	68.9	250	35	350	299	790	2.64	1.64	*2760*	442	0.00101	632	297.0
S6-6	68.9	250	35	350	299	790	2.64	1.64	*2760*	442	0.00101	632	287.2
S7-1	74.8	250	35	350	294	970	3.30	2.30	3284	433	*0.00105*	569	217.2
S7-2	74.8	250	35	350	294	970	3.30	2.30	3284	433	*0.00126*	569	205.4
S7-3	74.8	250	35	350	294	970	3.30	2.30	3284	433	*0.00157*	569	246.5
S7-4	74.8	250	35	350	294	970	3.30	2.30	3284	433	*0.00196*	569	273.6
S7-5	74.8	250	35	350	294	970	3.30	2.30	3284	433	*0.00224*	569	304.4
S7-6	74.8	250	35	350	294	970	3.30	2.30	3284	433	*0.00262*	569	310.6
S8-1	74.6	250	35	350	292	730	2.50	1.50	2046	452	*0.00105*	569	272.1
S8-2	74.6	250	35	350	292	730	2.50	1.50	2046	452	*0.00126*	569	250.9
S8-3	74.6	250	35	350	292	730	2.50	1.50	2046	452	*0.00157*	569	309.6
S8-4	74.6	250	35	350	292	730	2.50	1.50	2046	452	*0.00157*	569	265.8
S8-5	74.6	250	35	350	292	730	2.50	1.50	2046	452	*0.00196*	569	289.2
S8-6	74.6	250	35	350	292	730	2.50	1.50	2046	452	*0.00224*	569	283.9

Notes: (1) # flexure failure.

(2) The main parameter for each series of tests is highlighted in *italics* in Table 5.1.
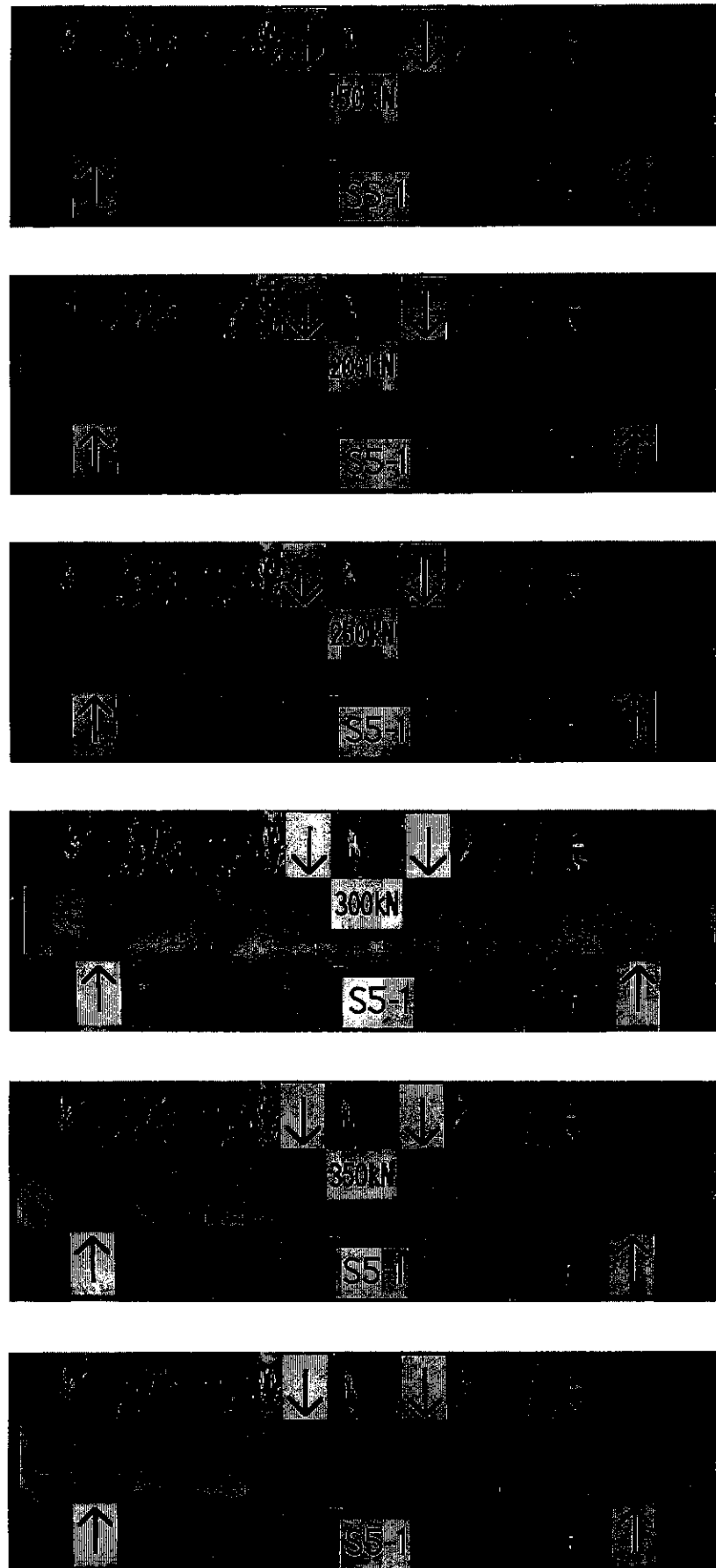
Figure 5.1 Progressive Cracking in the Back Face of Beam S5-1

99

was used to determined the effect of the concrete cover to shear reinforcement cage on the shear strength.

There were three pairs of identical beams, S1-1 and S1-2, S1-3 and S1-4, and S1-5 and S1-6. Table 5.1 indicates some scatter between the results of the pair beams. Beams S1-3 and S1-4 showed the largest difference in shear strength. Apart from the expected inherent scatter, the strain gauges used may have added to the variability of the results.

Average values of the shear strength of the three pairs of beams were 218 kN (S1-1 and S1-2), 242 kN (S1-3 and S1-4) and 239 kN (S1-5 and S1-6). There was no significant difference among these averages although S1-1 and S1-2 had slightly lower shear capacities.

If there should be any difference, then beams S1-1 and S1-2 should have the largest shear capacities since they had the smallest concrete cover and the widest stirrup cage effective for shear. This would then imply that the "spalled web width" assumption was valid. Evidently, the average of the shear capacities for S1-1 and S1-2 turned out to be the smallest and it can only be concluded that the full width of a beam should be taken as being effective for shear. In addition, spalling of concrete cover was not apparent in any of these test beams.

The nominal shear strength of the beams were plotted against concrete cover in Figure 5.2. The test trend indicates that there is almost negligible effect of the concrete cover on the shear strength. The shear strength only dropped slightly at the smallest concrete cover of 25 mm.

5.2.2.2   Shear Reinforcement Ratio

In Series 2, 7 and 8, the shear reinforcement ratio was the test parameter. Series 8 was a repeat test of Series 2 and their results complemented each other. Series 7 had a single point load at midspan instead of the two point loads used in Series 2 and 8.

Series 2 and 8 had an a/d_0 ratio of 2.50 and their concrete compressive strengths were respectively 72.5 and 74.6 MPa. Series 7 had an a/d_0 ratio of 3.30 and a concrete compressive strength of 74.8 MPa.

Figure 5.3 shows a plot of the shear strength versus the shear reinforcement ratio for Series 2 and 8. The scatter was very large and the test trend was not obvious. The test procedure was the same for all the test beams but the results still showed large variations. This anomaly could not be explained.

Figure 5.4 shows the shear strength versus shear reinforcement ratio relationship for Series 7. The trend of increasing shear strength with increase in the shear reinforcement ratio was clearly evident in this beam series. It seems that this trend is more obvious in beams with the larger a/d_0 ratio of 3.30 than in the beams with the a/d_0 ratio of 2.50. Greater degree of cracking due to flexure in the more slender beams may have caused the trend to be more pronounced in these beams than in the shorter beams.

5.2.2.3   Longitudinal Tensile Reinforcement Ratio

Series 3 and 6 were used to study the effect of the longitudinal tensile reinforcement ratio ($\rho_\ell = A_{s\ell}/b_v d_0$) on the shear strength of beams. In Series 3, there were three pairs of identical beams, S3-1 and S3-2, S3-3 and S3-4, and S3-5 and S3-6. The beams in Series 6 were identical to those in Series 3, except four point loads were used instead of two.

Series 6 was tested to investigate the shear behaviour of beams under a four point loading configuration. The main parameter of this series was also the longitudinal tensile reinforcement ratio. The shear force was stepped from -2P to +2P along the length of each beam. Four beams in the series, S6-3, S6-4, S6-5 and S6-6, failed in shear, and S6-1 and S6-2 failed in flexure. A general shear failure pattern is shown in Figure 5.5.

101
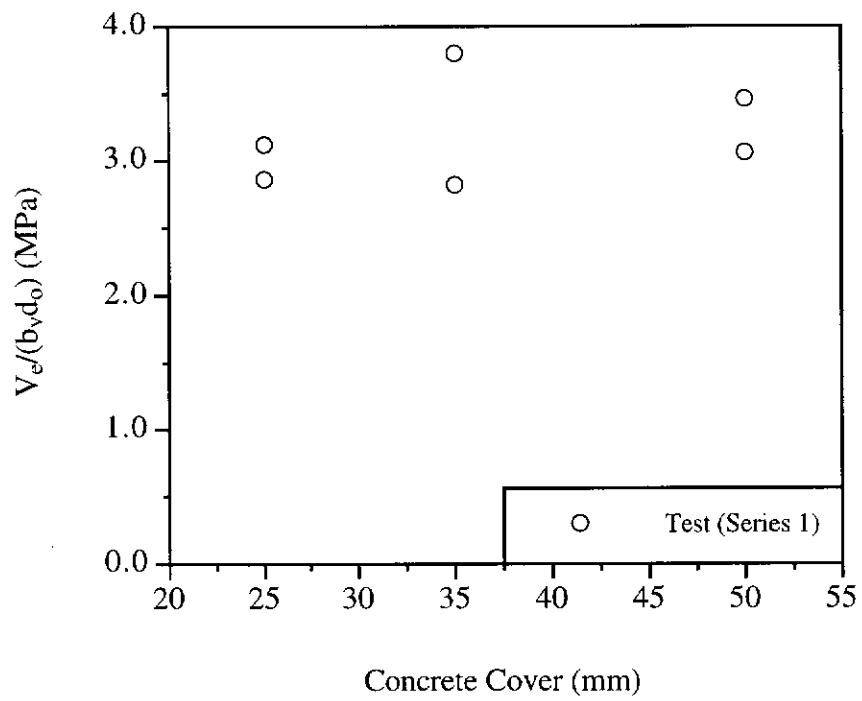
Figure 5.2 Shear Strength versus Concrete Cover to Shear Reinforcement Cage
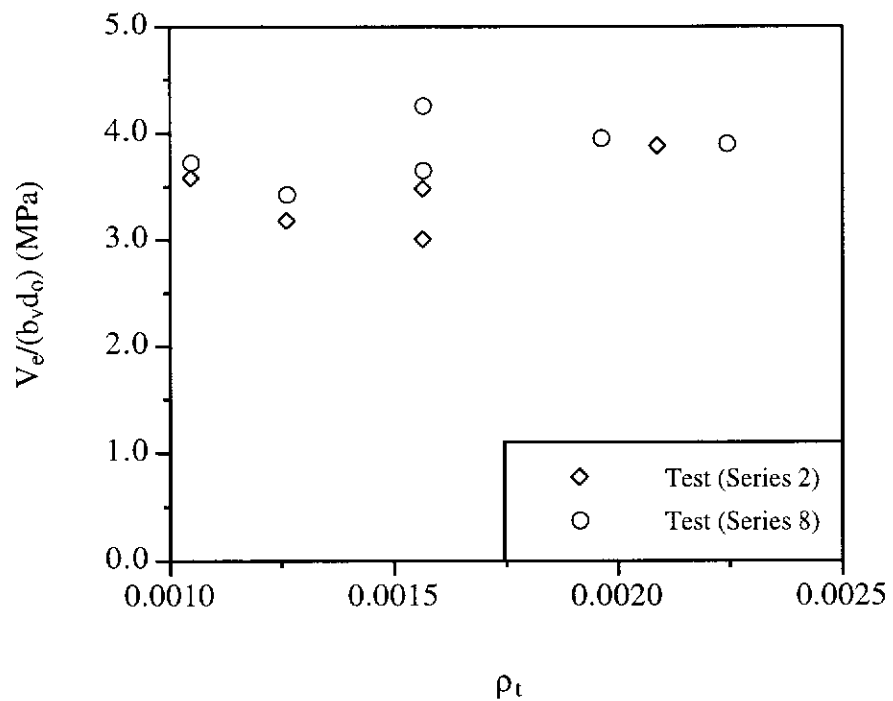
Figure 5.3 Shear Strength versus Shear Reinforcement Ratio

102
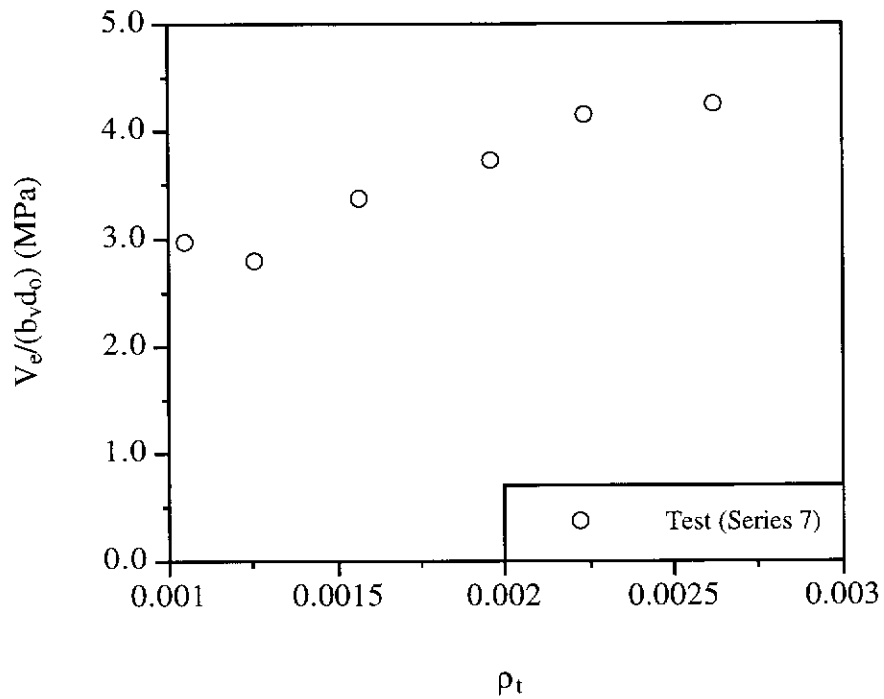
Figure 5.4   Shear Strength versus Shear Reinforcement Ratio
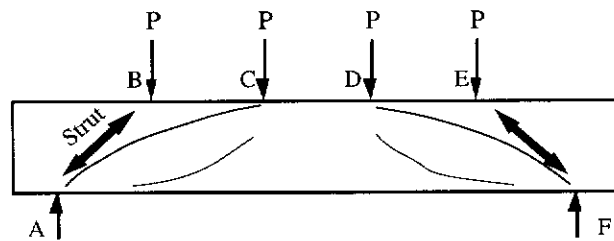
Figure 5.5   Shear Failure Pattern of Beams in Series 6

The concrete struts from A to B and E to F in Figure 5.5 did not show any sign of distress during the tests. This implied that the loads at B and E were transferred directly into the supports. The angles made by struts AB and EF with respect to the horizontal were about $40°$-$42°$. The loads at C and D were mainly causing the shearing action in the shear spans between A and C, and D and F. Shear failure was attributed

to the loads at C and D. Therefore, the shear strengths at failure for beams in Series 6 (Table 5.1) were taken as one quarter of the total failure load.

Although Series 3 had two point loads and Series 6 had four point loads, both these sets of results were combined together since two of the point loads nearer to the supports in each of the beams in Series 6 were directed straight into the supports and were ignored for shear. Therefore, considering only the two inner point loads in Series 6, the shear spans in Series 6 (a = 790, 800 or 810 mm) were only slightly longer than those in Series 3 (a = 720, 730 or 740 mm).

Figure 5.6 shows the shear strength plotted against the longitudinal tensile reinforcement ratio for both Series 3 and 6. The trend indicates a very small increase in the shear stress $V_e/b_v d_o$ from p_ℓ of 1.66% to 2.79%, which is in the range of longitudinal reinforcement ratios for typical reinforced concrete beams.
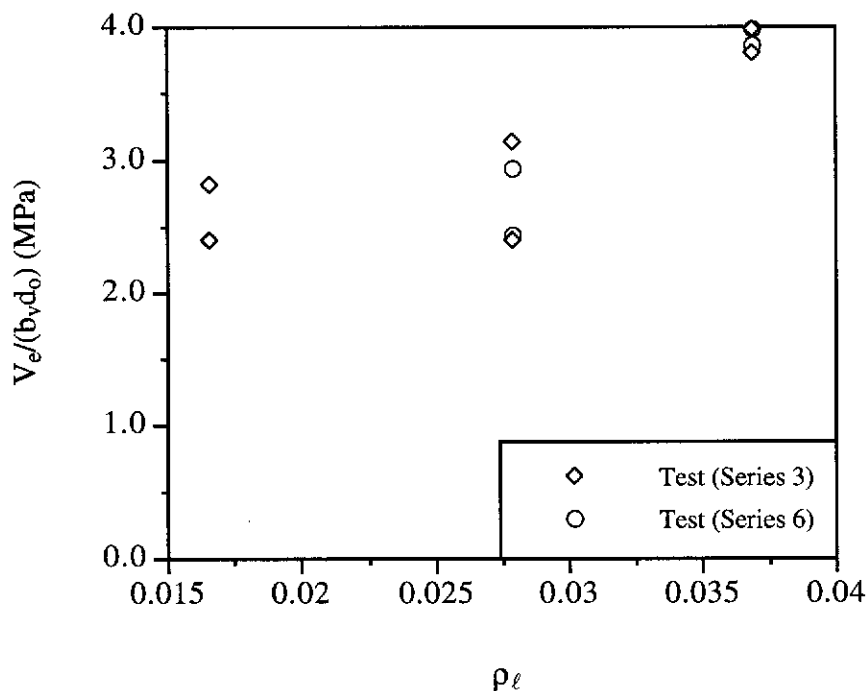
Figure 5.6   Shear Strength versus Longitudinal Tensile

Reinforcement Ratio

The shear strength increased with longitudinal tensile reinforcement ratio. However, there seems to be a sharper increase in the shear strength for $\rho_\ell = 3.69\%$. This may have been due to increased dowel action from the bundling of the longitudinal tensile bars in the beams with $\rho_\ell = 3.69\%$.

5.2.2.4 Overall Beam Depth

In Series 4, the overall beam depth was varied from 250 to 600 mm. Two of the failures in beams S4-2 and S4-5 were unexpected.

Beam S4-2 failed at a very high shear capacity with a loud explosion. Although all shear failures were sudden, this was the most catastrophic compared to all other beams. The damage to the concrete across the main shear crack was severe (Figure 5.7). The vertical legs of the stirrups fractured, and the compressive and tensile longitudinal bars bent due to the shearing effect. It was also noted that the failure crack was almost straight from the load point to the bottom of the beam towards the supports. This was different to other failure shear cracks which were curved and concave downwards in shape. This mode of failure is closer to the limit analysis failure mode predicted by the plasticity theory (Nielsen (1984)). The plasticity theory generally over-predicts the shear strength of reinforced concrete beams and may explain for the large test shear strength of beam S4-2.

In contrast, beam S4-5 failed in flexure. According to preliminary design calculations (based on AS 3600 (1994)), the ratio of the shear force for a shear failure to the shear force for a flexural failure was 0.76. Therefore, this beam should not have failed in flexure. It is suspected that the bundled bars may have contributed to the extra shear strength of the beam causing it to fail in flexure.

Figure 5.8 shows the nominal shear stress at failure plotted against the overall beam depth of the beams in Series 4.
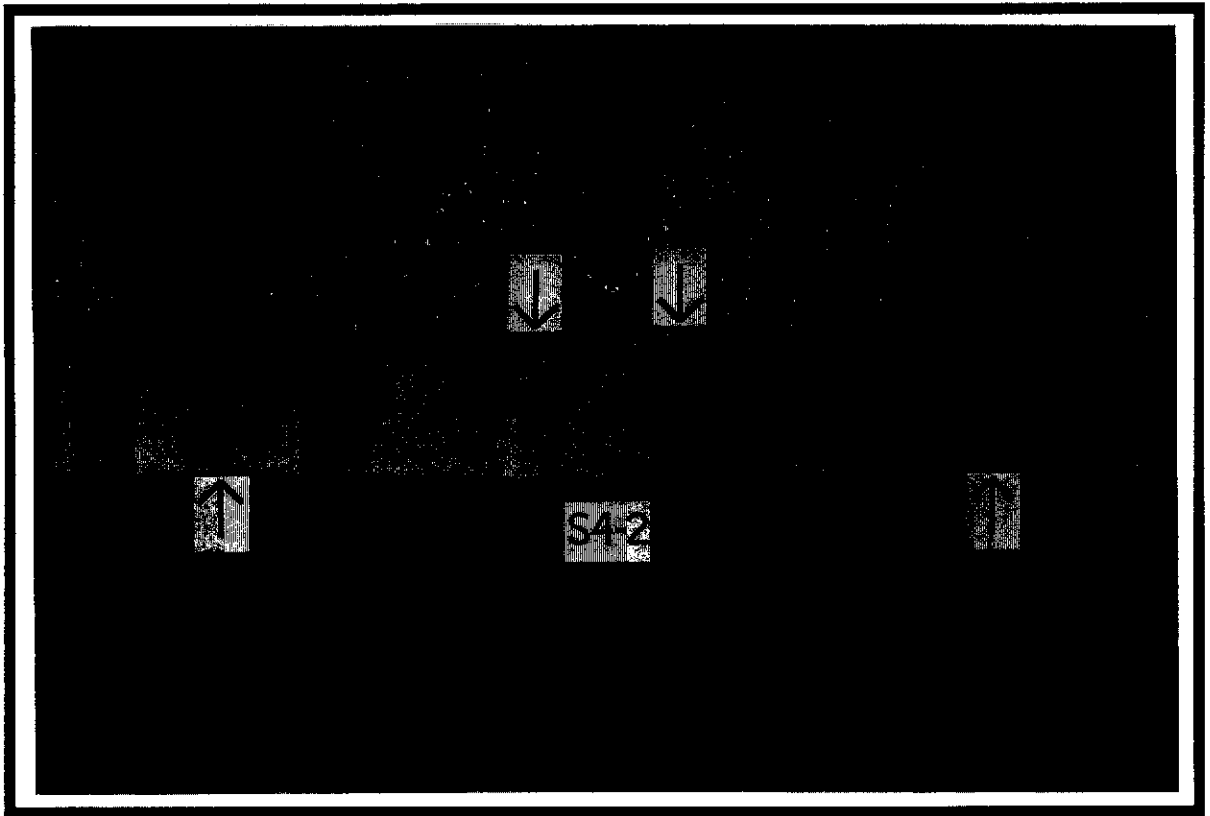
Figure 5.7 Failure Crack Pattern of Beam S4-2
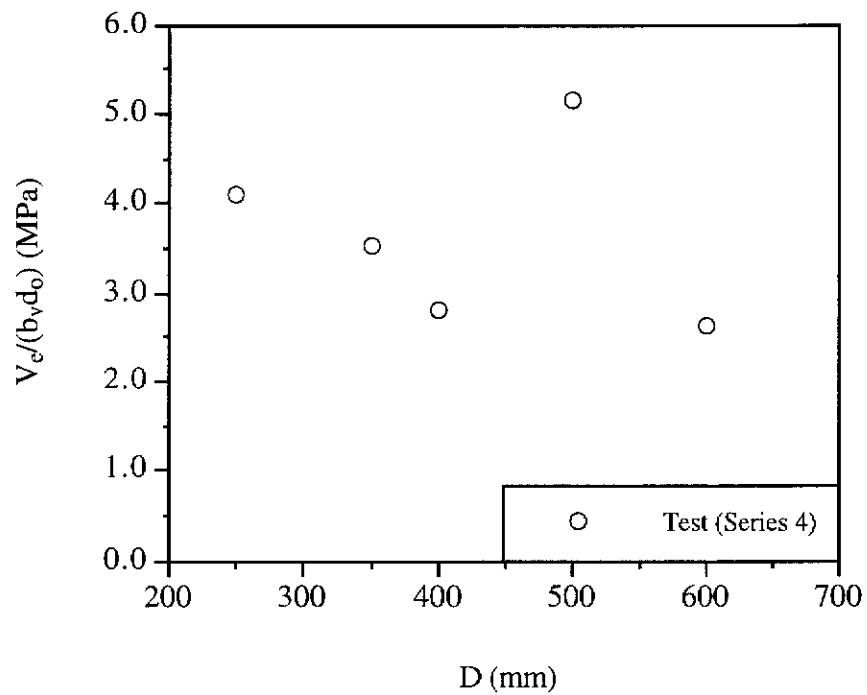
Figure 5.8 Shear Strength versus Overall Beam Depth

106

The test result for beam S4-5 was excluded from Figure 5.8 as the beam suffered a flexural failure. The shear strength for beam S4-2 was exceptionally high compared to the other beams. However, if the results of the four remaining beams are considered, it is clear that the shear stress at failure $V_e/b_v d_o$ decreased with an increase in beam depth. The loss of shear strength with increasing beam depth may be attributed to a decrease in aggregate interlock and dowel action for deeper slender beams.

Some recent tests published in the newsletter of the Public Works Research Institute of Japan confirmed the increase of the shear stress at failure with increasing depth.

5.2.2.5   Shear Span/Depth Ratio, a/d_o

The shear span-to-depth ratio a/d_o was varied from 1.51 to 3.01 in Series 5. Figure 5.9 is a plot of the shear strength versus the a/d_o ratio. The test result of beam S5-6 is not plotted in Figure 5.9 as the failure was flexure.
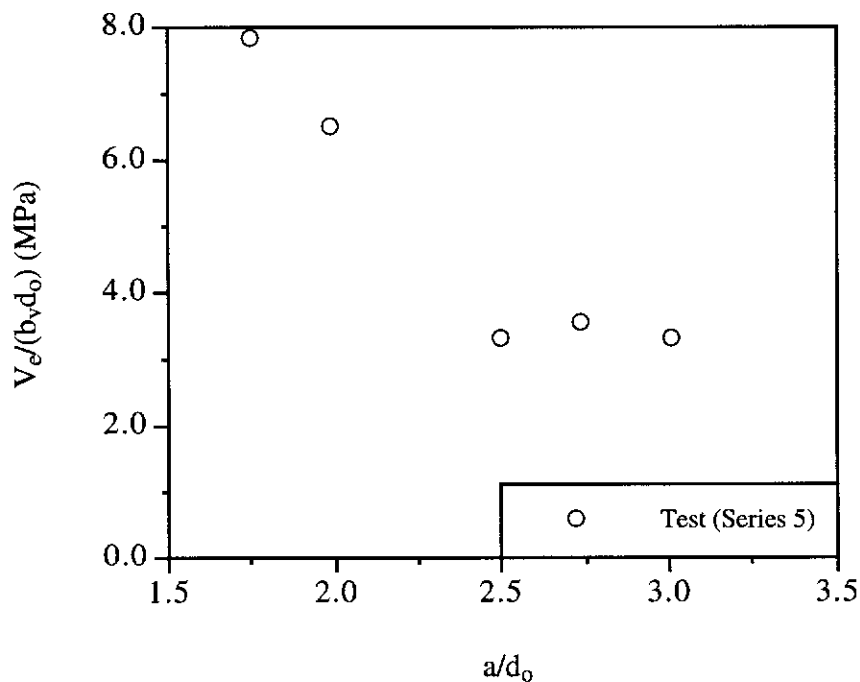
Figure 5.9   Shear Strength versus Shear Span/Depth Ratio

107

There is little difference in shear strength for a/d_o from 2.50 to 3.01. However, the shear strength increased sharply when a/d_o decreased below 2.50. The higher shear capacities of the short beams (i.e., beams S5-4 and S5-5) were due to arch action that must have developed in those beams.

5.2.2.6 Concrete Compressive Strength

The concrete compressive strength varied from 63.6 to 89.4 MPa in the tests. In order to study the test trend, the beams listed in Table 5.2 were considered. The results are plotted in Figure 5.10.

Table 5.2 Effect of Concrete Compressive Strength on Shear Strength

Beam Mark	f_c (MPa)	D (mm)	d_o (mm)	b (mm)	a/d_o	ρ_t	ρ_ℓ	V_e (kN)
S1-3	63.6	350	292	250	2.50	0.00157	0.0279	206.1
S1-4	63.6	350	292	250	2.50	0.00157	0.0279	277.9
S2-3	72.5	350	292	250	2.50	0.00157	0.0279	253.3
S2-4	72.5	350	292	250	2.50	0.00157	0.0279	219.4
S4-4	87.3	350	292	250	2.50	0.00157	0.0279	258.1
S5-3	89.4	350	292	250	2.50	0.00157	0.0279	243.8
S8-3	74.6	350	292	250	2.50	0.00157	0.0279	309.6
S8-4	74.6	350	292	250	2.50	0.00157	0.0279	265.8

Figure 5.10 shows that the concrete compressive strength within the range of 60 to 90 MPa had little influence on the shear strength of the beams. This is contrary to the conventionally accepted understanding of the effect of concrete compressive strength on shear strength.

108
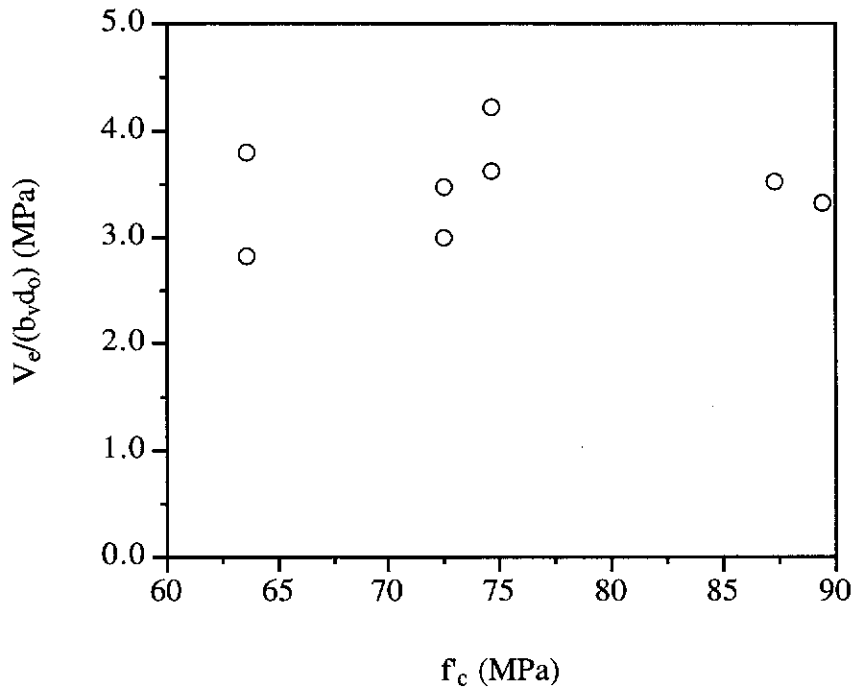
Figure 5.10   Shear Strength versus Concrete Compressive Strength

5.2.3   Deformation of Test Beams

The deformation of the test beams were monitored in various ways as discussed in Section 4.4. The test results are discussed in the following sub-sections.

From visual inspection during testing, the crack patterns of the reinforced HPC beams of the present study were similar to those reported for beams from previous research.

5.2.3.1   Vertical Midspan Deflection

Figure 5.11 shows the shear force versus midspan deflection curves for beams S1-1 to S1-6 which are typical for the test beams.

All the beams indicated a loss of stiffness as the shear force increased. This loss of stiffness was caused by the flexure and shear cracks propagating in the beams.

109
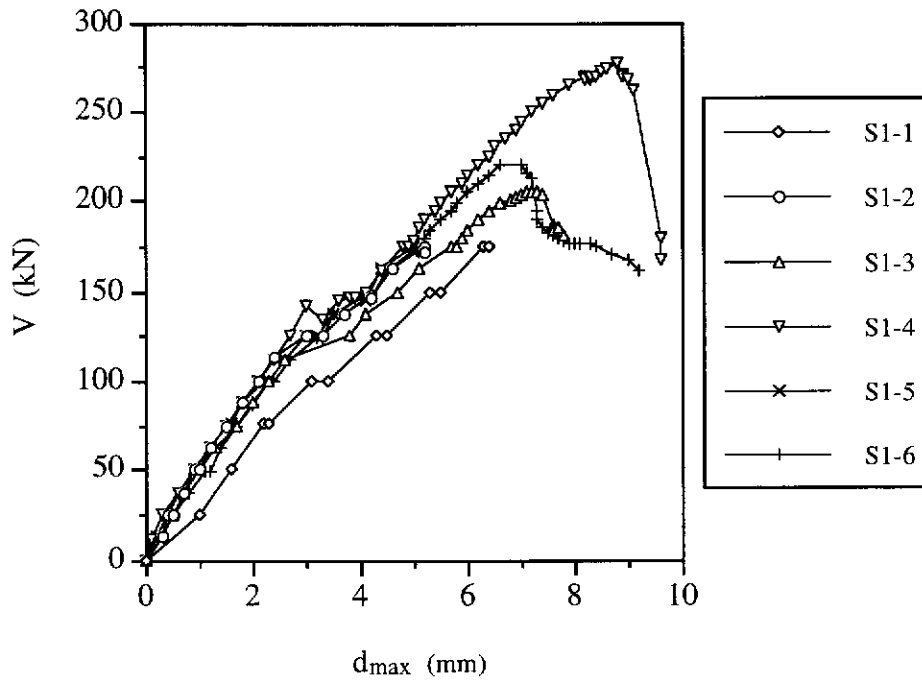
Figure 5.11   Shear Force versus Midspan Deflection for Series 1

For the prediction of the midspan deflection, Branson's formula (Warner, Rangan and Hall (1989)) was used to estimate the effective stiffness of the beam when determining the deflection component due to flexure. The shear strain $\gamma_{\ell t}$ from the present theory was assumed to apply to the whole shear span. Therefore, the deflection component due to shear was calculated as ($0.5\gamma_{\ell t}a$). The total midspan deflection was equal to the sum of the deflection contributions from shear and flexure. A detailed discussion and derivation of the formula for predicting the midspan deflection is given in Appendix C.

Theoretical and experimental shear force versus midspan deflection curves for all the test beams are compared in Appendix C.

5.2.3.2 Curvature of Test Beams

The curvature measurements were influenced by cracking. Figure 5.12 shows typical shear force versus curvature curves.

Curvature was measured in both the left hand side and right hand side shear spans.
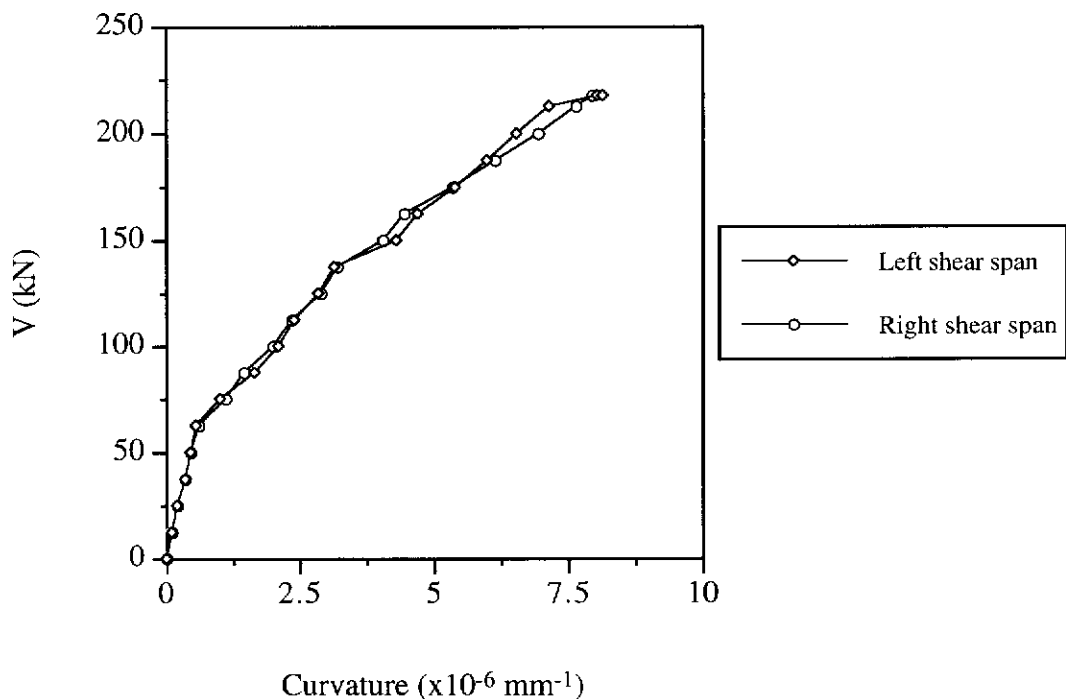
Figure 5.12 Shear Force versus Curvature of Beam S2-4

Most of the beams behaved similar to beam S2-4 where the curvature on both shear spans increased continuously until failure (Figure 5.12).

Test shear force versus curvature curves for all the beams are given in Appendix D.

5.2.3.3   Strains in Longitudinal Tensile Bars

Figures 5.13 and 5.14 show some typical curves of shear force versus strains in longitudinal tensile bars. The data from other beams were similar.

Test shear force versus tensile steel strains for the beams are given in Appendix E.

5.3   Correlation Of Test Results With Predictions By Theory

5.3.1   Shear Strength of Beams

The shear strength of test beams was calculated using the theory presented in Chapter 3. The specimens from previous investigations were included in the strength comparisons. The test results of the previous studies were given in Chapter 2.

Only beams that failed in shear were considered.

Before studying the correlation between measured and predicted shear strengths, the following points need attention:

- The concrete compressive strength of test beams from various investigations ranged from 20.7 MPa (beam G6 tested by Elzanaty, Nilson and Slate (1986)) to 125.3 MPa (beam 10 tested by Roller and Russell (1990)).

- Nearly all the test beams were simply supported and loaded by one or two concentrated loads. The critical section for shear failure was taken to be at a distance d_0 from the concentrated load in the direction of decreasing bending moment. Only beams with M/Vd_0 ratio at the critical section greater than or
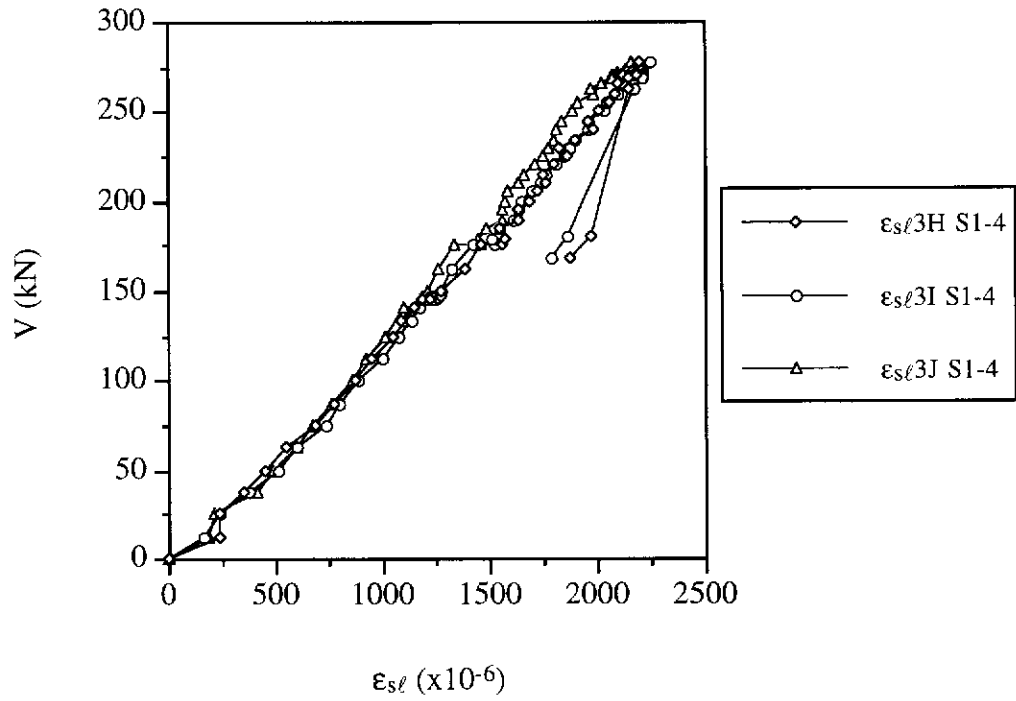
Figure 5.13   Shear Force versus Tensile Steel Strains for Beam S1-4
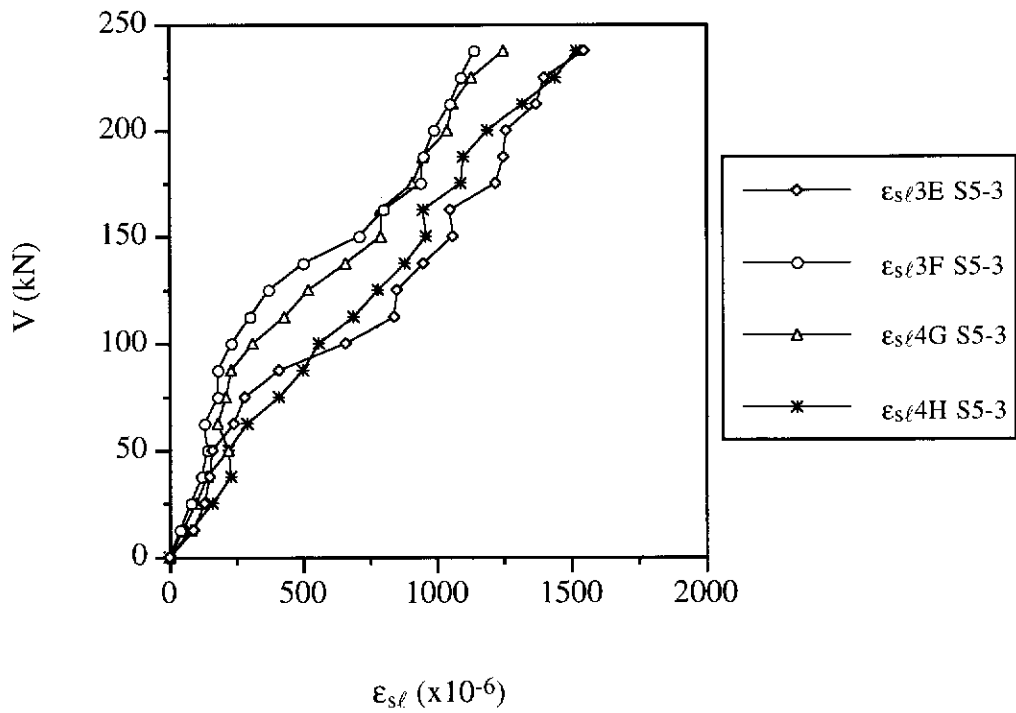
Figure 5.14   Shear Force versus Tensile Steel Strains for Beam S5-3

113

equal to 1.12 were considered (except for beams tested in reverse bending by Watanabe (1993) which had an M/Vd_o ratio of 1.04 and beams reported by Vecchio and Collins (1982) which had a critical section at the zero bending moment section).

In beams with very small M/Vd_o ratio, the failure region is disturbed by the proximity of the load and the support. In such cases, the concept of uniform stress field assumed in the development of the theory presented in Chapter 3 is not valid.

- The beams in Series 6 of the present study were subjected to four concentrated loads. It was observed that the two concentrated loads closest to the supports did not cause much distress in the beams. These loads must have been transferred directly into the supports. The critical section for failure was, therefore, assumed to be a distance d_o from the second (or third) concentrated load from the support.

- Figure 5.15 shows two possible cases of V-$\gamma_{\ell t}$ curves. Curve 1 depicts the usual shear response of a beam where the ultimate shear force, given as V_{u_1}, is greater than the predicted cracking shear, V_{cr}. However, when a beam has a high concrete compressive strength and a small insufficient amount of transverse reinforcement, then it is likely that the V-$\gamma_{\ell t}$ relationship will follow the path of Curve 2 as shown in Figure 5.15, where the ultimate shear capacity V_{u_2} is less than V_{cr}. This behaviour is also more likely to occur when the a/d_o ratio is large and the longitudinal steel area is insufficient to resist the combined effect of bending moment and shear force.

In the present analysis, the test beams with a predicted response similar to Curve 2 were considered to be inadequately detailed and ignored from the correlation study.

114

V

Curve 1 (Adequately detailed)

V_{u_1}

V_{cr}

V_{u_2}

Curve 2 (Inadequately detailed)

$\gamma_{\ell t}$
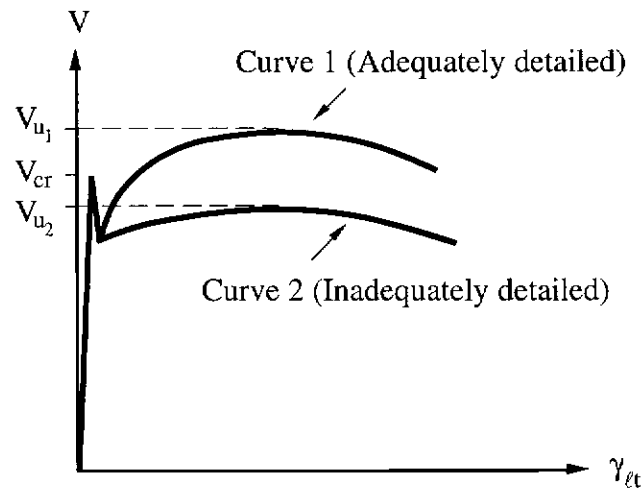
Figure 5.15   Shear Force versus Shear Strain Curves

Comparisons of test shear strength to prediction by the theory are presented in Table 5.3. There were 147 test results altogether. The mean V_e/V_p value of the ultimate shear strengths is 1.23 with a coefficient of variation of 32.8%. The correlation of test versus predicted shear strengths of the beams is shown in Figure 5.16. The majority of the test data fall either within a ±20% band of the ideal 1:1 test shear capacity versus predicted shear capacity line, or above this band.

A summary of correlation is given in Table 5.4.

Only the shear strengths of beams tested by Roller and Russell (1990) are greater than 800 kN. Most of the other results are lumped into the lower region of the graph in Figure 5.16. These results can be seen more clearly if the data points for Roller and Russell are excluded as shown in Figure 5.17.

The mean V_e/V_p value for the five beams reported by Vecchio and Collins (1982) is 1.03 with a coefficient of variation of 3.9%. The theory predicted the shear strength well.

115

Table 5.3 Correlation of Test and Predicted Shear Strengths

Source	Beam Mark	V_e (Experimental) (kN)	V_p (Theory) (kN)	$\dfrac{V_e}{V_p}$
Vecchio and Collins (1982)	SA3	730.0	707.8	1.03
	SK3	725.0	739.9	0.98
	SK4	601.0	597.5	1.01
	SM1	427.0	419.0	1.02
	SP0	436.0	401.7	1.09
Mphonde (1984)	B50-3-3	76.3	82.2	0.93
	B50-7-3	94.1	97.3	0.97
	B50-11-3	98.1	107.8	0.91
	B100-3-3	95.4	112.1	0.85
	B100-7-3	120.8	125.3	0.96
	B100-11-3	152.1	132.3	1.15
	B100-15-3	115.9	135.6	0.85
	B150-3-3	139.3	133.0	1.05
	B150-7-3	133.8	139.4	0.96
	B150-11-3	161.9	145.0	1.12
	B150-15-3	150.3	147.7	1.02
Elzanaty, Nilson and Slate (1986)	G4	150.0	125.8	1.19
	G5	112.0	102.3	1.09
	G6	78.0	94.7	0.82
Johnson and Ramirez (1989)	1	338.5	448.4	0.75
	2	221.9	349.8	0.63
	5	382.7	477.0	0.80
	7	280.8	381.0	0.74
	8	258.1	381.0	0.68
Ganwei and Nielsen (1990)	S-5-A	110.0	105.8	1.04
	S-7-A	140.0	151.0	0.93
	S-7-B	150.0	151.0	0.99
	S-8-A	125.0	133.7	0.93
	S-8-B	135.0	133.7	1.01
Roller and Russell (1990)	2	1099.1	909.7	1.21
	3	1657.5	1470.5	1.13
	4	1942.9	1934.6	1.00
	5	2237.9	2533.7	0.88
	10	1171.7	1246.9	0.94
Sarsam and Al-Musawi (1992)	AL2-N	114.7	95.1	1.21
	AS2-N	189.3	114.5	1.65
	AS2-H	201.0	125.4	1.60
	AS3-N	199.1	131.2	1.52
	AS3-H	199.1	139.6	1.43
	BL2-H	138.3	121.0	1.14
	BS2-H	223.5	137.9	1.62
	BS3-H	228.1	160.6	1.42
	BS4-H	206.9	177.4	1.17
	CL2-H	147.2	133.4	1.10
	CS2-H	247.2	141.5	1.75
	CS3-H	247.2	170.3	1.45
	CS4-H	220.7	194.2	1.14

Continued

116

Table 5.3 Correlation of Test and Predicted Shear Strengths *(Continued)*

| Source	Beam Mark	V_e (Experimental) (kN)	V_p (Theory) (kN)	$\dfrac{V_e}{V_p}$
Watanabe (1993)	PB-1	352.0	329.5	1.07
	PB-2	563.0	486.0	1.16
	PB-3	516.0	453.6	1.14
	PB-4	730.0	710.9	1.03
	B-1	161.0	171.4	0.94
	B-4	338.0	335.1	1.01
	B-5	478.0	416.1	1.15
	B-6	291.0	233.1	1.25
	B-7	435.0	402.1	1.08
	B-8	471.0	525.3	0.90
Gabrielsson (1993)	S2	172.5	124.4	1.39
	S3	210.0	142.8	1.47
	HS1	250.5	234.0	1.07
	HPS1	324.0	238.9	1.36
	HPS2	305.0	241.3	1.26
	HB2	322.0	258.6	1.25
Xie et al. (1994)	NNW-3	87.2	95.5	0.91
	NHW-3	102.6	126.1	0.81
	NHW-3a	108.5	133.4	0.81
	NHW-3b	122.8	141.4	0.87
	NHW-4	94.0	108.8	0.86
Thirugnanasundra-lingam et al. (1995)	7	111.0	157.5	0.70
	8	206.0	148.9	1.38
	9	113.0	142.2	0.79
Kriski and Loov (1996)	1	249.0	252.9	0.98
	2	383.5	265.4	1.44
	3	224.5	252.9	0.89
	4	444.5	274.7	1.62
	5	293.0	268.0	1.09
	6	331.0	284.9	1.16
	11	512.0	336.1	1.52
	12	594.5	333.0	1.79
Tests at Curtin University (1993)	A11	270.0	145.8	1.85
	A12	313.0	165.9	1.89
	A13	292.0	179.5	1.63
	A14	262.0	163.9	1.60
	A15	270.0	183.9	1.47
	B12	496.0	185.6	2.67
	B13	401.0	208.5	1.92
	B14	385.0	182.7	2.11
	B15	403.0	217.2	1.86
	C11	459.0	170.5	2.69
	C13	447.0	239.6	1.87
	C14	364.0	192.7	1.89
	C15	416.0	227.2	1.83
	D12	443.0	193.9	2.28
	D13	505.0	215.7	2.34
	D14	499.0	191.2	2.61
	D15	508.0	224.5	2.26
	B21	221.0	152.2	1.45
	B22	237.0	169.2	1.40
	B24	255.0	167.5	1.52
	C21	256.0	165.4	1.55
	C22	311.0	189.5	1.64
	C23	379.0	207.7	1.82
	C24	301.0	186.7	1.61
	D21	256.0	173.9	1.47
	D22	290.0	197.8	1.47
	D23	344.0	219.6	1.57
	D24	295.0	195.1	1.51
	D25	404.0	228.3	1.77

Continued

117

Table 5.3 Correlation of Test and Predicted Shear Strengths *(Continued)*

Source	Beam Mark	V_e (Experimental) (kN)	V_p (Theory) (kN)	$\dfrac{V_e}{V_p}$
	S1-1	228.3	237.9	0.96
	S1-2	208.3	237.9	0.88
	S1-3	206.1	237.9	0.87
	S1-4	277.9	237.9	1.17
	S1-5	253.3	237.9	1.06
	S1-6	224.1	237.9	0.94
	S2-1	260.3	215.0	1.21
	S2-2	232.5	227.4	1.02
	S2-3	253.3	242.4	1.04
	S2-4	219.4	242.4	0.91
	S2-5	282.1	262.7	1.07
	S3-3	228.6	216.9	1.05
	S3-4	174.9	216.9	0.81
	S3-5	296.6	234.6	1.26
	S3-6	282.9	234.6	1.21
	S4-1	354.0	483.1	0.73
	S4-2	572.8	386.7	1.48
	S4-3	243.4	300.7	0.81
	S4-4	258.1	249.1	1.04
Present	S4-6	202.9	166.6	1.22
Study	S5-1	241.7	232.7	1.04
	S5-2	259.9	241.9	1.07
	S5-3	243.8	250.0	0.98
	S6-3	178.4	213.6	0.84
	S6-4	214.4	213.6	1.00
	S6-5	297.0	233.6	1.27
	S6-6	287.2	233.6	1.23
	S7-1	217.2	232.1	0.94
	S7-2	205.4	246.2	0.83
	S7-3	246.5	267.5	0.92
	S7-4	273.6	289.0	0.95
	S7-5	304.4	300.9	1.01
	S7-6	310.6	314.4	0.99
	S8-1	272.1	216.3	1.26
	S8-2	250.9	228.5	1.10
	S8-3	309.6	243.4	1.27
	S8-4	265.8	243.4	1.09
	S8-5	289.2	259.0	1.12
	S8-6	283.9	268.6	1.06
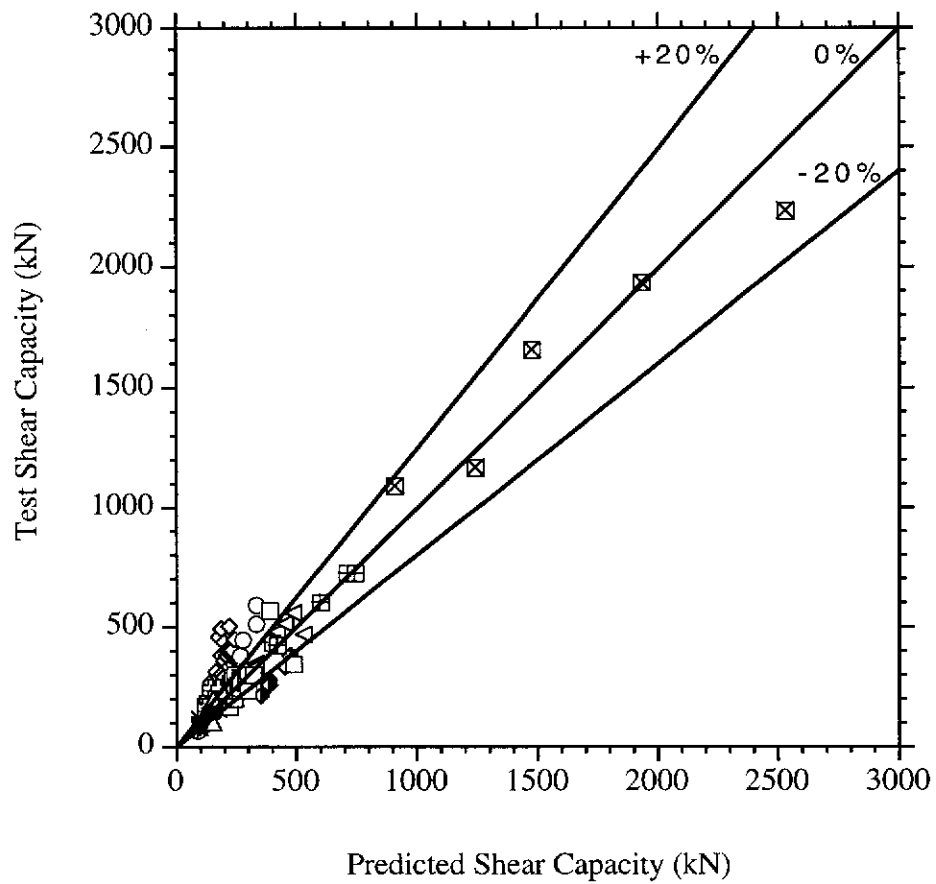
⊞	Vecchio and Collins	◁	Watanabe
⊕	Mphonde	▷	Gabrielsson
✕	Elzanaty et al.	▽	Xie et al.
◈	Johnson and Ramirez	△	Thirugnanasundralingam et al.
+	Ganwei and Nielsen	○	Kriski and Loov
⊠	Roller and Russell	◇	Tests at Curtin University
✢	Sarsam and Al-Musawi	□	Present Study

Figure 5.16   Correlation of Test and Predicted Shear Strengths

Table 5.4 Summary of Correlation

Source	Number of Beam Specimens	$\frac{V_e}{V_p}$ Ratio	
		Mean	Coefficient of Variation
Vecchio and Collins (1982)	5	1.03	3.9%
Mphonde (1984)	11	0.98	10.1%
Elzanaty, Nilson and Slate (1986)	3	1.03	18.5%
Johnson and Ramirez (1989)	5	0.72	9.2%
Ganwei and Nielsen (1990)	5	0.98	5.0%
Roller and Russell (1990)	5	1.03	13.2%
Sarsam and Al-Musawi (1992)	13	1.40	16.0%
Watanabe (1993)	10	1.07	10.0%
Gabrielsson (1993)	6	1.30	10.7%
Xie et al. (1994)	5	0.85	5.0%
Thirugnanasundralingam et al. (1995)	3	0.96	38.6%
Kriski and Loov (1996)	8	1.31	24.9%
Tests at Curtin University (1993)	29	1.85	20.6%
Present Study	39	1.04	15.4%
All Test Data	147	1.23	32.8%

For the beams tested by Mphonde (1984), the mean V_e/V_p value is 0.98 with a coefficient of variation of 10.1%. Beam B50-15-3 was inadequately detailed and the predicted V_{cr} and V_u values were 122.6 and 116.9 kN respectively. Therefore, this beam was not considered in the correlation of test and predicted shear strengths.

For the beams tested by Elzanaty, Nilson and Slate (1986), the prediction by the theory was more conservative for beam G4 with the highest concrete compressive strength of 62.8 MPa than for beam G6 with the lowest concrete compressive strength of 20.7 MPa. The overall mean V_e/V_p value is 1.03 for the three beams tested, with a fairly large a coefficient of variation of 18.5%.
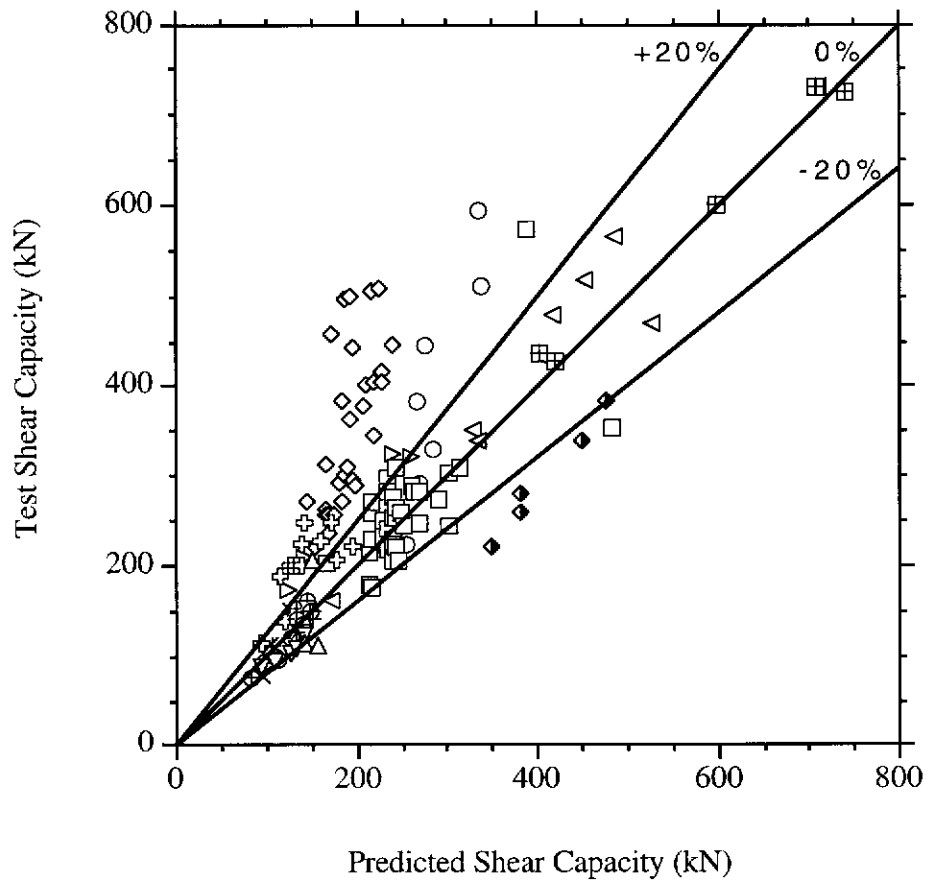
120

⊞	Vecchio and Collins	▷	Gabrielsson
⊕	Mphonde	∇	Xie et al.
×	Elzanaty et al.	△	Thirugnanasundralingam et al.
◈	Johnson and Ramirez	○	Kriski and Loov
+	Ganwei and Nielsen	◇	Tests at Curtin University
✛	Sarsam and Al-Musawi	□	Present Study
◁	Watanabe		

Figure 5.17   Correlation of Test and Predicted Shear Strengths

The specimens tested by Johnson and Ramirez (1989) gave a mean V_e/V_p value of 0.72 with a coefficient of variation of 9.2%. The theory over-predicted the shear strengths most severely in this set of data. A primary reason for the lower shear strength of these beams may be the attachment of as many as 18 strain gauges on the stirrups and longitudinal bars. Excessive number of these gauges might have debonded the steel reinforcement. These gauges might have also served as initiators of cracking and failure regions, which might have decreased the shear strength. Beams 3 and 4 were identical beams which were inadequately detailed with $V_{cr} = 432.9$ kN and $V_u = 414.4$ kN; and were not included in the correlation analysis.

For the beams reported by Ganwei and Nielsen (1990), the theory predicted the test strengths well, with a mean V_e/V_p value of 0.98 and a coefficient of variation of 5.0%.

The beams tested by Roller and Russell (1990) had fairly deep sections which gave some of the largest shear capacities compared to all other beams reported here. The mean V_e/V_p value is 1.03 for these beams, with a coefficient of variation of 13.2%. Beams 1, 6, 7, 8 and 9 were inadequately detailed with V_{cr} values of 647.7, 915.8, 918.1, 1207.9 and 1207.9 kN, and V_u values of 469.6, 736.3, 880.4, 876.9 and 1073.2 kN respectively. These beams were excluded from the correlation analysis.

For the beams tested by Sarsam and Al-Musawi, the mean V_e/V_p value is 1.40 with a coefficient of variation of 16.0%. The test results were conservative when compared with predictions from the theory. The small M/Vd_0 ratio of 1.50 contributed significantly to the conservative shear strengths of this set of beams. The beams with M/Vd_0 ratio of 3.00 (i.e., AL2-N, BL2-H and CL2-H) gave V_e/V_p values which were closer to 1.0 than the other beams with M/Vd_0 ratio of 1.50. Beam AL2-H was inadequately detailed with a V_{cr} value of 109.0 kN and a V_u value of 101.7 kN. This beam was excluded from the correlation of test and predicted shear strengths.

The beams tested by Watanabe (1993) under anti-symmetric moment distribution gave a mean V_e/V_p value of 1.07 with a coefficient of variation of 10.0%. The theory predicted the shear strength quite well for this set of beams.

The predictions for the beams tested by Gabrielsson (1993) were conservative with a mean V_e/V_p value of 1.30 and a coefficient of variation of 10.7%.

The beams tested by Xie et al. (1994) gave a mean V_e/V_p value of 0.85 and a coefficient of variation of 5.0%. The predictions were slightly unconservative.

There is much variation in the results for beams tested by Thirugnanasundralingam et al. (1995). The mean V_e/V_p value is 0.96 with a large coefficient of variation of 38.6%. The inconsistency in the test results may have been due to the low M/Vd_o ratio of 1.34.

For beams tested by Kriski and Loov (1996), the mean V_e/V_p value is 1.31 with a coefficient of variation of 24.9%. The predictions were conservative, particularly for beams 4, 6, 11 and 12, with an M/Vd_o ratio of 1.17. Beams 7, 8, 9 and 10 were inadequately detailed with V_{cr} values of 318.0, 325.4, 323.7 and 322.2 kN, and V_u values of 290.6, 313.0, 292.3 and 312.0 kN respectively; and were ignored in the correlation analysis.

Tests at Curtin University (1993) gave the most conservative results with a mean V_e/V_p value of 1.85 and a coefficient of variation of 20.6%. The large shear capacities were mainly due to beams with M/Vd_o ratios of 1.16 or 1.17. The scatter in the results may have been due to the small amount of shear reinforcement used in many beams, particularly those with less than the minimum shear reinforcement according to the AS 3600 method (i.e., beams A11, C11, B21, C21 and D21). In addition, the scatter was more pronounced in beams with the smaller M/Vd_o ratios of 1.16 or 1.17 than in beams with M/Vd_o ratios of 2.66 to 2.68.

The mean V_e/V_p value for the present study is 1.04 with a coefficient of variation of 15.4%. The theory predicted these test results well. Two pairs of identical beams, S3-1 and S3-2, and S6-1 and S6-2, were inadequately detailed with predicted V_{cr} values of 181.0 and 183.0 kN, and V_u values of 176.5 and 170.1 kN respectively. These beams were ignored in the correlation analysis. It is also noted that beams S6-1 and S6-2 were also excluded due to flexure failure.

In order to consider the effects of certain parameters on the predictions from the theory, the V_e/V_p values were grouped according to different categories of concrete compressive strength, amount of shear reinforcement and M/Vd_0 ratio. The results of the analysis are summarised in Table 5.5. Since the previous tests at Curtin University (1993) gave over-conservative results, the correlation analysis was performed not only for all the test results, but also after excluding this set of results (Table 5.5).

Table 5.5   Test Shear Strength/Predicted Shear Strength Values

| Parameter | Category | V_e/V_p Ratio | | | | | |
| | | All Test Results | | | Excluding Previous Tests at Curtin University (1993) | | |
		n	Mean	C.O.V.	n	Mean	C.O.V.
Conc. Compressive	$f_c < 50$ MPa	29	1.24	41.7%	25	1.06	23.9%
Strength	$f_c \geq 50$ MPa	118	1.23	30.5%	93	1.09	20.9%
Amount of	$A_{sv}/A_{sv.min} < 1.0$	9	1.37	46.7%	4	0.83	16.6%
Shear	$1.0 \leq A_{sv}/A_{sv.min} < 2.0$	78	1.27	33.4%	60	1.10	23.4%
Reinforcement	$A_{sv}/A_{sv.min} \geq 2.0$	60	1.17	28.2%	54	1.08	18.3%
Moment-to-Shear	$1.0 < M/Vd_0 < 2.0$	101	1.27	35.3%	84	1.11	23.0%
Ratio	$M/Vd_0 \geq 2.0$	46	1.16	24.3%	34	1.02	14.4%

Note: $A_{sv.min}$ refers to the minimum shear reinforcement given by Equation 2.14.

n is the number of beam specimens.

C.O.V. is the coefficient of variation.

From Table 5.5, it can be seen that f_c did not have a significant effect on the V_e/V_p values. The predictions were conservative for $f_c < 50$ MPa and $f_c \geq 50$ MPa.

124

The amount of shear reinforcement had a significant influence on the V_e/V_p values when the previous tests at Curtin University (1993) were not considered. When the amount of shear reinforcement used was less than the minimum amount required by the AS 3600 method, the predicted shear strength of a beam could be unconservative. For greater amount of shear reinforcement $(1.0 \leq A_{sv}/A_{sv.min} < 2.0$ or $A_{sv}/A_{sv.min} \geq 2.0)$, the theory gave conservative predictions of shear strength.

The M/Vd_o ratio had a discernible effect on the V_e/V_p values. The theory gave generally more conservative predictions for beams with small M/Vd_o ratios in the range of $1.0 < M/Vd_o < 2.0$ than for more slender beams with $M/Vd_o \geq 2.0$.

The previous tests at Curtin University (1993) contributed to the large scatter in the overall set of test results.

5.3.2   Load-Deformation Behaviour

The deformations from the theory could not be compared directly to test results from the present study. Firstly, the surface strains from the tests were affected by the development of cracks. Therefore, test shear strains could not be determined. Secondly, the predicted longitudinal steel strains from the theory are based on a smeared steel concept and these strains cannot be compared to the strains measured on the longitudinal tensile bars. Thirdly, the theory does not predict the deflection of beams although this was measured in the tests. However, when combined with Branson's method as described earlier, the midspan deflection for each beam was predicted. Figure 5.18 shows the comparison of a typical midspan deflection curve with the predicted curve. Other curves are given in Appendix C.

The midspan deflection was measured at the front and back faces of the beam. The predicted curve in Figure 5.18 is fairly close to the test curves although it shows greater stiffness compared to the test curves.

125

The deformation predicted by the theory can be compared with test results given by Vecchio and Collins (1982). Figures 5.19 to 5.23 compare shear force versus shear strain (V-$\gamma_{\ell t}$) test graphs with the predictions by the present theory and the Modified Compression Field Theory (Vecchio and Collins (1982)). The present theory predicted the V-$\gamma_{\ell t}$ relationships well for these beams.

5.4 Correlation Of Test Shear Strength With Predictions By Codes

Various code provisions for shear strength of concrete beams were described in Chapter 2. The experimental shear strengths of the 147 beams tested in the present study and previous investigations are compared to the predictions by the following:

    (i)   Australian Standard AS 3600

    (ii)   American Concrete Institute Building Code ACI 318-95

    (iii)   Eurocode EC2 Part 1

    (iv)   Canadian Standard CSA A23.3-94

The comparisons of test shear strengths to predictions by the AS 3600 and ACI 318-95 codes are given in Table 5.6. Similar comparisons with respect to the EC2 Part 1 and CSA A23.3-94 codes are given in Table 5.7. A summary of the correlation is given in Table 5.8.

The summary of correlation in Table 5.8 indicates significant scatter in the predictions by the codes. For the six methods of prediction, the coefficient of variation ranged from 36.2% (AS 3600) to 55.9% (Variable Strut Inclination Method of EC2 Part 1).

AS 3600 gave the best prediction with the smallest scatter. The mean V_e/V_p value is 1.22 with a coefficient of variation of 36.2%. Figures 5.24 and 5.25 show the correlation of test versus predicted shear strengths for this code method.

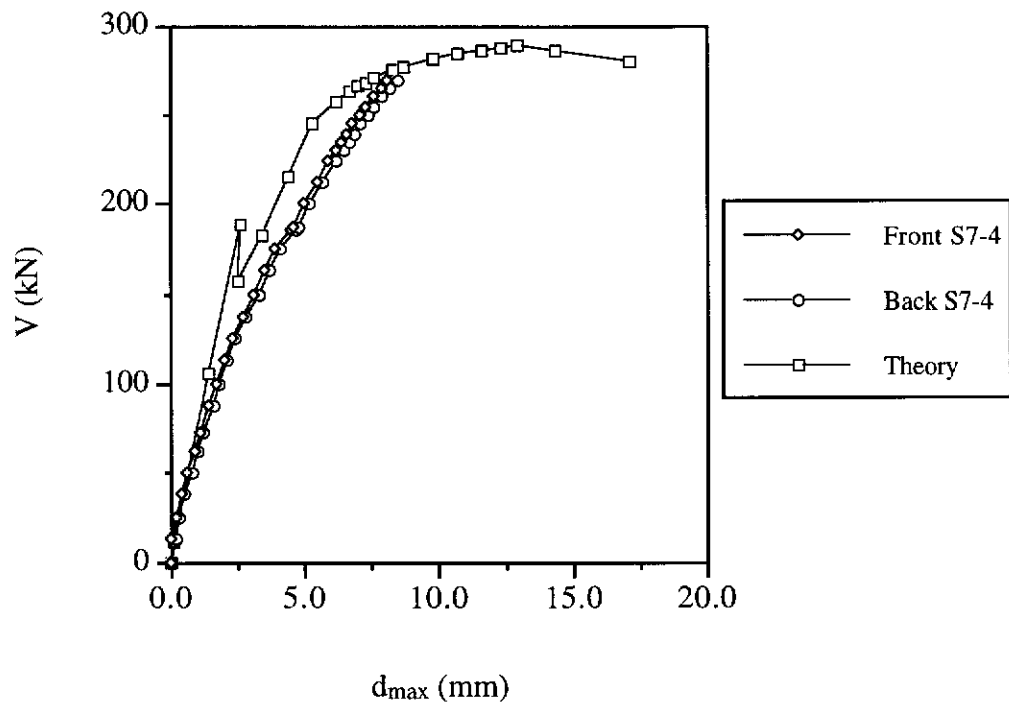**Figure 5.18   Test versus Predicted Midspan Deflection for Beam S7-4**
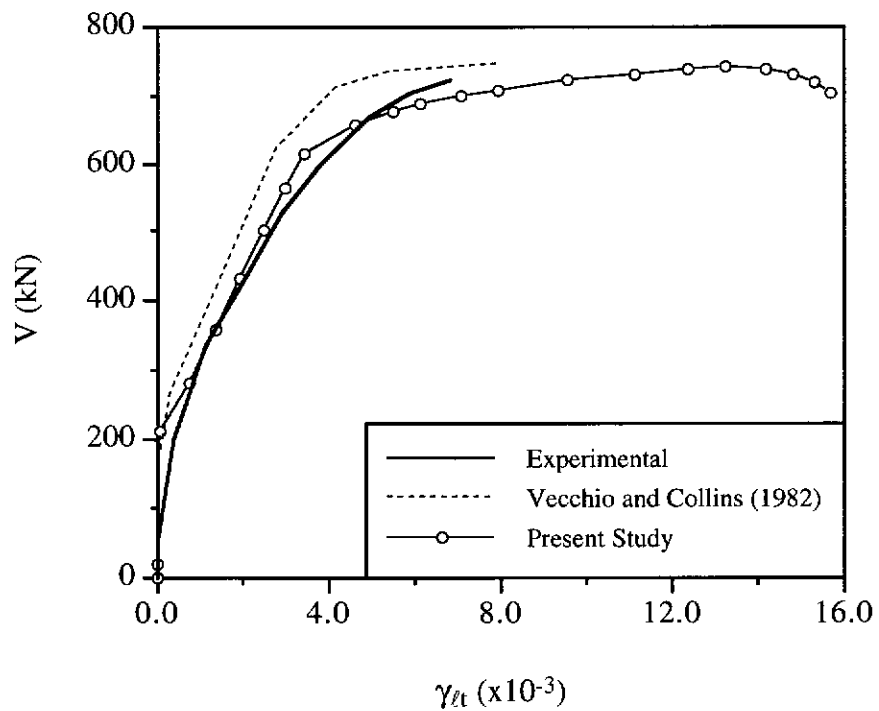

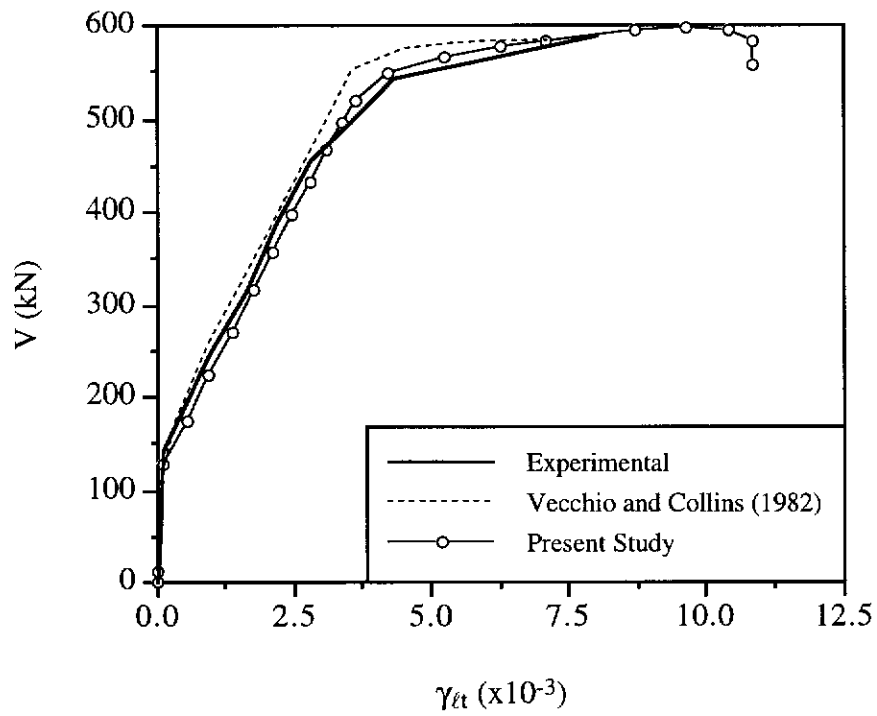**Figure 5.19   Shear Force versus Shear Strain for Beam SK3**

127

Figure 5.20 Shear Force versus Shear Strain for Beam SK4
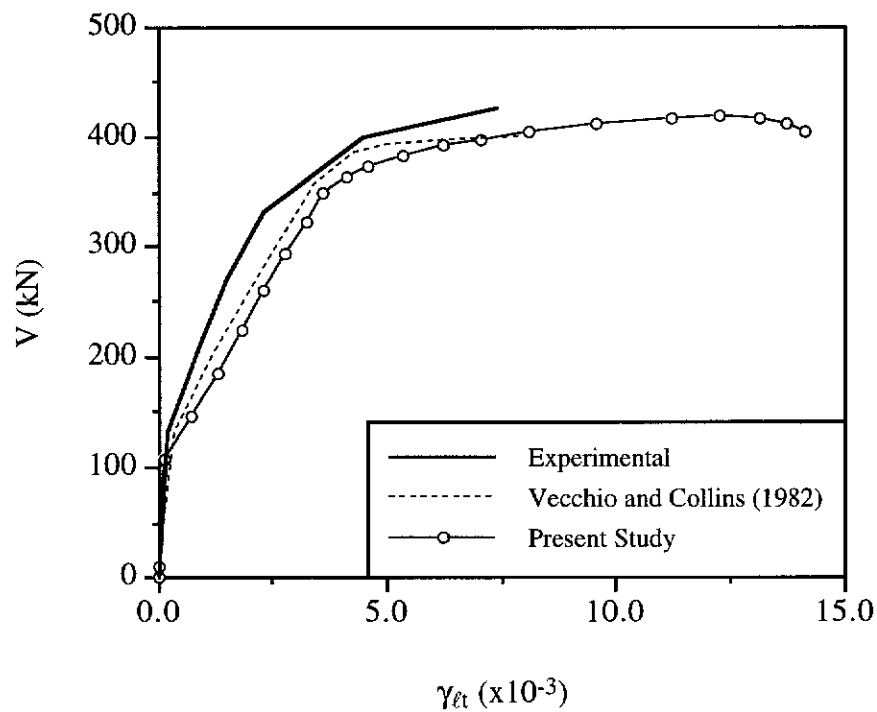

Figure 5.21 Shear Force versus Shear Strain for Beam SM1
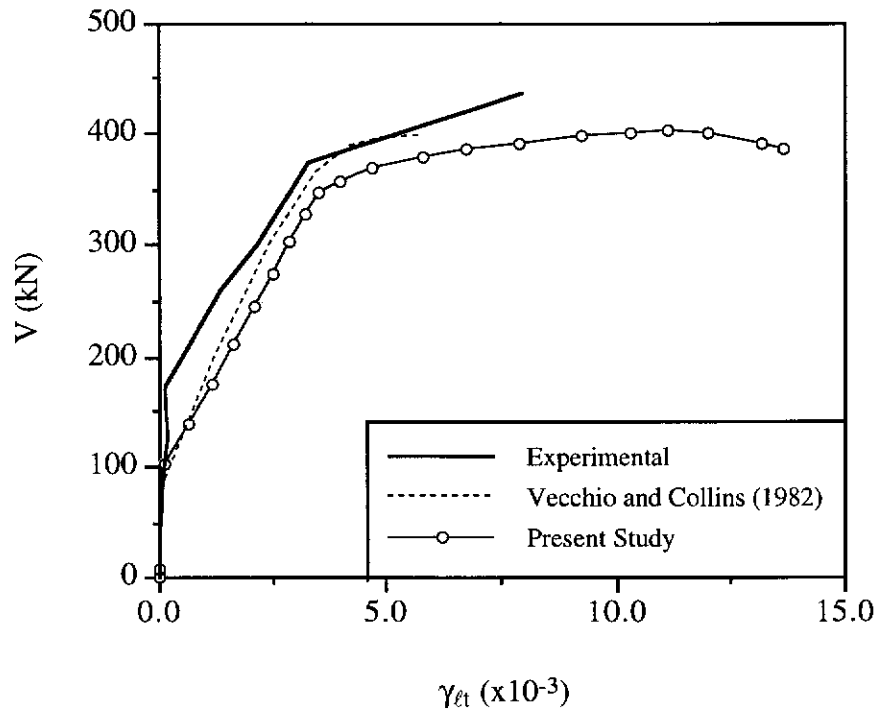
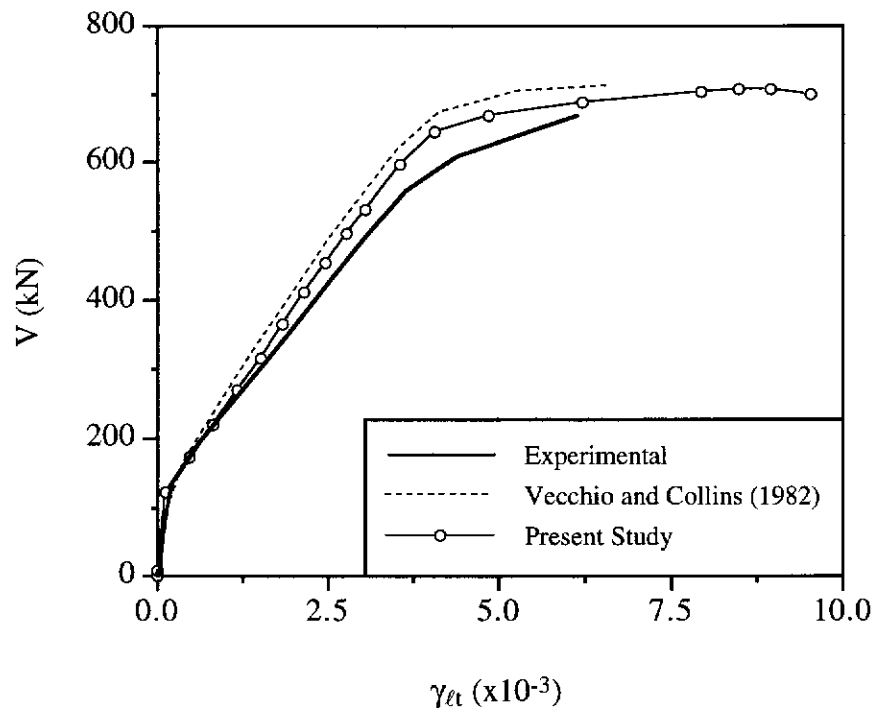**Figure 5.22   Shear Force versus Shear Strain for Beam SP0**

Figure 5.23   Shear Force versus Shear Strain for Beam SA3

129

Table 5.6 Correlation of Test and Predicted Shear Strengths

Beam Mark	V_e (Exp) (kN)	V_p (AS 3600) (kN)	$\dfrac{V_e}{V_p}$	V_p (ACI) (kN)	$\dfrac{V_e}{V_p}$
Vecchio and Collins	*(1982)*				
SA3	730.0	646.7	1.13	534.2	1.37
SK3	725.0	666.0	1.09	488.0	1.49
SK4	601.0	533.6	1.13	429.1	1.40
SM1	427.0	378.7	1.13	291.7	1.46
SP0	436.0	363.3	1.20	291.4	1.50
Mphonde	*(1984)*				
B50-3-3	76.3	85.6	0.89	52.3	1.46
B50-7-3	94.1	98.6	0.95	64.7	1.45
B50-11-3	98.1	108.8	0.90	75.6	1.30
B100-3-3	95.4	115.3	0.83	72.9	1.31
B100-7-3	120.8	129.2	0.93	85.1	1.42
B100-11-3	152.1	139.9	1.09	96.0	1.58
B100-15-3	115.9	145.3	0.80	101.9	1.14
B150-3-3	139.3	138.6	1.01	89.7	1.55
B150-7-3	133.8	154.0	0.87	101.0	1.32
B150-11-3	161.9	166.6	0.97	112.7	1.44
B150-15-3	150.3	172.2	0.87	118.5	1.27
Elzanaty et al.	*(1986)*				
G4	150.0	142.1	1.06	95.2	1.58
G5	112.0	122.1	0.92	82.2	1.36
G6	78.0	105.4	0.74	67.8	1.15
Johnson and Ramirez	*(1989)*				
1	338.5	398.0	0.85	291.5	1.16
2	221.9	295.5	0.75	230.0	0.96
5	382.7	430.7	0.89	331.6	1.15
7	280.8	318.0	0.88	261.6	1.07
8	258.1	318.0	0.81	261.6	0.99
Ganwei and Nielsen	*(1990)*				
S-5-A	110.0	128.6	0.86	86.7	1.27
S-7-A	140.0	176.2	0.79	106.2	1.32
S-7-B	150.0	176.2	0.85	106.2	1.41
S-8-A	125.0	141.6	0.88	83.0	1.51
S-8-B	135.0	141.6	0.95	83.0	1.63
Roller and Russell	*(1990)*				
2	1099.1	1035.7	1.06	755.0	1.46
3	1657.5	1848.4	0.90	1171.0	1.42
4	1942.9	2411.9	0.81	1514.6	1.28
5	2237.9	3169.8	0.71	1972.1	1.13
10	1171.7	1238.4	0.95	1023.7	1.14
Sarsam and Al-Musawi	*(1992)*				
AL2-N	114.7	115.2	1.00	78.0	1.47
AS2-N	189.3	114.4	1.65	77.2	2.45
AS2-H	201.0	129.6	1.55	93.5	2.15
AS3-N	199.1	139.4	1.43	94.2	2.11
AS3-H	199.1	155.8	1.28	109.5	1.82
BL2-H	138.3	135.9	1.02	94.0	1.47
BS2-H	223.5	135.2	1.65	93.3	2.40
BS3-H	228.1	161.2	1.42	109.2	2.09
BS4-H	206.9	188.8	1.10	127.8	1.62
CL2-H	147.2	139.7	1.05	91.7	1.61
CS2-H	247.2	139.8	1.77	91.7	2.70
CS3-H	247.2	167.6	1.47	109.6	2.26
CS4-H	220.7	192.9	1.14	126.0	1.75

Continued

130

Table 5.6 Correlation of Test and Predicted Shear Strengths (*Continued*)

Beam Mark	V_e (Exp) (kN)	V_p (AS 3600) (kN)	$\dfrac{V_e}{V_p}$	V_p (ACI) (kN)	$\dfrac{V_e}{V_p}$
Watanabe	*(1993)*				
PB-1	352.0	325.2	1.08	204.7	1.72
PB-2	563.0	531.8	1.06	361.4	1.56
PB-3	516.0	486.5	1.06	323.4	1.60
PB-4	730.0	887.4	0.82	802.6	0.91
B-1	161.0	164.2	0.98	105.1	1.53
B-4	338.0	352.0	0.96	279.4	1.21
B-5	478.0	410.7	1.16	611.4	0.78
B-6	291.0	227.3	1.28	148.2	1.96
B-7	435.0	447.6	0.97	337.3	1.29
B-8	471.0	595.4	0.79	676.0	0.70
Gabrielsson	*(1993)*				
S2	172.5	128.7	1.34	82.4	2.09
S3	210.0	154.2	1.36	100.1	2.10
HS1	250.5	237.2	1.06	160.0	1.57
HPS1	324.0	233.9	1.39	154.4	2.10
HPS2	305.0	235.9	1.29	156.3	1.95
HB2	322.0	258.9	1.24	164.6	1.96
Xie et al.	*(1994)*				
NNW-3	87.2	111.9	0.78	69.6	1.25
NHW-3	102.6	142.0	0.72	85.0	1.21
NHW-3a	108.5	158.6	0.68	94.6	1.15
NHW-3b	122.8	179.9	0.68	108.1	1.14
NHW-4	94.0	142.2	0.66	85.1	1.10
Thirugnanasun-	*(1995)*				
dralingam et al.					
7	111.0	159.0	0.70	115.0	0.97
8	206.0	145.6	1.41	106.9	1.93
9	113.0	136.5	0.83	101.5	1.11
Kriski and Loov	*(1996)*				
1	249.0	260.4	0.96	183.6	1.36
2	383.5	259.9	1.48	183.0	2.10
3	224.5	260.4	0.86	183.6	1.22
4	444.5	260.4	1.71	183.6	2.42
5	293.0	262.7	1.12	185.9	1.58
6	331.0	268.8	1.23	192.4	1.72
11	512.0	323.4	1.58	260.7	1.96
12	594.5	320.2	1.86	256.2	2.32
Tests at Curtin	*(1993)*				
University					
A11	270.0	136.4	1.98	105.9	2.55
A12	313.0	162.2	1.93	121.3	2.58
A13	292.0	184.3	1.58	135.0	2.16
A14	262.0	159.5	1.64	119.5	2.19
A15	270.0	193.4	1.40	140.5	1.92
B12	496.0	175.9	2.82	121.8	4.07
B13	401.0	198.0	2.03	135.5	2.96
B14	385.0	173.2	2.22	120.0	3.21
B15	403.0	207.1	1.95	141.0	2.86
C11	459.0	161.3	2.85	98.5	4.66
C13	447.0	209.1	2.14	125.3	3.57
C14	364.0	184.3	1.98	111.0	3.28
C15	416.0	218.2	1.91	130.2	3.20
D12	443.0	188.8	2.35	108.5	4.08
D13	505.0	210.4	2.40	121.3	4.16
D14	499.0	186.1	2.68	106.8	4.67
D15	508.0	219.2	2.32	126.4	4.02
B21	221.0	154.4	1.43	111.4	1.98
B22	237.0	180.4	1.31	126.8	1.87
B24	255.0	177.7	1.44	125.0	2.04

Continued

131

Table 5.6 Comparisons of Test to Predicted Shear Strengths (*Continued*)

Beam Mark	V_e (Exp) (kN)	V_p (AS 3600) (kN)	$\dfrac{V_e}{V_p}$	V_p (ACI) (kN)	$\dfrac{V_e}{V_p}$
Tests at Curtin University	*(1993)*				
C21	256.0	165.5	1.55	102.6	2.50
C22	311.0	191.5	1.62	116.8	2.66
C23	379.0	212.5	1.78	128.3	2.95
C24	301.0	188.7	1.60	115.1	2.62
D21	256.0	173.6	1.47	103.2	2.48
D22	290.0	199.5	1.45	117.6	2.47
D23	344.0	221.7	1.55	130.5	2.64
D24	295.0	196.8	1.50	115.9	2.55
D25	404.0	230.9	1.75	135.5	2.98
Present Study					
S1-1	228.3	237.7	0.96	164.2	1.39
S1-2	208.3	237.7	0.88	164.2	1.27
S1-3	206.1	237.7	0.87	164.2	1.26
S1-4	277.9	237.7	1.17	164.2	1.69
S1-5	253.3	237.7	1.07	164.2	1.54
S1-6	224.1	237.7	0.94	164.2	1.36
S2-1	260.3	208.1	1.25	149.2	1.74
S2-2	232.5	222.5	1.04	157.9	1.47
S2-3	253.3	243.9	1.04	170.9	1.48
S2-4	219.4	243.9	0.90	170.9	1.28
S2-5	282.1	278.7	1.01	192.7	1.46
S3-3	228.6	210.0	1.09	148.8	1.54
S3-4	174.9	210.0	0.83	148.8	1.18
S3-5	296.6	226.6	1.31	145.7	2.04
S3-6	282.9	226.6	1.25	145.7	1.94
S4-1	354.0	424.9	0.83	325.2	1.09
S4-2	572.8	363.2	1.58	265.6	2.16
S4-3	243.4	293.8	0.83	206.0	1.18
S4-4	258.1	253.0	1.02	181.2	1.42
S4-6	202.9	178.3	1.14	122.9	1.65
S5-1	241.7	254.2	0.95	182.6	1.32
S5-2	259.9	254.2	1.02	182.6	1.42
S5-3	243.8	254.2	0.96	182.6	1.34
S6-3	178.4	211.0	0.85	149.9	1.19
S6-4	214.4	211.0	1.02	149.9	1.43
S6-5	297.0	227.7	1.30	146.8	2.02
S6-6	287.2	227.7	1.26	146.8	1.96
S7-1	217.2	233.4	0.93	143.6	1.51
S7-2	205.4	248.0	0.83	151.9	1.35
S7-3	246.5	269.6	0.91	164.3	1.50
S7-4	273.6	296.0	0.92	179.8	1.52
S7-5	304.4	314.5	0.97	190.9	1.59
S7-6	310.6	338.8	0.92	205.7	1.51
S8-1	272.1	209.4	1.30	150.7	1.81
S8-2	250.9	223.9	1.12	159.4	1.57
S8-3	309.6	245.3	1.26	172.4	1.80
S8-4	265.8	245.3	1.08	172.4	1.54
S8-5	289.2	271.6	1.06	188.7	1.53
S8-6	283.9	290.0	0.98	200.4	1.42

Table 5.7 Correlation of Test and Predicted Shear Strengths

Beam Mark	V_e (Exp) (kN)	V_p (EC2,S) (kN)	$\dfrac{V_e}{V_p}$	V_p (EC2,V) (kN)	$\dfrac{V_e}{V_p}$	V_p (CAN,S) (kN)	$\dfrac{V_e}{V_p}$	V_p (CAN,G) (kN)	$\dfrac{V_e}{V_p}$
Vecchio and Collins	*(1982)*								
SA3	730.0	508.0	1.44	665.9	1.10	530.3	1.38	667.0	1.09
SK3	725.0	475.2	1.53	763.4	0.95	514.2	1.41	618.0	1.17
SK4	601.0	407.9	1.47	580.8	1.03	444.9	1.35	535.0	1.12
SM1	427.0	280.2	1.52	448.7	0.95	305.5	1.40	361.0	1.18
SP0	436.0	276.7	1.58	423.5	1.03	304.3	1.43	363.0	1.20
Mphonde	*(1984)*								
B50-3-3	76.3	63.3	1.21	36.3	2.10	58.7	1.30	58.0	1.32
B50-7-3	94.1	86.7	1.09	36.3	2.59	73.3	1.28	70.0	1.34
B50-11-3	98.1	109.1	0.90	36.3	2.70	86.1	1.14	78.0	1.26
B100-3-3	95.4	86.0	1.11	72.5	1.32	80.1	1.19	78.0	1.22
B100-7-3	120.8	109.8	1.10	72.5	1.67	94.4	1.28	89.0	1.36
B100-11-3	152.1	132.8	1.15	72.5	2.10	107.3	1.42	97.0	1.57
B100-15-3	115.9	145.8	0.79	72.5	1.60	114.2	1.01	102.0	1.14
B150-3-3	139.3	101.7	1.37	109.0	1.28	97.0	1.44	94.0	1.48
B150-7-3	133.8	123.8	1.08	109.0	1.23	110.3	1.21	101.0	1.32
B150-11-3	161.9	148.3	1.09	109.0	1.49	124.0	1.31	109.0	1.49
B150-15-3	150.3	161.2	0.93	109.0	1.38	130.8	1.15	114.0	1.32
Elzanaty et al.	*(1986)*								
G4	150.0	133.2	1.13	69.6	2.16	106.5	1.41	95.0	1.58
G5	112.0	105.9	1.06	69.6	1.61	91.3	1.23	79.0	1.42
G6	78.0	78.1	1.00	69.6	1.12	74.3	1.05	69.0	1.13
Johnson and Ramirez	*(1989)*								
1	338.5	311.7	1.09	276.4	1.22	321.2	1.05	296.0	1.14
2	221.9	256.4	0.87	138.2	1.61	259.8	0.85	241.0	0.92
5	382.7	378.0	1.01	276.4	1.38	368.4	1.04	326.0	1.17
7	280.8	308.1	0.91	138.2	2.03	260.3	1.08	224.0	1.25
8	258.1	308.1	0.84	138.2	1.87	260.3	0.99	224.0	1.15
Ganwei and Nielsen	*(1990)*								
S-5-A	110.0	118.0	0.93	107.6	1.02	93.5	1.18	83.0	1.33
S-7-A	140.0	131.2	1.07	155.2	0.90	112.8	1.24	105.0	1.33
S-7-B	150.0	131.2	1.14	155.2	0.97	112.8	1.33	105.0	1.43
S-8-A	125.0	110.4	1.13	103.1	1.21	89.6	1.40	87.0	1.44
S-8-B	135.0	110.4	1.22	103.1	1.31	89.6	1.51	87.0	1.55
Roller and Russell	*(1990)*								
2	1099.1	875.5	1.26	864.6	1.27	820.4	1.34	716.0	1.54
3	1657.5	1249.9	1.33	1800.5	0.92	1236.4	1.34	1149.0	1.44
4	1942.9	1559.2	1.25	2573.7	0.75	1580.0	1.23	1512.0	1.28
5	2237.9	1970.9	1.14	3603.1	0.62	2037.6	1.10	2059.0	1.09
10	1171.7	1240.5	0.94	812.4	1.44	1140.7	1.03	942.0	1.24
Sarsam and Al-Musawi	*(1992)*								
AL2-N	114.7	100.4	1.14	72.6	1.58	86.0	1.33	73.0	1.57
AS2-N	189.3	98.8	1.92	72.6	2.61	85.1	2.22	80.0	2.37
AS2-H	201.0	135.8	1.48	71.7	2.80	104.4	1.93	94.0	2.14
AS3-N	199.1	114.8	1.73	109.3	1.82	102.2	1.95	98.0	2.03
AS3-H	199.1	148.4	1.34	109.3	1.82	120.2	1.66	106.0	1.88
BL2-H	138.3	136.5	1.01	72.0	1.92	105.0	1.32	86.0	1.61
BS2-H	223.5	134.8	1.66	72.0	3.10	104.1	2.15	100.0	2.24
BS3-H	228.1	148.9	1.53	108.3	2.11	120.0	1.90	112.0	2.04
BS4-H	206.9	169.4	1.22	143.9	1.44	139.0	1.49	129.0	1.60
CL2-H	147.2	131.1	1.12	72.0	2.04	102.2	1.44	90.0	1.64
CS2-H	247.2	131.2	1.88	72.0	3.43	102.3	2.42	102.0	2.42
CS3-H	247.2	149.6	1.65	108.3	2.28	120.4	2.05	120.0	2.06
CS4-H	220.7	165.3	1.34	143.9	1.53	136.9	1.61	136.0	1.62

Continued

Table 5.7 Correlation of Test and Predicted Shear Strengths (*Continued*)

Beam Mark	V_e (Exp) (kN)	V_p (EC2,S) (kN)	$\dfrac{V_e}{V_p}$	V_p (EC2,V) (kN)	$\dfrac{V_e}{V_p}$	V_p (CAN,S) (kN)	$\dfrac{V_e}{V_p}$	V_p (CAN,G) (kN)	$\dfrac{V_e}{V_p}$
Watanabe	*(1993)*								
PB-1	352.0	247.4	1.42	306.5	1.15	216.8	1.62	215.0	1.64
PB-2	563.0	388.3	1.45	658.9	0.85	373.4	1.51	336.0	1.68
PB-3	516.0	354.2	1.46	573.5	0.90	335.5	1.54	327.0	1.58
PB-4	730.0	785.5	0.93	908.7	0.80	403.0	1.81	697.0	1.05
B-1	161.0	127.3	1.26	130.3	1.24	113.5	1.42	116.0	1.39
B-4	338.0	284.1	1.19	377.2	0.90	277.7	1.22	262.0	1.29
B-5	478.0	444.9	1.07	444.9	1.07	277.7	1.72	445.0	1.07
B-6	291.0	178.5	1.63	205.6	1.42	158.2	1.84	154.0	1.89
B-7	435.0	348.7	1.25	511.7	0.85	334.4	1.30	282.0	1.54
B-8	471.0	645.0	0.73	639.0	0.74	334.4	1.41	587.0	0.80
Gabrielsson	*(1993)*								
S2	172.5	115.1	1.50	86.2	2.00	90.2	1.91	83.0	2.08
S3	210.0	139.0	1.51	114.7	1.83	108.8	1.93	95.0	2.21
HS1	250.5	209.8	1.19	180.4	1.39	174.1	1.44	157.0	1.60
HPS1	324.0	212.3	1.53	176.7	1.83	167.8	1.93	161.0	2.01
HPS2	305.0	216.9	1.41	176.7	1.73	170.0	1.79	163.0	1.87
HB2	322.0	225.2	1.43	211.7	1.52	177.0	1.82	183.0	1.76
Xie et al.	*(1994)*								
NNW-3	87.2	83.2	1.05	92.1	0.95	74.7	1.17	72.0	1.21
NHW-3	102.6	118.9	0.86	93.5	1.10	92.7	1.11	88.0	1.17
NHW-3a	108.5	124.6	0.87	119.2	0.91	101.9	1.06	97.0	1.12
NHW-3b	122.8	141.5	0.87	143.0	0.86	116.0	1.06	108.0	1.14
NHW-4	94.0	119.3	0.79	93.5	1.01	92.8	1.01	80.0	1.18
Thirugnanasun-dralingam et al.	*(1995)*								
7	111.0	168.2	0.66	90.5	1.23	128.2	0.87	123.0	0.90
8	206.0	160.9	1.28	72.4	2.85	120.1	1.71	113.0	1.82
9	113.0	156.1	0.72	60.2	1.88	114.7	0.99	110.0	1.03
Kriski and Loov	*(1996)*								
1	249.0	217.2	1.15	157.6	1.58	203.6	1.22	189.0	1.32
2	383.5	216.1	1.77	157.6	2.43	202.9	1.89	194.0	1.98
3	224.5	217.2	1.03	157.6	1.42	203.6	1.10	189.0	1.19
4	444.5	240.5	1.85	157.6	2.82	203.6	2.18	201.0	2.21
5	293.0	221.4	1.32	157.6	1.86	206.3	1.42	197.0	1.49
6	331.0	259.3	1.28	157.6	2.10	214.0	1.55	210.0	1.58
11	512.0	417.3	1.23	157.6	3.25	294.3	1.74	265.0	1.93
12	594.5	406.2	1.46	157.6	3.77	289.0	2.06	261.0	2.28
Tests at Curtin University	*(1993)*								
A11	270.0	165.7	1.63	57.8	4.67	118.9	2.27	95.0	2.84
A12	313.0	179.5	1.74	92.5	3.38	135.5	2.31	126.0	2.48
A13	292.0	191.9	1.52	123.3	2.37	149.2	1.96	138.0	2.12
A14	262.0	177.5	1.48	89.0	2.94	133.6	1.96	123.0	2.13
A15	270.0	195.9	1.38	136.8	1.97	154.5	1.75	144.0	1.88
B12	496.0	182.0	2.73	92.5	5.36	136.1	3.64	139.0	3.57
B13	401.0	194.4	2.06	123.3	3.25	149.8	2.68	153.0	2.62
B14	385.0	179.8	2.14	89.0	4.33	134.2	2.87	137.0	2.81
B15	403.0	197.9	2.04	136.8	2.95	155.1	2.60	159.0	2.53
C11	459.0	147.8	3.11	53.3	8.61	111.7	4.11	102.0	4.50
C13	447.0	171.9	2.60	113.6	3.93	138.5	3.23	148.0	3.02
C14	364.0	158.5	2.30	82.0	4.44	124.2	2.93	131.0	2.78
C15	416.0	175.1	2.38	126.0	3.30	143.3	2.90	152.0	2.74
D12	443.0	151.2	2.93	86.7	5.11	120.8	3.67	131.0	3.38
D13	505.0	162.7	3.10	115.5	4.37	133.7	3.78	150.0	3.37
D14	499.0	149.2	3.34	83.4	5.98	119.1	4.19	133.0	3.75
D15	508.0	166.2	3.06	128.2	3.96	138.6	3.67	158.0	3.22
B21	221.0	158.6	1.39	57.8	3.82	125.2	1.77	96.0	2.30
B22	237.0	172.5	1.37	92.5	2.56	141.9	1.67	123.0	1.93
B24	255.0	170.8	1.49	89.0	2.87	140.0	1.82	121.0	2.11

Continued

Table 5.7 Correlation of Test and Predicted Shear Strengths (*Continued*)

Beam Mark	V_e (Exp) (kN)	V_p (EC2,S) (kN)	$\dfrac{V_e}{V_p}$	V_p (EC2,V) (kN)	$\dfrac{V_e}{V_p}$	V_p (CAN,S) (kN)	$\dfrac{V_e}{V_p}$	V_p (CAN,G) (kN)	$\dfrac{V_e}{V_p}$
Tests at Curtin	*(1993)*								
University									
C21	256.0	148.6	1.72	53.3	4.80	116.5	2.20	92.0	2.78
C22	311.0	161.3	1.93	85.2	3.65	130.7	2.38	124.0	2.51
C23	379.0	170.3	2.23	113.6	3.34	142.0	2.67	134.0	2.83
C24	301.0	159.7	1.88	82.0	3.67	129.0	2.33	122.0	2.47
D21	256.0	148.1	1.73	54.2	4.72	117.2	2.18	98.0	2.61
D22	290.0	161.1	1.80	86.7	3.34	131.6	2.20	130.0	2.23
D23	344.0	172.7	1.99	115.5	2.98	144.4	2.38	141.0	2.44
D24	295.0	159.5	1.85	83.4	3.54	129.8	2.27	128.0	2.30
D25	404.0	177.0	2.28	128.2	3.15	149.3	2.71	147.0	2.75
Present Study									
S1-1	228.3	218.5	1.04	146.8	1.56	181.7	1.26	178.0	1.28
S1-2	208.3	218.5	0.95	146.8	1.42	181.7	1.15	178.0	1.17
S1-3	206.1	218.5	0.94	146.8	1.40	181.7	1.13	178.0	1.16
S1-4	277.9	218.5	1.27	146.8	1.89	181.7	1.53	178.0	1.56
S1-5	253.3	218.5	1.16	146.8	1.73	181.7	1.39	178.0	1.42
S1-6	224.1	218.5	1.03	146.8	1.53	181.7	1.23	178.0	1.26
S2-1	260.3	213.5	1.22	97.9	2.66	167.8	1.55	157.0	1.66
S2-2	232.5	221.3	1.05	117.4	1.98	176.5	1.32	168.0	1.38
S2-3	253.3	233.0	1.09	146.8	1.73	189.6	1.34	179.0	1.42
S2-4	219.4	233.0	0.94	146.8	1.49	189.6	1.16	179.0	1.23
S2-5	282.1	252.6	1.12	195.7	1.44	211.3	1.34	199.0	1.42
S3-3	228.6	208.9	1.09	104.7	2.18	166.8	1.37	158.0	1.45
S3-4	174.9	208.9	0.84	104.7	1.67	166.8	1.05	158.0	1.11
S3-5	296.6	204.9	1.45	102.6	2.89	163.4	1.82	165.0	1.80
S3-6	282.9	204.9	1.38	102.6	2.76	163.4	1.73	165.0	1.71
S4-1	354.0	398.9	0.89	263.4	1.34	361.9	0.98	349.0	1.01
S4-2	572.8	345.2	1.66	215.2	2.66	295.6	1.94	285.0	2.01
S4-3	243.4	284.2	0.86	166.9	1.46	229.3	1.06	214.0	1.14
S4-4	258.1	256.0	1.01	146.8	1.76	201.7	1.28	188.0	1.37
S4-6	202.9	183.2	1.11	99.5	2.04	136.7	1.48	128.0	1.59
S5-1	241.7	259.2	0.93	146.8	1.65	203.3	1.19	179.0	1.35
S5-2	259.9	259.2	1.00	146.8	1.77	203.3	1.28	184.0	1.41
S5-3	243.8	259.2	0.94	146.8	1.66	203.3	1.20	190.0	1.28
S6-3	178.4	210.8	0.85	104.7	1.70	168.1	1.06	159.0	1.12
S6-4	214.4	210.8	1.02	104.7	2.05	168.1	1.28	159.0	1.35
S6-5	297.0	207.3	1.43	102.6	2.89	164.7	1.80	166.0	1.79
S6-6	287.2	207.3	1.39	102.6	2.80	164.7	1.74	166.0	1.73
S7-1	217.2	208.5	1.04	93.2	2.33	161.6	1.34	156.0	1.39
S7-2	205.4	216.0	0.95	111.8	1.84	169.9	1.21	167.0	1.23
S7-3	246.5	227.2	1.08	139.8	1.76	182.3	1.35	177.0	1.39
S7-4	273.6	241.1	1.13	174.7	1.57	197.9	1.38	196.0	1.40
S7-5	304.4	251.1	1.21	199.7	1.52	209.0	1.46	203.0	1.50
S7-6	310.6	264.4	1.17	232.9	1.33	223.7	1.39	214.0	1.45
S8-1	272.1	216.8	1.26	97.9	2.78	169.6	1.60	159.0	1.71
S8-2	250.9	224.6	1.12	117.4	2.14	178.3	1.41	170.0	1.48
S8-3	309.6	236.4	1.31	146.8	2.11	191.3	1.62	180.0	1.72
S8-4	265.8	236.4	1.12	146.8	1.81	191.3	1.39	180.0	1.48
S8-5	289.2	251.1	1.15	183.5	1.58	207.7	1.39	194.0	1.49
S8-6	283.9	261.6	1.09	209.7	1.35	219.3	1.29	207.0	1.37

Table 5.8   Summary of Correlation of Code Predictions

Code Method	$\dfrac{V_e}{V_p}$ Ratio	
	Mean	Coefficient of Variation
AS 3600	1.22	36.2%
ACI 318-95	1.81	41.4%
Standard Method of EC2 Part 1	1.37	36.9%
Variable Strut Inclination Method of EC2 Part 1	2.14	55.9%
Simplified Method of CSA A23.3-94	1.66	39.3%
General Method of CSA A23.3-94	1.72	37.0%

In Figure 5.24, most of the results fall either within the ±20% band, or above this band. For beams 3, 4 and 5 tested by Roller and Russell (1990), the predictions by AS 3600 were unconservative. These three beams had fairly large depths (D = 718 to 743 mm) and were most heavily reinforced. If the minimum shear reinforcement requirement according to AS 3600 was used as a datum, then beams 3, 4 and 5 contained approximately 6, 9 and 12 times the minimum shear reinforcement respectively. These beams were also the most heavily reinforced in the longitudinal direction with nominal longitudinal reinforcement ratio $A_{s\ell}/b_v d_o$ of 3.8%, 5.1% and 5.7% respectively.

Only the test shear capacities of the beams tested by Roller and Russell (1990) are in the range of 800 to 2200 kN. Figure 5.25 shows a clearer picture of the correlation between the test shear strength and shear strength predicted by AS 3600 after removing the data by Roller and Russell (1990).

All other code methods apart from AS 3600 gave overall conservative predictions. The most conservative predictions were given by the Variable Strut Inclination Method of EC2 Part 1 followed by the ACI code method, the Canadian code methods and the Standard Method of EC2 Part 1.

136

Figure 5.24   Correlation of Test Shear Strength versus Shear Strength Predicted by AS 3600

Figure 5.25 Correlation of Test Shear Strength versus Shear Strength Predicted by AS 3600

The figure's legend:

Symbol	Name	Symbol	Name
⊞	Vecchio and Collins	▷	Gabrielsson
⊕	Mphonde	▽	Xie et al.
×	Elzanaty et al.	△	Thirugnanasundralingam et al.
◈	Johnson and Ramirez	○	Kriski and Loov
+	Ganwei and Nielsen	◇	Tests at Curtin University
⊕	Sarsam and Al-Musawi	□	Present Study
◁	Watanabe		

The comparisons in Section 5.3.1 and above identified the present theory and the AS 3600 method as the most promising methods for determining the shear strength of slender NSC and HPC beams with vertical shear reinforcement.

5.5 Trends Of Test Parameters

This section compares the trends of test parameters with those predicted by the theory and the AS 3600 method. The parameters considered are the concrete cover to shear reinforcement cage, shear reinforcement ratio, longitudinal tensile reinforcement ratio, overall beam depth, shear span-to-depth ratio and concrete compressive strength.

5.5.1 Shear Strength versus Cover to Shear Reinforcement Cage

The concrete cover to shear reinforcement cage was the variable in beam Series 1. Figure 5.26 compares the test results with predicted trends.

Figure 5.26 shows that the shear strength was not significantly affected by the concrete cover. Both the theory and the AS 3600 method gave similar predictions. This contradicts the "spalled width" concept advanced by Vecchio and Collins (1982). It is reasonable to consider the full width of a beam as being effective for shear.

5.5.2 Shear Strength versus Shear Reinforcement Ratio

In Series 2, 7 and 8, the transverse steel ratio was the test variable. The results from Series 8 complemented those from Series 2. After combining the results for Series 2 and 8, a plot of the shear strength versus the shear reinforcement ratio is shown in Figure 5.27.
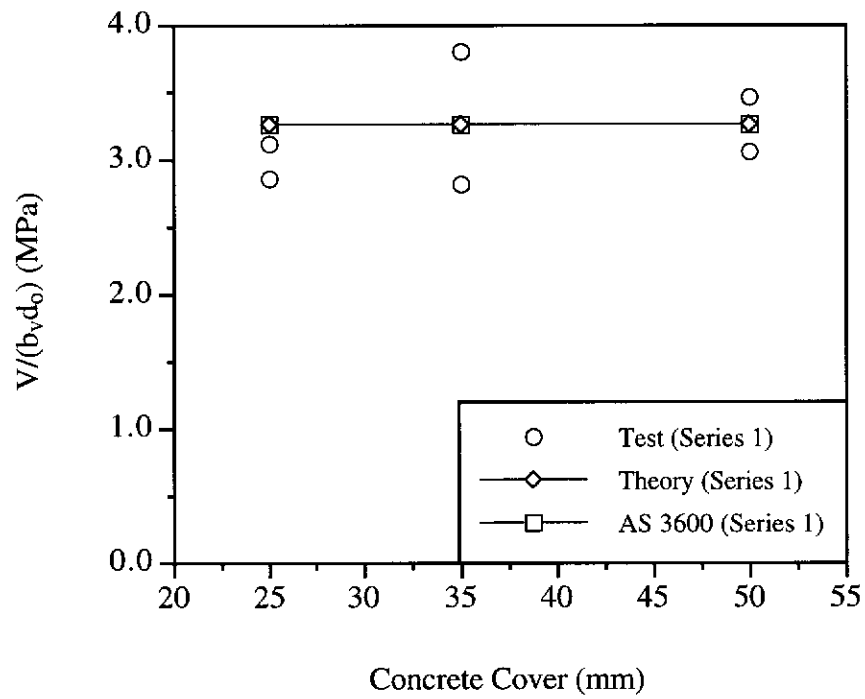
Figure 5.26   Shear Strength versus Concrete Cover to Shear Reinforcement Cage
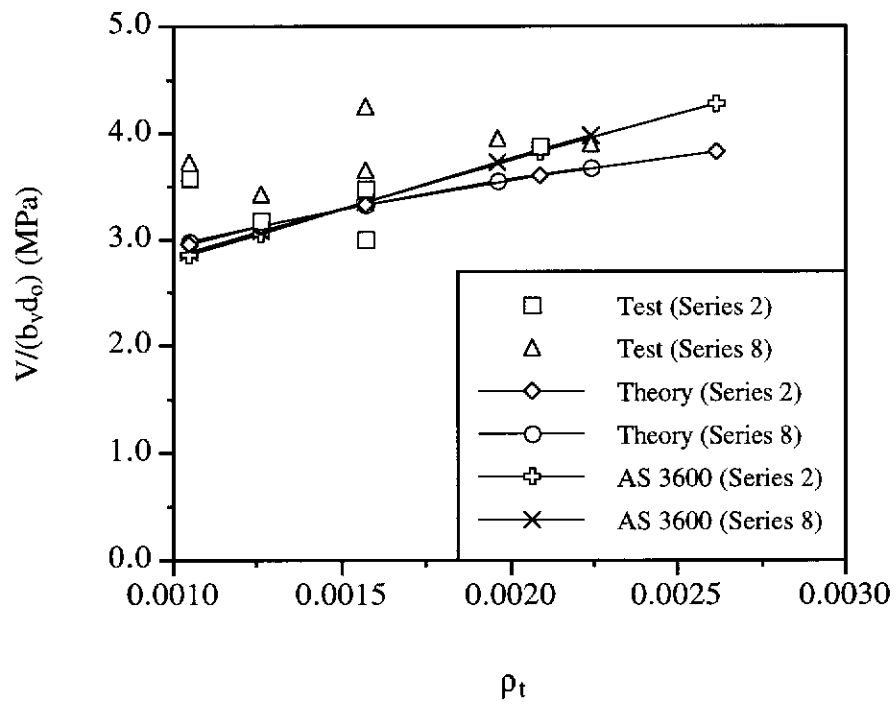
Figure 5.27   Shear Strength versus Shear Reinforcement Ratio for Series 2 and 8

140

The theory and the AS 3600 method predicted the test results reasonably well although the predictions were slightly conservative. For larger ρ_t values, the test results are closer to the predictions by the AS 3600 method. The AS 3600 method is less conservative for shear reinforcement ratio greater than about $\rho_t = 0.0015$. However, the trend shows that the code predictions are still relatively conservative.

The shear strength versus shear reinforcement ratio for Series 7 is shown in Figure 5.28.

The test trend is similar to that predicted by the theory. It is clear that increasing the amount of shear reinforcement in a beam will lead to an increase in the shear strength.

The AS 3600 method also has a trend similar to the tests but it is less conservative for ρ_t greater than about 0.0015, which is consistent with the trends observed for Series 2 and 8 in Figure 5.27.

5.5.3 Shear Strength versus Longitudinal Tensile Reinforcement Ratio

In Series 3 and 6, the longitudinal tensile reinforcement ratio ($\rho_\ell = A_{s\ell}/b_v d_o$) was the test parameter. Figure 5.29 shows the test shear strengths and the predicted trends.

The test results follow the trends given by the theory and the AS 3600 method reasonably well except at $\rho_\ell = 3.69\%$. The large increase in shear strength when $\rho_\ell = 3.69\%$ may have been due to the bundling of the tensile bars resulting in greater shear strength.

The test results, the theory and the AS 3600 method indicate that the shear strength increased with the longitudinal tensile reinforcement ratio.
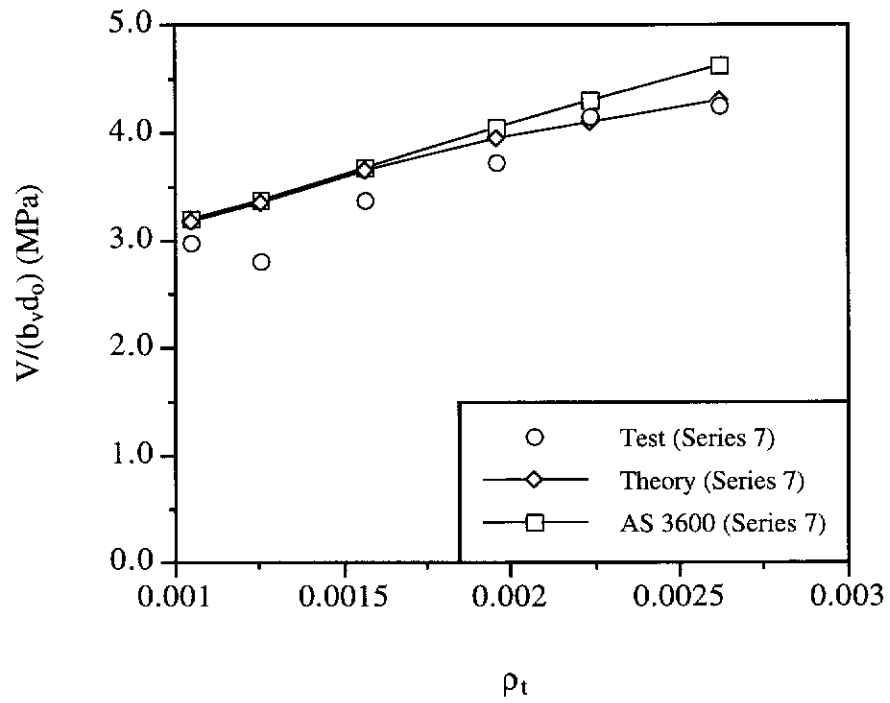
Figure 5.28   Shear Strength versus Shear Reinforcement Ratio for Series 7
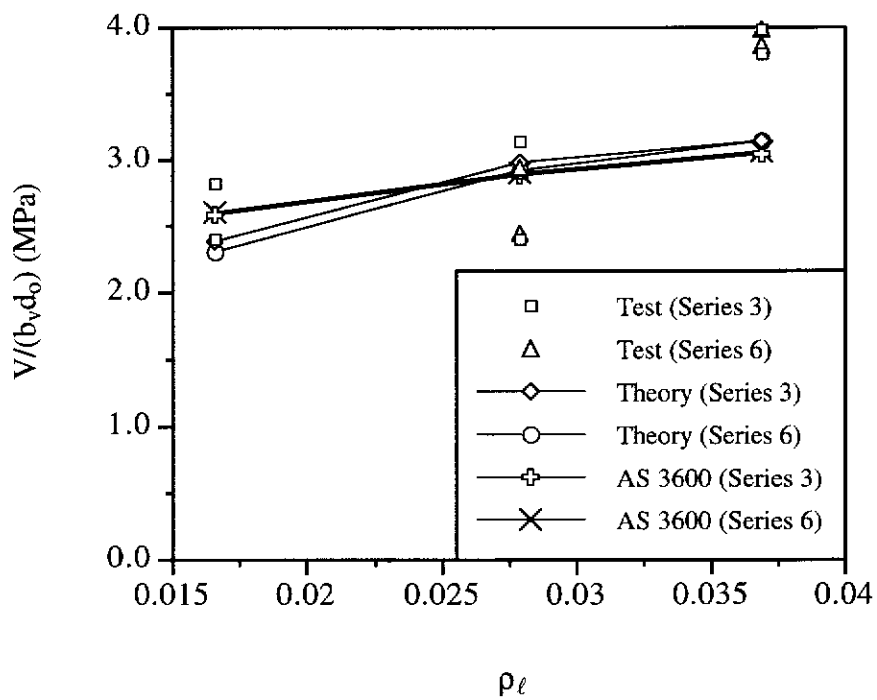
Figure 5.29   Shear Strength versus Longitudinal Tensile Reinforcement Ratio

142

5.5.4 Shear Strength versus Overall Beam Depth

The effect of overall beam depth on the shear strength was studied in Series 4. The test results and predictions by the theory and the AS 3600 method are shown in Figure 5.30.

Beam S4-2 had a very high shear strength at failure ($V_e/b_v d_o$ = 5.16 MPa). If this result is ignored, then the trends predicted by the theory and the AS 3600 method are fairly close to the test data points. The theory predicted an almost horizontal trend, with an almost negligible increase in shear strength as the overall depth increased. In contrast, the AS 3600 method predicted a slight decrease in the shear stress at failure $V/b_v d_o$ with an increase in the overall beam depth. Indeed, the test results (apart from beam S4-2) confirmed that the shear stress at failure decreased with increasing D. Therefore, the theory was not as conservative as the AS 3600 method at large D values. Both methods of prediction overestimated the shear strength at D = 400 and 600 mm.

5.5.5 Shear Strength versus Shear Span/Depth Ratio

The a/d_o ratio was varied from 1.51 to 3.01 in Series 5. A comparison of the test results and theoretical predictions are given in Figure 5.31.

Results for the beams with $a/d_o \geq 2.50$ (S5-1, S5-2 and S5-3) agreed well with the predictions by the theory and the AS 3600 method. However, for short beams with $a/d_o < 2.50$, both the theory and the AS 3600 method severely underestimated the shear strength. A strut-and-tie method would be more appropriate in such cases for determining the shear strength of the beams.

It is noted that the test shear strength did not vary greatly for slender beams where $a/d_o \geq 2.50$.
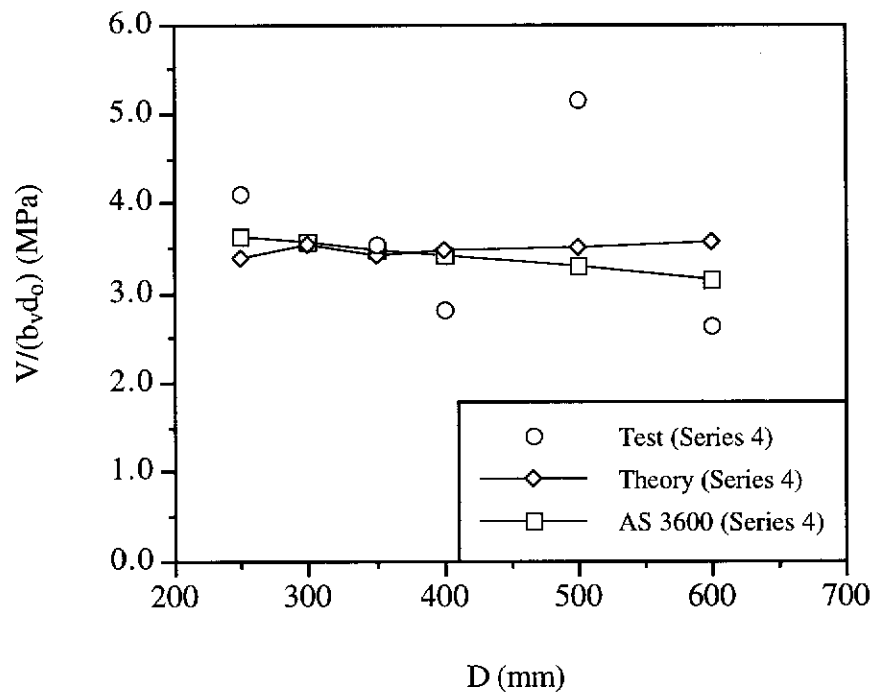
Figure 5.30 Shear Strength versus Overall Beam Depth
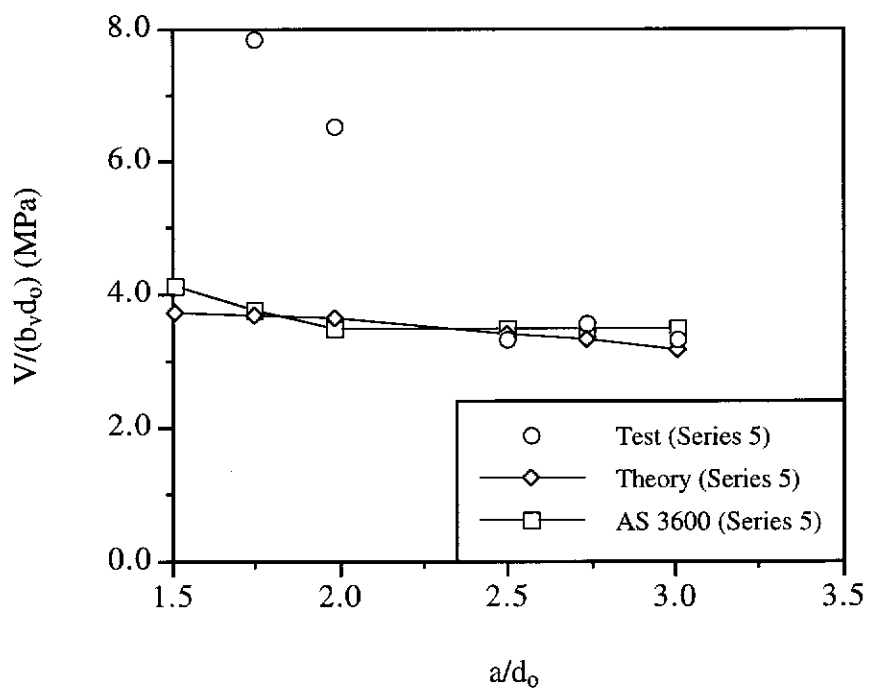
Figure 5.31 Shear Strength versus Shear Span/Depth Ratio

5.5.6 Shear Strength versus Concrete Compressive Strength

The comparison of shear strength versus concrete compressive strength for beams S1-3, S1-4, S2-3, S2-4, S4-4, S5-3, S8-3 and S8-4 is shown in Figure 5.32. In these beams, the concrete compressive strength was the test variable.
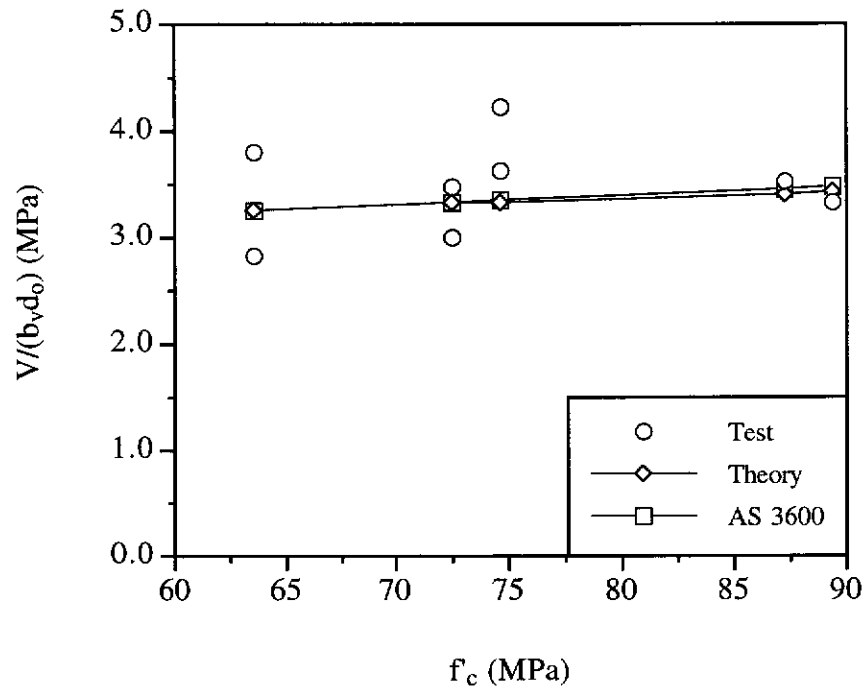
Figure 5.32   Shear Strength versus Concrete Compressive Strength

Figure 5.32 shows that the shear strength is not significantly affected by the concrete compressive strength. The theory predicted an increase of 5.1% in the shear strength when the concrete compressive strength was increased from 63.6 MPa ($V_p = 237.9$ kN) to 89.4 MPa ($V_p = 250.0$ kN). The trend shown by the AS 3600 method is almost identical to that of the theory.

Conclusions And Recommendations

6.1 Introduction

This chapter presents the conclusions of the present study. The findings from the experimental and analytical work with regard to the response and shear strength of reinforced Normal Strength Concrete (NSC) and High Performance Concrete (HPC) beams subjected to combined bending moment and shear force are highlighted here.

The analytical work involved the development of a theory capable of predicting the deformation and shear strength of a reinforced concrete beam. The theory was based on a truss analogy approach, with due consideration given to equilibrium, compatibility and material relationships.

In the theory, the stirrups were assumed to be uniformly smeared. The longitudinal tensile steel was divided into two parts, one part for sustaining the bending moment at the critical section of a beam and the other part for resisting the shear force. That part of the longitudinal tensile steel attributed to shear was also assumed to be smeared.

The experimental part of the study involved testing of eight series of beams, totalling to forty-eight specimens. Of the forty-eight beams tested, forty-three beams failed in shear and the remainder failed in flexure. The parameters studied were concrete cover to shear reinforcement cage, shear reinforcement ratio, longitudinal tensile steel ratio, overall beam depth, shear span-to-depth ratio and concrete compressive strength. Most of the beams were subjected to two symmetrically placed concentrated loads. Some beams were subjected to one or four concentrated loads. The deformations in terms of midspan deflection, curvature and strain in the longitudinal steel bars were monitored during the tests. Most of the beams were 250 mm wide and 350 mm deep, with an effective span of about 2 metres. However, there were other beam sizes with the largest beam being 250 mm wide and 600 mm deep with an effective span of 3.1 metres. The concrete compressive strength ranged from 63.6 to 89.4 MPa. In most cases, the shear span-to-depth ratio was approximately 2.5.

Test results from previous investigations were also studied. The shear design provisions given by the Australian Standard AS 3600 (1994), American Concrete Institute Building Code ACI 318-95, Eurocode EC2 Part 1 and Canadian Standard CSA A23.3-94 were also examined. Comparisons were made between the test shear strength and predictions by the various codes of practice.

Recommendations for future work are proposed at the end of the chapter.

6.2 Conclusions

6.2.1 Effect of Test Parameters

- There was no significant difference in the shear strength of the reinforced HPC beams with different concrete cover to shear reinforcement cage. The full beam width was effective for shear.

- An increase in the shear reinforcement ratio increased the shear strength of the reinforced HPC beams.

- An increase in the longitudinal tensile reinforcement ratio increased the shear strength of the reinforced HPC beams.

- An increase in the overall beam depth caused a decrease in the nominal shear stress at failure $V_e/b_v d_o$ of the reinforced HPC beams.

- When the shear span-to-depth ratio $a/d_o \geq 2.5$, there was no significant difference in the shear strength. However, for beams with $a/d_o < 2.5$, the shear strength increased significantly with a decrease in the a/d_o ratio.

- There was negligible influence of the concrete compressive strength on the shear strength of the reinforced HPC beams within the range of 63.6 to 89.4 MPa.

6.2.2 Shear Strength of Beams

- The theory predicted the shear strength of the reinforced HPC beams in the present study well. Of the forty-three beams that failed in shear, beams S3-1 and S3-2 were inadequately detailed, and beams S5-4 and S5-5 were short beams with $a/d_o < 2.0$. Hence, these four beams were not considered in the correlation analysis between the test and predicted shear strengths. For the remaining 39 beams, the mean test/predicted shear strength ratio V_e/V_p was 1.04 and the coefficient of variation was 15.4%.

- The theory also predicted the shear strength of reinforced NSC and HPC beams from other investigations well. For 147 beams from the present and previous investigations, the mean test/predicted shear strength ratio V_e/V_p was 1.23 with a coefficient of variation of 32.8%.

- The V_e/V_p ratio was not affected much by the concrete compressive strength and the moment-to-shear ratio M/Vd_o, provided that the amount of shear reinforcement was not less than the minimum specified by the Australian Standard AS 3600.

- The AS 3600 method gave the best prediction of shear strength among the various code methods considered. For 147 beams, the mean test/predicted shear strength ratio V_e/V_p was 1.22 with a coefficient of variation of 36.2%.

- All other code methods were generally conservative. The most conservative code method was the Variable Strut Inclination Method of the Eurocode EC2 Part 1, followed by the ACI code method, the Canadian code methods and the Standard Method of the Eurocode EC2 Part 1.

6.2.3 Deformation of Beams

- Prediction of the midspan deflection of beams by combining the theory with Branson's method compared reasonably well with test results.

- The theory gave good prediction of the shear force versus shear strain relationship for the beams reported by Vecchio and Collins (1982).

- Crack patterns of the reinforced HPC beams of the present study were similar to those reported for beams from previous research.

6.3 Recommendations For Further Research

The following is a list of areas where future research may be directed:

- The bundling of bars may contribute to an increase in the shear strength of a beam. More tests should be done to confirm this behaviour.

- Very few reinforced HPC beams with large depths have been tested before. More tests on beams with overall depth greater than 1.0 m should be carried out.

- Tests with multiple point loads and uniformly distributed load should be done.

- The minimum shear reinforcement requirement stipulated in the codes of practice should be examined in the light of rational shear strength calculation methods.

- Beams with thin webs, for example I, T or rectangular hollow section beams, should be tested to extend the theory to such specimens. These beams should also be tested for web crushing to examine the accuracy of the theory in predicting the response and strength of beams which are over-reinforced with shear reinforcement.

- Axially loaded beams and prestressed concrete beams should be tested to determine whether the rational theory is applicable to such beams.

References

ACI Committee 318 (1995)
Building Code Requirements for Reinforced Concrete.
American Concrete Institute, Detroit.

AS 3600 (1994)
Concrete Structures.
Standards Association of Australia, Sydney.

ASCE-ACI Task Committee 426 (1973)
The Shear Strength of Reinforced Concrete Members.
Journal of the Structural Division, Proceedings of the American Society of Civil
Engineers, Vol. 99, No. ST6, June, pp. 1091-1187.

Canadian Standards Association (1994)
Design of Concrete Structures A23.3-94.
Canadian Standards Association, Rexdale, Ontario.

Carrasquillo, R.L., Nilson, A.H. and Slate, F.O. (1981)
Properties of High Strength Concrete Subject to Short-Term Loads.
ACI Journal, Proc. Vol. 78, No. 3, May-June, pp. 171-178.

Clark, A.P. (1951)
Diagonal Tension in Reinforced Concrete Beams.
ACI Journal, Vol. 23, No. 2, October, pp. 145-155.

Collins, M.P. (1972)
Torque-Twist Characteristics of Reinforced Concrete Beams.
Symposium on Inelasticity and Non-Linearity in Structural Concrete, University of
Waterloo Press, pp. 211-231.

151

Collins, M.P. (1978)

Towards a Rational Theory for RC Members in Shear.

Journal of the Structural Division, American Society of Civil Engineers, Vol. 104, No. ST4, April, pp. 649-666.

Collins, M.P., Mitchell, D., Adebar, P. and Vecchio, F.J. (1996)

A General Shear Design Method.

ACI Structural Journal, Vol. 93, No. 1, January-February, pp. 36-45.

EC2 Part 1 (Year not available)

Eurocode No. 2 - Design of Concrete Structures. Part 1: General Rules and Rules for Buildings.

Eurocode 2 Editorial Group, final text after harmonization with French and German versions, October 1991.

Elzanaty, A.H., Nilson, A.H. and Slate, F.O. (1986)

Shear Capacity of Reinforced Concrete Beams Using High-Strength Concrete.

ACI Journal, Vol. 83, No. 2, March-April, pp. 290-296.

Gabrielsson, H. (1993a)

Shear Capacity of Beams of Reinforced High Performance Concrete, September 1992, and *Bending and Shear Tests on Reinforced High Performance Concrete Beams,* May 1993.

Division of Structural Engineering, Lulea University of Technology, Internal Report K1:1, 52 and 59 pp..

Gabrielsson, H. (1993b)

High Performance Concrete Beams Tested in Shear. Comparison Between the Traditional Approach and the Modified Compression Field Theory.

Proceedings of the Third International Symposium on Utilisation of High-Strength Concrete, Lillehammer, Norway, 20-24 June, pp. 169-176.

Ganwei, C. and Nielsen, M.P. (1990)

Shear Strength of Beams of High Strength Concrete.

Department of Structural Engineering, Technical University of Denmark, Report Ser R No. 258, 23 pp..

Hsu, T.T.C. (1988)

Softened Truss Model Theory for Shear and Torsion.

ACI Structural Journal, Vol. 85, No. 6, November-December, pp. 624-635.

Hsu, T.T.C. (1993)

Unified Theory of Reinforced Concrete.

CRC Press Inc., Florida, 313 pp..

Ilyas, M.B.M. (1993)

Private Discussion on the Details of Tests Performed on Thirty Two Reinforced HPC Beams with Shear Reinforcement, School of Civil Engineering, Curtin University of Technology, Western Australia.

Johnson, M.K. and Ramirez, J.A. (1989)

Minimum Shear Reinforcement in Beams with Higher Strength Concrete.

ACI Structural Journal, Vol. 86, No. 4, July-August, pp. 376-382.

Kani, G.N.J., Huggins, M.W. and Wittkopp, R.R. (1979)

Kani on Shear in Reinforced Concrete.

Department of Civil Engineering, University of Toronto, Toronto.

Krauthammer, T. (1992)

Minimum Shear Reinforcement Based on Interface Shear Transfer.

ACI Structural Journal, Vol. 89, No. 1, January-February, pp. 99-105.

Kriski, W. and Loov, R. (1996)

Strength of Beams Based on Shear-Friction.

Paper to be presented at the 1996 Annual Conference of the Canadian Society for Civil Engineering, Edmonton, Canada, May 29-June 1, 1996.

Lloyd, N.A. and Rangan, B.V. (1993)

High Strength Concrete: A Review.

Research Report No. 1/93 January 1993, School of Civil Engineering, Curtin University of Technology, W. Australia, 132 pp..

Mphonde, A.G. (1984)

Shear Strength of High Strength Concrete Beams.

Thesis for the Degree of Doctor of Philosophy of the University of Connecticut, published by UMI Dissertation Services, Michigan, 249 pp..

Nielsen, M.P. (1984)

Limit Analysis and Concrete Plasticity.

Prentice-Hall, Inc., Englewood Cliffs, New Jersey, 421 pp..

Roller, J.J. and Russell, H.G. (1990)

Shear Strength of High Strength Concrete Beams with Web Reinforcement.

ACI Structural Journal, Vol. 87, No. 2, March-April, pp. 191-198.

Sarsam, K.F. and Al-Musawi, J.M.S. (1992)

Shear Design of High- and Normal Strength Concrete Beams with Web Reinforcement.

ACI Structural Journal, Vol. 89, No. 6, November-December, pp. 658-664.

Thirugnanasundralingam, K., Sanjayan, G. and Hollins, P. (1995)

Shear Strength of High Strength Concrete Beams.

Paper presented at the 14th Australasian Conference on the Mechanics of Structures and Materials, Hobart, Australia.

Thirugnanasundralingam, K. (1996)

Private Communication By Facsimile Concerning the Yield Stresses of Steel Reinforcement Used in Tests by Thirugnanasundralingam, K., Sanjayan, G. and Hollins, P. (1995).

Thorenfeldt, E., Tomaszewicz, A. and Jensen, J.J. (1987)

Mechanical Properties of High-Strength Concrete and Application in Design.

Proceedings of Symposium on Utilization of High Strength Concrete, 1987, Stavanger, Norway, pp. 149-159.

Vecchio, F.J. and Collins, M.P. (1981)

Stress-Strain Characteristics of Reinforced Concrete in Pure Shear.

IABSE Colloquium on Advanced Mechanics of Reinforced Concrete, Delft, Netherlands, pp. 211-225.

Vecchio, F.J. and Collins, M.P. (1982)

The Response of Reinforced Concrete to In-Plane Shear and Normal Stresses.

Publication No. 82-03, Department of Civil Engineering, University of Toronto, Toronto, 332 pp..

Vecchio, F.J. and Collins, M.P. (1986)

The Modified Compression-Field Theory for Reinforced Concrete Elements Subjected to Shear.

ACI Journal, Proc. Vol. 83, No. 2, March-April, pp. 219-231.

Vecchio, F.J. and Collins, M.P. (1988)

Predicting the Response of Reinforced Concrete Beams Subjected to Shear Using Modified Compression Field Theory.

ACI Structural Journal, Vol. 85, No. 3, May-June, pp. 258-268.

Vecchio, F.J. and Collins, M.P. (1993)

Compression Response of Cracked Reinforced Concrete.

Journal of Structural Engineering, Vol. 119, No. 12, December, pp. 3590-3610.

Warner, R.F., Rangan, B.V. and Hall, A.S. (1989)

Reinforced Concrete (3rd. Edition).

Longman Cheshire Pty. Ltd., Melbourne, 553 pp..

Watanabe, F. (1993)

Shear Strength of Beams.

Multilateral Project on the Use of High Strength Concrete, Kyoto, 19-21 May 1993.

Xie, Y., Ahmad, S.H., Yu, T., Hino, S. and Chung, W. (1994)

Shear Ductility of Reinforced Concrete Beams of Normal and High-Strength Concrete.

ACI Structural Journal, Vol. 91, No. 2, March-April, pp. 140-149.

Zia, P., Leming, M.L. and Ahmad, S.H. (1991)

High Performance Concretes, A State of the Art Report.

SHRP-C/FR-91-103, Strategic Highway Research Program, National Research Council, Washington DC, 246 pp..

Zsutty, T.C. (1968)

Beam Shear Strength Prediction by Analysis of Existing Data.

ACI Journal, Proceedings Vol. 65, No. 11, November, pp. 943-951.

Bibliography

The publications or sources of information given below served as supplementary materials to this work.

ACI Committee 363 (1984)
State-of-the-Art Report on High-Strength Concrete.
ACI Journal, Proc. Vol. 81, No. 4, July-August, pp. 364-411.

ACI-ASCE 445 Shear And Torsion (1995)
New Approaches to Shear Design in Structural Concrete - State-of-the-Art Report (Draft).
August 1995.

Adebar, P. and Collins, M.P. (1994)
Shear Design of Concrete Offshore Structures.
ACI Structural Journal, Vol. 91, No. 3, May-June, pp. 324-335.

Adebar, P. and Collins, M.P. (1996)
Shear Strength of Members Without Transverse Reinforcement.
Canadian Journal of Civil Engineering, No. 23, pp. 30-41.

Ahmad, S.H., Khaloo, A.R. and Poveda, A. (1986)
Shear Capacity of Reinforced High-Strength Concrete Beams.
ACI Journal, Vol. 83, No. 2, March-April, pp. 297-305.

Ahmad, S.H. and Lue, D.M. (1987)
Flexure-Shear Interaction of Reinforced High-Strength Concrete Beams.
ACI Structural Journal, Vol. 84, No. 4, July-August, pp. 330-341.

Ahmad, S.H., Xie, Y. and Yu, T. (1994)

Shear Strength of Reinforced Lightweight Concrete Beams of Normal and High Strength Concrete.

Magazine of Concrete Research, Vol. 46, No. 166, March, pp. 57-66.

Al-Nahlawi, K.A. and Wight, J.K. (1992)

Beam Analysis using Concrete Tensile Strength in Truss Models.

ACI Structural Journal, Vol. 89, No. 3, May-June, pp. 284-289.

American Concrete Institute (1973)

ACI Manual of Concrete Practice 1973 - Part 2.

American Concrete Institute, Detroit.

AS 3600 - Supplementary 1 (1990)

Concrete Structures - Commentary (Supplement to AS 3600 -1988).

Standards Association of Australia, Sydney.

Bazant, Z.P. and Kim, J.K. (1984)

Size Effect in Shear Failure of Longitudinally Reinforced Beams.

ACI Journal, Proc. Vol. 81, September-October, pp. 456-468.

Bazant, Z.P. and Sun, H.H. (1987)

Size Effect in Diagonal Shear Failure: Influence of Aggregate Size and Stirrups.

ACI Materials Journal, Vol. 84, No. 4, July-August, pp. 259-272.

Belarbi, A. and Hsu, T.T.C. (1991)

Constitutive Laws of Reinforced Concrete in Biaxial Tension-Compression.

Research Report UHCEE 91-2, Department of Civil and Environmental Engineering, University of Houston, Houston, Texas 77204, July, 155 pp..

Belarbi, A. and Hsu, T.T.C. (1995)

Constitutive Laws of Softened Concrete in Biaxial Tension-Compression.

ACI Structural Journal, Vol. 92, No. 5, September-October, pp. 562-573.

Bhide, S.B. and Collins, M.P. (1989)

Influence of Axial Tension on the Shear Capacity of Reinforced Concrete Members.

ACI Structural Journal, Vol. 86, No. 5, September-October, pp. 570-581.

BS 8110 Part 1 (1985)

Structural Use of Concrete: Code of Practice for Design and Construction.

British Standards Institution, London.

Canadian Portland Cement Association (1985)

Concrete Design Handbook.

Canadian Portland Cement Association, Ontario.

Carino, N.J. and Clifton, J.R. (1991)

High Performance Concrete: Research Needs to Enhance Its Use.

Concrete International: Design and Construction, Vol. 13, No. 9, September, pp. 70-76.

Carrasquillo, R.L., Slate, F.O. and Nilson, A.H. (1981)

Microcracking and Behaviour of High Strength Concrete Subject to Short-Term Loading.

ACI Journal, Proc. Vol. 78, No. 3, May-June, pp. 179-186.

Chana, P.S. (1987)

Investigation of the Mechanism of Shear Failure of Reinforced Concrete Beams.

Magazine of Concrete Research, Vol. 39, No. 141, December, pp. 196-204.

Chung, W. and Ahmad, S.H. (1994)

Model for Shear Critical High-Strength Concrete Beams.

ACI Structural Journal, Vol. 91, No. 1, January-February, pp. 31-41.

Clarke, J.L. (1987)

Shear Capacity of High Strength Concrete Beams.

Concrete (London), Vol. 21, No. 3, March, pp. 24-26.

Collins, M.P. (1993a)

Shear Design of High-Strength Concrete Structures.

Proceedings of the Third International Symposium on Utilisation of High-Strength Concrete, Lillehammer, Norway, 20-24 June, pp. 128-135.

Collins, M.P. (1993b)

The Use of Rational Design Methods for Shear.

Proceedings of the Tom Paulay Symposium: Recent Developments in Lateral Force Transfer in Buildings, University of California, San Diego, September, pp. 359-381.

Collins, M.P. and Mitchell, D. (1980)

Shear and Torsion Design of Prestressed and Non-Prestressed Concrete Beams.

PCI Journal, Vol. 25, No. 5, September-October, pp. 32-100.

Collins, M.P. and Porasz, A. (1989)

Shear Design for High Strength Concrete.

Proceedings of the Workshop on Design Aspects of High Strength Concrete, Dubrovnik, Comite Euro-International du Beton Bulletin d'Information, No. 193, December, pp. 77-83.

Collins, M.P., Mitchell, D. and MacGregor, J.G. (1993)

Structural Design Considerations for High-Strength Concrete.

Concrete International, Vol. 15, No. 5, May, pp. 27-34.

Gerwick, B.C. Jr. (1992)

High-Performance Concrete. Present and Future.

Concrete Construction, Vol. 37, No. 5, May, pp. 355-357.

Hsiung, W. and Frantz, G.C. (1985)

Transverse Stirrup Spacing in R/C Beams.

Journal of Structural Engineering, Vol. 111, No. 2, February, pp. 353-362.

Hsu, L.S. and Hsu, C.T.T. (1994)

Complete Stress-Strain Behaviour of High-Strength Concrete Under Compression.

Magazine of Concrete Research, Vol. 46, No. 169, December, pp. 301-312.

Hsu, T.T.C. (1991)

Nonlinear Analysis of Concrete Membrane Elements.

ACI Structural Journal, Vol. 88, No. 5, September-October, pp. 552-561.

Hsu, T.T.C. (1996)

In Search of "Contribution of Concrete" (V_c) in Membrane Elements.

Paper to the Members and Associate Members of the ACI-ASCE Committee 445 on Shear and Torsion; from the University of Houston, Cullen College of Engineering, Department of Civil and Environmental Engineering, Houston.

Hsu, T.T.C. and Mo, Y.L. (1985)

Softening of Concrete in Torsional Members - Theory and Tests.

ACI Journal, Proc. Vol. 82, No. 3, May-June, pp. 290-303.

Hsu, T.T.C., Mau, S.T. and Chen, B. (1987)
Theory on Shear Transfer Strength of Reinforced Concrete.
ACI Structural Journal, Vol. 84 , No. 2, March-April, pp. 149-160.

Jenq, Y.S. and Shah, S.P. (1989)
Shear Resistance of Reinforced Concrete Beams - A Fracture Mechanics Approach.
Fracture Mechanics: Application to Concrete, edited by Li, V.C. and Bazant, Z.P.,
SP-118, American Concrete Institute, Detroit, pp. 237-258.

Kani, G.N.J. (1964)
The Riddle of Shear Failure and Its Solution.
ACI Journal, Proc. Vol. 61, No. 4, April, pp. 441-467.

Kani, G.N.J. (1966)
Basic Facts Concerning Shear Failure.
ACI Journal, Proc. Vol. 63, No. 6, June, pp. 675-692.

Discussion of the paper *Basic Facts Concerning Shear Failure* by G.N.J. Kani (1966),
by De Cossio, R.D. and Loera, S.; Smith, R.B.L.; Iyengar, K.T.S.R. and Rangan,
B.V.; and Kani, G.N.J..
ACI Journal, Proc. Vol. 63, No. 12, December, pp. 1511-1528.

Kani, G.N.J. (1967)
How Safe Are Our Large Reinforced Concrete Beams?
ACI Journal, Proc. Vol. 64, March, pp. 128-141.

Kani, G.N.J. (1969)
A Rational Theory for the Function of Web Reinforcement.
ACI Journal, Vol. 66, No. 3, March, pp. 185-197.

Kotsovos, M.D. (1988)
Compressive Force Path Concept; Basis for Reinforced Concrete Ultimate Limit State Design.
ACI Structural Journal, Vol. 85, No. 1, January-February, pp. 68-75.

Kotsovos, M.D. and Bobrowski, J. (1993)
Design Model for Structural Concrete based on the Concept of the Compressive Force Path.
ACI Structural Journal, Vol. 90, No. 1, January-February, pp. 12-20.

Krefeld, W.J. and Thurston, C.W. (1966)
Contribution of Longitudinal Steel to Shear Resistance of Reinforced Concrete Beams.
ACI Journal, Proc. Vol. 63, pp. 325-344.

MacGregor, J.G. (1988)
Reinforced Concrete: Mechanics and Design.
Prentice-Hall International, Englewood Cliffs, New Jersey, 799 pp..

Malier, Y. (1991)
French Approach to Using HPC.
Concrete International, Vol. 13, No. 7, July, pp. 28-32.

Marti, P. (1985)
Basic Tools of Reinforced Concrete Beam Design.
ACI Journal, Vol. 82, No. 1, January-February, pp. 46-56.

Mitchell, D. and Collins, M.P. (1974)
Diagonal Compression Field Theory - A Rational Model for Structural Concrete in Pure Torsion.
ACI Journal, Proc. Vol. 71, No. 8, August, pp. 396-408.

Mphonde, A.G. (1988)
Aggregate Interlock in High Strength Reinforced Concrete Beams.
Proceedings of the Institution of Civil Engineers (London), Vol. 85, Part 2, September, pp. 397-413.

Mphonde, A.G. and Frantz, G.C. (1984)
Shear Strength of High Strength Reinforced Concrete Beams.
Report No. CE 84-157, Civil Engineering Department, University of Connecticut, Storrs, June, 260 pp..

Mphonde, A.G. and Frantz, G.C. (1985)
Shear Tests of High- and Low-Strength Concrete Beams With Stirrups.
ACI Special Publication, SP-87, pp. 179-196.

Pang, X.B. and Hsu, T.T.C. (1992)
Constitutive Laws of Reinforced Concrete in Shear.
Research Report UHCEE 92-1, Department of Civil and Environmental Engineering, University of Houston, Houston, Texas 77204, 180 pp..

Pang, X.B. and Hsu, T.T.C. (1996)
Fixed Angle Softened Truss Model for Reinforced Concrete.
ACI Structural Journal, Vol. 93, No. 2, March-April, pp. 197-207.

Placas, A., Regan, P.E. and Baker, A.L.L. (1971)
Shear Failure of Reinforced Concrete Beams.
ACI Journal, Proc. Vol. 68, No. 10, October, pp. 763-773.

Polak, M.A. and Vecchio, F.J. (1994)
Reinforced Concrete Shell Elements Subjected to Bending and Membrane Loads.
ACI Structural Journal, Vol. 91, No. 3, May-June, pp. 261-268.

Rahal, K.N. and Collins, M.P. (1995)
Effect of Thickness of Concrete Cover on Shear-Torsion Interaction - An Experimental Investigation.
ACI Structural Journal, Vol. 92, No. 3, May-June, pp. 334-342.

Rangan, B.V. (1987)
Shear and Torsion Design in the Australian Standard for Concrete Structures.
Civil Engineering Transactions, Institution of Engineers Australia, Vol. CE 29, No. 3, August, pp. 148-156.

Rangan, B.V. (1991)
Web Crushing Strength of Reinforced and Prestressed Concrete Beams.
ACI Structural Journal, Vol. 88, No. 1, January-February, pp. 12-16.

Regan, P.E. (1993)
Research on Shear: A Benefit to Humanity or a Waste of Time?
The Structural Engineer, Vol. 71, No. 19, 5 October 1993, pp. 337-347.

Ryan, W.G. and Samarin, A. (1992)
Australian Concrete Technology.
Longman Cheshire Pty. Ltd., Australia.

Setunge, S., Darvall, P.LeP. and Attard, M.M. (1989)
A Preliminary Study of Very High Strength Concrete Beams.
Civil Engineering Research Report, Report No. 5/1989, Monash University, Melbourne, 60 pp..

So, K.O. and Karihaloo, B.L. (1993)

Shear Capacity of Longitudinally Reinforced Beams - A Fracture Mechanics Approach.

ACI Structural Journal, Vol. 90, No. 6, November-December, pp. 591-600.

Tan, K.H., Murugappan, K. and Paramasivam, P. (1993)

Shear Behaviour of Steel Fiber Reinforced Concrete Beams.

ACI Structural Journal, Vol. 89, No. 6, November-December, pp. 3-11.

Vecchio, F.J. and Chan, C.C.L. (1990)

Reinforced Concrete Membrane Elements with Perforations.

Journal of Structural Engineering, Vol. 116, No. 9, September, pp. 2344-2360.

Vecchio, F.J. and Emara, M.B. (1992)

Shear Deformations in Reinforced Concrete Frames.

ACI Structural Journal, Vol. 89, No. 1, January-February, pp. 46-56.

Vecchio, F.J., Collins, M.P. and Aspiotis, J. (1994)

High-Strength Concrete Elements Subjected to Shear.

ACI Structural Journal, Vol. 91, No. 4, July-August, pp. 423-433.

Walraven, J.C. (1981)

Fundamental Analysis of Aggregate Interlock.

Journal of the Structural Division, ASCE, Vol. 107, ST 11, November, pp. 2245-2270.

Test Data

Table A.1 Test Data for Beam S1-1

V (kN)	Curv. (Left) $(x10^{-6}\ mm^{-1})$	Curv. (Right) $(x10^{-6}\ mm^{-1})$	d_{max} (mm)
0.0	0.00	0.00	0.0
25.3	0.23	0.09	1.0
50.5	0.62	0.57	1.6
50.5	0.63	0.64	1.6
75.4	1.29	1.18	2.2
75.7	1.42	1.22	2.3
100.6	2.58	1.78	3.1
100.6	2.68	1.70	3.4
125.8	3.57	2.01	4.3
125.9	3.46	2.04	4.5
150.1	3.71	2.32	5.3
150.1	3.72	2.35	5.5
175.1	4.10	2.62	6.3
175.2	4.11	2.62	6.4
185.1	4.22	2.71	-
195.0	4.40	2.81	-
201.1	4.50	2.84	-
205.1	4.57	2.86	-
210.1	4.66	2.90	-
215.1	4.76	2.93	-
220.1	4.84	2.93	-
225.1	4.95	2.93	-

Table A.2 Test Data for Beam S1-2

V (kN)	Curv. (Left) ($\times 10^{-6}$ mm^{-1})	Curv. (Right) ($\times 10^{-6}$ mm^{-1})	d_{max} (mm)
0.0	0.00	0.00	0.0
12.7	0.08	0.05	0.3
25.2	0.27	0.24	0.4
25.0	0.30	0.26	0.5
37.8	0.47	0.46	0.7
50.2	0.73	0.89	0.9
50.0	0.84	1.02	1.0
62.8	1.15	1.49	1.2
75.3	1.64	2.04	1.5
75.3	1.62	2.04	1.5
74.8	1.65	2.10	1.5
87.8	1.85	2.46	1.8
100.4	2.19	2.91	2.1
99.8	2.32	2.97	2.1
113.2	2.67	3.26	2.4
125.4	3.06	2.95	3.0
126.0	2.84	2.89	3.3
137.6	2.83	2.89	3.7
148.1	2.89	2.87	4.2
146.6	2.88	2.87	4.2
162.5	3.01	2.93	4.6
175.1	3.12	3.00	5.2
172.6	3.12	3.00	5.2
175.9	3.12	3.00	-
180.1	3.14	3.01	-
185.1	3.21	3.04	-
190.1	3.25	3.04	-
195.1	3.26	3.05	-
200.1	3.30	3.02	-
205.1	3.31	2.94	-
202.8	3.27	3.50	-

Table A.3 Test Data for Beam S1-3

V (kN)	Curv. (Left) (x10⁻⁶ mm⁻¹)	Curv. (Right) (x10⁻⁶ mm⁻¹)	d_{max} (mm)	$\varepsilon_{s\ell}1A$ (x10⁻⁶)	$\varepsilon_{s\ell}1B$ (x10⁻⁶)	$\varepsilon_{s\ell}1C$ (x10⁻⁶)	$\varepsilon_{s\ell}2D$ (x10⁻⁶)	$\varepsilon_{s\ell}2E$ (x10⁻⁶)	$\varepsilon_{s\ell}2F$ (x10⁻⁶)	$\varepsilon_{s\ell}2G$ (x10⁻⁶)
0.0	0.00	0.00	0.0	0	0	0	0	0	0	0
12.4	0.08	0.12	0.3	115	153	204	139	159	158	188
25.0	0.22	0.30	0.5	184	277	208	180	205	196	230
37.5	0.29	0.74	0.7	305	370	287	267	328	275	316
50.0	0.37	1.43	1.0	448	507	350	365	445	438	471
62.5	0.46	1.91	1.3	558	608	422	430	514	527	593
75.1	0.62	2.46	1.7	657	717	524	543	645	631	710
87.8	0.77	2.92	2.0	728	653	601	606	718	712	812
100.3	0.97	3.41	2.3	837	768	698	699	803	831	899
112.7	1.19	3.80	2.6	920	933	773	796	928	928	963
125.3	1.20	4.45	3.8	1044	1075	969	926	1019	1050	1104
137.4	1.31	4.74	4.1	1086	1193	1039	960	1102	1131	1177
149.6	1.29	5.09	4.7	1180	1264	1100	1092	1190	1192	1231
162.5	1.34	5.39	5.1	1272	1353	1167	1129	1216	1270	1288
174.9	1.32	5.89	5.7	1377	1473	1222	1267	1320	1363	1387
175.4	1.30	5.90	5.8	1355	1461	1242	1279	1310	1349	1381
179.7	1.32	5.99	5.9	1363	1481	1259	1290	1345	1367	1383
184.8	1.34	6.13	6.0	1412	1486	1285	1322	1357	1380	1421
190.0	1.36	6.24	6.2	1439	1541	1328	1349	1393	1431	1444
194.9	1.37	6.34	6.4	1494	1567	1334	1385	1420	1465	1456
199.9	1.37	6.49	6.6	1504	1604	1367	1426	1469	1504	1496
200.2	1.37	6.68	6.8	1518	1626	1399	1450	1456	1494	1468
200.3	1.37	6.72	6.8	1516	1595	1436	1426	1461	1475	1488
200.9	1.37	6.77	6.8	1540	1624	1428	1432	1461	1490	1498
202.3	1.38	6.84	6.9	1532	1606	1446	1450	1461	1477	1488
204.4	1.38	6.99	7.0	1553	1642	1438	1454	1479	1514	1499
204.6	1.38	7.31	7.1	1557	1648	1452	1461	1491	1518	1507
204.7	1.38	7.37	7.2	1563	1652	1469	1459	1493	1506	1509
204.9	1.38	7.42	7.2	1559	1654	1444	1485	1491	1502	1507
205.3	1.39	7.54	7.3	1581	1657	1434	1473	1499	1516	1494
204.1	1.39	7.92	7.4	1547	1648	1434	1475	1489	1526	1501
187.8	1.28	8.54	7.6	1508	1555	1346	1420	1424	1467	1426
184.5	1.26	8.63	7.6	1457	1539	1401	1408	1428	1459	1422
185.8	1.26	8.79	7.7	1473	1535	1360	1418	1422	1475	1399
185.0	1.26	8.94	7.7	1487	1526	1358	1375	1414	1467	1385
181.8	1.24	9.34	7.8	1459	1514	1328	1401	1404	1463	1365

Table A.4 Test Data for Beam S1-4

V (kN)	Curv. (Left) ($\times 10^{-6}$ mm^{-1})	Curv. (Right) ($\times 10^{-6}$ mm^{-1})	d_{max} (mm)	ε_{st}3H ($\times 10^{-6}$)	ε_{st}3I ($\times 10^{-6}$)	ε_{st}3J ($\times 10^{-6}$)	ε_{st}4K ($\times 10^{-6}$)	ε_{st}4L ($\times 10^{-6}$)	ε_{st}4M ($\times 10^{-6}$)	ε_{st}4N ($\times 10^{-6}$)
0.0	0.00	0.00	0.0	0	0	0	0	0	0	0
12.2	0.08	0.08	0.1	236	169	187	153	172	139	157
24.8	0.22	0.31	0.3	246	244	217	177	197	191	163
37.3	0.79	1.34	0.6	360	378	411	290	299	330	376
50.0	1.41	1.91	0.9	449	511	497	401	414	432	477
62.3	1.94	2.38	1.2	560	610	603	504	522	521	544
75.0	2.20	2.89	1.5	696	737	677	601	631	614	624
87.4	2.53	3.36	1.8	773	808	769	672	738	689	683
100.1	2.96	3.85	2.1	883	889	869	770	801	783	760
112.3	3.31	4.29	2.4	960	1000	927	835	928	858	834
125.0	3.78	4.76	2.7	1060	1085	1014	948	1007	953	905
141.4	4.62	5.32	3.0	1152	1185	1098	1041	1112	1032	988
134.1	4.57	4.62	3.3	1091	1140	1120	1041	1073	1028	1004
145.4	5.17	4.83	3.6	1188	1197	1183	1135	1146	1103	1055
146.9	5.59	4.88	3.8	1239	1227	1187	1190	1140	1109	1045
146.0	5.55	4.88	3.9	1262	1215	1179	1204	1140	1095	1047
146.0	5.52	4.88	3.9	1231	1243	1189	1171	1159	1097	1061
147.1	5.52	4.88	3.9	1274	1235	1207	1208	1138	1099	1073
150.1	5.58	4.96	4.1	1278	1274	1211	1220	1207	1139	1079
162.2	5.81	5.17	4.4	1392	1335	1263	1288	1246	1213	1140
174.6	6.15	5.45	4.8	1470	1432	1346	1381	1337	1279	1207
175.1	6.15	5.43	4.9	1562	1528	1462	1430	1376	1348	1302
178.9	6.22	5.48	5.0	1580	1513	1460	1456	1434	1360	1278
184.9	6.34	5.60	5.1	1550	1550	1497	1485	1447	1397	1339
189.6	6.44	5.70	5.2	1639	1621	1561	1514	1487	1431	1355
194.8	6.57	5.77	5.4	1639	1636	1568	1569	1491	1435	1406
199.9	6.69	5.83	5.5	1689	1656	1578	1571	1532	1482	1390
204.6	6.81	5.90	5.7	1725	1707	1594	1618	1623	1515	1426
209.8	6.94	5.97	5.9	1766	1742	1644	1660	1601	1557	1475
214.6	7.05	6.02	6.0	1758	1772	1672	1689	1627	1592	1512
219.9	7.20	6.10	6.2	1803	1817	1721	1720	1668	1621	1520
224.6	7.33	6.14	6.4	1865	1851	1755	1761	1719	1671	1548
229.9	7.46	6.22	6.5	1826	1878	1779	1791	1735	1700	1589
234.5	7.59	6.26	6.7	1898	1902	1808	1818	1739	1741	1609
239.8	7.74	6.32	6.9	1986	1964	1822	1840	1776	1767	1650
244.4	7.87	6.38	7.0	1963	1972	1842	1881	1819	1798	1658
249.6	8.02	6.44	7.2	2021	2047	1895	1906	1833	1828	1717
254.7	8.17	6.51	7.4	2062	2056	1919	1949	1884	1871	1723
259.6	8.31	6.95	7.6	2097	2107	1988	1969	1914	1920	1770
264.7	8.47	7.78	7.9	2101	2134	2033	2018	1941	1991	1791
269.3	8.61	8.76	8.2	2177	2168	2087	2061	1947	2087	1831
268.9	8.64	9.21	8.2	2130	2193	2073	2047	1945	2104	1835
268.5	8.63	9.40	8.3	2156	2185	2092	2029	1986	2087	1831
269.1	8.64	9.59	8.3	2119	2144	2124	2053	1961	2120	1829
269.9	8.66	9.69	8.4	2129	2160	2108	2061	1977	2116	1829
272.2	8.74	9.99	8.5	2175	2211	2140	2096	2016	2134	1843
274.6	8.81	10.27	8.6	2201	2209	2156	2104	1994	2151	1825
277.0	8.87	10.49	8.8	2205	2252	2166	2112	2014	2165	1839
271.4	8.85	10.92	8.9	2195	2213	2104	2092	2018	2161	1827
269.6	8.84	11.00	8.9	2195	2213	2075	2070	2012	2161	1839
268.7	8.82	11.13	9.0	2158	2221	2075	2072	1996	2161	1833
262.1	8.72	11.84	9.1	2150	2183	1978	2084	1961	2122	1780
180.2	-	-	9.6	1973	1862	-	1740	1686	-	-
168.1	-	-	9.6	1875	1792	-	1752	1664	-	-

Table A.5 Test Data for Beam S1-5

V (kN)	Curv. (Left) ($\times 10^{-6}$ mm^{-1})	Curv. (Right) ($\times 10^{-6}$ mm^{-1})	d_{max} (mm)
0.0	0.00	0.00	0.0
12.5	0.05	0.07	0.2
25.0	0.14	0.22	0.4
25.1	0.16	0.23	0.4
37.5	0.29	0.40	0.6
50.1	0.47	0.85	0.9
50.3	0.50	0.98	1.0
62.6	0.75	1.49	1.2
75.3	1.31	2.19	1.5
75.4	1.37	2.30	1.6
87.7	1.63	2.64	1.8
100.3	2.00	3.65	2.2
100.4	2.06	3.99	2.3
112.7	2.29	5.01	2.6
125.2	2.67	6.11	3.0
125.2	2.64	6.36	3.2
137.8	2.79	6.84	3.5
148.2	2.75	7.90	4.1
144.8	2.73	7.90	4.1
162.6	2.84	8.55	4.4
175.1	2.89	9.46	5.0
172.8	2.89	9.45	5.0
179.8	2.92	9.62	-
184.7	2.94	9.82	-
189.8	2.98	10.05	-
194.9	3.00	10.31	-
199.4	3.01	10.59	-
204.8	3.03	10.87	-
209.9	3.03	11.16	-
214.8	3.03	11.44	-
219.9	3.05	11.70	-
225.1	3.05	11.98	-
229.8	3.06	12.25	-
235.1	3.06	12.57	-
239.9	3.04	12.89	-
244.9	3.07	13.21	-
249.6	3.04	13.55	-

Table A.6 Test Data for Beam S1-6

V (kN)	Curv. (Left) ($\times 10^{-6}$ mm^{-1})	Curv. (Right) ($\times 10^{-6}$ mm^{-1})	d_{max} (mm)
0.0	0.00	0.00	0.0
12.4	0.05	0.05	0.3
24.8	0.13	0.27	0.5
24.8	0.14	0.30	0.5
37.2	0.25	0.60	0.8
49.8	0.67	1.18	1.1
49.8	0.71	1.23	1.2
62.3	0.97	1.58	1.4
74.9	1.44	1.91	1.7
75.0	1.52	2.02	1.7
87.3	1.84	2.55	2.0
100.0	2.43	4.08	2.3
100.1	2.58	4.72	2.4
112.5	2.92	5.74	2.7
124.8	3.60	7.17	3.2
124.8	3.87	7.39	3.3
137.4	4.26	8.04	3.5
149.1	6.65	9.27	4.2
146.4	6.79	9.25	4.2
162.1	7.49	10.02	4.5
174.6	8.68	11.22	5.1
171.7	8.68	11.22	5.1
174.6	8.75	11.29	5.1
180.0	8.93	11.52	5.2
184.6	9.16	11.79	5.3
189.8	9.46	12.12	5.5
194.7	9.80	12.48	5.7
199.4	10.09	12.84	5.8
204.6	10.30	13.23	6.0
209.9	10.52	13.67	6.2
214.5	10.75	14.15	6.4
219.7	11.00	14.64	6.6
220.8	11.21	16.39	7.0
215.8	11.12	16.85	7.1
212.4	11.02	17.37	7.2
194.7	10.53	18.22	7.3
190.1	10.40	18.57	7.3
185.4	10.27	19.03	7.4
182.0	10.17	19.44	7.5
180.4	10.13	19.87	7.6
179.8	10.09	20.15	7.7
179.2	10.08	20.39	7.7
178.9	10.07	20.61	7.8
178.6	10.05	20.79	7.8
177.3	10.03	21.23	7.9
177.1	10.01	21.52	8.0
176.8	10.01	21.70	8.1
176.0	-	-	8.3
174.6	-	-	8.4
170.8	-	-	8.7
166.9	-	-	9.0
161.1	-	-	9.2

Table A.7 Test Data for Beam S2-1

V (kN)	Curv. (Left) ($\times 10^{-6}$ mm^{-1})	Curv. (Right) ($\times 10^{-6}$ mm^{-1})	d_{max} (Front) (mm)	d_{max} (Back) (mm)
0.0	0.00	0.00	0.0	0.0
12.6	0.01	0.04	0.6	-1.1
25.1	0.04	0.10	0.7	-0.6
37.5	0.16	0.19	0.8	-0.3
50.2	0.56	0.24	1.1	0.2
62.7	0.81	0.31	1.4	0.5
75.2	1.08	0.40	1.7	0.9
87.7	1.38	0.52	1.9	1.2
100.2	2.09	1.44	2.3	1.6
112.8	2.42	1.72	2.6	1.9
125.1	2.86	2.13	2.9	2.2
137.5	3.25	2.45	3.3	2.5
149.9	3.96	2.97	3.7	2.9
162.6	5.12	3.66	4.4	3.5
174.9	5.77	4.42	4.9	3.9
180.0	6.04	4.84	5.1	4.1
184.9	6.31	5.19	5.3	4.3
189.9	6.60	5.45	5.6	4.5
194.9	6.87	5.69	5.8	4.7
200.1	7.18	5.96	6.0	4.9
204.9	7.42	6.20	6.2	5.0
207.5	7.55	6.33	6.3	5.1
209.9	7.70	6.45	6.4	5.2
212.5	7.90	6.58	6.5	5.3
214.9	8.03	6.72	6.6	5.4
217.4	8.17	6.85	6.7	5.5
219.9	8.30	6.99	6.8	5.6
222.4	8.44	7.15	6.9	5.7
225.1	8.59	7.29	7.1	5.8
227.5	8.74	7.43	7.2	5.9
229.9	8.89	7.56	7.3	6.0
232.6	9.07	7.72	7.4	6.2
235.1	9.24	7.86	7.6	6.3
237.4	9.40	7.97	7.7	6.4
240.4	9.59	8.13	7.9	6.5
242.5	9.71	8.26	8.0	6.6
244.9	9.84	8.42	8.2	6.8
247.8	10.00	8.58	8.4	7.0
249.9	10.12	8.74	8.6	7.1
252.4	10.25	8.92	8.8	7.3
255.1	10.43	9.09	9.0	7.5
257.5	10.59	9.39	9.3	7.7
259.9	10.76	9.79	9.6	8.0
260.0	10.78	10.01	9.7	8.1
259.4	10.78	10.19	9.8	8.2
257.4	10.77	10.52	10.0	8.4
249.5	10.61	11.50	10.5	9.1
179.1	8.74	16.34	12.7	11.1
150.4	7.69	23.71	15.2	13.6

Table A.8 Test Data for Beam S2-2

V (kN)	Curv. (Left) ($\times 10^{-6}$ mm^{-1})	Curv. (Right) ($\times 10^{-6}$ mm^{-1})	d_{max} (Front) (mm)	d_{max} (Back) (mm)
0.0	0.00	0.00	0.0	0.0
13.1	0.05	0.12	1.0	-0.8
25.6	0.19	0.25	1.2	-0.4
38.0	0.31	0.39	1.4	0.0
50.8	0.44	0.53	1.7	0.4
63.2	0.78	0.62	1.9	0.9
75.3	1.24	0.66	2.2	1.3
88.2	1.56	0.72	2.5	1.7
100.8	1.98	0.75	2.8	2.1
113.2	4.76	1.34	3.5	2.7
125.8	5.51	1.88	3.9	3.1
138.1	6.04	2.15	4.3	3.5
150.4	6.69	2.67	4.8	4.0
162.9	7.42	3.50	5.2	4.4
175.4	8.20	4.03	5.7	4.8
187.9	9.14	4.52	6.2	5.3
200.4	10.40	5.05	6.7	5.8
205.4	10.92	5.25	6.9	6.0
210.2	11.41	5.59	7.2	6.2
215.4	11.97	5.84	7.4	6.5
220.6	12.57	6.11	7.7	6.7
225.6	13.25	6.36	8.0	7.0
229.9	14.14	6.60	8.4	7.4

Table A.10 Test Data for Beam S2-4

V (kN)	Curv. (Left) (x10⁻⁶ mm⁻¹)	Curv. (Right) (x10⁻⁶ mm⁻¹)	d_{max} (Front) (mm)	d_{max} (Back) (mm)	ε_{st}3F (x10⁻⁶)	ε_{st}3G (x10⁻⁶)	ε_{st}3H (x10⁻⁶)	ε_{st}4I (x10⁻⁶)	ε_{st}4J (x10⁻⁶)
0.0	0.00	0.00	0.0	0.0	0	0	0	0	0
12.6	0.07	0.09	0.3	0.1	74	76	116	129	74
24.9	0.19	0.20	0.5	0.3	83	154	119	168	200
37.6	0.33	0.34	0.7	0.6	152	268	147	218	304
50.0	0.44	0.45	1.0	0.9	235	340	211	277	377
62.5	0.55	0.57	1.3	1.2	319	413	281	368	459
75.2	0.97	1.10	1.6	1.6	393	505	382	428	561
87.6	1.62	1.45	1.9	1.9	454	603	412	475	622
100.3	2.09	2.00	2.3	2.4	524	654	518	523	661
112.8	2.36	2.32	2.6	2.7	579	679	643	599	723
125.3	2.85	2.89	3.0	3.2	693	772	707	689	751
137.6	3.12	3.19	3.4	3.5	853	853	733	748	839
150.0	4.27	4.05	3.9	4.0	871	922	785	848	881
162.1	4.70	4.45	4.3	4.4	965	992	895	889	1020
174.8	5.37	5.31	4.8	4.8	1071	1103	909	1013	1074
187.4	5.96	6.14	5.3	5.3	1139	1177	960	1108	1221
199.7	6.53	6.92	5.7	5.8	1157	1263	1093	1272	1248
212.7	7.14	7.61	6.2	6.3	1224	1369	1106	1305	1368
217.9	8.03	7.95	6.7	6.7	1265	1403	1172	1386	1396
217.9	8.13	7.95	6.8	6.7	1317	1443	1134	1449	1381
148.7	15.51	5.74	8.9	8.8	-	-	-	-	-
107.3	23.70	5.44	10.1	10.0	-	-	-	-	-
108.7	25.99	5.48	10.7	10.5	-	-	-	-	-
104.5	27.04	5.45	10.8	10.6	-	-	-	-	-

Table A.11 Test Data for Beam S2-5

V (kN)	Curv. (Left) (x10⁻⁶ mm⁻¹)	Curv. (Right) (x10⁻⁶ mm⁻¹)	d_{max} (Front) (mm)	d_{max} (Back) (mm)
0.0	0.00	0.00	0.0	0.0
12.4	0.07	0.08	0.3	0.0
25.0	0.20	0.21	0.5	0.3
37.4	0.34	0.35	0.6	0.5
50.0	0.44	0.43	0.9	0.9
62.4	0.55	0.52	1.2	1.2
74.9	0.67	0.97	1.5	1.6
87.6	1.32	1.26	1.8	1.9
99.8	1.71	1.58	2.1	2.2
112.7	1.99	1.84	2.4	2.5
125.1	2.37	2.27	2.8	2.8
137.3	2.71	4.08	3.3	3.3
149.9	5.06	4.59	4.0	4.0
162.1	5.42	4.99	4.4	4.3
174.6	5.87	5.49	4.8	4.7
187.1	6.36	5.98	5.2	5.1
188.1	6.52	6.20	5.5	5.3
199.8	6.84	6.58	5.8	5.7
212.1	7.29	7.02	6.3	6.1
224.6	7.79	7.59	6.8	6.5
229.6	7.98	7.80	6.9	6.7
234.6	8.18	8.03	7.1	6.9
239.6	8.36	8.28	7.4	7.1
244.6	8.54	8.53	7.6	7.3
249.5	8.73	8.83	7.8	7.5
254.7	8.92	8.99	8.0	7.7
259.6	9.11	9.18	8.3	7.9
264.5	9.31	9.40	8.5	8.1
269.5	9.51	9.66	8.8	8.4
272.2	9.62	9.81	8.9	8.5
274.6	9.73	9.98	9.1	8.7
277.0	9.82	10.10	9.2	8.8
279.6	9.93	10.25	9.4	8.9
280.5	10.01	10.72	9.6	9.1
280.0	10.01	10.79	9.6	9.2
279.1	9.99	13.04	9.9	9.4
247.4	9.47	13.55	10.0	9.4
243.4	9.40	13.58	9.9	9.4
240.4	9.35	13.58	9.9	9.4
237.0	9.26	13.56	9.8	9.3
241.1	9.21	13.61	9.9	9.4
241.5	9.21	13.63	9.9	9.4
243.6	9.23	14.08	10.0	9.5

Table A.12 Test Data for Beam S2-6

V (kN)	Curv. (Left) ($\times 10^{-6}$ mm^{-1})	Curv. (Right) ($\times 10^{-6}$ mm^{-1})	d_{max} (Front) (mm)	d_{max} (Back) (mm)
0.0	0.00	0.00	0.0	0.0
13.5	0.09	0.12	0.5	-0.1
25.2	0.22	0.24	0.7	0.1
37.5	0.34	0.38	0.8	0.4
50.2	0.45	0.49	1.1	0.8
62.8	0.58	0.61	1.4	1.1
75.2	0.73	0.73	1.6	1.3
87.9	1.49	1.32	1.9	1.7
100.2	1.94	1.68	2.1	1.9
112.9	2.34	2.03	2.4	2.2
125.2	3.02	2.52	2.7	2.5
137.4	3.42	2.79	3.0	2.7
149.9	4.24	3.22	3.4	3.1
162.4	4.62	3.64	3.7	3.4
174.9	5.29	4.22	4.0	3.7
187.4	5.80	4.65	4.4	4.1
199.9	6.60	5.14	4.7	4.4
212.4	7.36	5.67	5.1	4.7
224.9	8.04	6.45	5.5	5.1
237.2	8.69	7.29	5.9	5.5
249.8	9.35	7.85	6.3	5.9
254.9	9.59	8.04	6.5	6.0
259.8	9.83	8.24	6.6	6.2
264.9	10.07	8.45	6.8	6.3
269.9	10.31	8.62	6.9	6.5
274.8	10.54	8.75	7.1	6.6
279.6	10.78	8.92	7.3	6.8
284.9	11.02	9.08	7.4	6.9
289.8	11.25	9.21	7.6	7.1
295.0	11.48	9.39	7.8	7.2
299.8	11.73	9.56	7.9	7.4
302.5	11.85	9.65	8.0	7.5
304.9	11.97	9.75	8.1	7.6
306.7	12.05	9.83	8.1	7.6
307.5	12.09	9.86	8.2	7.6
308.2	12.14	9.89	8.2	7.7
309.8	12.22	9.95	8.3	7.7
312.5	12.35	10.04	8.3	7.8
314.8	12.47	10.12	8.4	7.9
317.5	12.60	10.22	8.5	8.0
319.9	12.72	10.30	8.6	8.1
322.5	12.85	10.38	8.7	8.2
323.7	12.91	10.42	8.8	8.2
324.1	12.93	10.44	8.8	8.2
324.6	12.97	10.46	8.8	8.2
327.4	13.11	10.57	8.9	8.3
329.9	13.23	10.67	9.0	8.4
332.4	13.39	10.78	9.1	8.6
335.0	13.50	10.88	9.3	8.7
337.4	13.63	10.99	9.4	8.8
339.9	13.77	11.12	9.5	8.9
342.4	13.89	11.25	9.6	9.0
344.8	14.05	11.40	9.8	9.2

Continued

Table A.12 Test Data for Beam S2-6 (*Continued*)

V (kN)	Curv. (Left) (x10⁻⁶ mm⁻¹)	Curv. (Right) (x10⁻⁶ mm⁻¹)	d_{max} (Front) (mm)	d_{max} (Back) (mm)
347.8	14.22	11.57	10.0	9.3
350.0	14.36	11.69	10.1	9.5
354.9	14.66	11.98	10.4	9.8
355.7	14.76	12.06	10.6	10.0
355.2	14.76	12.06	10.7	10.1
354.6	14.76	12.05	10.8	10.1
354.2	14.76	12.04	10.9	10.3
354.3	14.76	12.04	11.1	10.4
354.5	14.76	12.04	11.2	10.5
354.8	14.76	12.04	11.3	10.6
355.0	14.76	12.05	11.5	10.7
355.8	14.77	12.07	11.7	10.8
356.4	14.79	12.09	11.9	11.0
357.8	14.85	12.14	12.5	11.4
357.4	14.91	12.16	14.2	12.4
347.6	14.56	12.01	15.2	12.8
345.5	14.42	11.99	-	12.4
344.7	14.35	11.98	-	13.0
343.2	14.27	11.97	-	-
336.6	14.17	11.93	-	-
327.0	13.94	11.86	-	-
325.6	13.77	11.61	-	-
313.9	13.54	11.60	-	-
312.0	13.46	11.55	-	-
310.3	13.39	11.52	-	-
308.5	13.34	11.50	-	-
308.6	13.32	11.50	-	-
308.2	13.29	11.48	-	-
307.9	13.26	11.48	-	-
308.4	13.24	11.48	-	-
307.4	13.15	11.44	-	-
303.0	13.05	11.40	-	-
301.9	13.03	11.36	-	-
301.8	13.01	11.34	-	-
300.5	12.99	11.32	-	-
299.2	12.96	11.27	-	-
297.1	12.91	11.21	-	-
292.4	12.76	11.11	-	-

Table A.13 Test Data for Beam S3-1

V (kN)	Curv. (Left) (x10^-6 mm^-1)	Curv. (Right) (x10^-6 mm^-1)	d_{max} (Front) (mm)	d_{max} (Back) (mm)
0.0	0.00	0.00	0.0	0.0
12.6	0.10	0.04	1.0	-0.8
24.9	0.24	0.15	1.2	-0.5
37.5	0.38	0.29	1.4	0.0
50.0	0.51	0.40	1.9	0.6
62.5	0.70	0.68	2.2	1.1
75.1	1.62	2.19	2.8	1.7
87.6	2.16	3.03	3.3	2.2
100.1	2.73	3.86	3.8	2.7
112.7	4.15	4.75	4.4	3.2
125.1	4.99	5.82	4.9	3.7
137.3	6.60	6.95	5.6	4.4
149.9	8.26	8.02	6.3	5.0
154.8	9.21	8.41	6.7	5.4
159.7	9.61	8.82	6.9	5.7
164.6	10.00	9.22	7.2	5.9
169.6	10.39	9.64	7.5	6.2
174.6	10.83	10.08	7.8	6.4
179.6	11.27	10.51	8.1	6.7
184.6	11.70	10.97	8.4	7.0
189.7	12.17	11.47	8.7	7.3
194.9	12.69	12.03	9.1	7.7
199.4	13.13	12.55	9.5	8.0
204.5	13.77	13.24	10.0	8.5

Table A.14 Test Data for Beam S3-2

V (kN)	Curv. (Left) (x10^-6 mm^-1)	Curv. (Right) (x10^-6 mm^-1)	d_{max} (Front) (mm)	d_{max} (Back) (mm)
0.0	0.00	0.00	0.0	0.0
12.5	0.07	0.05	0.6	-0.5
24.9	0.18	0.15	0.8	-0.1
37.5	0.31	0.28	1.0	0.4
50.0	0.40	0.39	1.4	0.9
62.5	0.48	1.14	1.8	1.4
75.1	0.93	1.77	2.3	1.9
87.6	1.52	2.80	2.7	2.4
99.9	1.83	3.81	3.2	2.9
112.4	2.23	4.76	3.6	3.3
125.1	2.68	5.76	4.1	3.8
137.4	3.12	9.05	5.2	4.8
149.8	5.48	10.21	6.3	5.7
154.8	6.05	10.62	6.7	6.0
159.7	6.54	11.09	7.0	6.4
164.6	6.95	11.61	7.4	6.7
169.8	7.31	12.16	7.7	7.0
174.9	7.71	12.91	8.1	7.4

Table A.15 Test Data for Beam S3-3

V (kN)	Curv. (Left) ($\times 10^{-6}$ mm^{-1})	Curv. (Right) ($\times 10^{-6}$ mm^{-1})	d_{max} (Front) (mm)	d_{max} (Back) (mm)	$\varepsilon_{s\ell}1A$ ($\times 10^{-6}$)	$\varepsilon_{s\ell}1B$ ($\times 10^{-6}$)	$\varepsilon_{s\ell}2C$ ($\times 10^{-6}$)	$\varepsilon_{s\ell}2D$ ($\times 10^{-6}$)	$\varepsilon_{s\ell}2E$ ($\times 10^{-6}$)
0.0	0.00	0.00	0.0	0.0	0	0	0	0	0
12.5	0.00	0.04	0.3	0.0	76	103	79	100	67
25.0	0.05	0.12	0.4	0.2	107	135	119	144	119
37.5	0.13	0.23	0.7	0.5	168	172	147	282	198
50.0	0.19	0.33	0.9	0.8	290	290	225	326	305
62.6	0.38	0.41	1.2	1.2	340	360	282	441	330
75.1	0.67	0.79	1.5	1.5	429	400	303	521	477
87.9	1.06	1.20	1.8	1.7	506	496	384	558	473
100.1	1.33	1.65	2.2	2.0	583	587	438	607	605
112.7	1.69	2.36	2.6	2.4	712	661	473	783	625
125.2	2.43	3.04	3.1	2.8	728	776	584	957	796
137.6	2.97	4.09	3.6	3.3	835	811	686	956	856
149.8	3.56	4.90	4.1	3.7	990	888	738	1101	885
154.9	3.87	5.21	4.3	3.9	1074	906	766	1144	957
160.0	4.16	5.71	4.6	4.2	1080	959	797	1144	1022
164.9	4.76	6.06	4.9	4.4	1074	902	847	1080	1047
169.9	5.10	6.31	5.1	4.6	1084	1025	812	1270	1015
174.9	5.46	6.54	5.3	4.8	1179	1002	828	1199	1119
179.8	5.91	6.78	5.5	5.0	1162	1064	859	1324	1195
184.9	6.41	7.02	5.8	5.3	1215	1158	890	1268	1164
189.9	6.70	7.29	6.0	5.5	1333	1131	937	1382	1190
194.9	6.95	7.53	6.2	5.7	1280	1175	871	1332	1184
199.9	7.26	7.82	6.4	5.9	1321	1230	1021	1334	1184
204.8	7.57	8.12	6.7	6.1	1329	1273	991	1452	1230
209.9	7.86	8.41	6.9	6.3	1350	1369	1008	1445	1245
214.9	8.14	8.71	7.1	6.5	1423	1325	1110	1556	1284
219.9	8.44	9.01	7.4	6.8	1519	1362	1151	1535	1376
224.9	8.74	9.36	7.6	7.0	1524	1463	1109	1586	1387
220.6	8.95	11.84	8.9	8.4	1593	1405	1210	-	-

A.15

Table A.16 Test Data for Beam S3-4

V (kN)	Curv. (Left) ($\times 10^{-6}$ mm^{-1})	Curv. (Right) ($\times 10^{-6}$ mm^{-1})	d_{max} (Front) (mm)	d_{max} (Back) (mm)	ε_{st}3F ($\times 10^{-6}$)	ε_{st}3G ($\times 10^{-6}$)	ε_{st}3H ($\times 10^{-6}$)	ε_{st}4I ($\times 10^{-6}$)	ε_{st}4J ($\times 10^{-6}$)
0.0	0.00	0.00	0.0	0.0	0	0	0	0	0
12.8	0.07	0.01	0.3	0.1	74	110	37	79	71
25.1	0.13	0.06	0.5	0.2	120	148	93	142	134
37.7	0.21	0.10	0.8	0.4	187	254	146	254	187
50.2	0.30	0.16	1.1	0.7	276	359	178	373	294
62.9	0.38	0.34	1.4	1.0	325	396	265	416	368
75.2	0.62	0.66	1.7	1.3	443	510	279	527	515
87.8	1.40	0.95	2.1	1.6	475	579	390	733	557
100.3	1.70	1.25	2.4	1.9	638	701	410	843	699
112.8	1.99	1.83	2.7	2.2	701	754	511	983	747
123.6	2.72	5.17	3.5	3.0	751	877	578	1052	877
124.1	2.91	5.17	3.5	3.0	779	893	571	1081	896
137.6	4.50	5.96	4.3	3.6	951	930	622	1187	955
150.0	5.27	6.68	4.8	4.1	1058	967	693	1380	1037
155.1	5.61	6.96	5.0	4.3	1054	1052	767	1516	1075
165.0	6.22	7.51	5.5	4.7	1166	1116	812	1540	1209
170.1	6.50	7.75	5.7	4.9	1219	1191	853	1661	1220
174.9	7.27	8.08	6.2	5.5	1330	1237	910	1749	1226

Table A.17 Test Data for Beam S3-5

V (kN)	Curv. (Left) (x10⁻⁶ mm⁻¹)	Curv. (Right) (x10⁻⁶ mm⁻¹)	d_{max} (Front) (mm)	d_{max} (Back) (mm)
0.0	0.00	0.00	0.0	0.0
12.4	0.02	0.04	0.3	0.0
24.8	0.10	0.13	0.5	0.2
37.4	0.21	0.24	0.8	0.4
49.9	0.45	0.31	1.0	0.7
62.5	0.63	0.47	1.2	0.9
74.9	0.81	0.63	1.4	1.1
87.5	1.02	0.82	1.7	1.4
99.9	1.25	1.03	1.9	1.6
112.4	1.46	1.27	2.1	1.8
122.5	1.65	1.54	2.3	2.0
125.6	1.70	1.87	2.4	2.1
137.4	1.91	2.86	2.8	2.5
149.6	2.18	3.68	3.2	2.8
162.1	4.18	4.37	3.8	3.4
174.6	4.90	4.97	4.3	3.8
187.1	5.49	5.46	4.6	4.1
199.6	6.00	5.94	5.0	4.5
204.6	6.21	6.14	5.1	4.6
209.6	6.41	6.35	5.3	4.8
214.4	6.61	6.55	5.4	4.9
219.7	6.83	6.76	5.6	5.1
224.5	7.04	6.95	5.7	5.2
229.6	7.25	7.15	5.9	5.3
234.6	7.45	7.35	6.1	5.5
239.6	7.66	7.57	6.2	5.6
244.7	7.87	7.78	6.4	5.8
249.4	8.07	7.99	6.5	5.9
254.6	8.29	8.21	6.7	6.1
259.6	8.49	8.44	6.9	6.3
264.5	8.70	8.66	7.0	6.4
269.5	8.92	8.88	7.2	6.6
274.5	9.14	9.12	7.4	6.8
279.5	9.36	9.36	7.6	6.9
284.5	9.60	9.62	7.8	7.1
289.5	9.85	9.90	8.0	7.3
294.6	10.20	10.18	8.2	7.5

Table A.18 Test Data for Beam S3-6

V (kN)	Curv. (Left) (x10⁻⁶ mm⁻¹)	Curv. (Right) (x10⁻⁶ mm⁻¹)	d_{max} (Front) (mm)	d_{max} (Back) (mm)
0.0	0.00	0.00	0.0	0.0
12.2	0.03	0.04	0.3	-0.1
24.7	0.07	0.16	0.5	0.1
37.3	0.11	0.31	0.6	0.4
49.8	0.18	0.50	0.8	0.6
62.3	0.27	0.71	1.0	0.8
74.8	0.54	0.92	1.3	1.1
87.3	0.78	1.13	1.5	1.3
99.8	1.08	1.32	1.7	1.5
112.4	1.32	1.58	1.9	1.7
124.8	1.58	1.83	2.2	1.9
136.9	1.91	2.11	2.4	2.1
142.4	2.78	2.39	2.7	2.3
142.4	3.08	2.41	2.7	2.4
141.8	3.41	2.42	2.8	2.4
142.9	3.59	2.44	2.8	2.5
149.4	3.97	3.91	3.3	2.9
161.9	4.60	4.40	3.7	3.3
174.1	5.10	4.87	4.1	3.6
179.2	5.31	5.10	4.2	3.7
184.4	5.53	5.30	4.4	3.9
189.4	5.78	5.48	4.5	4.0
194.4	6.01	5.66	4.7	4.1
199.0	6.21	5.85	4.8	4.2
204.4	6.46	6.06	5.0	4.4
209.4	6.67	6.24	5.2	4.5
214.4	6.89	6.43	5.3	4.6
219.4	7.11	6.61	5.5	4.8
224.4	7.35	6.82	5.6	4.9
229.2	7.57	7.00	5.8	5.1
234.4	7.78	7.20	5.9	5.2
239.2	7.99	7.37	6.1	5.3
244.4	8.21	7.57	6.3	5.5
249.1	8.41	7.75	6.4	5.6
254.4	8.65	7.97	6.6	5.8
259.4	8.86	8.16	6.8	5.9
264.2	9.09	8.35	6.9	6.1
269.5	9.34	8.56	7.1	6.2
274.4	9.61	8.76	7.3	6.4
279.4	9.96	8.95	7.5	6.5

Table A.19 Test Data for Beam S4-1

V (kN)	Curv. (Left) ($\times 10^{-6}$ mm^{-1})	Curv. (Right) ($\times 10^{-6}$ mm^{-1})	d_{max} (Front) (mm)	d_{max} (Back) (mm)	$\varepsilon_{s\ell}1A$ ($\times 10^{-6}$)	$\varepsilon_{s\ell}1B$ ($\times 10^{-6}$)	$\varepsilon_{s\ell}2C$ ($\times 10^{-6}$)	$\varepsilon_{s\ell}2D$ ($\times 10^{-6}$)
0.0	0.00	0.00	0.0	0.0	0	0	0	0
12.4	0.05	0.05	0.3	0.2	25	19	24	25
25.0	0.06	0.06	0.5	0.4	64	36	28	34
37.5	0.10	0.11	0.7	0.6	50	68	70	52
50.0	0.15	0.15	0.9	0.7	146	105	61	73
62.6	0.21	0.20	1.1	0.9	171	79	71	105
75.1	0.27	0.24	1.3	1.0	181	132	126	206
87.7	0.33	0.28	1.4	1.2	223	141	121	233
99.9	0.46	0.29	1.8	1.5	260	167	161	273
112.7	0.56	0.31	2.0	1.8	241	168	130	250
125.1	0.70	0.35	2.3	2.0	258	120	140	273
137.5	0.84	0.40	2.5	2.2	250	204	165	301
149.6	0.97	0.67	2.8	2.5	347	219	241	362
174.4	1.12	0.83	3.2	2.9	340	324	240	480
187.4	1.23	0.93	3.4	3.1	419	373	279	508
199.5	1.33	1.06	3.8	3.4	385	358	360	574
212.5	1.40	1.24	4.2	3.8	437	432	300	564
224.6	1.47	1.21	4.4	4.1	394	396	323	587
237.2	1.57	1.17	4.8	4.5	478	450	403	635
249.9	1.64	1.18	5.1	4.8	517	465	431	616
262.1	1.62	1.27	5.5	5.2	565	546	529	682
274.8	1.47	1.44	6.1	5.7	603	617	633	788
288.4	1.46	1.55	6.5	6.2	572	575	631	857
299.7	1.45	1.64	7.0	6.6	679	649	665	806
312.4	1.31	1.79	7.5	7.1	719	718	767	863
324.6	1.23	1.97	8.0	7.6	718	737	795	903
337.1	1.17	2.12	8.5	8.1	843	776	863	924
349.7	1.12	2.27	9.3	8.9	844	803	921	945

Table A.20 Test Data for Beam S4-2

V (kN)	Curv. (Left) ($\times 10^{-6}$ mm^{-1})	Curv. (Right) ($\times 10^{-6}$ mm^{-1})	d_{max} (Front) (mm)	d_{max} (Back) (mm)
0.0	0.00	0.00	0.0	0.0
12.2	0.06	0.06	0.4	0.3
26.1	0.08	0.07	0.6	0.4
37.3	0.13	0.13	0.7	0.6
49.9	0.21	0.20	0.9	0.8
62.3	0.28	0.27	1.1	1.0
74.8	0.39	0.39	1.3	1.2
87.6	0.45	0.52	1.6	1.4
100.0	0.62	0.76	1.9	1.7
112.6	0.75	0.92	2.1	1.9
124.9	1.05	1.16	2.3	2.2
137.3	1.24	1.32	2.6	2.4
149.6	1.48	1.56	2.8	2.7
163.5	1.67	1.72	3.1	2.9
174.4	1.85	1.94	3.3	3.1
187.3	2.02	2.23	3.5	3.4
199.2	2.44	2.49	3.9	3.7
212.0	2.96	2.79	4.5	4.3
224.0	3.12	3.35	4.8	4.6
237.1	3.26	3.63	5.1	4.9
249.6	3.38	3.92	5.4	5.2
262.1	3.53	4.27	5.8	5.6
274.5	3.67	4.49	6.1	5.9
287.0	3.83	4.68	6.5	6.3
299.6	3.98	4.88	6.8	6.6
311.8	4.13	5.09	7.2	7.0
324.6	4.29	5.33	7.5	7.3
337.0	4.44	5.55	7.8	7.6
349.6	4.59	5.76	8.1	7.9
362.0	4.76	5.96	8.5	8.3
374.5	4.91	6.15	8.8	8.6
387.1	5.06	6.33	9.1	9.0
399.5	5.21	6.51	9.5	9.3
412.5	5.36	6.69	9.8	9.7
425.0	5.70	7.02	10.4	10.2
437.5	5.88	7.24	10.7	10.5
450.0	6.04	7.44	11.1	10.9
462.5	6.20	7.66	11.5	11.3
475.0	6.36	7.91	11.8	11.6
487.5	6.52	8.18	12.2	12.0
500.0	6.70	8.48	12.7	12.5
512.5	6.87	8.78	13.1	12.9
525.0	7.11	9.22	13.7	13.5
537.5	7.32	9.70	14.2	14.0
550.0	7.56	10.34	14.9	14.7
562.5	7.81	11.06	15.6	15.4

Table A.21 Test Data for Beam S4-3

V (kN)	Curv. (Left) (x10⁻⁶ mm⁻¹)	Curv. (Right) (x10⁻⁶ mm⁻¹)	d_{max} (Front) (mm)	d_{max} (Back) (mm)
0.0	0.00	0.00	0.0	0.0
13.1	0.12	0.10	0.4	0.3
27.0	0.18	0.13	0.6	0.5
37.9	0.27	0.22	0.8	0.7
50.7	0.37	0.34	1.0	0.9
62.9	0.48	0.46	1.3	1.3
75.6	0.72	0.80	1.6	1.6
88.2	0.92	1.03	1.8	1.9
100.7	1.19	1.46	2.1	2.2
113.2	1.40	1.84	2.4	2.5
125.6	1.60	2.19	2.6	2.8
137.4	1.79	2.60	2.9	3.1
150.6	2.49	4.14	3.7	3.9
162.6	3.00	4.59	4.3	4.5
175.1	3.33	4.78	4.7	4.9
187.6	3.56	5.03	5.1	5.3
200.4	3.79	5.30	5.6	5.7
212.7	3.94	5.57	6.0	6.1
225.1	4.11	5.83	6.5	6.6
237.9	4.27	6.13	7.1	7.2

Table A.22 Test Data for Beam S4-4

V (kN)	Curv. (Left) (x10⁻⁶ mm⁻¹)	Curv. (Right) (x10⁻⁶ mm⁻¹)	d_{max} (Front) (mm)	d_{max} (Back) (mm)	$\varepsilon_{s\ell}3E$ (x10⁻⁶)	$\varepsilon_{s\ell}3F$ (x10⁻⁶)	$\varepsilon_{s\ell}4G$ (x10⁻⁶)	$\varepsilon_{s\ell}4H$ (x10⁻⁶)
0.0	0.00	0.00	0.0	0.0	0	0	0	0
12.6	0.18	0.09	0.4	0.2	160	48	70	89
25.0	0.22	0.12	0.6	0.4	228	107	100	178
37.5	0.38	0.21	0.8	0.6	286	110	189	191
50.0	0.60	0.31	1.1	0.8	368	149	238	312
62.6	0.92	0.40	1.4	1.1	447	242	298	366
75.2	1.22	0.47	1.7	1.4	416	276	328	422
87.8	1.46	1.04	2.1	1.7	631	295	371	535
100.2	2.01	1.56	2.4	2.1	593	408	433	646
112.8	2.49	2.16	2.8	2.4	702	405	452	721
125.2	2.92	2.59	3.1	2.7	803	473	518	765
137.4	4.04	3.47	3.7	3.2	993	594	635	825
149.9	4.81	4.43	4.2	3.7	1099	697	722	969
162.4	5.30	5.14	4.7	4.1	1059	815	759	991
175.1	5.75	5.73	5.1	4.5	1188	874	842	1112
187.4	6.15	6.20	5.5	4.9	1194	962	916	1177
199.9	6.70	6.87	6.0	5.4	1224	952	998	1214
212.3	7.23	7.53	6.4	5.8	1349	1059	1075	1402
224.9	7.72	8.12	6.9	6.3	1439	1179	1110	1488
237.2	8.20	8.71	7.4	6.7	1480	1187	1144	1498
249.8	8.73	9.45	8.0	7.3	1582	1246	1235	1594

Table A.25 Test Data for Beam S5-1

V (kN)	Curv. (Left) (x10⁻⁶ mm⁻¹)	Curv. (Right) (x10⁻⁶ mm⁻¹)	d_{max} (Front) (mm)	d_{max} (Back) (mm)	$\varepsilon_{s\ell}1A$ (x10⁻⁶)	$\varepsilon_{s\ell}1B$ (x10⁻⁶)	$\varepsilon_{s\ell}2C$ (x10⁻⁶)	$\varepsilon_{s\ell}2D$ (x10⁻⁶)
0.0	0.00	0.00	0.0	0.0	0	0	0	0
12.6	0.13	0.18	0.5	0.1	135	92	93	108
25.1	0.20	0.25	0.7	0.3	323	238	199	159
37.7	0.38	0.45	1.0	0.7	386	312	224	255
50.1	1.05	0.81	1.5	1.2	492	285	270	267
62.8	1.78	2.00	2.0	1.7	725	383	510	485
75.3	2.33	2.76	2.5	2.2	864	547	600	646
87.8	2.65	3.32	2.9	2.6	932	674	716	750
100.2	2.99	4.07	3.4	3.1	975	699	692	818
112.8	3.37	4.62	3.8	3.5	1211	829	837	973
125.2	3.81	5.40	4.3	4.0	1125	910	903	1172
137.3	4.19	5.92	4.7	4.4	1277	968	966	1102
149.6	4.82	6.95	5.3	5.0	1365	1109	1070	1236
162.3	5.14	7.80	6.2	5.8	1503	1324	1210	1451
174.6	5.25	9.53	7.2	6.7	1659	1373	1330	1626
187.2	5.23	10.77	7.9	7.4	1703	1494	1345	1705
199.6	5.20	11.79	8.6	8.1	1783	1457	1448	1803
212.4	5.19	12.76	9.4	8.8	1805	1570	1628	1881
224.7	5.32	13.67	10.1	9.5	1913	1689	1684	1958
237.4	5.72	14.66	11.0	10.3	2070	1826	1781	2107

Table A.26 Test Data for Beam S5-2

V (kN)	Curv. (Left) (x10⁻⁶ mm⁻¹)	Curv. (Right) (x10⁻⁶ mm⁻¹)	d_{max} (Front) (mm)	d_{max} (Back) (mm)
0.0	0.00	0.00	0.0	0.0
12.9	0.17	0.12	0.3	0.2
25.2	0.22	0.18	0.5	0.4
37.7	0.38	0.32	0.8	0.7
50.0	0.60	0.45	1.1	1.1
62.7	1.06	0.62	1.5	1.5
75.2	1.59	1.01	1.9	1.9
87.7	1.96	1.44	2.2	2.2
100.2	2.57	2.08	2.7	2.6
113.0	2.96	2.36	2.9	2.9
125.1	3.66	3.11	3.4	3.4
137.6	4.14	3.42	3.7	3.8
150.0	5.82	4.34	4.5	4.4
162.9	6.50	4.83	4.9	4.9
174.9	7.35	5.52	5.4	5.4
187.4	7.98	5.99	5.9	5.8
199.8	8.89	6.84	6.5	6.4
212.2	9.68	7.83	7.1	7.0
224.7	10.39	8.57	7.6	7.5
237.3	11.12	9.36	8.2	8.1
249.8	12.03	10.18	8.9	8.7

Table A.30 Test Data for Beam S5-6

V (kN)	d_{max} (Front) (mm)	d_{max} (Back) (mm)	$\varepsilon_{s\ell}5I$ (x10^{-6})	$\varepsilon_{s\ell}6J$ (x10^{-6})	$\varepsilon_{s\ell}6K$ (x10^{-6})
0.0	0.0	0.0	0	0	0
12.4	0.2	0.1	89	36	66
25.1	0.3	0.2	138	77	88
37.8	0.3	0.3	211	106	142
50.2	0.4	0.3	300	173	151
62.7	0.4	0.4	304	241	200
75.1	0.5	0.6	390	269	235
87.8	0.6	0.6	463	268	265
100.1	0.7	0.7	563	326	333
112.7	0.8	0.8	579	325	347
125.1	0.9	0.9	657	390	420
137.4	1.0	1.0	680	441	421
149.6	1.1	1.2	728	513	487
162.4	1.2	1.3	820	531	512
174.1	1.5	1.4	870	553	577
187.2	1.6	1.6	921	611	642
199.1	1.7	1.7	992	615	618
212.2	1.8	1.8	1029	668	660
224.0	2.0	1.9	1176	753	726
237.2	2.0	2.0	1177	756	767
249.6	2.2	2.1	1247	810	817
262.1	2.3	2.2	1256	847	842
272.1	2.4	2.3	1317	874	884
287.2	2.5	2.4	1309	847	786
299.6	2.6	2.5	1370	943	985
311.9	2.7	2.7	1410	1031	998
324.6	2.8	2.8	1502	901	932
337.0	2.9	2.9	1552	1060	1069
349.8	3.0	3.0	1625	1046	1106
362.0	3.2	3.1	1648	1152	1157
374.6	3.3	3.2	1685	1173	1146
387.0	3.4	3.3	1749	1150	1213
399.5	3.5	3.4	1780	1229	1287
412.5	3.6	3.5	1887	1273	1303
425.0	3.7	3.6	1953	1359	1393
437.5	3.9	3.7	1999	1445	1380
450.0	4.0	3.8	2061	1463	1427
462.5	4.1	3.9	2153	1503	1512
475.0	4.2	4.1	2193	1475	1520
487.5	4.3	4.2	2201	1590	1535
500.0	4.5	4.3	2286	1641	1571
512.5	4.6	4.4	2282	1555	1625
525.0	4.7	4.5	2402	1596	1637
537.5	4.9	4.7	2393	1647	1732
550.0	5.0	4.8	2466	1713	1696
562.5	5.2	4.9	2499	1752	1826
575.0	5.3	5.1	2576	1790	1810
587.5	5.5	5.3	2765	1870	1850
600.0	5.7	5.5	3116	1876	1852
612.5	6.0	5.7	3213	2016	1933
625.0	6.3	5.9	3345	2108	1953
637.5	6.9	6.4	3479	2230	2102

Table A.31 Test Data for Beam S6-1

V (kN)	Curv. (Left) (x10^-6 mm^-1)	Curv. (Right) (x10^-6 mm^-1)	d_{max} (Front) (mm)	d_{max} (Back) (mm)
0.0	0.00	0.00	0.0	0.0
6.3	0.01	0.03	0.4	0.0
12.5	0.03	0.09	0.6	0.1
18.7	0.11	0.16	0.9	0.3
25.0	0.21	0.29	1.2	0.7
31.2	0.30	0.87	1.6	1.1
37.5	0.81	1.25	2.1	1.6
43.8	1.24	1.61	2.4	2.0
50.1	1.76	1.97	2.7	2.4
56.3	2.23	3.27	3.2	2.7
62.5	2.68	3.84	3.5	3.1
68.7	3.26	4.34	3.9	3.4
74.8	3.75	4.95	4.3	3.7
81.2	4.25	5.52	4.6	4.1
87.3	4.85	6.15	5.0	4.4
93.6	5.48	6.84	5.4	4.8
99.9	6.03	7.59	5.8	5.2
102.3	6.27	7.97	6.0	5.3
104.8	6.56	8.38	6.2	5.5
107.3	6.85	8.70	6.3	5.7
109.8	7.15	9.05	6.5	5.8
112.3	7.43	9.40	6.7	6.0
114.8	7.74	9.70	6.9	6.2
117.4	8.09	10.00	7.2	6.4
119.8	8.47	10.23	7.4	6.6
122.3	9.08	10.49	7.6	6.9
124.8	9.62	10.75	7.9	7.1
127.3	10.07	11.03	8.2	7.3
129.8	10.46	11.30	8.4	7.6
132.3	10.88	11.62	8.7	7.8
134.8	11.31	11.94	8.9	8.0
137.3	11.69	12.30	9.2	8.3
139.8	12.13	12.69	9.5	8.6
142.2	12.53	13.21	9.8	8.9
144.7	13.00	13.79	10.2	9.2
147.3	13.53	14.35	10.7	9.7
149.9	13.97	14.83	13.0	12.0
151.1	14.68	15.54	15.1	14.0
151.2	14.70	15.54	15.3	14.2
151.1	14.71	15.53	15.5	14.4
151.1	14.73	15.54	15.8	14.7
152.3	14.92	15.67	16.6	15.5
152.9	15.10	15.78	17.1	16.0
153.2	15.24	15.86	17.5	16.4
152.2	15.30	15.93	18.7	17.5
152.5	15.30	15.93	19.0	17.8
153.4	15.31	16.03	19.5	18.4
154.4	15.50	16.30	20.8	19.6
154.8	15.56	16.45	21.5	20.3

Table A.32 Test Data for Beam S6-2

V (kN)	Curv. (Left) (x10⁻⁶ mm⁻¹)	Curv. (Right) (x10⁻⁶ mm⁻¹)	d_{max} (Front) (mm)	d_{max} (Back) (mm)
0.0	0.00	0.00	0.0	0.0
6.3	0.01	0.03	-0.5	0.8
13.0	0.03	0.09	-0.4	0.9
18.8	0.08	0.15	-0.1	1.1
25.1	0.10	0.22	0.2	1.3
31.5	0.15	0.26	0.7	1.7
37.6	0.17	0.39	1.1	2.0
43.8	0.81	1.16	1.5	2.4
50.1	1.16	1.96	1.8	2.7
56.4	1.50	2.50	2.1	3.0
62.6	1.84	2.97	2.5	3.3
68.7	2.20	3.37	2.8	3.6
74.9	2.62	3.87	3.1	3.9
81.2	2.99	4.30	3.4	4.2
87.5	3.32	4.69	3.8	4.5
93.7	3.74	5.12	4.1	4.9
100.0	4.14	5.56	4.5	5.2
102.4	4.26	5.75	4.6	5.3
104.9	4.44	5.93	4.8	5.5
107.3	4.65	6.15	4.9	5.6
109.8	4.97	6.50	5.1	5.8
112.3	5.27	6.77	5.3	6.0
115.9	6.56	7.06	5.7	6.4
117.4	6.93	7.27	5.8	6.5
119.9	7.28	7.68	6.1	6.8
122.4	7.57	7.99	6.3	6.9
124.9	7.96	8.45	6.5	7.2
127.4	8.41	9.16	6.8	7.5
129.8	8.79	9.61	7.1	7.8
132.4	9.16	10.03	7.3	8.0
135.1	9.53	10.60	7.6	8.3
137.3	9.85	11.09	7.8	8.5
139.9	10.17	11.56	8.1	8.7
142.4	10.54	11.99	8.3	9.0
144.9	10.92	12.42	8.6	9.3
147.3	11.43	12.86	9.0	9.7
149.9	11.99	13.26	9.5	10.1
152.3	12.41	13.48	11.3	11.9
153.6	12.61	13.62	12.2	12.8
154.8	12.85	13.76	13.0	13.5
154.9	13.01	13.88	13.6	14.2
154.4	13.04	13.88	13.9	14.5
153.6	13.04	13.87	14.2	14.8
153.4	13.04	13.87	14.4	15.0
153.2	13.04	13.87	14.6	15.2
153.4	13.04	13.87	14.9	15.5
153.6	13.04	13.89	15.1	15.7
153.7	13.04	13.91	15.3	15.9
153.8	13.04	13.92	15.5	16.2
154.2	13.11	14.03	16.4	17.0
154.6	13.17	14.09	16.9	17.5
154.9	13.25	14.16	17.4	18.0
154.9	13.30	14.20	17.9	18.5
146.2	13.31	13.95	18.7	19.2

Table A.33 Test Data for Beam S6-3

V (kN)	Curv. (Left) (x10^{-6} mm^{-1})	Curv. (Right) (x10^{-6} mm^{-1})	d$_{max}$ (Front) (mm)	d$_{max}$ (Back) (mm)	$\varepsilon_{s\ell}$1A (x10^{-6})	$\varepsilon_{s\ell}$1B (x10^{-6})	$\varepsilon_{s\ell}$2C (x10^{-6})	$\varepsilon_{s\ell}$2D (x10^{-6})	$\varepsilon_{s\ell}$2E (x10^{-6})
0.0	0.00	0.00	0.0	0.0	0	0	0	0	0
6.1	0.00	0.05	0.3	0.0	60	56	43	65	21
12.4	0.01	0.10	0.5	0.1	119	92	109	117	26
18.7	0.01	0.15	0.7	0.3	235	151	149	178	42
25.0	0.03	0.21	0.9	0.5	263	216	204	257	34
31.2	0.05	0.26	1.2	0.8	334	259	198	289	40
37.5	0.10	0.59	1.4	1.0	403	283	275	429	98
43.8	0.84	0.90	1.7	1.3	493	317	352	459	60
50.0	1.08	1.14	2.0	1.5	462	425	393	553	111
56.3	1.28	1.34	2.2	1.7	571	503	514	593	80
62.6	1.50	1.56	2.4	1.9	599	521	551	687	125
68.6	1.69	1.76	2.6	2.1	656	664	547	734	115
75.2	1.91	1.97	2.9	2.3	697	694	626	838	273
81.1	2.14	2.17	3.2	2.5	795	696	671	814	330
87.3	2.26	2.31	3.4	2.7	840	743	718	934	379
93.6	2.43	2.46	3.6	2.9	952	894	797	975	432
99.8	2.65	2.63	3.9	3.2	964	919	862	1095	444
106.1	2.88	2.85	4.1	3.4	1088	1007	952	1130	530
112.2	3.19	3.01	4.4	3.7	1085	1029	1049	1226	521
118.6	3.74	3.18	4.7	4.0	1201	1112	1159	1285	609
124.8	4.29	3.33	5.0	4.3	1219	1115	1213	1338	633
131.1	5.26	3.50	5.5	4.7	1269	1207	1192	1418	658
137.3	5.96	3.66	5.8	5.1	1352	1203	1217	1478	711
143.5	6.68	3.79	6.2	5.4	1388	1277	1266	1548	742
149.8	7.42	3.92	6.6	5.8	1457	1375	1313	1595	802
152.2	7.63	4.44	6.8	6.0	1474	1379	1346	1626	817
154.8	7.88	4.55	7.0	6.2	1523	1436	1354	1685	857
157.3	8.10	4.63	7.1	6.3	1562	1502	1403	1695	864
159.8	8.32	4.70	7.3	6.5	1591	1486	1393	1777	898
162.3	8.57	4.78	7.4	6.6	1550	1572	1435	1769	898
164.9	8.83	4.86	7.6	6.7	1603	1556	1435	1796	931
167.2	9.05	4.93	7.7	6.9	1642	1554	1468	1812	911
169.8	9.30	5.01	7.9	7.0	1632	1574	1532	1792	943
172.3	9.56	5.08	8.0	7.2	1704	1587	1521	1878	946
174.7	9.81	5.14	8.2	7.3	1738	1634	1546	1923	986
177.2	10.13	5.19	8.4	7.5	1734	1714	1579	1923	1041

Table A.34 Test Data for Beam S6-4

V (kN)	Curv. (Left) (x10⁻⁶ mm⁻¹)	Curv. (Right) (x10⁻⁶ mm⁻¹)	d_{max} (Front) (mm)	d_{max} (Back) (mm)	$\varepsilon_{s\ell}3F$ (x10⁻⁶)	$\varepsilon_{s\ell}3G$ (x10⁻⁶)	$\varepsilon_{s\ell}3H$ (x10⁻⁶)	$\varepsilon_{s\ell}4I$ (x10⁻⁶)	$\varepsilon_{s\ell}4J$ (x10⁻⁶)
0.0	0.00	0.00	0.0	0.0	0	0	0	0	0
6.2	0.00	0.03	0.2	0.2	61	31	30	61	17
12.4	0.02	0.08	0.4	0.3	122	77	51	131	38
18.6	0.09	0.14	0.6	0.5	185	51	73	202	48
25.0	0.15	0.21	0.8	0.7	221	77	75	277	98
31.2	0.20	0.26	1.1	0.9	294	114	109	277	64
37.4	0.67	0.35	1.4	1.1	381	124	174	431	86
43.7	0.84	1.09	1.6	1.4	438	161	245	506	98
50.0	1.05	1.37	1.9	1.6	505	243	246	569	102
56.2	1.26	1.61	2.1	1.8	557	302	299	644	106
62.5	1.49	1.86	2.4	2.1	600	286	332	688	94
68.6	1.72	2.11	2.6	2.3	647	371	423	823	140
74.8	1.94	2.34	2.8	2.5	681	467	423	883	142
81.1	2.18	2.59	3.1	2.7	828	482	481	978	134
87.3	2.44	2.86	3.3	3.0	832	495	488	1010	147
93.6	2.74	3.21	3.7	3.4	889	640	573	1048	196
99.8	3.07	3.29	4.0	3.7	991	691	602	1136	222
106.1	3.41	3.37	4.3	3.9	1138	681	663	1249	263
112.3	3.74	3.46	4.6	4.2	1203	774	757	1289	322
118.5	4.10	3.56	4.8	4.4	1259	791	756	1310	397
124.8	4.62	3.65	5.1	4.7	1308	842	871	1357	385
131.0	5.33	3.77	5.5	5.0	1365	862	977	1453	425
137.2	6.52	3.89	5.9	5.4	1495	907	1095	1580	472
143.5	7.09	4.01	6.2	5.8	1551	999	1133	1605	490
149.8	7.52	4.10	6.5	6.1	1623	1072	1230	1669	566
152.2	7.69	4.12	6.6	6.2	1605	1105	1210	1661	572
154.7	7.97	4.12	6.8	6.3	1629	1140	1294	1698	552
157.2	8.38	4.13	6.9	6.5	1705	1154	1398	1738	582
159.8	8.68	4.12	7.1	6.6	1672	1210	1399	1774	609
162.2	8.92	4.11	7.2	6.8	1719	1228	1460	1763	609
164.8	9.39	4.09	7.4	6.9	1705	1249	1565	1829	654
167.3	9.59	4.09	7.6	7.1	1728	1286	1563	1848	621
169.6	9.75	4.09	7.7	7.2	1765	1282	1588	1835	654
172.3	9.93	4.07	7.8	7.4	1841	1372	1608	1927	641
174.6	10.09	4.08	8.0	7.5	1855	1451	1636	1979	664
177.2	10.28	4.09	8.1	7.6	1867	1435	1692	1956	690
179.8	10.46	4.10	8.2	7.8	1865	1505	1692	1969	688
182.3	10.64	4.11	8.4	7.9	1892	1458	1736	1996	693
184.8	10.82	4.12	8.5	8.0	1937	1559	1766	2014	699
186.1	10.91	4.12	8.6	8.1	1982	1567	1746	2097	688
187.3	10.98	4.12	8.7	8.2	2032	1589	1758	2111	688
188.5	11.08	4.12	8.7	8.3	2013	1616	1782	2090	695
189.8	11.16	4.12	8.8	8.3	1942	1575	1844	2085	693
191.2	11.26	4.22	8.9	8.4	1973	1649	1787	2085	707
192.4	11.34	4.30	9.0	8.5	2081	1671	1842	2088	678
193.6	11.42	4.35	9.0	8.6	2067	1632	1844	2103	701
194.7	11.50	4.42	9.1	8.6	2097	1663	1842	2187	688
196.2	11.61	4.50	9.2	8.7	2116	1632	1846	2175	670
197.3	11.69	4.55	9.3	8.8	2089	1684	1865	2128	685
198.6	11.78	4.61	9.4	8.9	2096	1674	1881	2116	687
199.7	11.85	4.79	9.5	9.0	2139	1690	1941	2191	658
201.0	11.94	5.23	9.6	9.1	2134	1766	1906	2208	678

Continued

Table A.34 Test Data for Beam S6-4 (*Continued*)

V (kN)	Curv. (Left) ($\times 10^{-6}$ mm^{-1})	Curv. (Right) ($\times 10^{-6}$ mm^{-1})	d_{max} (Front) (mm)	d_{max} (Back) (mm)	ε_{st}3F ($\times 10^{-6}$)	ε_{st}3G ($\times 10^{-6}$)	ε_{st}3H ($\times 10^{-6}$)	ε_{st}4I ($\times 10^{-6}$)	ε_{st}4J ($\times 10^{-6}$)
202.3	12.05	5.55	9.7	9.2	2151	1706	1934	2197	713
203.5	12.16	5.81	9.9	9.4	2172	1772	1929	2231	719
204.7	12.25	6.04	10.0	9.5	2161	1827	1953	2245	727
207.5	12.34	6.21	10.1	9.6	2166	1789	1915	2168	744
210.0	12.44	6.42	10.2	9.7	2223	1809	1976	2257	760
212.5	12.54	6.66	10.3	9.8	2250	1865	1982	2273	784
209.2	12.62	6.89	10.5	10.0	2193	1840	1951	2274	780
205.5	12.75	7.12	10.7	10.2	2250	1844	2011	2272	829
199.2	12.93	7.32	11.0	10.4	-	-	-	-	-
186.8	13.17	7.71	11.3	10.8	-	-	-	-	-

Table A.35 Test Data for Beam S6-5

V (kN)	Curv. (Left) (x10⁻⁶ mm⁻¹)	Curv. (Right) (x10⁻⁶ mm⁻¹)	d_{max} (Front) (mm)	d_{max} (Back) (mm)
0.0	0.00	0.00	0.0	0.0
6.2	0.02	0.01	0.2	0.1
11.2	0.03	0.03	0.4	0.3
12.4	0.06	0.03	0.4	0.3
18.7	0.12	0.08	0.6	0.5
25.0	0.21	0.12	0.8	0.7
31.3	0.35	0.12	1.0	0.9
37.5	0.50	0.12	1.2	1.1
43.8	0.63	0.16	1.4	1.3
50.0	0.79	0.25	1.6	1.5
56.3	1.00	0.34	1.7	1.7
62.6	1.23	0.47	1.9	1.9
68.7	1.42	0.61	2.1	2.0
74.8	1.59	0.76	2.3	2.2
81.2	1.76	0.93	2.4	2.4
87.3	1.91	1.13	2.6	2.6
93.6	2.10	1.57	2.8	2.7
99.8	2.50	1.86	3.0	2.9
106.1	3.13	2.27	3.3	3.2
112.4	3.51	3.04	3.6	3.4
118.6	3.85	3.41	3.8	3.6
124.8	4.15	3.70	4.0	3.9
131.0	4.41	3.95	4.2	4.0
137.2	4.66	4.21	4.5	4.3
143.6	4.90	4.49	4.7	4.5
149.8	5.14	4.74	4.9	4.7
156.1	5.40	4.97	5.1	4.9
169.9	6.25	5.50	5.7	5.4
174.7	6.44	5.65	5.9	5.6
181.1	6.71	5.85	6.1	5.8
187.4	7.00	6.06	6.3	6.0
193.5	7.28	6.25	6.6	6.2
199.7	7.59	6.44	6.8	6.5
202.2	7.71	6.50	6.9	6.5
204.8	7.86	6.57	7.1	6.7
207.5	8.02	6.63	7.2	6.8
210.0	8.15	6.68	7.3	6.9
212.5	8.27	6.68	7.4	7.0
215.0	8.40	6.64	7.6	7.2
217.5	8.53	6.64	7.7	7.3
220.0	8.68	6.64	7.8	7.4
222.5	8.80	6.64	7.9	7.5
225.0	8.92	6.66	8.0	7.6
227.5	9.06	6.68	8.1	7.7
230.0	9.18	6.71	8.2	7.8
232.5	9.31	6.75	8.4	7.9
235.0	9.45	6.84	8.5	8.1
237.5	9.58	6.94	8.6	8.2
240.0	9.72	7.03	8.7	8.3
242.5	9.86	7.11	8.8	8.4
245.0	9.99	7.20	8.9	8.5
247.5	10.21	7.28	9.1	8.6
250.0	10.34	7.35	9.2	8.7

Continued

A.33

Table A.35 Test Data for Beam S6-5 (*Continued*)

V (kN)	Curv. (Left) ($\times 10^{-6}$ mm^{-1})	Curv. (Right) ($\times 10^{-6}$ mm^{-1})	d_{max} (Front) (mm)	d_{max} (Back) (mm)
252.5	10.49	7.44	9.3	8.8
255.0	10.64	7.51	9.4	9.0
257.5	10.79	7.61	9.5	9.1
260.0	10.95	7.69	9.6	9.2
262.5	11.11	7.77	9.8	9.3
265.0	11.26	7.85	9.9	9.4
267.5	11.41	7.95	10.0	9.6
270.0	11.56	8.03	10.1	9.7
272.5	11.74	8.11	10.3	9.9
275.0	11.84	8.18	10.4	10.0
277.5	11.82	8.32	10.6	10.2
280.0	11.71	8.41	10.8	10.4
282.5	11.71	8.49	11.0	10.6
285.0	11.73	8.55	11.2	10.7
287.5	11.79	8.60	11.3	10.9
290.0	11.91	8.66	11.5	11.1
292.5	12.03	8.71	11.7	11.3
295.0	12.17	8.77	12.0	11.6

Table A.36 Test Data for Beam S6-6

V (kN)	Curv. (Left) (x10^{-6} mm^{-1})	Curv. (Right) (x10^{-6} mm^{-1})	d_{max} (Front) (mm)	d_{max} (Back) (mm)
0.0	0.00	0.00	0.0	0.0
6.2	0.02	0.02	0.2	0.1
12.5	0.04	0.05	0.4	0.3
18.7	0.09	0.10	0.5	0.4
25.0	0.15	0.13	0.7	0.6
31.2	0.21	0.15	0.9	0.8
37.5	0.35	0.21	1.1	1.0
43.7	0.50	0.26	1.3	1.2
50.0	0.67	0.33	1.5	1.3
56.3	0.89	0.44	1.7	1.5
62.5	1.11	0.62	1.8	1.7
68.6	1.33	0.97	2.0	1.9
74.9	1.62	1.19	2.2	2.1
81.1	1.88	1.41	2.4	2.3
87.3	2.13	1.62	2.6	2.5
93.7	3.39	1.86	2.9	2.8
99.9	3.76	2.09	3.1	3.0
106.1	4.05	2.30	3.3	3.2
112.4	4.37	2.54	3.5	3.4
118.6	4.68	3.05	3.8	3.6
124.9	5.02	3.38	4.0	3.9
131.1	5.33	3.83	4.3	4.1
137.4	5.64	4.18	4.5	4.3
143.6	5.96	4.48	4.7	4.6
149.9	6.25	4.75	4.9	4.8
156.1	6.54	5.01	5.2	5.0
162.4	6.84	5.27	5.4	5.2
168.6	7.15	5.54	5.6	5.4
174.9	7.47	5.78	5.8	5.6
177.8	7.62	5.87	5.9	5.8
179.9	7.73	5.94	6.0	5.8
182.3	7.90	6.06	6.2	6.0
184.7	8.03	6.13	6.3	6.1
187.3	8.14	6.14	6.4	6.2
189.9	8.26	6.19	6.5	6.3
192.4	8.37	6.24	6.6	6.4
194.9	8.48	6.29	6.7	6.5
197.2	8.80	6.32	7.0	6.8
199.9	9.10	6.39	7.2	7.0
202.4	9.18	6.45	7.3	7.1
204.9	9.26	6.53	7.4	7.2
207.5	9.36	6.59	7.5	7.3
210.0	9.45	6.62	7.6	7.4
212.5	9.54	6.64	7.7	7.5
215.0	9.63	6.68	7.8	7.6
217.5	9.73	6.71	7.9	7.7
220.0	9.82	6.73	8.1	7.8
222.5	9.93	6.74	8.2	7.9
225.0	10.03	6.77	8.3	8.0
227.5	10.13	6.79	8.4	8.1
230.0	10.25	6.82	8.5	8.3
232.5	10.35	6.87	8.6	8.4
235.0	10.46	6.91	8.7	8.5

Continued

A.35

Table A.36 Test Data for Beam S6-6 (*Continued*)

V (kN)	Curv. (Left) ($\times 10^{-6}$ mm^{-1})	Curv. (Right) ($\times 10^{-6}$ mm^{-1})	d_{max} (Front) (mm)	d_{max} (Back) (mm)
237.5	10.57	6.99	8.8	8.6
240.0	10.69	7.02	9.0	8.7
242.5	10.81	7.08	9.1	8.8
245.0	10.93	7.15	9.2	8.9
247.5	11.05	7.22	9.3	9.1
250.0	11.18	7.30	9.4	9.2
252.5	11.30	7.38	9.6	9.3
255.0	11.42	7.46	9.7	9.4
257.5	11.55	7.56	9.8	9.6
260.0	11.67	7.65	10.0	9.7
262.5	11.79	7.77	10.2	9.9
265.0	12.07	8.01	10.5	10.2
267.5	12.28	8.21	10.8	10.5
270.0	12.51	8.34	11.0	10.7
272.5	12.74	8.45	11.2	10.9
275.0	12.92	8.57	11.5	11.1
277.5	13.15	8.68	11.7	11.4
280.0	13.36	8.79	12.0	11.7
282.5	13.59	8.91	12.3	12.0
285.0	13.80	9.02	12.7	12.4

Table A.37 Test Data for Beam S7-1

V (kN)	Curv. (Left) ($\times 10^{-6}$ mm^{-1})	Curv. (Right) ($\times 10^{-6}$ mm^{-1})	d_{max} (Front) (mm)	d_{max} (Back) (mm)
0.0	0.00	0.00	0.0	0.0
12.1	0.06	0.07	0.5	0.0
24.6	0.24	0.24	0.7	0.0
37.2	0.57	0.54	0.9	0.5
49.8	0.99	0.90	1.2	0.4
62.2	1.52	1.26	1.5	0.8
74.7	1.89	1.91	1.8	1.2
87.3	2.29	2.40	2.1	1.5
99.8	2.67	2.83	2.3	1.5
112.4	3.13	3.07	2.7	2.2
124.8	4.20	3.50	3.1	2.4
132.4	4.27	3.90	3.5	3.0
137.2	4.24	4.07	3.7	3.2
149.6	4.29	4.37	4.3	3.7
162.1	4.42	4.35	5.1	4.4
174.5	4.50	4.52	5.7	4.9
187.1	4.49	4.82	6.3	5.8
199.6	4.40	5.17	7.0	6.5
204.5	4.31	5.31	7.3	6.7
209.4	4.19	5.56	7.7	7.0
214.4	3.75	5.75	8.2	7.6
214.6	3.00	5.79	8.5	8.0
211.9	2.51	5.72	8.6	8.1
210.9	1.68	5.48	8.9	8.6

Table A.38 Test Data for Beam S7-2

V (kN)	Curv. (Left) ($\times 10^{-6}$ mm^{-1})	Curv. (Right) ($\times 10^{-6}$ mm^{-1})	d_{max} (Front) (mm)	d_{max} (Back) (mm)
0.0	0.00	0.00	0.0	0.0
12.6	0.07	0.08	0.1	0.1
25.2	0.31	0.24	0.3	0.3
37.7	0.56	0.45	0.5	0.5
50.2	0.83	0.72	0.7	0.7
62.8	1.42	1.23	0.9	0.9
75.2	1.98	1.54	1.1	1.2
87.8	2.50	1.87	1.4	1.4
100.3	3.11	2.28	1.6	1.7
112.9	3.62	2.66	1.9	2.0
125.4	4.10	3.05	2.2	2.3
137.6	4.75	3.50	2.5	2.7
142.9	5.15	4.31	3.0	3.2
145.8	5.15	4.37	3.1	3.2
147.2	5.18	4.40	3.1	3.3
147.8	5.21	4.40	3.1	3.3
149.9	5.31	4.43	3.2	3.4
162.5	5.81	4.62	3.7	3.9
175.0	5.58	4.64	4.3	4.6
187.6	4.22	4.61	5.7	6.1
199.9	3.22	4.55	6.8	7.3
204.9	2.09	4.55	7.6	8.0

Table A.39 Test Data for Beam S7-3

V (kN)	Curv. (Left) (x10⁻⁶ mm⁻¹)	Curv. (Right) (x10⁻⁶ mm⁻¹)	d_{max} (Front) (mm)	d_{max} (Back) (mm)	$\varepsilon_{st}1A$ (x10⁻⁶)	$\varepsilon_{st}1B$ (x10⁻⁶)	$\varepsilon_{st}2C$ (x10⁻⁶)	$\varepsilon_{st}2D$ (x10⁻⁶)	$\varepsilon_{st}2E$ (x10⁻⁶)
0.0	0.00	0.00	0.0	0.0	0	0	0	0	0
12.6	0.10	0.15	0.2	0.2	55	58	44	62	29
25.0	0.31	0.43	0.4	0.5	79	142	69	136	93
37.7	0.53	0.75	0.6	0.7	137	194	103	202	125
50.2	0.77	1.09	0.8	0.9	236	253	183	227	164
62.7	1.07	1.49	1.1	1.1	308	320	229	301	216
75.2	1.40	1.95	1.3	1.4	348	389	252	354	224
87.8	1.86	2.26	1.6	1.7	345	409	317	434	301
100.2	2.47	2.64	1.9	2.0	411	487	376	458	340
112.8	2.93	3.07	2.2	2.3	521	588	400	568	452
125.3	3.37	3.50	2.5	2.6	586	640	459	589	509
137.4	3.81	3.98	2.8	2.9	739	769	582	702	664
146.9	4.20	4.16	3.3	3.4	868	982	751	728	879
147.8	4.20	4.13	3.3	3.5	855	945	743	744	902
147.8	4.20	4.01	3.4	3.5	935	1008	847	772	885
148.1	4.21	3.99	3.4	3.6	894	1037	745	758	871
148.9	4.22	3.99	3.4	3.6	884	929	776	734	898
149.5	4.24	4.01	3.5	3.6	872	974	786	784	906
149.9	4.26	4.03	3.5	3.6	843	1000	804	770	910
162.4	5.07	4.21	4.2	4.3	984	1076	866	813	986
174.9	5.49	4.46	4.6	4.8	1082	1197	948	891	1094
187.3	5.92	4.66	5.1	5.3	1229	1263	1003	1000	1164
193.5	5.74	4.69	5.6	5.8	1234	1288	1253	1024	1170
194.6	5.72	4.70	5.6	5.8	-	-	-	-	-
195.4	5.70	4.70	5.7	5.8	1276	1312	1226	1018	1183
195.9	5.70	4.71	5.7	5.9	1285	1343	1171	1016	1205
196.4	5.69	4.72	5.7	5.9	1242	1271	1313	1019	1213
199.8	5.70	4.77	5.9	6.1	1285	1341	1253	1095	1303
212.3	5.88	4.81	6.5	6.7	1418	1415	1380	1168	1344
222.5	5.88	5.26	7.4	7.5	1514	1617	1427	1174	1451
223.7	5.88	5.38	7.5	7.6	1465	1702	1458	1207	1447
224.4	5.88	5.45	7.5	7.6	-	-	-	-	-
224.8	5.89	5.50	7.5	7.6	1496	1743	1460	1217	1494
225.1	5.90	5.53	7.5	7.6	1443	1673	1432	1214	1454
229.9	5.92	5.83	7.8	7.9	1538	1724	1554	1206	1494
234.9	5.94	5.91	8.1	8.2	1545	1788	1539	1314	1540
239.8	5.93	5.91	8.5	8.6	1553	1830	1640	1358	1577
244.8	5.90	5.80	8.9	9.0	1644	1864	1645	1410	1587

Table A.40 Test Data for Beam S7-4

V (kN)	Curv. (Left) (x10⁻⁶ mm⁻¹)	Curv. (Right) (x10⁻⁶ mm⁻¹)	d_{max} (Front) (mm)	d_{max} (Back) (mm)	$\varepsilon_{s\ell}3F$ (x10⁻⁶)	$\varepsilon_{s\ell}3G$ (x10⁻⁶)	$\varepsilon_{s\ell}3H$ (x10⁻⁶)	$\varepsilon_{s\ell}4I$ (x10⁻⁶)	$\varepsilon_{s\ell}4J$ (x10⁻⁶)
0.0	0.00	0.00	0.0	0.0	0	0	0	0	0
12.6	0.01	0.19	0.0	0.2	77	78	65	69	57
25.1	0.02	0.41	0.2	0.3	141	169	130	140	155
37.7	0.29	0.73	0.4	0.5	237	205	206	190	236
50.2	0.58	1.24	0.6	0.8	322	334	278	263	307
62.8	0.90	1.81	0.9	1.0	384	387	344	376	445
72.8	1.13	2.26	1.1	1.2	395	434	417	407	465
87.8	1.88	2.86	1.4	1.6	472	569	539	525	541
100.2	2.29	3.37	1.7	1.8	558	618	562	604	617
112.8	2.81	3.91	2.0	2.1	655	722	620	623	721
125.4	3.38	4.70	2.3	2.4	693	773	718	699	799
137.6	3.95	5.60	2.7	2.8	826	947	798	837	906
150.1	4.93	6.35	3.1	3.3	925	976	868	853	940
162.4	5.52	6.95	3.5	3.7	1049	1101	921	924	1037
174.9	6.10	7.63	3.9	4.1	1146	1185	1011	986	1078
184.9	6.90	8.17	4.5	4.7	1185	1273	1069	1062	1180
185.6	6.93	8.20	4.5	4.7	1204	1240	1059	1042	1133
187.5	7.02	8.29	4.6	4.8	1204	1308	1073	1083	1180
199.9	7.51	8.96	5.0	5.2	1320	1374	1158	1237	1306
212.4	8.05	9.63	5.5	5.7	1369	1450	1137	1304	1295
224.9	8.63	10.31	5.9	6.2	1530	1597	1327	1375	1479
230.9	8.91	10.62	6.2	6.5	1553	1659	1424	1468	1500
234.8	9.11	10.80	6.4	6.7	1583	1604	1367	1381	1524
239.9	9.38	11.01	6.6	6.9	1613	1698	1520	1511	1620
244.9	9.64	11.24	6.8	7.1	1642	1659	1468	1446	1598
249.8	9.91	11.46	7.1	7.4	1746	1661	1635	1567	1682
254.9	10.22	11.70	7.3	7.6	1778	1700	1629	1580	1706
259.9	10.54	11.95	7.6	7.9	1800	1793	1702	1681	1701
264.9	10.88	12.27	7.9	8.2	1874	1809	1743	1817	1731
269.8	11.17	12.50	8.1	8.5	1928	1882	1755	1836	1864

Table A.41 Test Data for Beam S7-5

V (kN)	Curv. (Left) ($\times 10^{-6}$ mm^{-1})	Curv. (Right) ($\times 10^{-6}$ mm^{-1})	d_{max} (Front) (mm)	d_{max} (Back) (mm)
0.0	0.00	0.00	0.0	0.0
12.6	0.14	0.16	0.2	0.2
25.1	0.36	0.40	0.4	0.4
37.7	0.76	0.85	0.6	0.6
50.2	1.11	1.34	0.9	0.9
62.8	1.37	1.62	1.1	1.1
75.3	1.68	1.85	1.4	1.4
87.8	1.99	2.14	1.6	1.6
100.3	2.33	2.45	1.9	1.9
112.9	2.72	2.74	2.1	2.1
125.4	3.11	3.04	2.4	2.4
137.6	3.46	3.33	2.7	2.7
149.9	3.81	3.75	3.1	3.1
162.4	4.14	4.24	3.5	3.5
174.9	4.43	4.48	3.9	4.0
187.4	4.73	4.69	4.3	4.4
199.9	5.05	5.06	4.7	4.9
212.4	5.37	5.55	5.2	5.3
224.8	5.65	6.07	5.8	5.9
237.3	6.14	6.46	6.3	6.4
249.9	6.40	6.97	6.8	7.0
254.9	6.50	7.22	7.1	7.3
259.8	6.58	7.40	7.3	7.5
264.8	6.67	7.58	7.5	7.7
269.8	6.77	7.76	7.8	8.0
274.8	6.86	7.98	8.0	8.3
279.9	6.94	8.15	8.3	8.5
284.9	7.02	8.32	8.6	8.9
290.0	7.08	8.47	8.9	9.2
294.8	7.10	8.62	9.2	9.5
299.8	7.12	8.75	9.5	9.8

Table A.42 Test Data for Beam S7-6

V (kN)	Curv. (Left) ($\times10^{-6}$ mm^{-1})	Curv. (Right) ($\times10^{-6}$ mm^{-1})	d_{max} (Front) (mm)	d_{max} (Back) (mm)
0.0	0.00	0.00	0.0	0.0
12.5	0.09	0.10	0.1	0.3
25.0	0.30	0.30	0.3	0.7
37.6	0.78	0.72	0.6	1.1
50.1	1.27	1.12	0.8	1.5
62.8	1.71	1.49	1.1	1.8
75.2	2.15	1.83	1.3	2.2
87.8	2.57	2.18	1.5	2.5
100.3	2.82	2.51	1.8	2.8
112.7	3.18	2.86	2.0	3.2
122.8	3.55	3.15	2.2	3.5
137.4	4.10	3.75	2.6	3.9
149.8	4.58	4.17	2.9	4.3
162.4	5.06	4.57	3.3	4.7
174.8	5.62	5.04	3.7	5.2
187.3	6.22	5.60	4.2	5.6
199.8	6.75	6.11	4.6	6.1
212.1	7.66	6.64	5.2	6.5
224.7	8.33	7.08	5.6	7.0
237.2	8.91	7.46	6.0	7.4
249.7	9.47	7.88	6.4	7.9
262.2	10.06	8.28	6.9	8.4
274.7	10.72	8.67	7.5	8.9
287.4	11.39	9.18	8.2	9.5
299.6	11.67	9.62	8.9	10.3
309.9	12.34	9.84	9.8	11.3
308.6	12.36	9.82	9.9	11.4
308.9	12.43	9.81	9.9	11.4
309.1	12.58	9.81	10.0	11.5

Table A.43 Test Data for Beam S8-1

V (kN)	Curv. (Left) ($\times 10^{-6}$ mm^{-1})	Curv. (Right) ($\times 10^{-6}$ mm^{-1})	d_{max} (Front) (mm)	d_{max} (Back) (mm)
0.0	0.00	0.00	0.0	0.0
12.7	0.02	0.07	0.2	0.2
25.2	0.13	0.15	0.4	0.4
37.7	0.25	0.24	0.6	0.7
50.4	0.38	0.25	0.9	0.9
62.8	0.61	0.31	1.2	1.2
75.3	0.81	0.43	1.4	1.5
88.0	1.08	0.64	1.7	1.7
100.7	1.41	1.04	2.1	2.1
113.2	1.85	1.41	2.4	2.4
125.4	2.81	1.94	2.9	2.9
137.5	3.64	3.58	3.7	3.7
149.9	4.44	4.22	4.2	4.2
162.4	5.18	4.82	4.7	4.7
174.6	5.84	5.32	5.2	5.1
187.5	6.51	5.87	5.7	5.6
201.4	7.23	6.38	6.2	6.2
204.7	7.49	6.48	6.4	6.3
210.0	8.02	6.66	6.6	6.5
214.7	8.28	6.82	6.7	6.7
220.1	8.56	7.01	7.0	6.9
224.8	8.82	7.17	7.1	7.1
229.4	9.06	7.34	7.3	7.2
234.9	9.33	7.52	7.5	7.5
239.7	9.58	7.72	7.8	7.7
244.8	9.85	7.94	8.0	7.9
249.8	10.10	8.14	8.2	8.1
254.9	10.40	8.36	8.5	8.3
259.8	10.67	8.57	8.7	8.6
264.7	10.96	8.88	9.0	8.9
269.7	11.26	9.21	9.4	9.3
270.8	11.42	9.22	9.8	9.6

Table A.44 Test Data for Beam S8-2

V (kN)	Curv. (Left) ($\times 10^{-6}$ mm^{-1})	Curv. (Right) ($\times 10^{-6}$ mm^{-1})	d_{max} (Front) (mm)	d_{max} (Back) (mm)
0.0	0.00	0.00	0.0	0.0
12.5	0.02	0.09	0.3	0.2
24.9	0.10	0.19	0.5	0.4
37.6	0.23	0.31	0.8	0.7
50.1	0.32	0.61	1.1	0.9
62.8	0.36	0.91	1.4	1.2
75.3	0.47	1.18	1.6	1.5
87.8	0.74	1.42	1.9	1.7
100.2	1.19	1.92	2.2	2.1
112.7	2.06	2.81	2.6	2.5
125.3	2.67	5.92	3.5	3.3
137.4	3.26	6.68	4.0	3.7
149.8	4.50	7.33	4.5	4.2
162.1	5.28	7.93	4.9	4.7
175.1	6.04	8.53	5.3	5.1
187.2	6.68	9.13	5.8	5.5
199.9	7.38	9.72	6.2	6.0
204.5	7.61	9.96	6.4	6.1
209.8	7.86	10.21	6.6	6.3
214.8	8.09	10.45	6.8	6.5
219.7	8.31	10.69	6.9	6.7
224.7	8.60	10.94	7.1	6.9
229.6	8.91	11.22	7.3	7.0
234.5	9.21	11.49	7.5	7.2
239.8	9.55	11.79	7.8	7.5
245.2	9.88	12.16	8.0	7.7
249.5	10.13	12.50	8.2	7.9

Table A.45 Test Data for Beam S8-3

V (kN)	Curv. (Left) ($\times 10^{-6}$ mm^{-1})	Curv. (Right) ($\times 10^{-6}$ mm^{-1})	d_{max} (Front) (mm)	d_{max} (Back) (mm)
0.0	0.00	0.00	0.0	0.0
12.6	0.03	0.06	0.3	0.3
25.2	0.12	0.14	0.5	0.5
37.8	0.23	0.22	0.8	0.8
49.9	0.34	0.32	1.0	1.0
62.7	0.47	0.82	1.4	1.4
75.2	0.99	1.21	1.7	1.7
88.0	1.24	1.55	1.9	2.0
101.5	1.55	2.28	2.3	2.3
112.6	1.82	3.06	2.6	2.6
125.4	2.32	5.29	3.3	3.3
137.4	2.91	6.13	3.7	3.8
149.9	3.49	6.90	4.1	4.2
162.3	4.32	7.53	4.6	4.7
174.8	5.12	8.07	5.0	5.1
187.3	5.96	8.63	5.4	5.5
199.6	6.82	9.10	5.8	5.9
212.5	7.54	9.67	6.3	6.3
224.8	8.30	10.24	6.7	6.7
237.2	9.03	10.86	7.1	7.2
249.6	9.69	11.55	7.5	7.6
262.8	10.35	12.37	8.0	8.1
274.8	10.99	13.19	8.5	8.5
287.4	11.68	14.19	9.0	9.0
299.8	12.50	15.38	9.6	9.6

Table A.46 Test Data for Beam S8-4

V (kN)	Curv. (Left) ($\times 10^{-6}$ mm^{-1})	Curv. (Right) ($\times 10^{-6}$ mm^{-1})	d_{max} (Front) (mm)	d_{max} (Back) (mm)
0.0	0.00	0.00	0.0	0.0
12.4	0.01	0.09	0.3	0.2
25.1	0.06	0.21	0.5	0.3
37.5	0.13	0.31	0.8	0.6
50.0	0.20	0.33	1.2	0.9
62.6	0.23	0.37	1.5	1.2
75.3	0.24	0.45	1.8	1.4
87.5	0.25	0.71	2.1	1.8
101.1	0.38	0.98	2.5	2.1
112.5	0.56	1.54	2.8	2.5
125.2	1.04	3.89	3.5	3.3
137.3	1.99	4.49	4.0	3.7
150.8	3.34	4.99	4.5	4.3
162.3	3.92	5.46	4.9	4.7
175.1	4.66	5.96	5.4	5.1
187.3	5.38	6.41	5.8	5.5
199.6	6.47	7.06	6.3	6.0
212.3	7.08	7.69	6.7	6.4
225.1	7.68	8.38	7.2	6.9
237.4	8.26	9.10	7.6	7.4
250.5	8.87	9.98	8.1	7.9
262.2	9.45	11.14	8.7	8.5

Table A.47 Test Data for Beam S8-5

V (kN)	Curv. (Left) $(\times 10^{-6} \text{ mm}^{-1})$	Curv. (Right) $(\times 10^{-6} \text{ mm}^{-1})$	d_{max} (Front) (mm)	d_{max} (Back) (mm)
0.0	0.00	0.00	0.0	0.0
12.5	0.04	0.05	0.4	0.1
25.0	0.14	0.13	0.7	0.3
37.7	0.33	0.24	1.0	0.5
50.1	0.73	0.38	1.3	0.8
62.6	0.98	0.58	1.6	1.1
75.2	1.35	0.84	1.9	1.3
87.6	1.74	1.16	2.1	1.6
100.0	2.15	1.47	2.4	1.9
112.8	2.71	1.85	2.8	2.3
125.2	3.20	3.06	3.3	2.7
137.4	3.74	4.20	3.8	3.3
149.9	4.27	4.88	4.2	3.7
162.1	4.85	5.34	4.6	4.1
174.8	5.47	5.80	5.1	4.6
187.2	6.07	6.25	5.5	5.0
199.7	7.02	6.74	6.0	5.5
212.3	7.63	7.26	6.4	5.9
224.8	8.23	7.76	6.9	6.4
237.1	8.80	8.29	7.4	6.9
249.4	9.37	8.83	8.0	7.4
254.7	9.61	9.06	8.2	7.7
259.7	9.84	9.27	8.4	7.9
264.5	10.10	9.51	8.6	8.1
269.6	10.40	9.75	8.9	8.3
274.4	10.69	9.99	9.1	8.6
279.7	10.96	10.25	9.4	8.8
284.6	11.27	10.57	9.7	9.1

Table A.48 Test Data for Beam S8-6

V (kN)	Curv. (Left) ($\times 10^{-6}$ mm^{-1})	Curv. (Right) ($\times 10^{-6}$ mm^{-1})	d_{max} (Front) (mm)	d_{max} (Back) (mm)
0.0	0.00	0.00	0.0	0.0
12.6	0.00	0.07	0.4	0.2
20.2	0.04	0.11	0.5	0.3
25.0	0.08	0.14	0.6	0.3
37.5	0.20	0.21	0.8	0.5
50.0	0.35	0.26	1.1	0.8
62.7	0.50	0.30	1.4	1.1
75.2	0.73	0.32	1.7	1.4
87.8	1.12	0.36	2.0	1.6
100.3	1.59	0.43	2.3	1.9
112.8	1.95	0.48	2.6	2.2
125.0	2.84	1.93	3.1	2.7
137.4	4.45	3.19	3.8	3.3
149.8	5.11	3.99	4.3	3.8
162.4	5.67	4.45	4.7	4.2
174.9	6.22	4.89	5.1	4.5
187.3	6.83	5.30	5.5	4.9
199.7	7.37	5.72	5.9	5.2
212.1	7.94	6.17	6.3	5.6
224.7	8.53	6.60	6.7	6.0
237.4	9.10	7.06	7.1	6.4
249.6	9.72	7.53	7.5	6.8
262.1	10.38	8.06	8.0	7.2
274.6	11.16	8.69	8.5	7.7
279.6	11.53	8.97	8.8	7.9

Crack Pattern Of Test Beams

Photographs showing the crack patterns of the front and back faces of each test beam of the present study are given in the following pages.
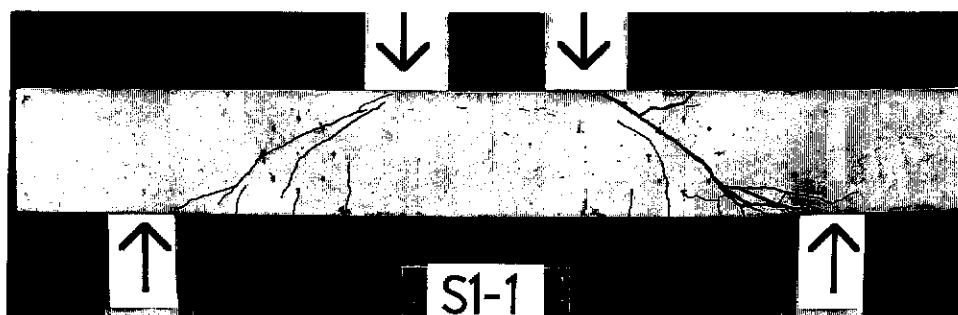
Figure B.1 Crack Pattern of the Front Face of Beam S1-1
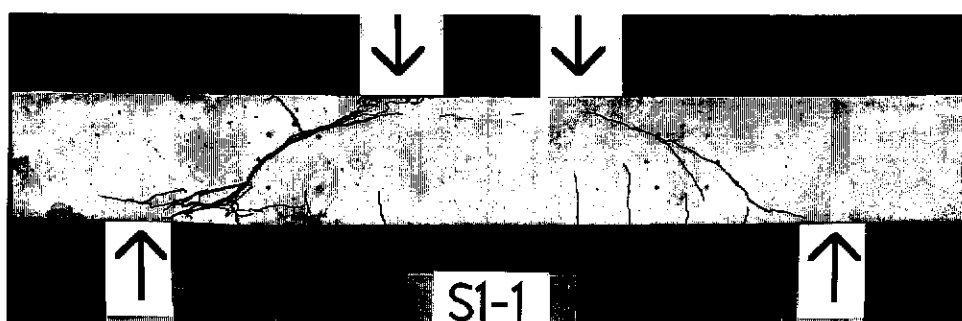
Figure B.2 Crack Pattern of the Back Face of Beam S1-1
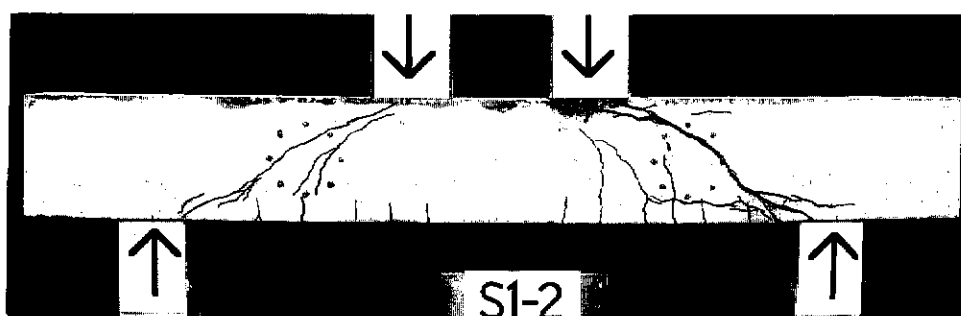
Figure B.3 Crack Pattern of the Front Face of Beam S1-2
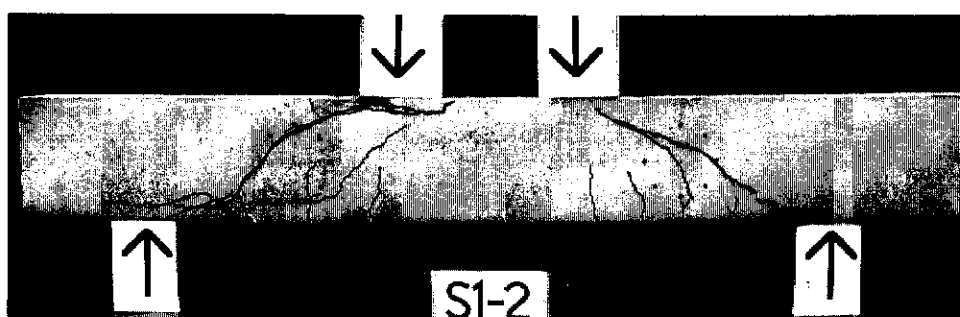
Figure B.4 Crack Pattern of the Back Face of Beam S1-2
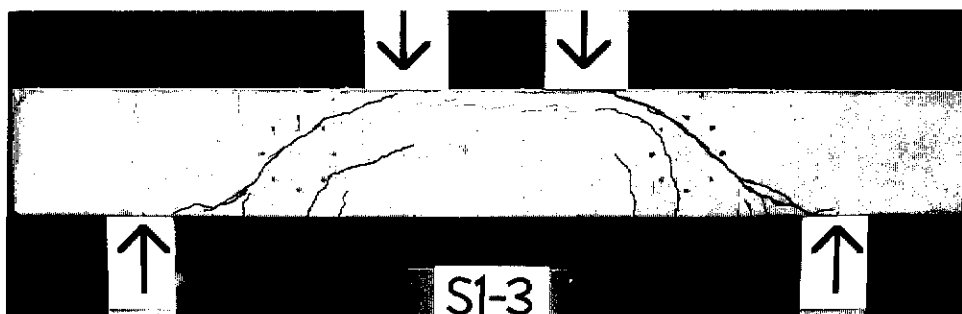
Figure B.5 Crack Pattern of the Front Face of Beam S1-3
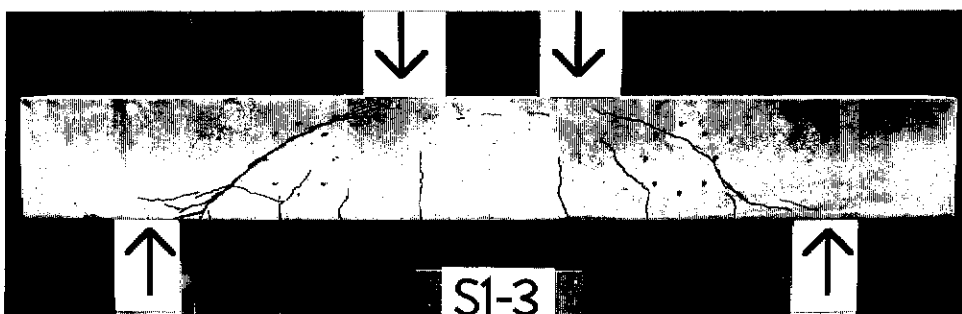
Figure B.6 Crack Pattern of the Back Face of Beam S1-3
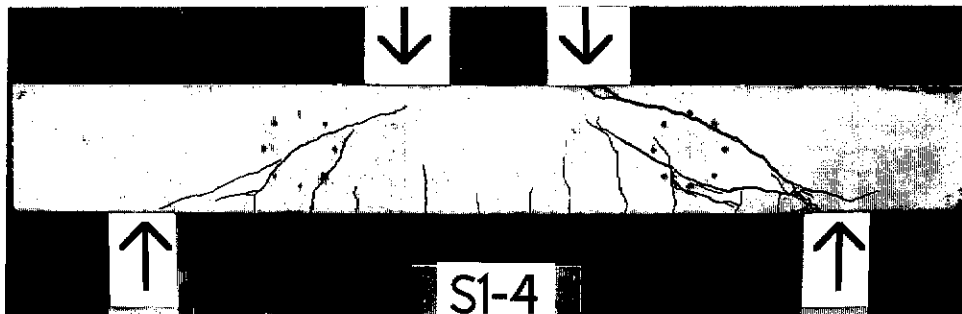
Figure B.7 Crack Pattern of the Front Face of Beam S1-4
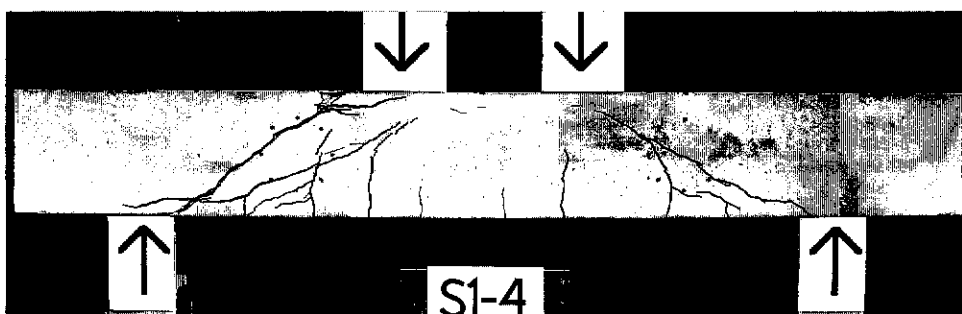
Figure B.8 Crack Pattern of the Back Face of Beam S1-4
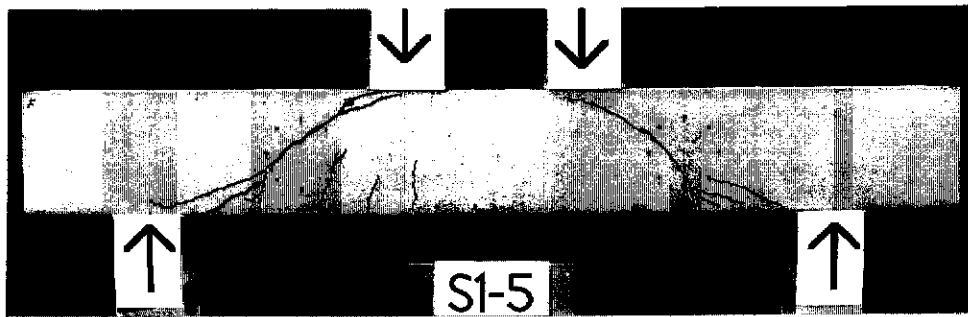
Figure B.9 Crack Pattern of the Front Face of Beam S1-5
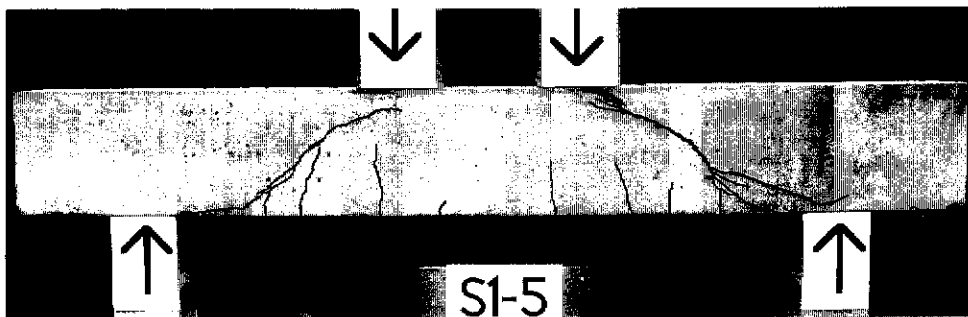
Figure B.10 Crack Pattern of the Back Face of Beam S1-5
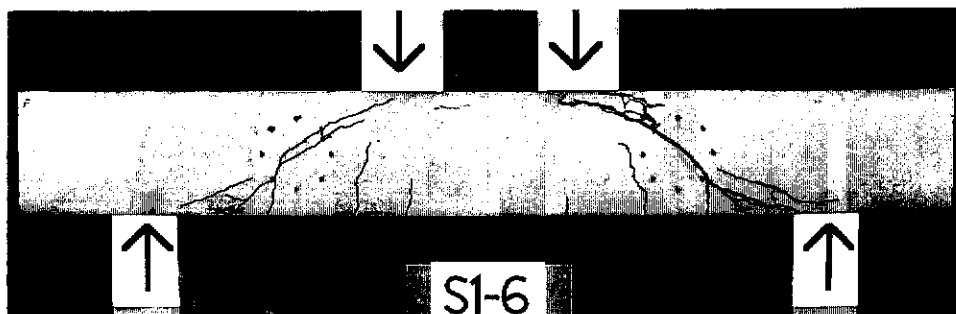
Figure B.11 Crack Pattern of the Front Face of Beam S1-6
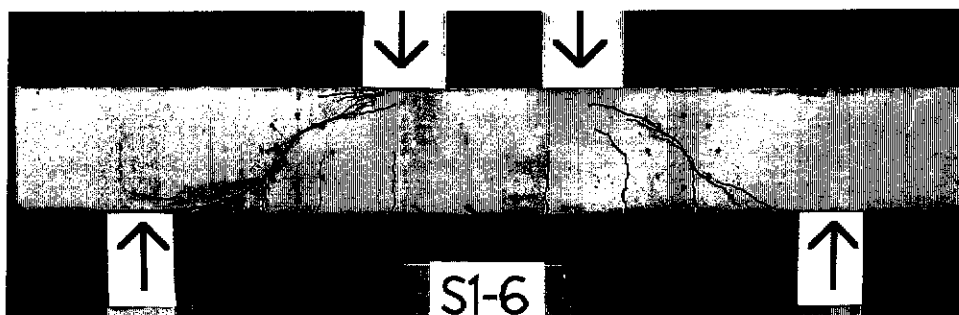
Figure B.12 Crack Pattern of the Back Face of Beam S1-6
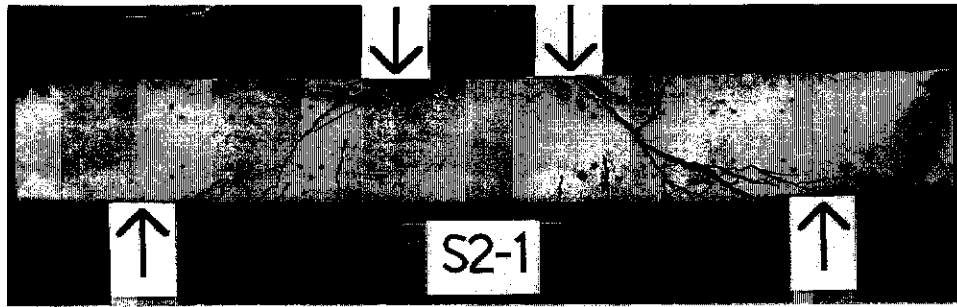
Figure B.13 Crack Pattern of the Front Face of Beam S2-1
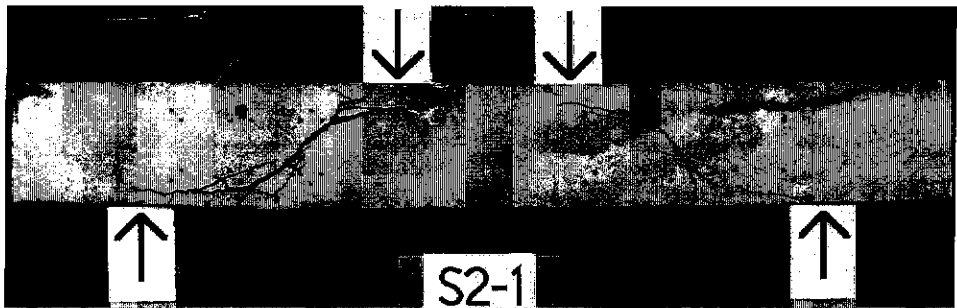
Figure B.14 Crack Pattern of the Back Face of Beam S2-1
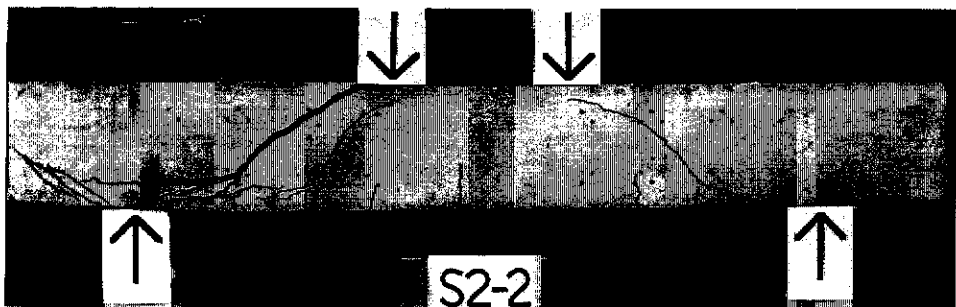
Figure B.15 Crack Pattern of the Front Face of Beam S2-2
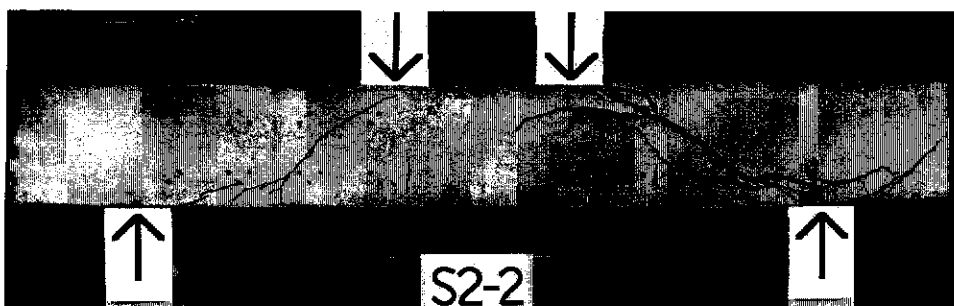
Figure B.16 Crack Pattern of the Back Face of Beam S2-2
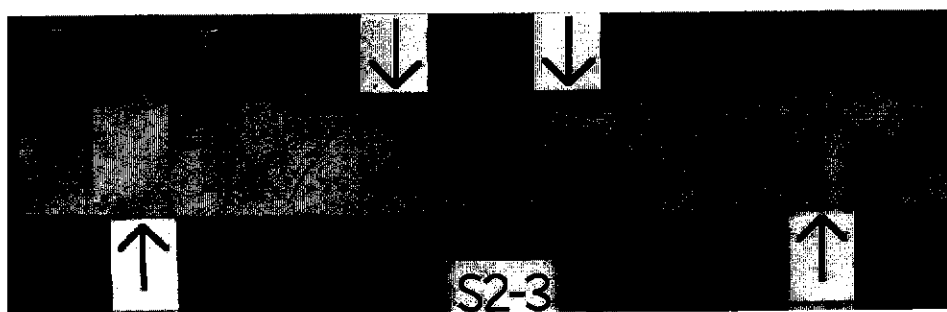
Figure B.17 Crack Pattern of the Front Face of Beam S2-3
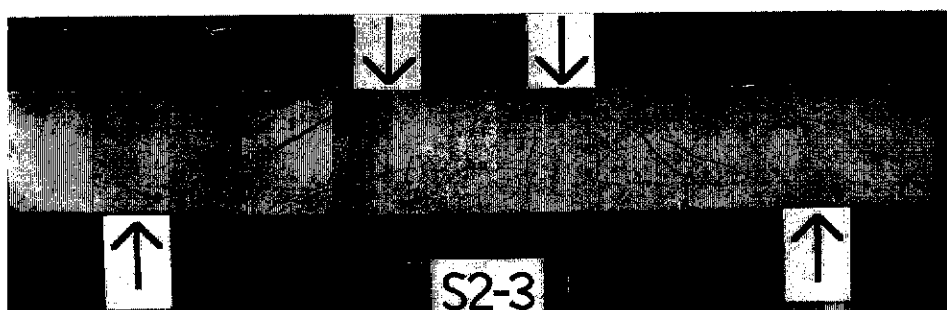
Figure B.18 Crack Pattern of the Back Face of Beam S2-3
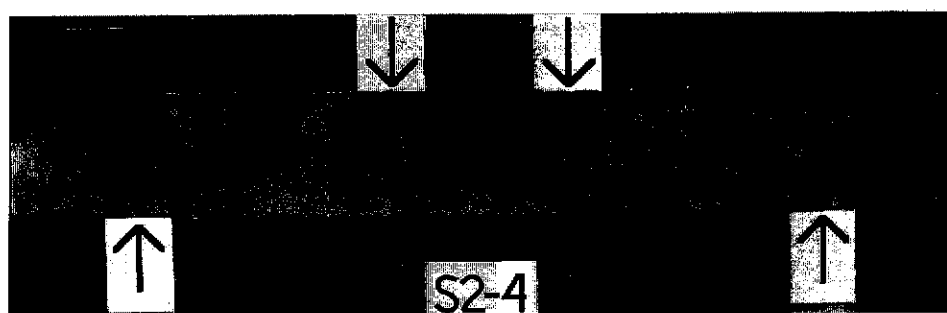
Figure B.19 Crack Pattern of the Front Face of Beam S2-4
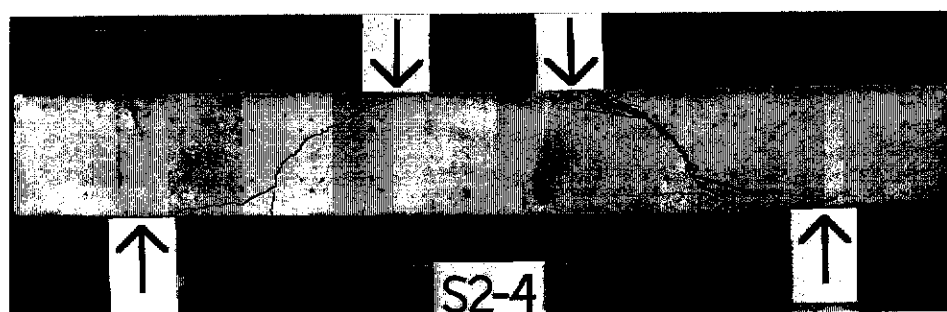
Figure B.20 Crack Pattern of the Back Face of Beam S2-4
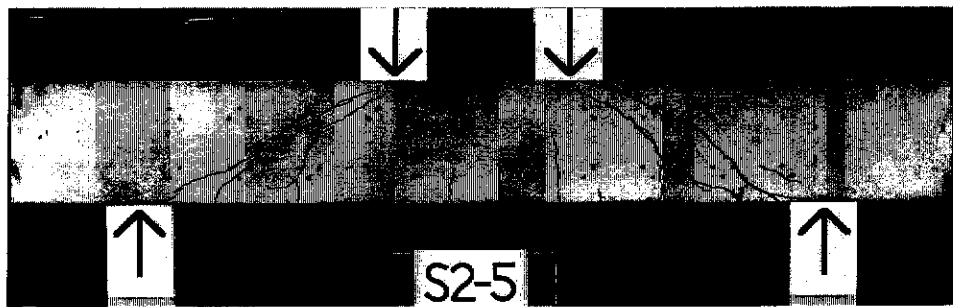
Figure B.21 Crack Pattern of the Front Face of Beam S2-5
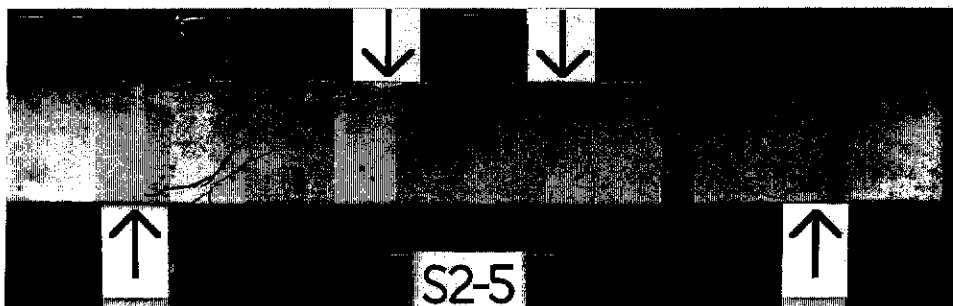
Figure B.22 Crack Pattern of the Back Face of Beam S2-5
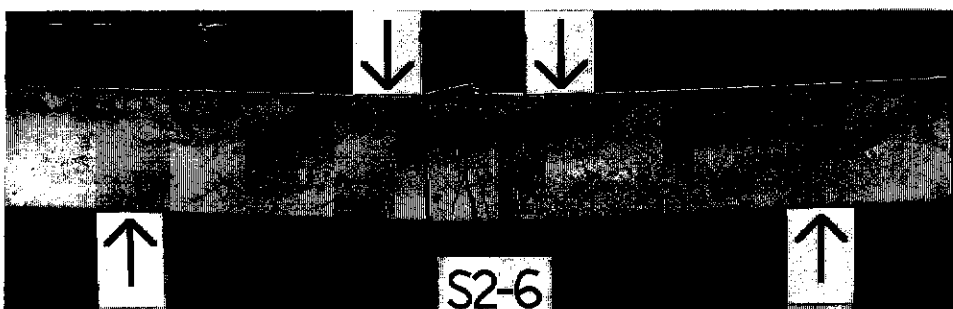
Figure B.23 Crack Pattern of the Front Face of Beam S2-6
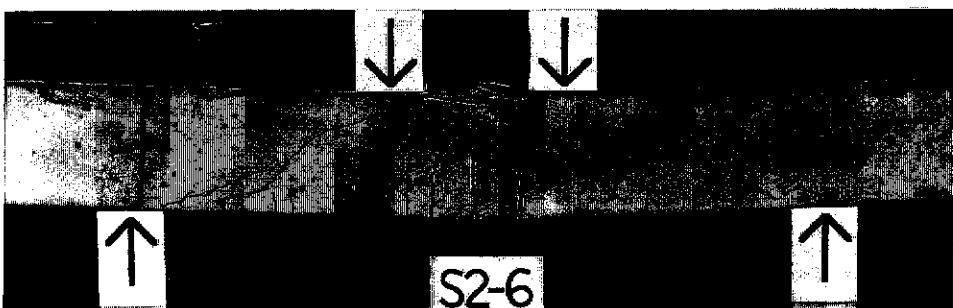
Figure B.24 Crack Pattern of the Back Face of Beam S2-6
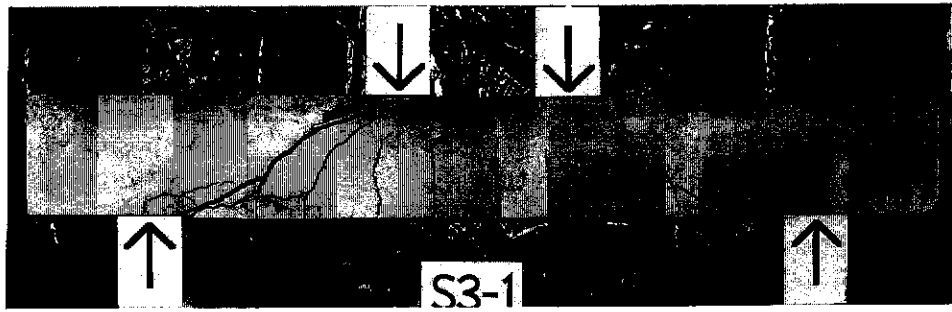
Figure B.25 Crack Pattern of the Front Face of Beam S3-1
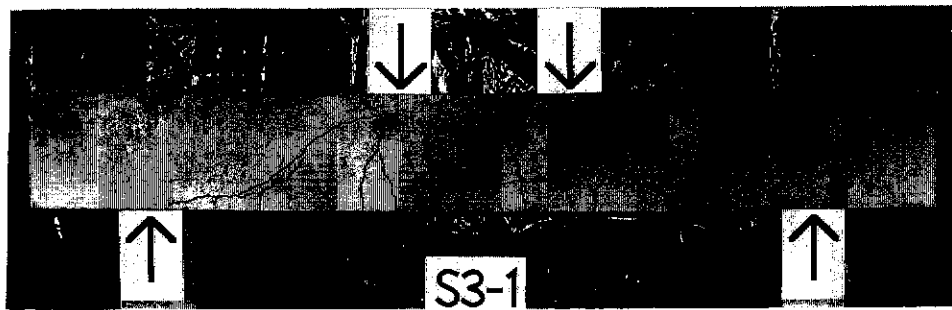
Figure B.26 Crack Pattern of the Back Face of Beam S3-1
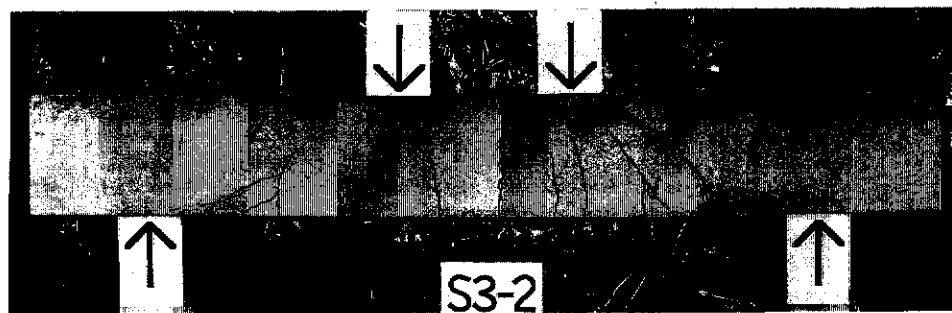
Figure B.27 Crack Pattern of the Front Face of Beam S3-2
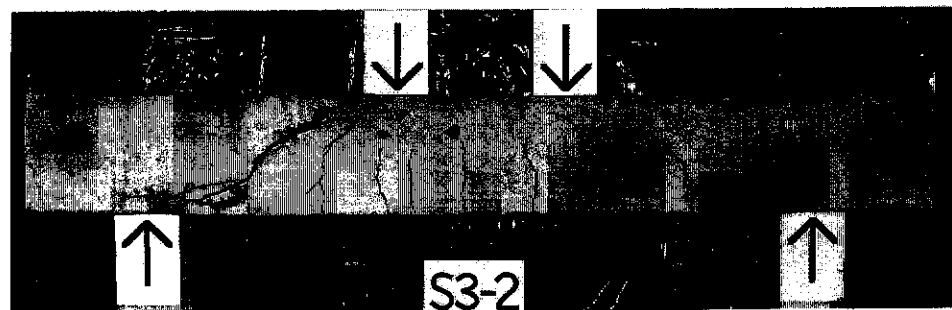
Figure B.28 Crack Pattern of the Back Face of Beam S3-2
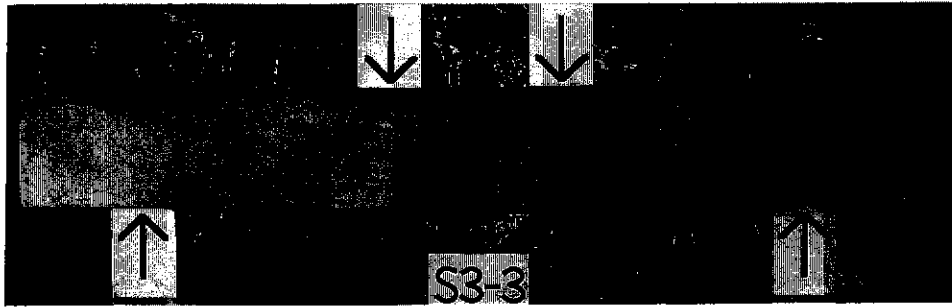
Figure B.29 Crack Pattern of the Front Face of Beam S3-3
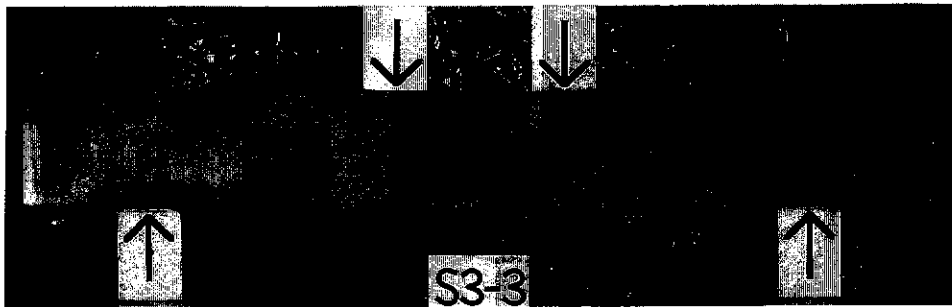
Figure B.30 Crack Pattern of the Back Face of Beam S3-3
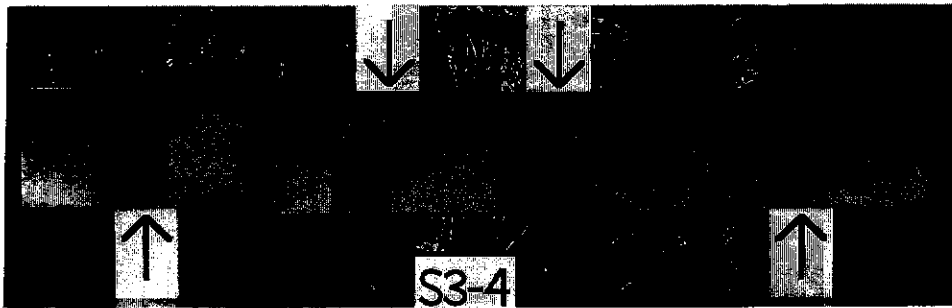
Figure B.31 Crack Pattern of the Front Face of Beam S3-4
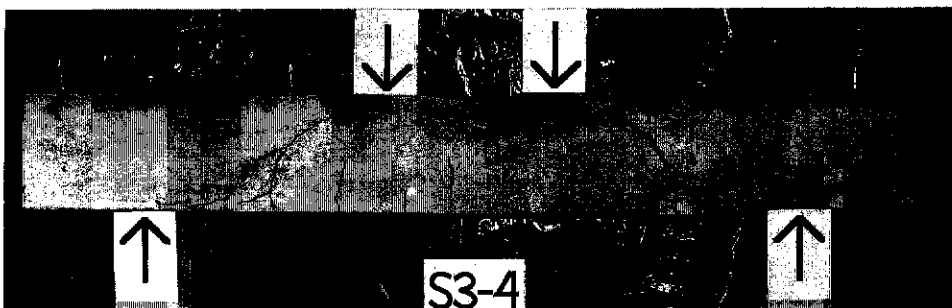
Figure B.32 Crack Pattern of the Back Face of Beam S3-4
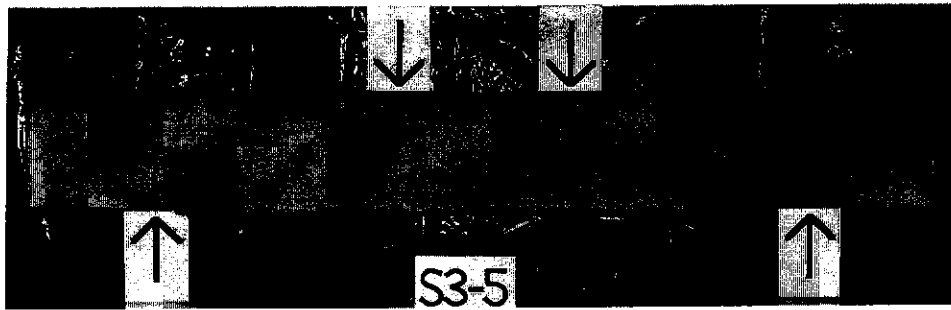
Figure B.33 Crack Pattern of the Front Face of Beam S3-5
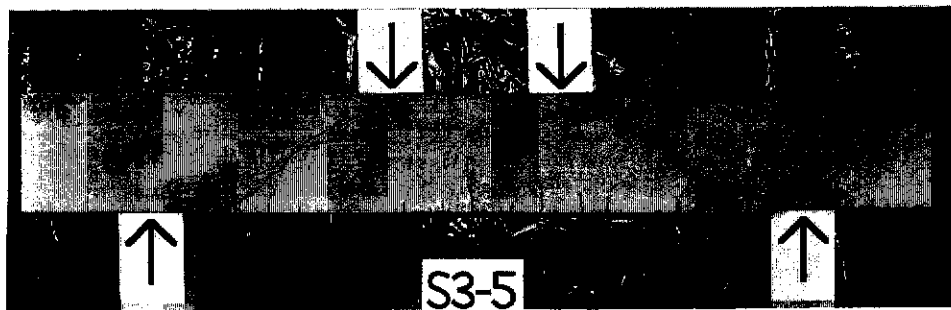
Figure B.34 Crack Pattern of the Back Face of Beam S3-5
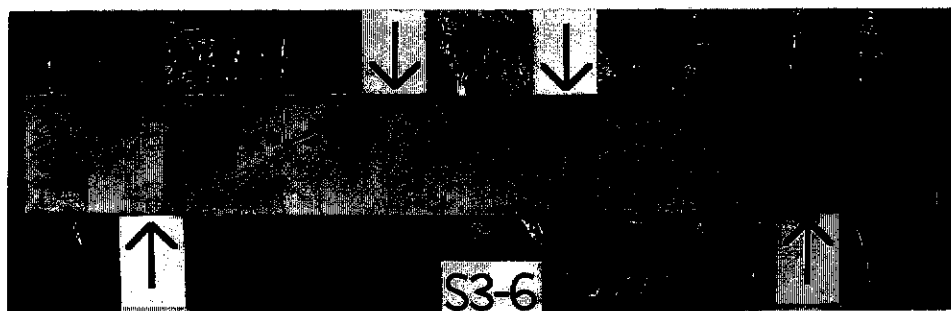
Figure B.35 Crack Pattern of the Front Face of Beam S3-6
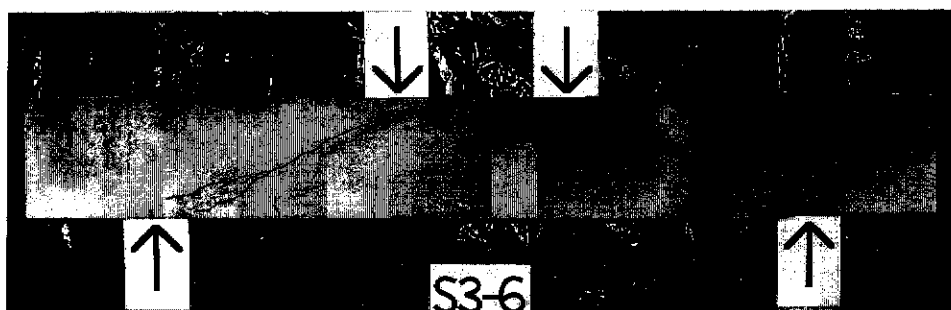
Figure B.36 Crack Pattern of the Back Face of Beam S3-6
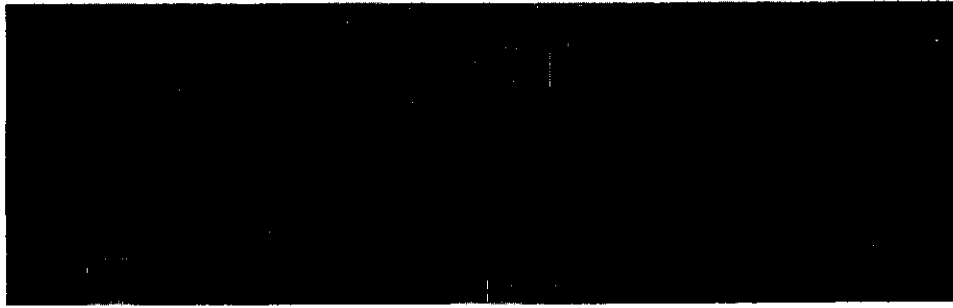
Figure B.37 Crack Pattern of the Front Face of Beam S4-1
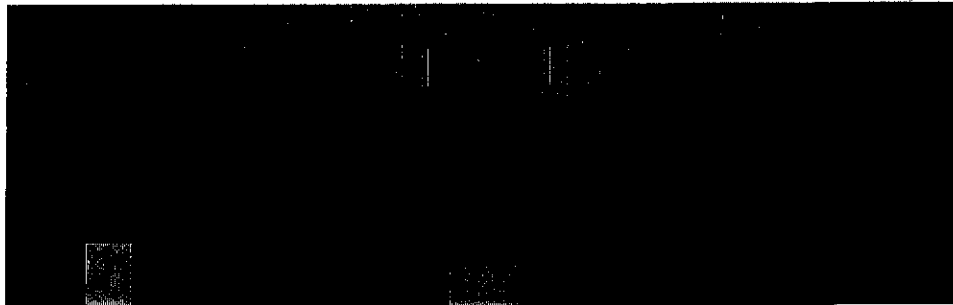
Figure B.38 Crack Pattern of the Back Face of Beam S4-1
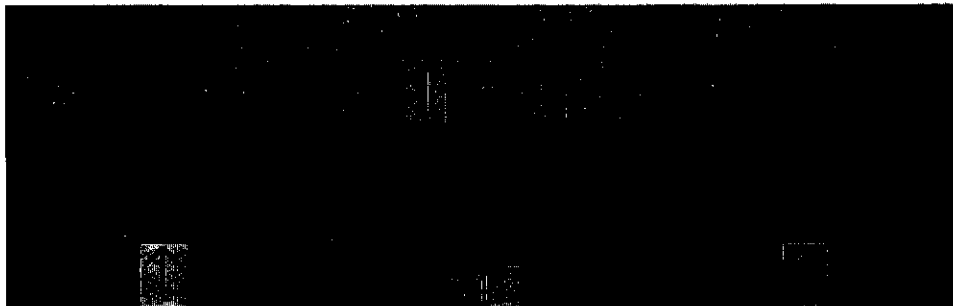
Figure B.39 Crack Pattern of the Front Face of Beam S4-2
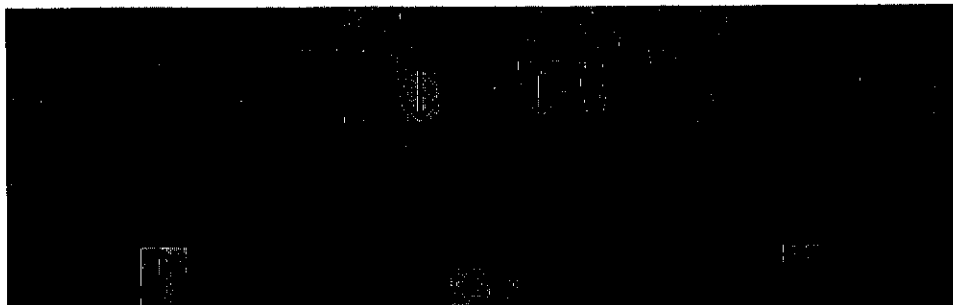
Figure B.40 Crack Pattern of the Back Face of Beam S4-2
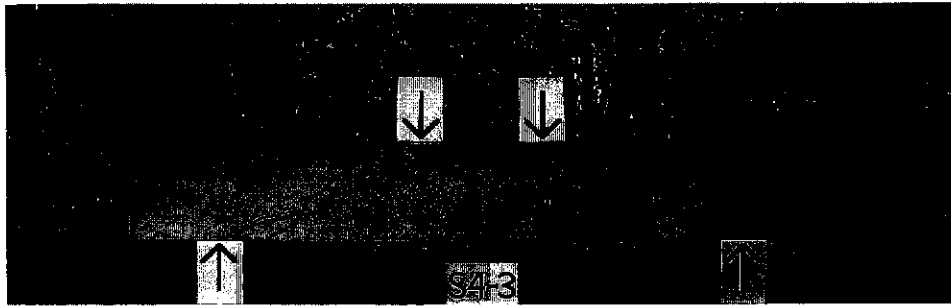
Figure B.41 Crack Pattern of the Front Face of Beam S4-3

Figure B.42 Crack Pattern of the Back Face of Beam S4-3

Figure B.43 Crack Pattern of the Front Face of Beam S4-4
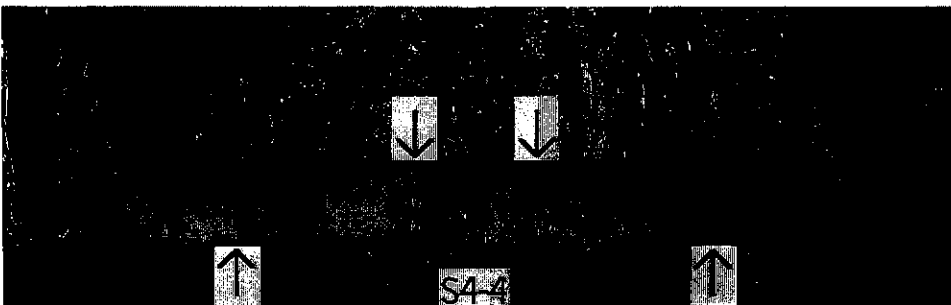
Figure B.44 Crack Pattern of the Back Face of Beam S4-4

Figure B.45 Crack Pattern of the Front Face of Beam S4-5
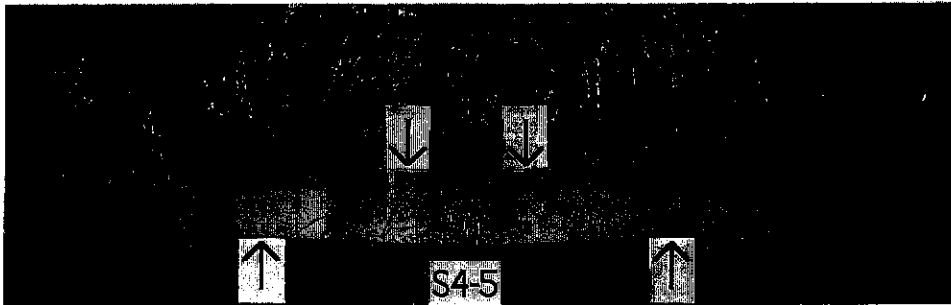
Figure B.46 Crack Pattern of the Back Face of Beam S4-5
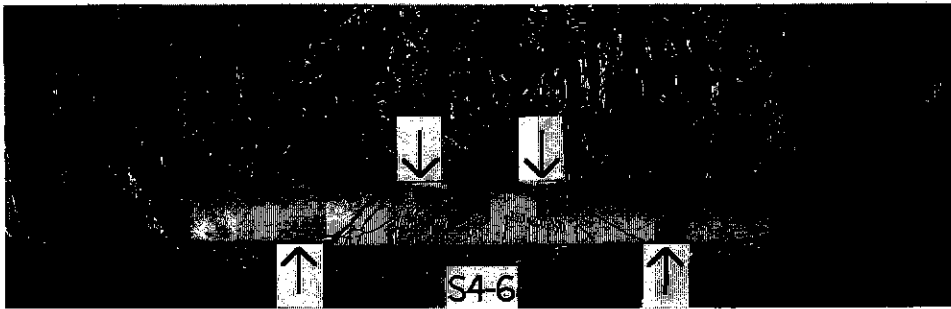
Figure B.47 Crack Pattern of the Front Face of Beam S4-6

Figure B.48 Crack Pattern of the Back Face of Beam S4-6
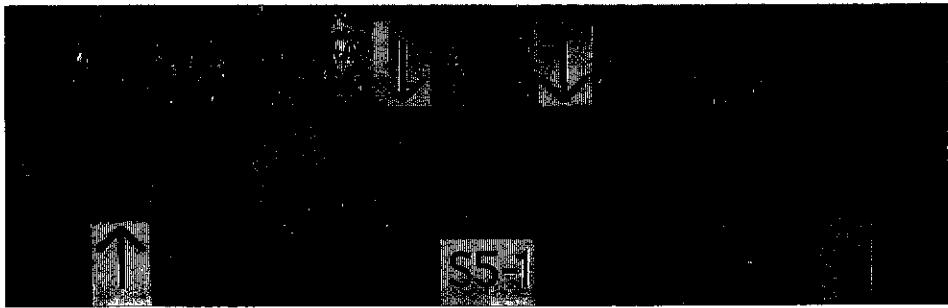
Figure B.49 Crack Pattern of the Front Face of Beam S5-1
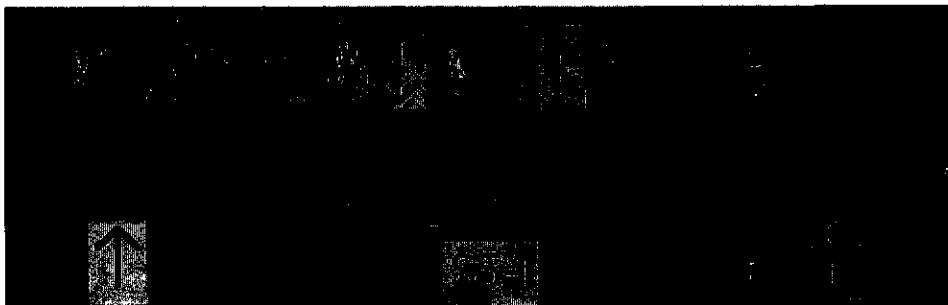
Figure B.50 Crack Pattern of the Back Face of Beam S5-1

Figure B.51 Crack Pattern of the Front Face of Beam S5-2
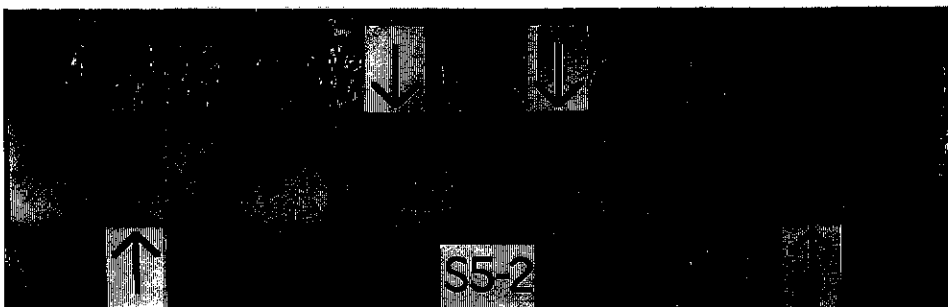
Figure B.52 Crack Pattern of the Back Face of Beam S5-2

B.14
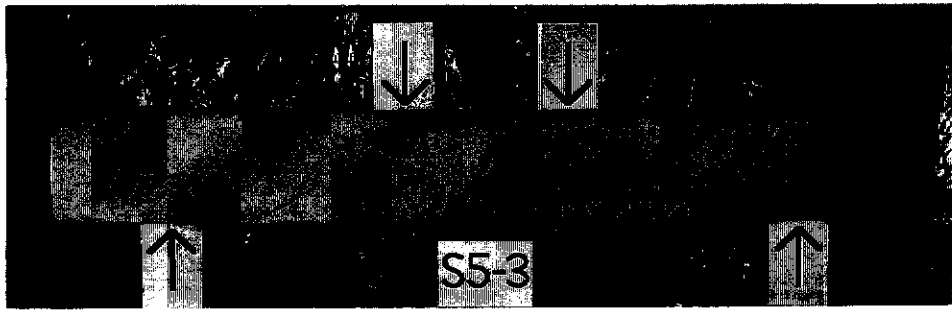
Figure B.53 Crack Pattern of the Front Face of Beam S5-3
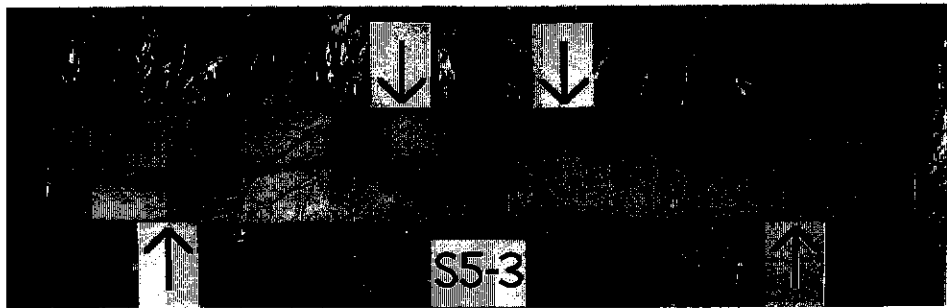
Figure B.54 Crack Pattern of the Back Face of Beam S5-3
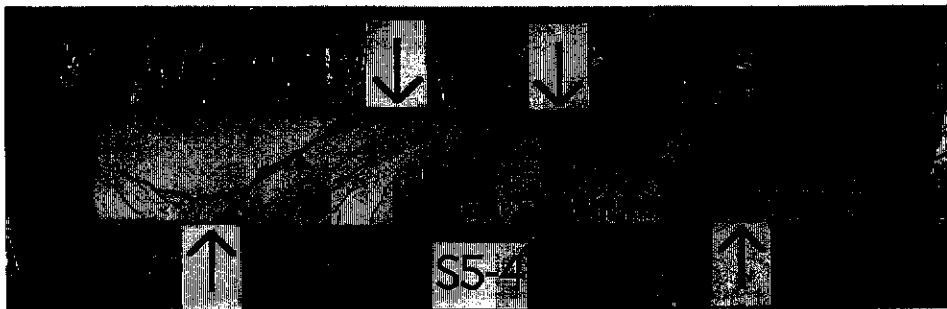
Figure B.55 Crack Pattern of the Front Face of Beam S5-4
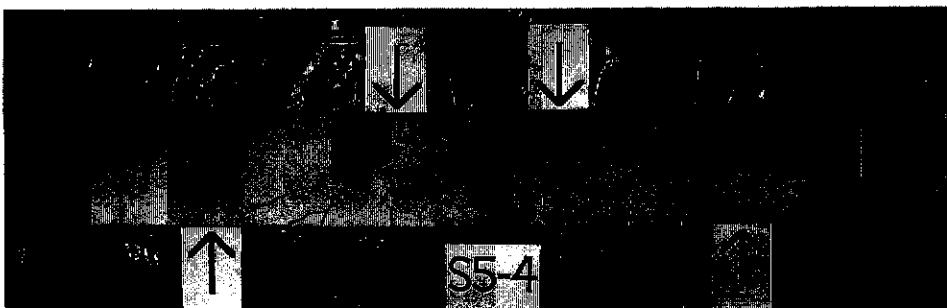
Figure B.56 Crack Pattern of the Back Face of Beam S5-4

B.15
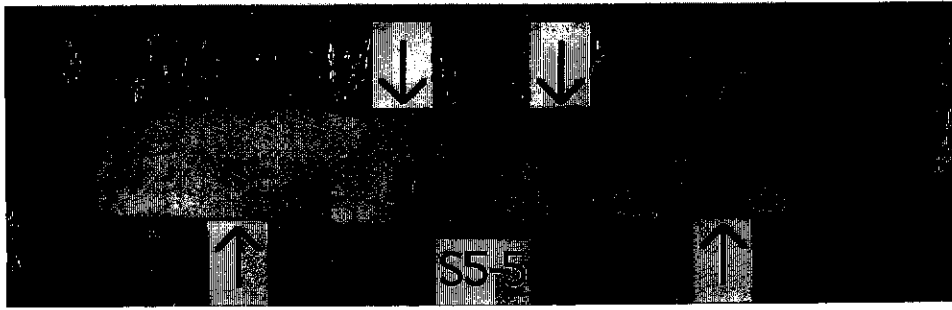
Figure B.57 Crack Pattern of the Front Face of Beam S5-5
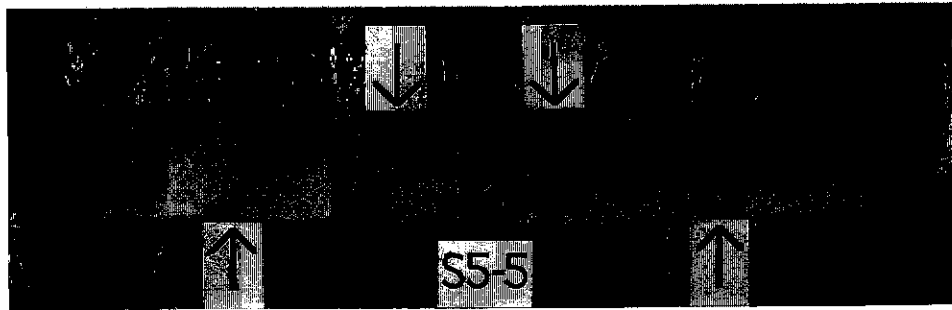
Figure B.58 Crack Pattern of the Back Face of Beam S5-5
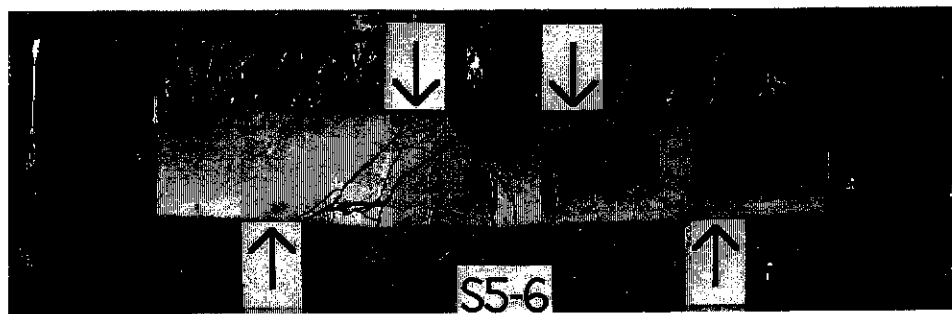
Figure B.59 Crack Pattern of the Front Face of Beam S5-6
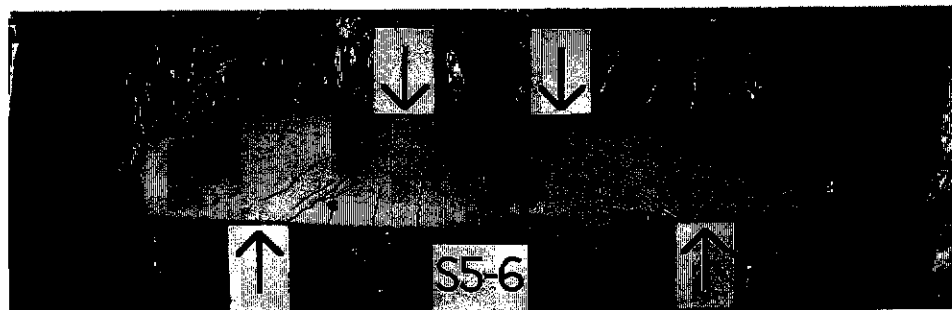
Figure B.60 Crack Pattern of the Back Face of Beam S5-6
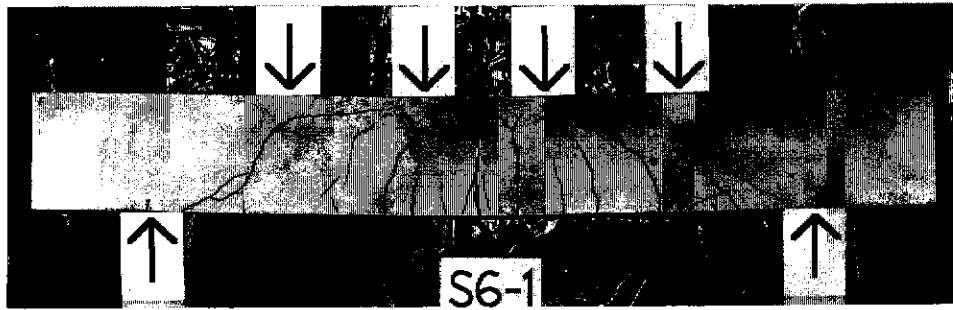
Figure B.61 Crack Pattern of the Front Face of Beam S6-1
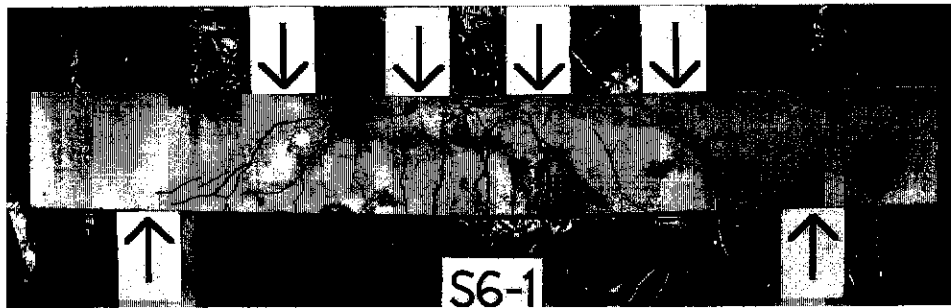
Figure B.62 Crack Pattern of the Back Face of Beam S6-1
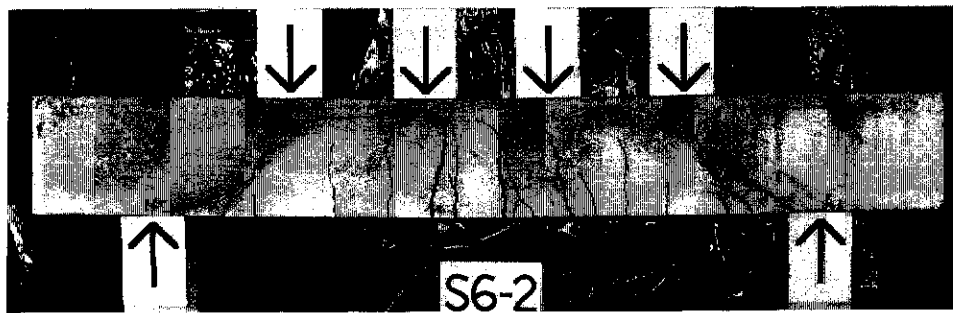
Figure B.63 Crack Pattern of the Front Face of Beam S6-2
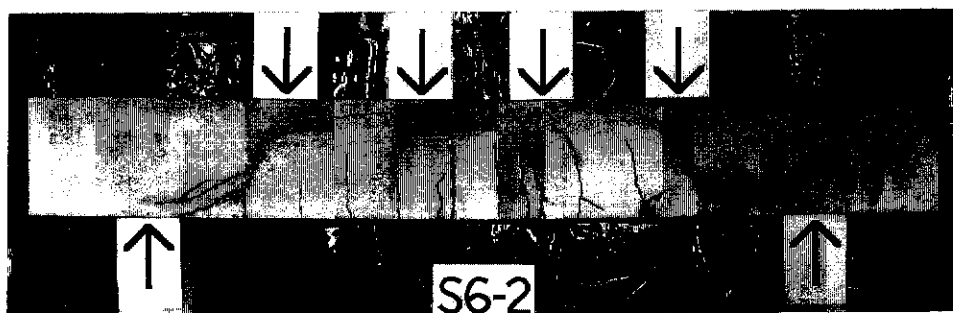
Figure B.64 Crack Pattern of the Back Face of Beam S6-2
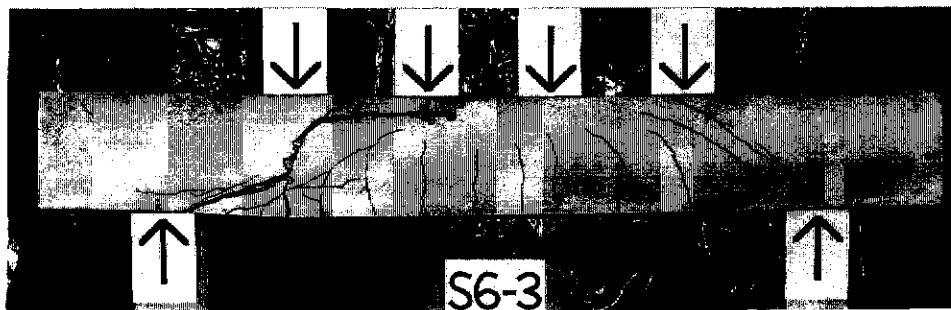
Figure B.65 Crack Pattern of the Front Face of Beam S6-3
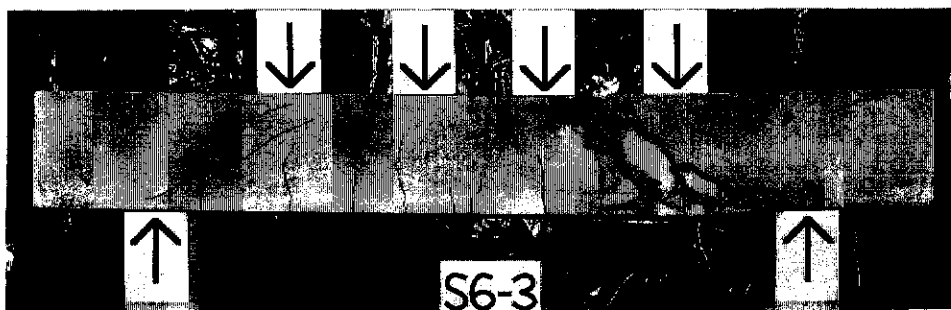
Figure B.66 Crack Pattern of the Back Face of Beam S6-3
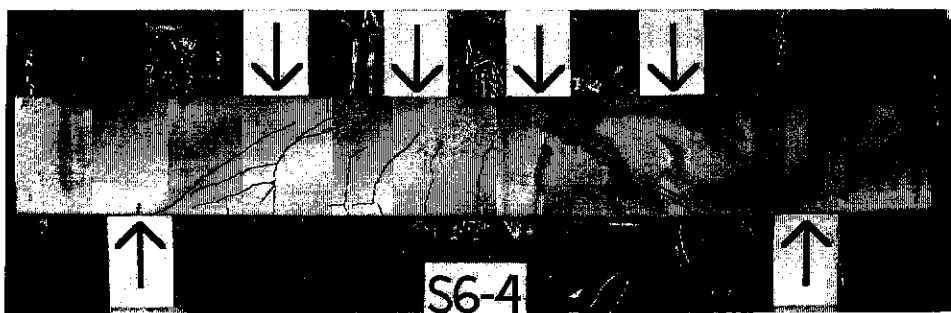
Figure B.67 Crack Pattern of the Front Face of Beam S6-4
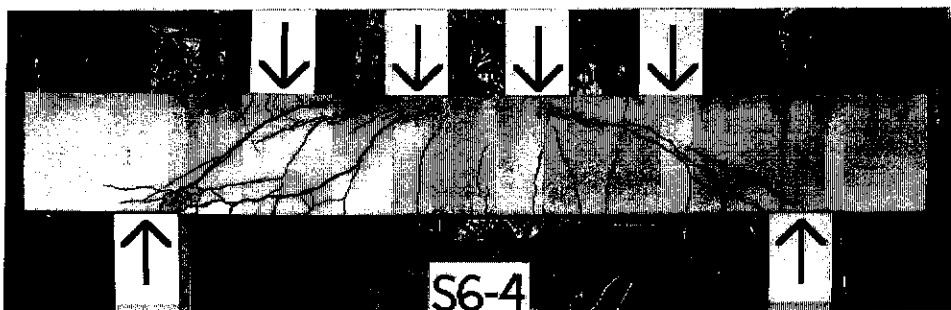
Figure B.68 Crack Pattern of the Back Face of Beam S6-4
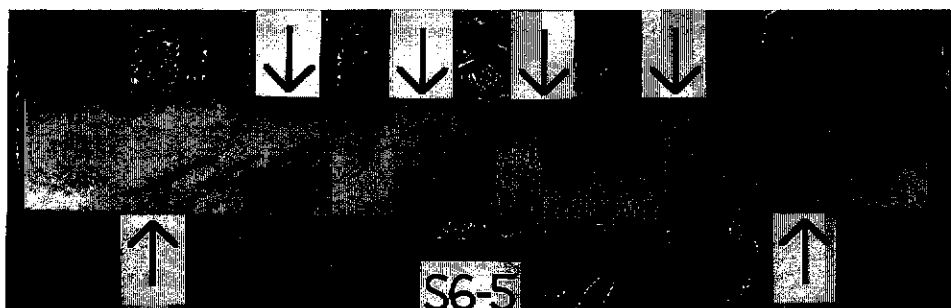
Figure B.69 Crack Pattern of the Front Face of Beam S6-5
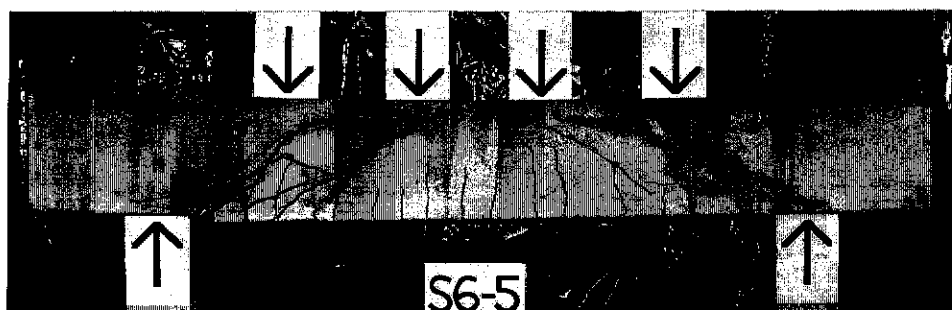
Figure B.70 Crack Pattern of the Back Face of Beam S6-5

Figure B.71 Crack Pattern of the Front Face of Beam S6-6
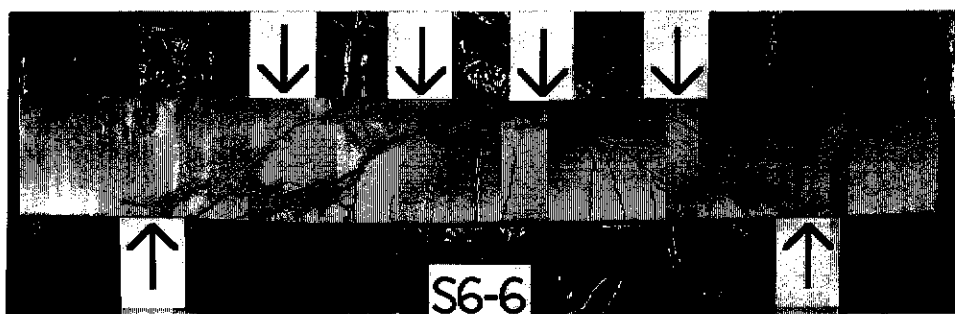
Figure B.72 Crack Pattern of the Back Face of Beam S6-6
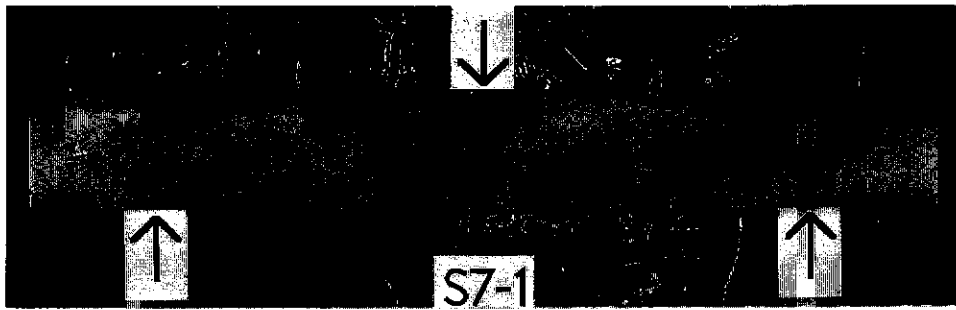
Figure B.73 Crack Pattern of the Front Face of Beam S7-1
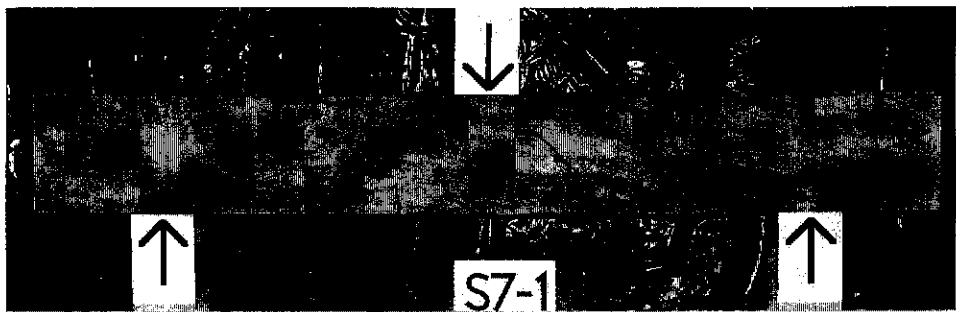
Figure B.74 Crack Pattern of the Back Face of Beam S7-1
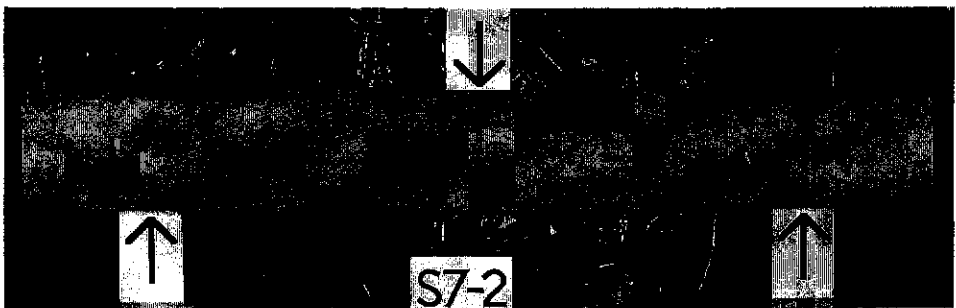
Figure B.75 Crack Pattern of the Front Face of Beam S7-2
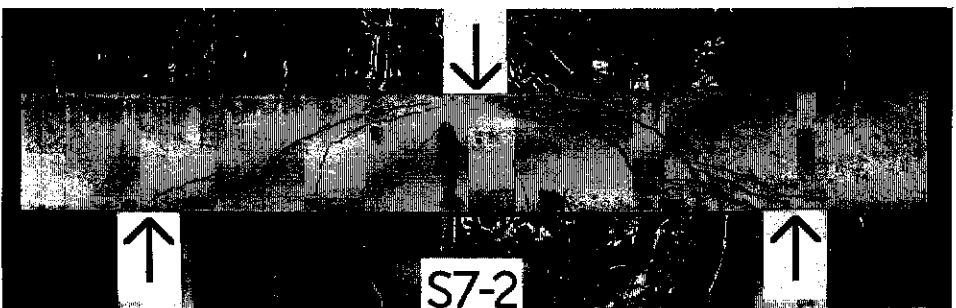
Figure B.76 Crack Pattern of the Back Face of Beam S7-2
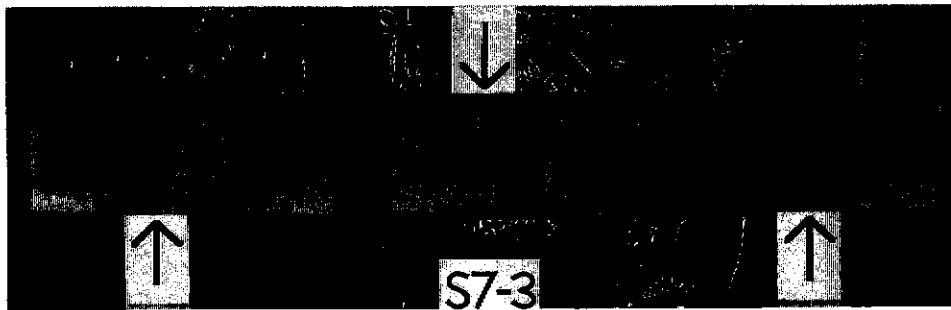
Figure B.77 Crack Pattern of the Front Face of Beam S7-3
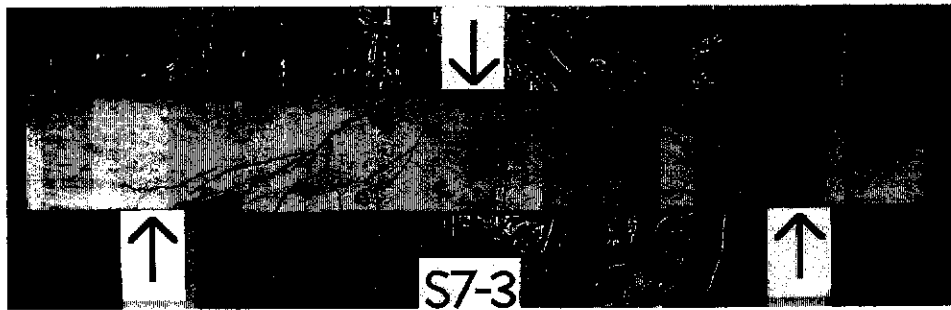
Figure B.78 Crack Pattern of the Back Face of Beam S7-3
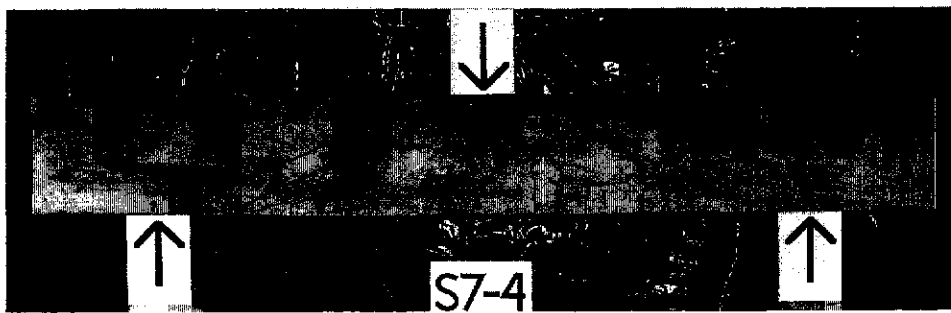
Figure B.79 Crack Pattern of the Front Face of Beam S7-4
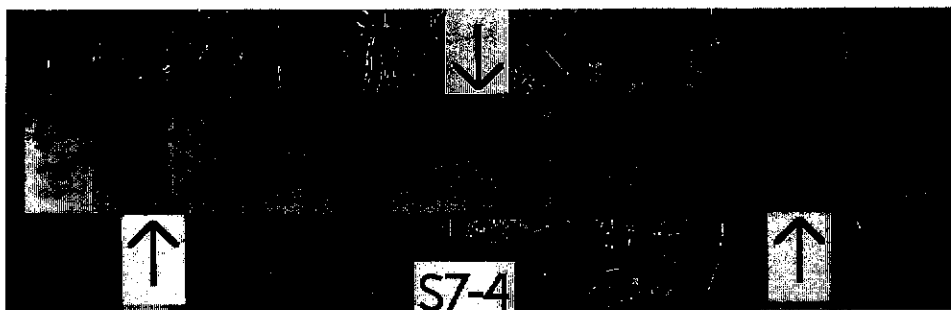
Figure B.80 Crack Pattern of the Back Face of Beam S7-4
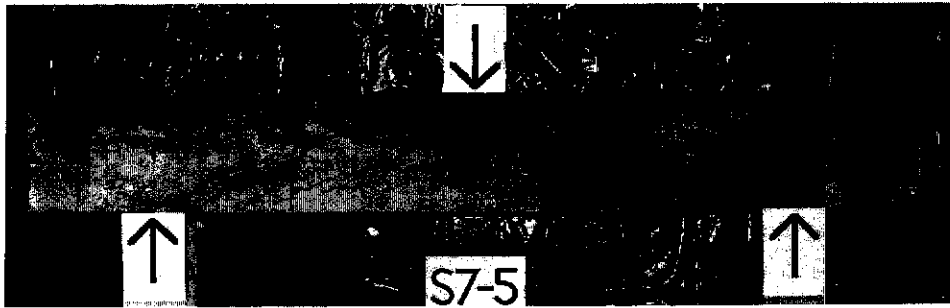
Figure B.81 Crack Pattern of the Front Face of Beam S7-5
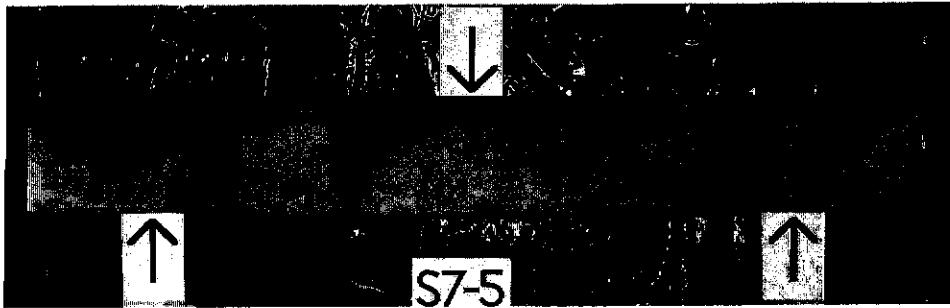
Figure B.82 Crack Pattern of the Back Face of Beam S7-5
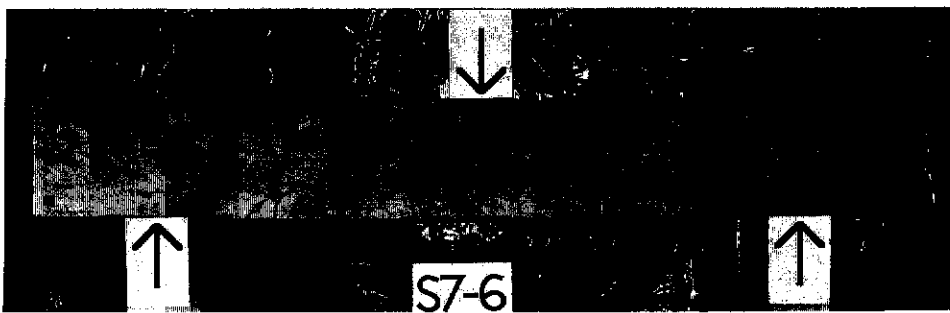
Figure B.83 Crack Pattern of the Front Face of Beam S7-6
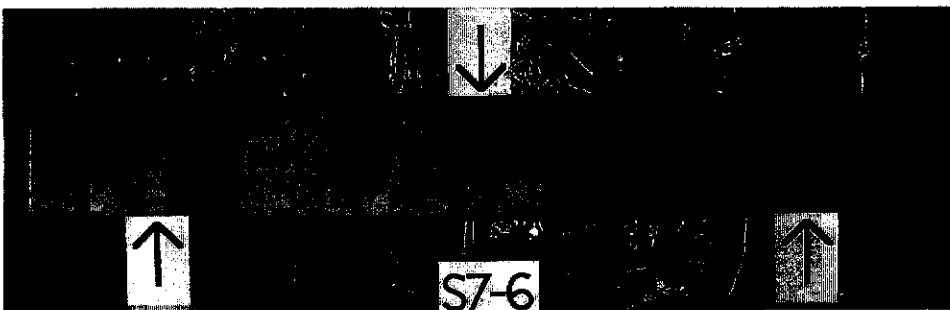
Figure B.84 Crack Pattern of the Back Face of Beam S7-6
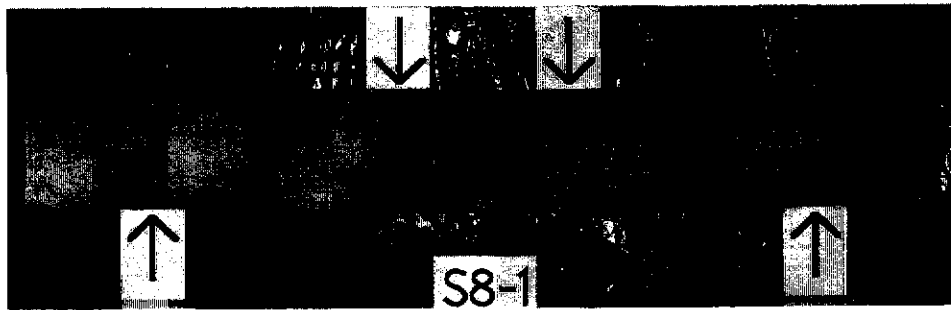
Figure B.85 Crack Pattern of the Front Face of Beam S8-1
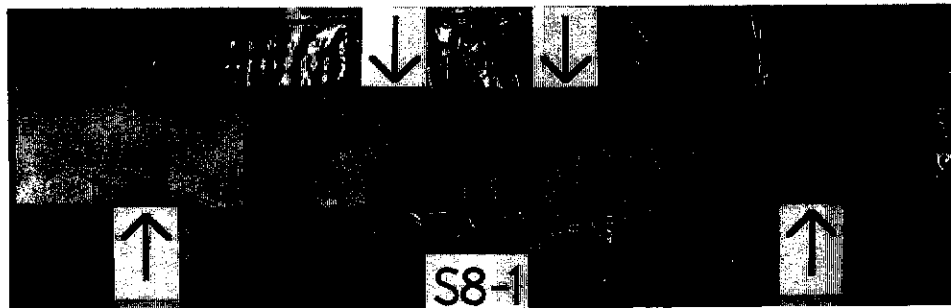
Figure B.86 Crack Pattern of the Back Face of Beam S8-1
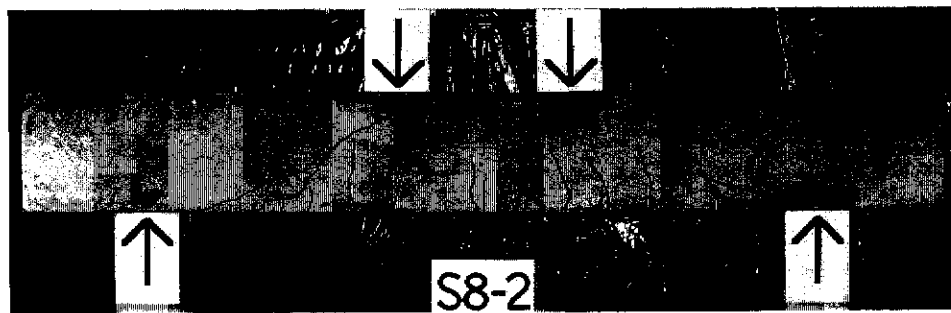
Figure B.87 Crack Pattern of the Front Face of Beam S8-2
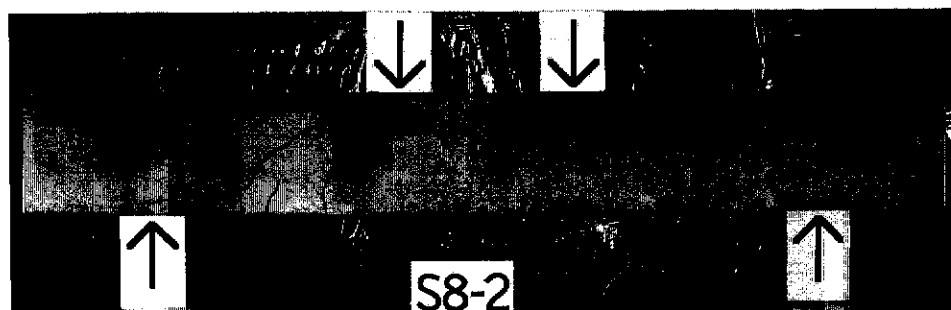
Figure B.88 Crack Pattern of the Back Face of Beam S8-2

B.23

Figure B.89 Crack Pattern of the Front Face of Beam S8-3

Figure B.90 Crack Pattern of the Back Face of Beam S8-3
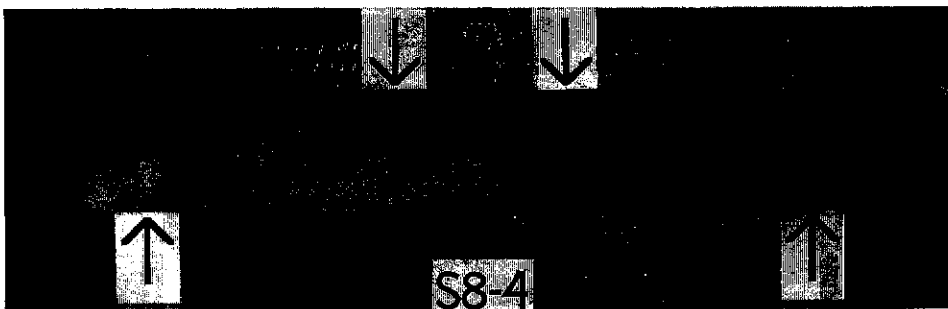
Figure B.91 Crack Pattern of the Front Face of Beam S8-4
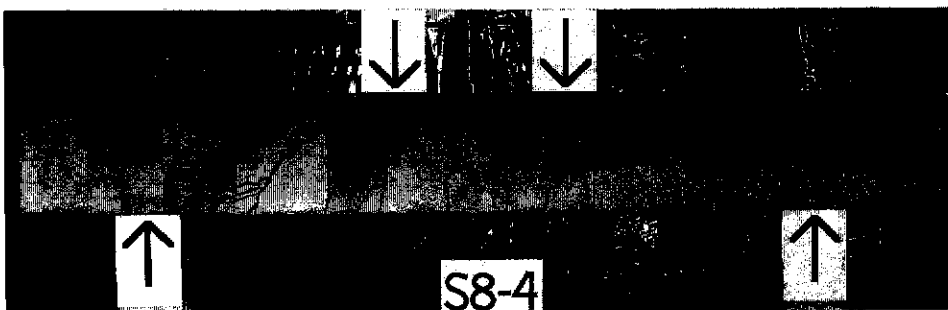
Figure B.92 Crack Pattern of the Back Face of Beam S8-4
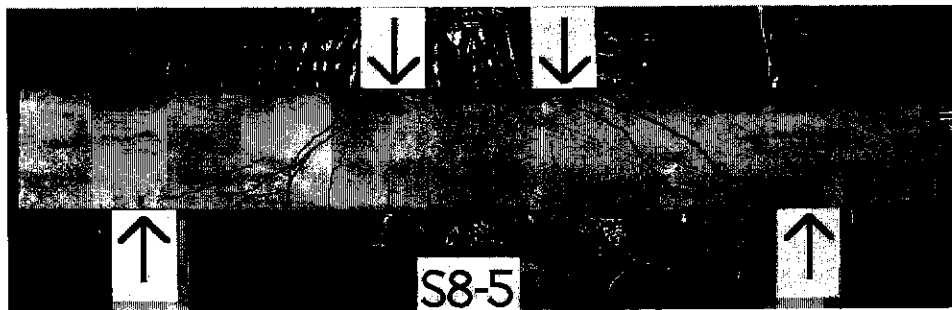
Figure B.93 Crack Pattern of the Front Face of Beam S8-5
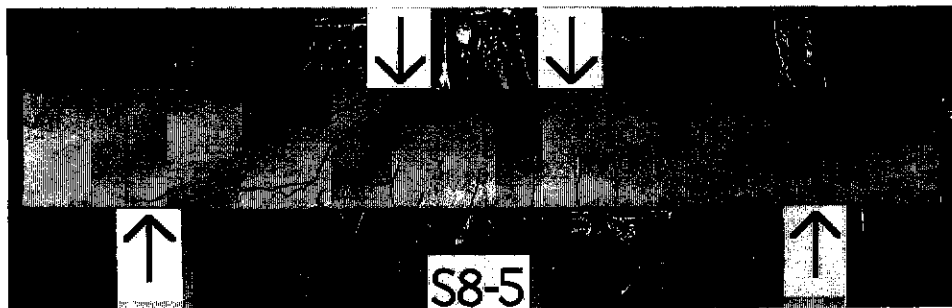
Figure B.94 Crack Pattern of the Back Face of Beam S8-5
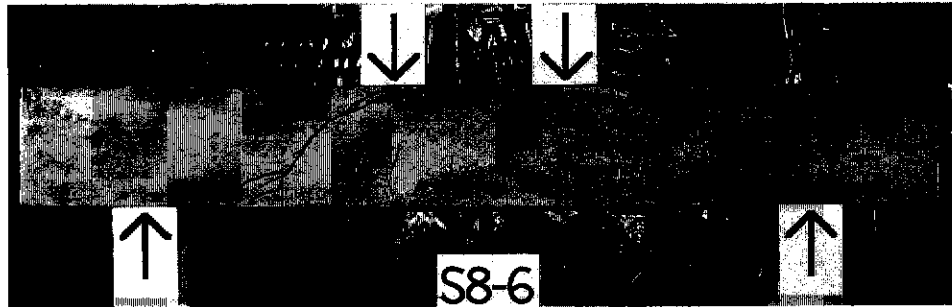
Figure B.95 Crack Pattern of the Front Face of Beam S8-6
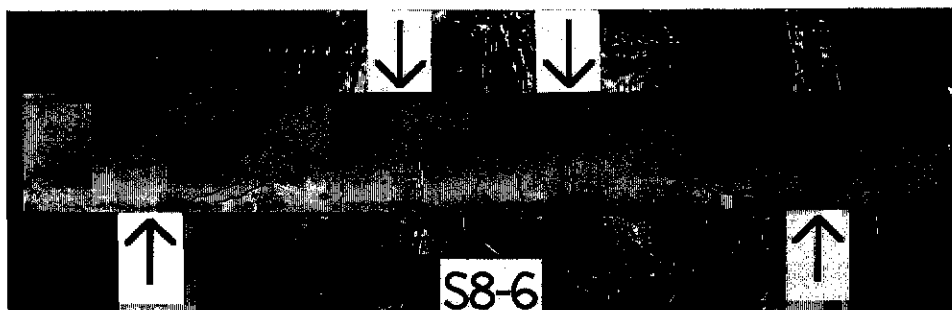
Figure B.96 Crack Pattern of the Back Face of Beam S8-6

Vertical Midspan Deflection Of Test Beams

C.1 Deflection Due To Flexure And Shear

The effective moment of inertia (I_e) of a reinforced concrete beam section after cracking has occurred lies in the range of:

$$I_{cr} < I_e < I_g$$

where

$$I_{cr} \quad = \quad \text{moment of inertia of a completely cracked section, and}$$

$$I_g \quad = \quad \text{moment of inertia of an uncracked section.}$$

Branson's equation (Warner, Rangan and Hall (1989)) is commonly used for determining I_e:

$$I_e \quad = \quad I_{cr} + (I_g - I_{cr})\left(\frac{M_{cr}}{M_s}\right)^3 \qquad (C.1)$$

where

M_s = maximum bending moment at the beam section, based on the short-term serviceability load

M_{cr} = bending moment causing cracking of the beam section

= $Z\, f_{cf}$

Z = section modulus of the uncracked section, taken to the extreme tensile fibre at which cracking occurs

= $\dfrac{I_g}{y_{bot}}$

f_{cf} = flexural tensile strength = $0.6 \sqrt{f_c}$, and

y_{bot} = distance from neutral axis of uncracked section to extreme tensile fibre in concrete just prior to cracking.

The sectional stiffness varies according to the following conditions:

(i) if $M_s < M_{cr}$, the stiffness is $E_c I_g$

(ii) if $M_s \geq M_{cr}$, the stiffness is $E_c I_e$

The following details the analysis of a solid rectangular beam with multiple layers of longitudinal steel.

Uncracked Beam Section

Figure C.1 shows an uncracked beam cross-section where the gross section is effective. The cross-sectional areas for the steel reinforcement are transformed using the modular ratio between steel and concrete.
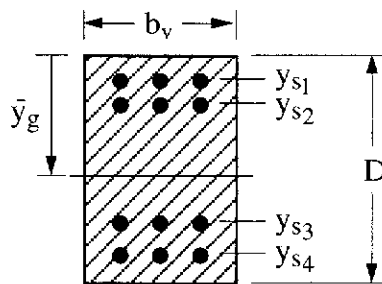
Figure C.1 Uncracked Beam Section

The distance from the top of the beam to the neutral axis ($\bar{y}_g$) can be found from the following equation:

$$\bar{y}_g = \frac{\displaystyle\sum_{i=1}^{i=k} A_{s_i}(n-1)y_{s_i} + \frac{b_v D^2}{2}}{\displaystyle\sum_{i=1}^{i=k} A_{s_i}(n-1) + b_v D} \tag{C.2}$$

where

n = modular ratio = E_s/E_c

A_{s_i} = cross-sectional area of a longitudinal steel bar

y_{s_i} = distance from the top of the beam to the centroid of a longitudinal steel bar, and

k = number of longitudinal bars in the reinforced concrete section.

The moment of inertia for the uncracked section is given by:

$$I_g = \sum_{i=1}^{i=k} A_{s_i}(n-1)(y_{s_i} - \bar{y}_g)^2 + \left[\frac{b_v D^3}{12} + b_v D \left(\bar{y}_g - \frac{D}{2}\right)^2 \right]$$

$$\tag{C.3}$$

Cracked Beam Section

For the cracked section, concrete below the neutral axis is assumed to be unable to sustain any tensile stress (Figure C.2).
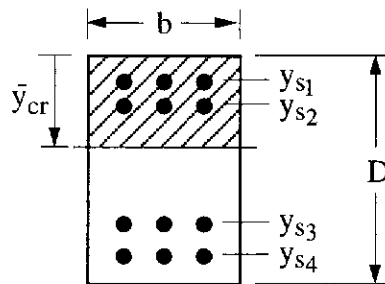
Figure C.2 Cracked Beam Section

After cracking, the longitudinal steel bars are not yielded and the modular ratio can still be applied to determine the height $\bar{y}_{cr}$ from the top of the beam to the neutral axis. The first moment of the transformed section about the neutral axis equals zero:

$$\Sigma A.y = (b_v\bar{y}_{cr})\left(\frac{\bar{y}_{cr}}{2}\right) + \sum_{i=1}^{i=j}A_{s_i}(n-1)(\bar{y}_{cr} - y_{s_i}) + \sum_{i=j+1}^{i=k}A_{s_i}n(\bar{y}_{cr} - y_{s_i}) = 0$$

(C.4)

where j is the number of steel bars in the compression zone.

Solving for Equation C.4, $\bar{y}_{cr}$ is found to be:

$$\bar{y}_{cr} = \frac{-B + \sqrt{B^2 - 4AC}}{2A}$$

(C.5)

where

$$A = \left(\frac{b_v}{2}\right)$$

$$B = \sum_{i=1}^{i=j}A_{s_i}(n-1) + \sum_{i=j+1}^{i=k}A_{s_i}n$$

$$C = -\left(\sum_{i=1}^{i=j}A_{s_i}(n-1)y_{s_i} + \sum_{i=j+1}^{i=k}A_{s_i}ny_{s_i}\right)$$

The moment of inertia for a cracked section can then be calculated as:

$$I_{cr} = \left(\frac{b_v\bar{y}_{cr}^3}{3}\right) + \sum_{i=1}^{i=j}A_{s_i}(n-1)(\bar{y}_{cr} - y_{s_i})^2 + \sum_{i=j+1}^{i=k}A_{s_i}n(\bar{y}_{cr} - y_{s_i})^2$$

(C.6)

Vertical Midspan Deflection

The actual moment of inertia varies between I_g and I_{cr} along the length of a beam with a clear span L and equal shear spans a on both ends, as shown in Figure C.3.

C.4
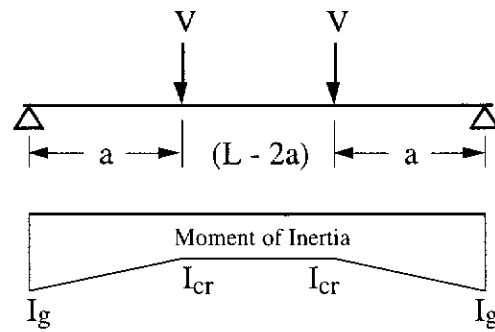
Figure C.3 Moment of Inertia Along A Beam

For simplicity, it is convenient to apply I_e to the full span of the simply supported beam based on the level of loading M_{cr}/M_s. Using this I_e value, the deflection due to flexure can be estimated from the first and second moment of area methods.

In solving for the first moment of area method, the rotation at the end of the beam is (Figure C.4):

$$\theta \quad = \quad \frac{1}{2EI} \int M \, dx \quad = \quad \frac{V\,a}{2EI} (L - a) \tag{C.7}$$
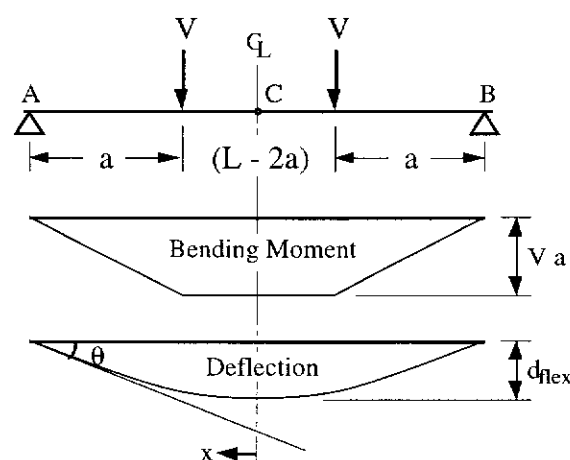
Figure C.4 Bending Moment and Deflection Diagrams for A Beam

Applying the second moment of area method between A and C, the vertical displacement of point C with respect to the tangent emanating from A is found as:

$$\Delta_{C/A} \quad = \quad \frac{1}{EI} \int M x \, dx \quad = \quad \frac{V a}{2EI} \left[\frac{a^2}{3} + \frac{a(L - 2a)}{2} + \frac{(L - 2a)^2}{4} \right] \quad \text{(C.8)}$$

The midspan vertical deflection due to flexure can be determined as:

$$d_{flex} \quad = \quad \frac{\theta L}{2} - \Delta_{C/A} \quad\quad\quad\quad\quad \text{(C.9)}$$

Using the modulus of elasticity of concrete E_c and the moment of inertia I_e, the deflection is determined from:

$$d_{flex} \quad = \quad \frac{V a}{2 E_c I_e} \left[\frac{2a^2}{3} + a(L - 2a) + \frac{(L - 2a)^2}{4} \right] \quad\quad \text{(C.10)}$$

However, Equation C.10 only gives the flexure contribution to vertical deflection at point C. The contribution due to shear is estimated from the present theory. The whole of each shear span is assumed to have a constant shear strain of $0.5\gamma_{\ell t}$ as a result of the shear force V (Figure C.5). The value of $\gamma_{\ell t}$ at each stage of loading is assumed to be the shear strain calculated at the critical section for shear.
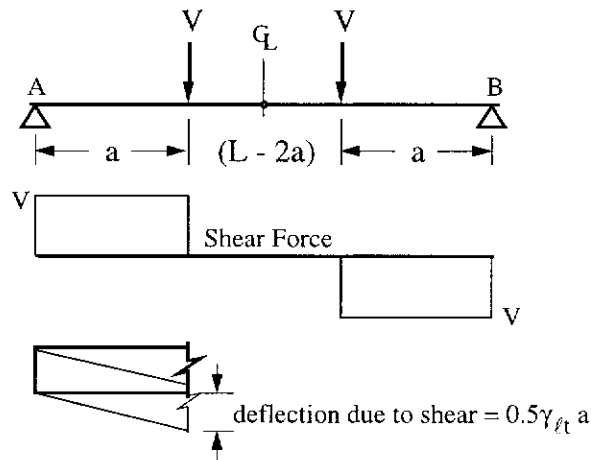
Figure C.5 Deflection Contribution Due to Shear Force

The deflection contribution due to shear is approximated as:

$$d_{shear} = 0.5\gamma_{\ell t}\, a \qquad\qquad (C.11)$$

Hence, the total predicted vertical deflection is estimated by adding the flexure and shear contributions as given in Equations C.10 and C.11:

$$d_{max} = \frac{V\,a}{2E_c I_e}\left[\frac{2a^2}{3} + a\,(L - 2a) + \frac{(L - 2a)^2}{4}\right] + 0.5\gamma_{\ell t}\, a \qquad (C.12)$$

Test shear force versus midspan deflection curves are plotted for each of the beams and these graphs are given in the pages that follow. The predicted curves using Equation C.12 are also plotted in these graphs.

Theoretical predictions are not available for short beams S5-4, S5-5 and S5-6 as the the truss theory does not apply in these cases.

C.2 Shear Force Versus Midspan Deflection Curves
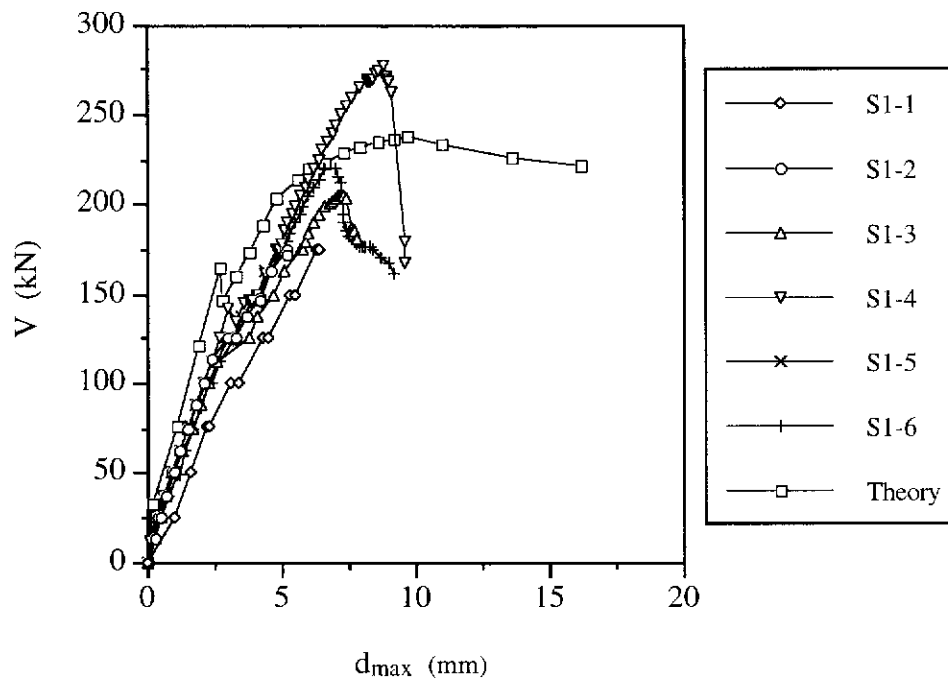
Figure C.6 Shear Force versus Midspan Deflection for Series 1
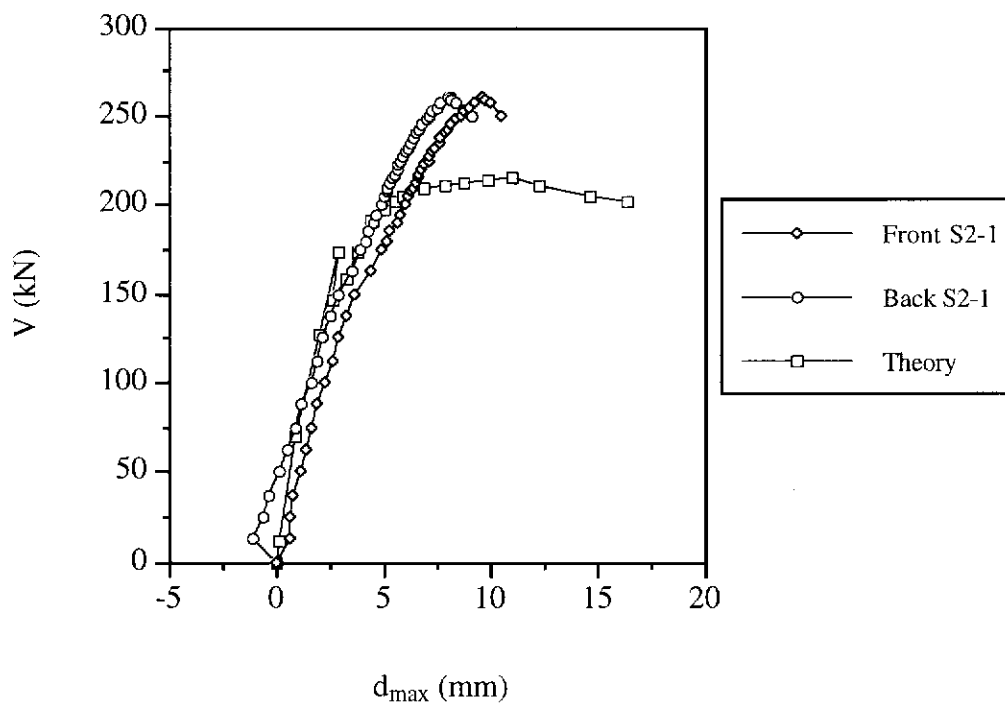
Figure C.7 Shear Force versus Midspan Deflection for Beam S2-1
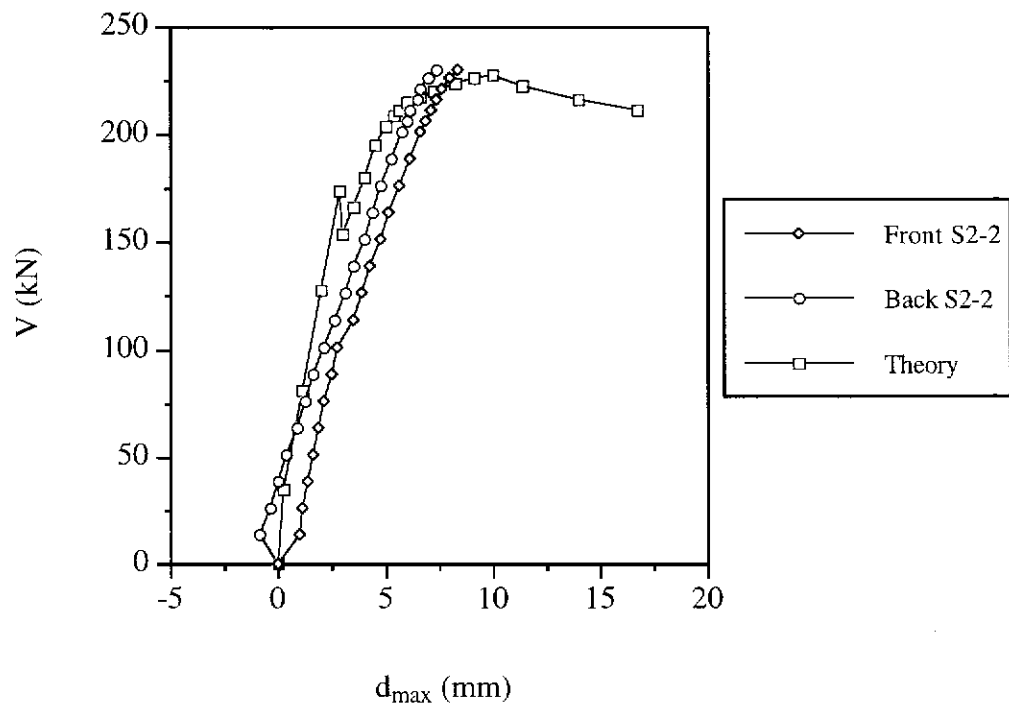
Figure C.8 Shear Force versus Midspan Deflection for Beam S2-2
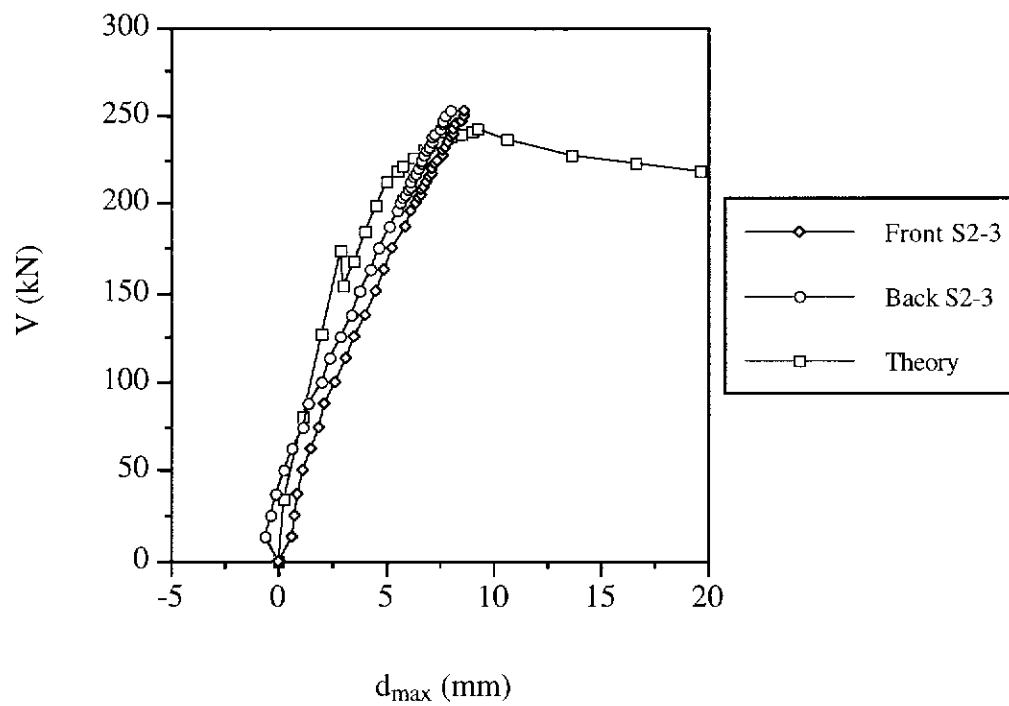
Figure C.9 Shear Force versus Midspan Deflection for Beam S2-3
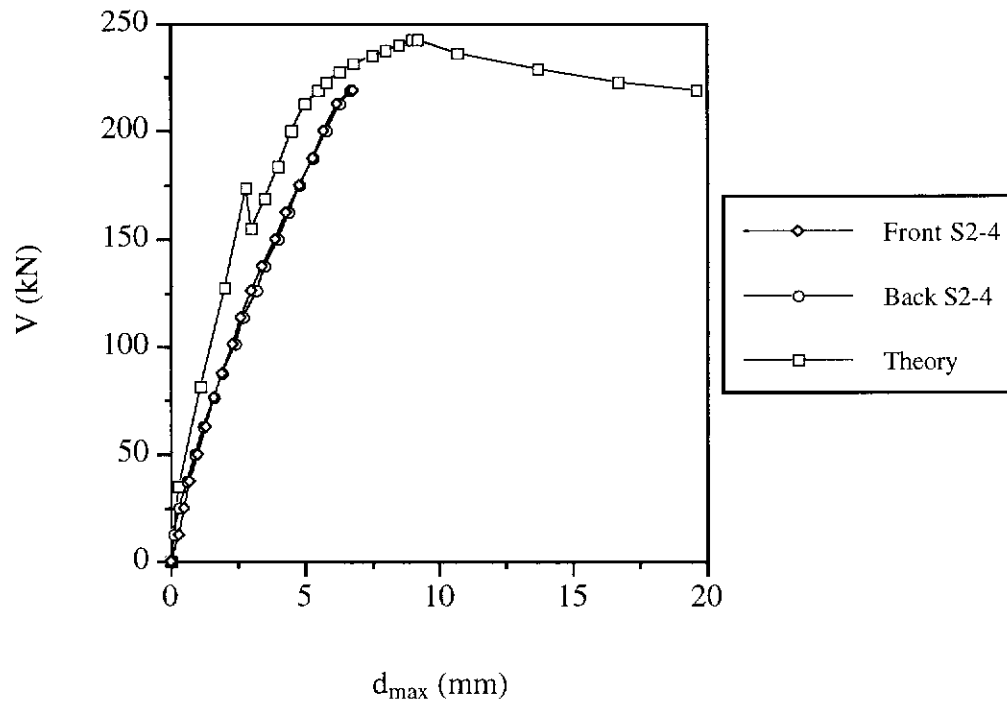
Figure C.10 Shear Force versus Midspan Deflection for Beam S2-4
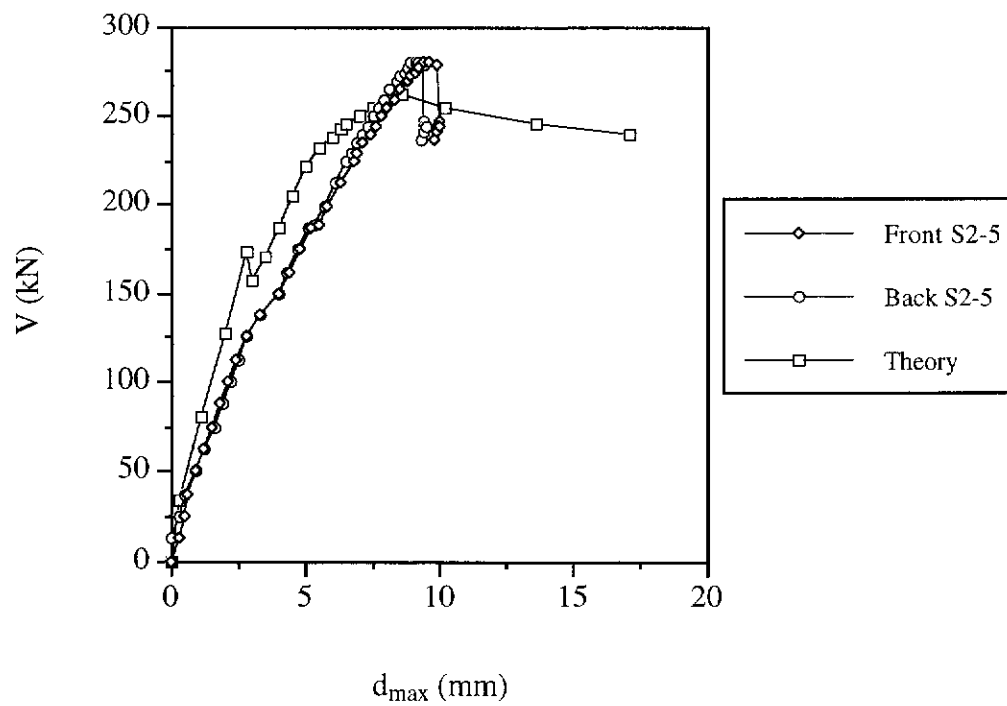
Figure C.11 Shear Force versus Midspan Deflection for Beam S2-5
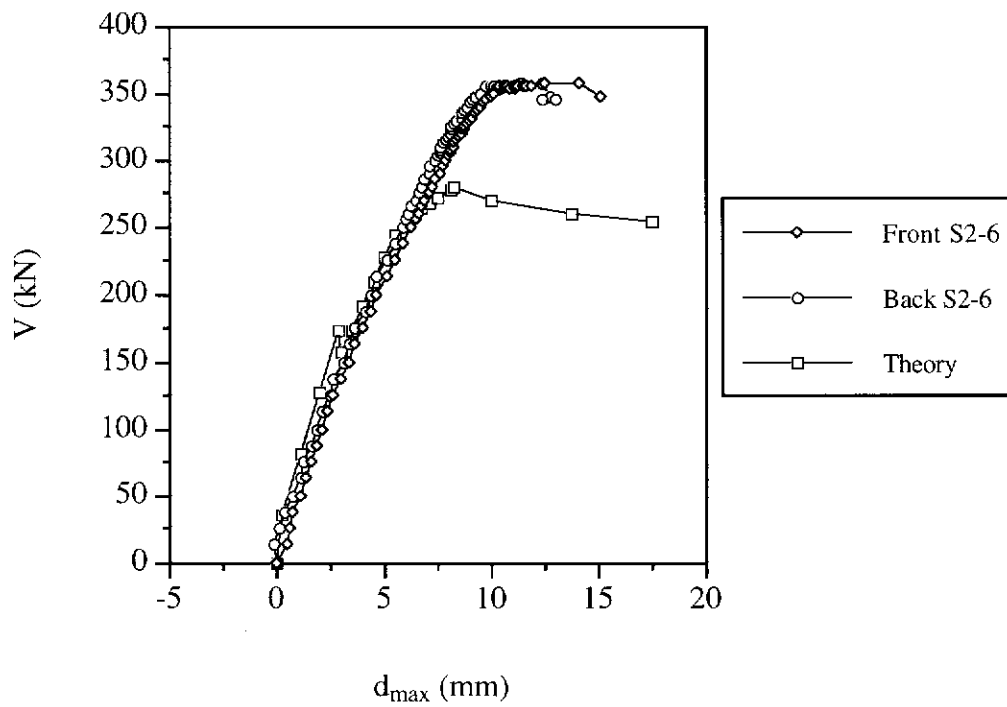
Figure C.12 Shear Force versus Midspan Deflection for Beam S2-6
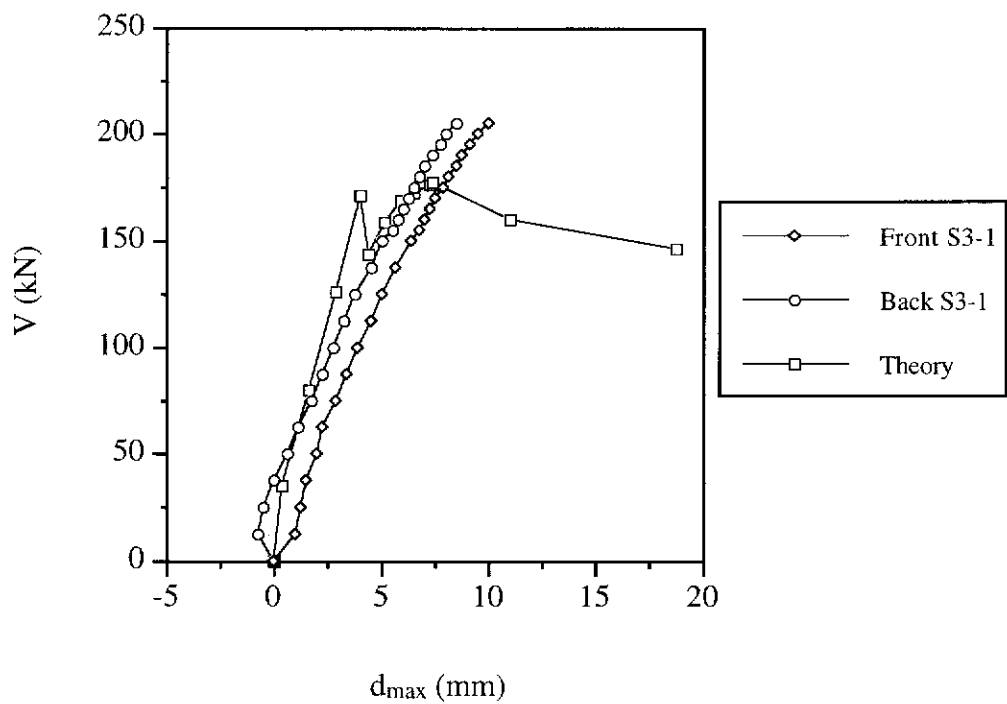
Figure C.13 Shear Force versus Midspan Deflection for Beam S3-1
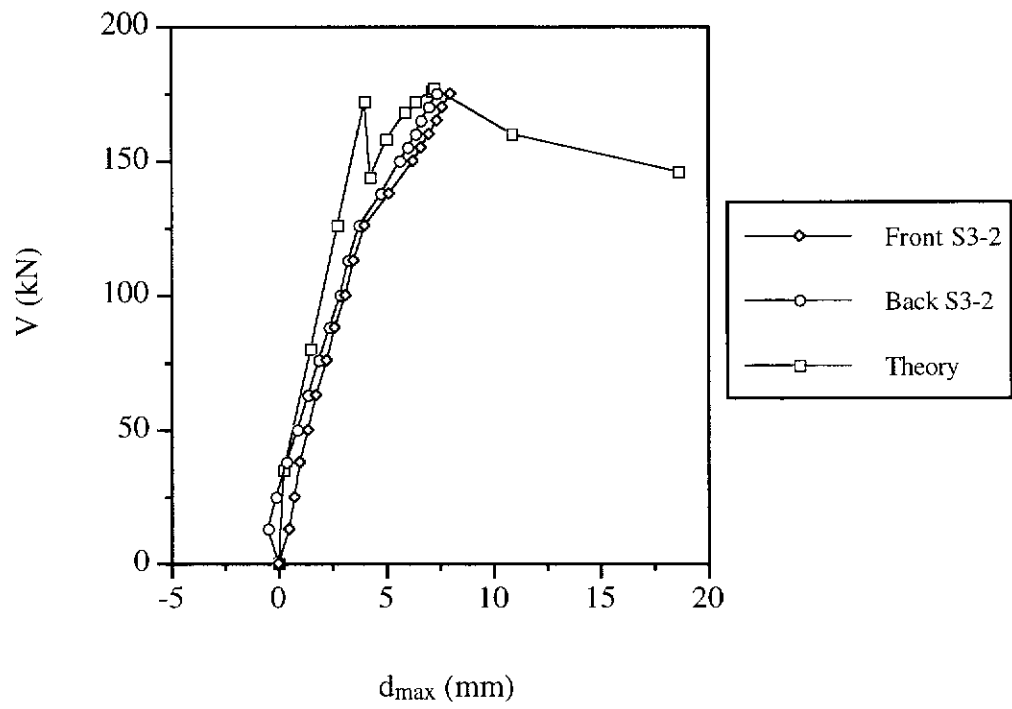
Figure C.14 Shear Force versus Midspan Deflection for Beam S3-2
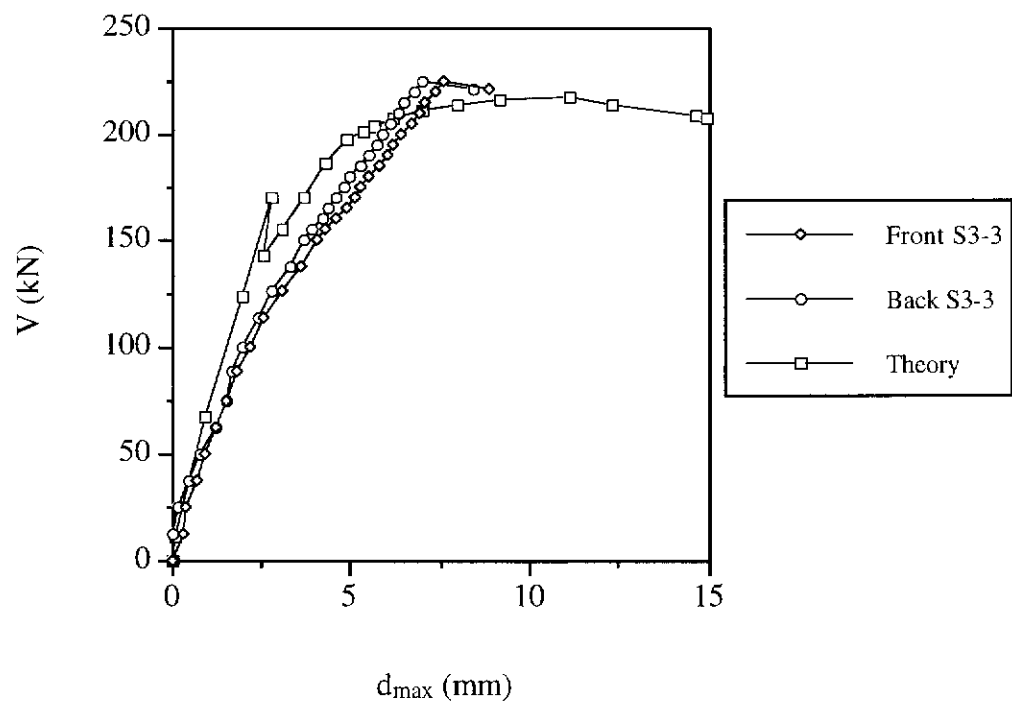
Figure C.15 Shear Force versus Midspan Deflection for Beam S3-3
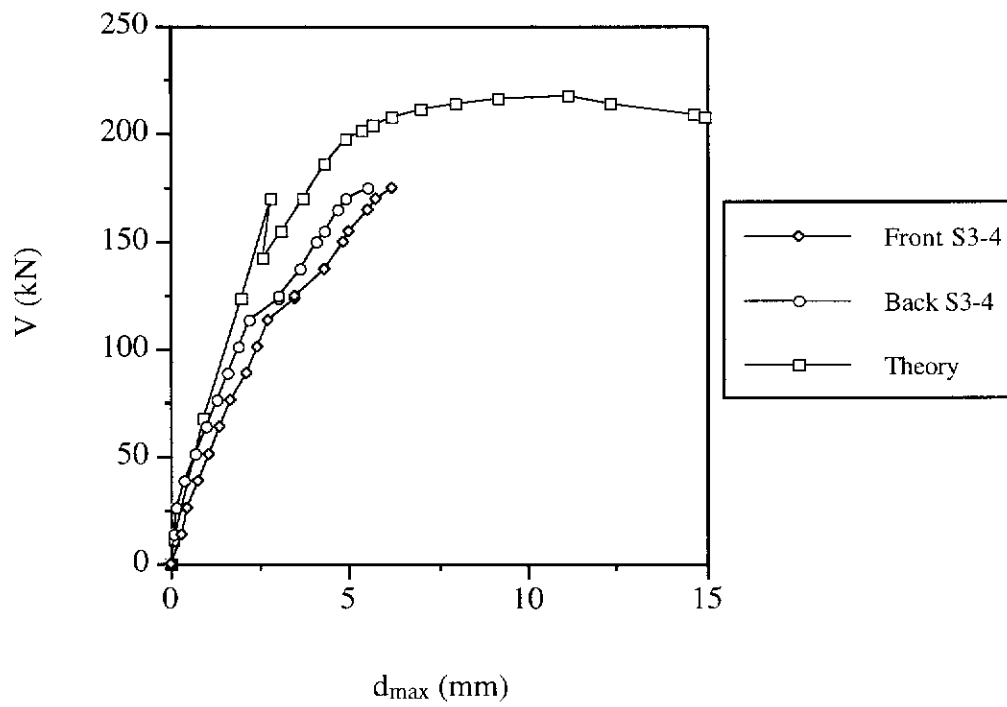
Figure C.16 Shear Force versus Midspan Deflection for Beam S3-4
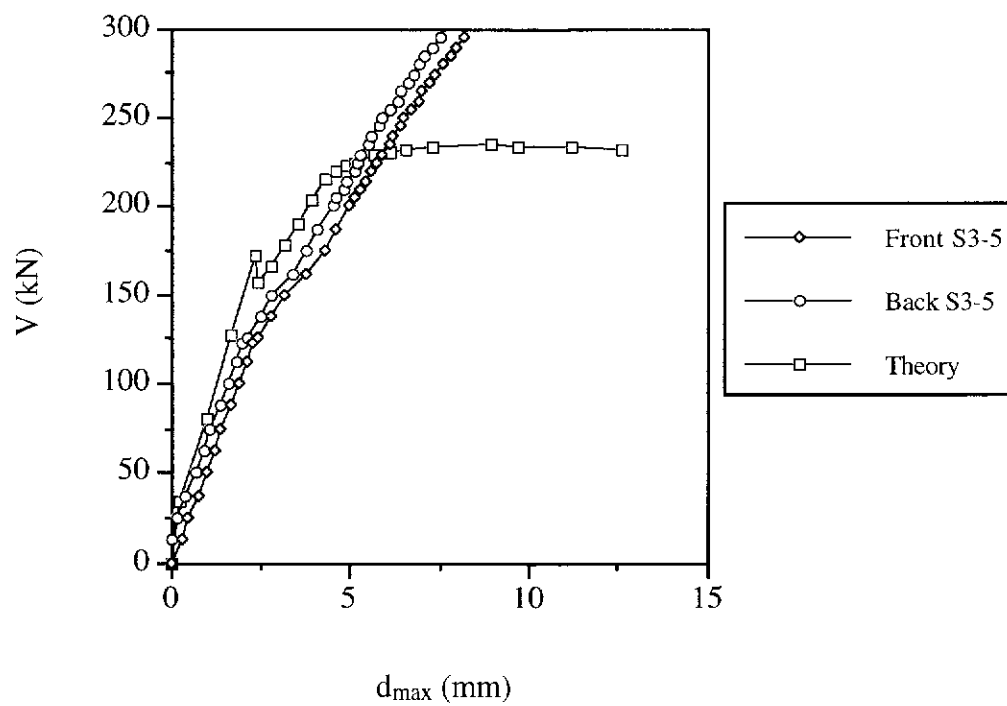
Figure C.17 Shear Force versus Midspan Deflection for Beam S3-5
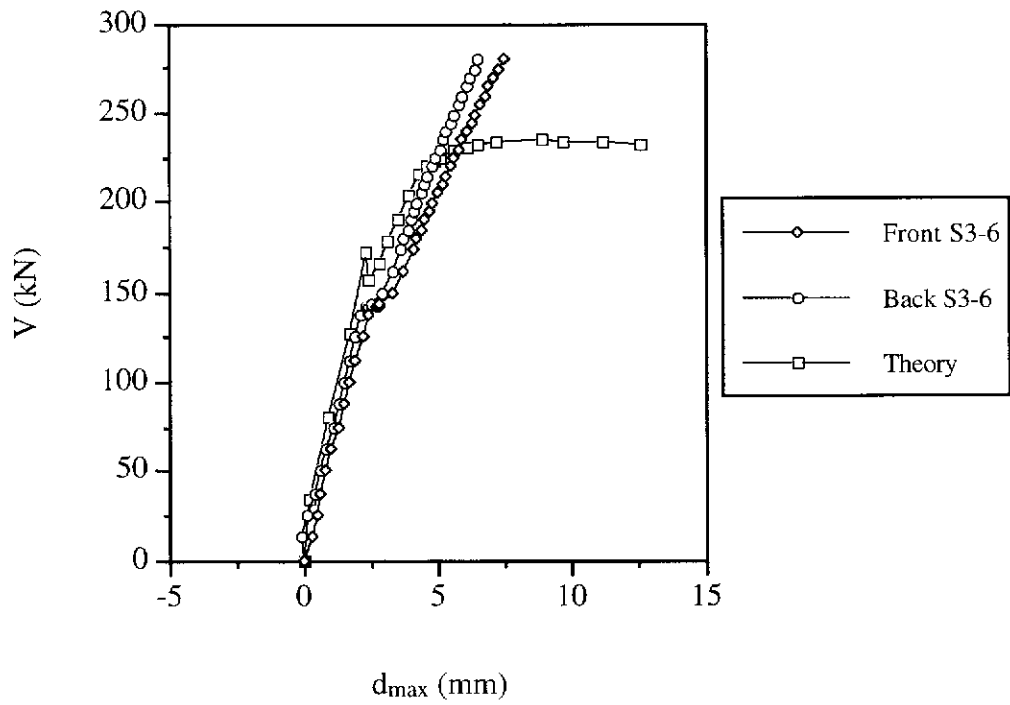
Figure C.18 Shear Force versus Midspan Deflection for Beam S3-6
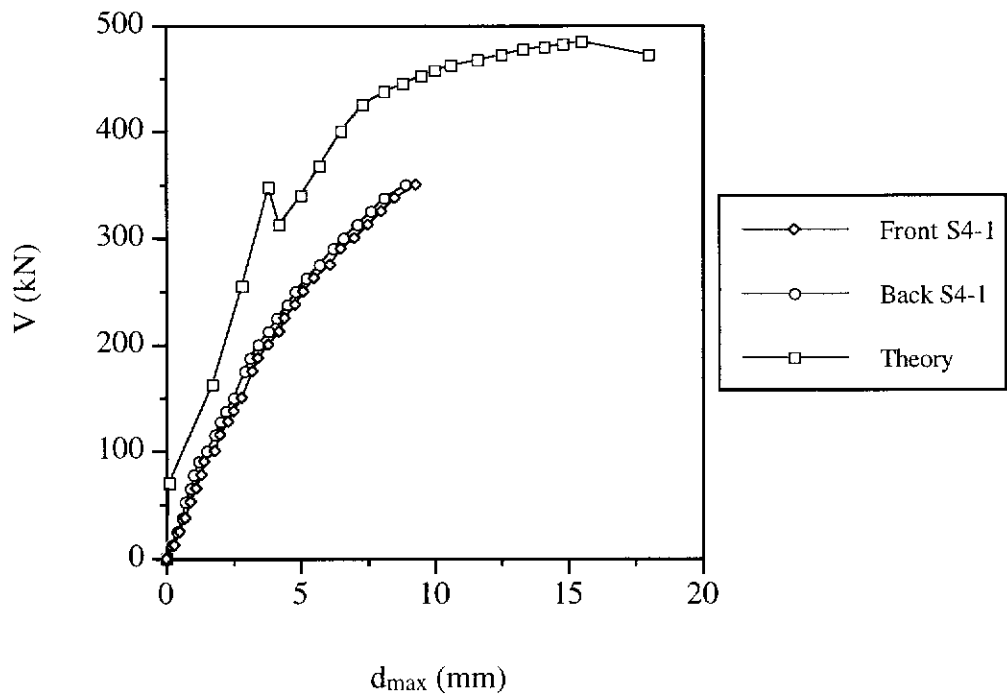
Figure C.19 Shear Force versus Midspan Deflection for Beam S4-1
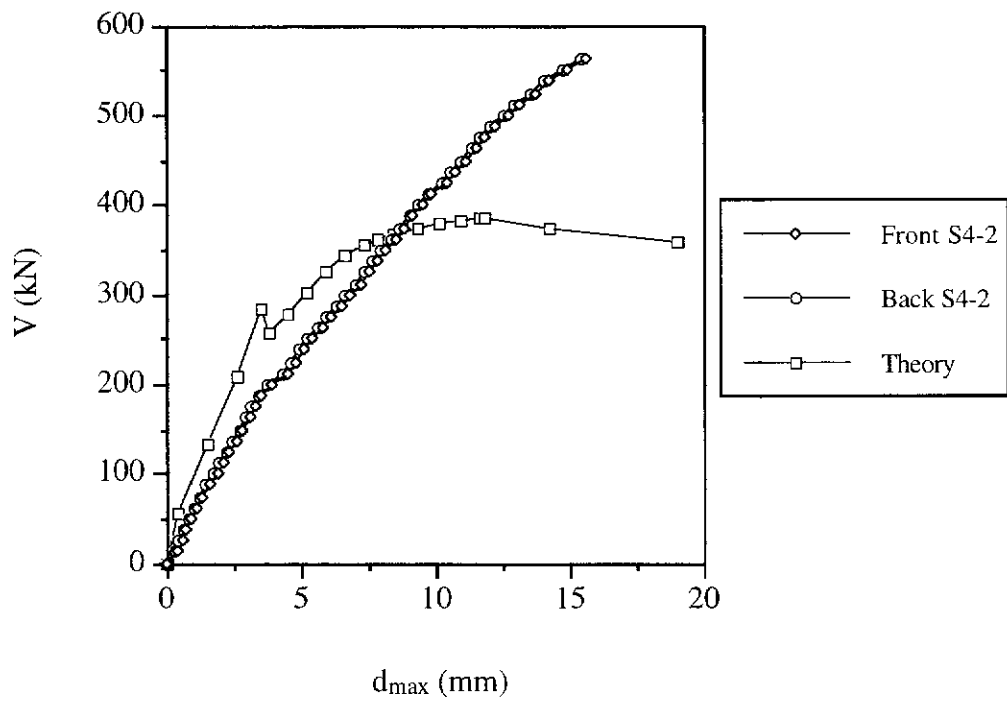
Figure C.20 Shear Force versus Midspan Deflection for Beam S4-2
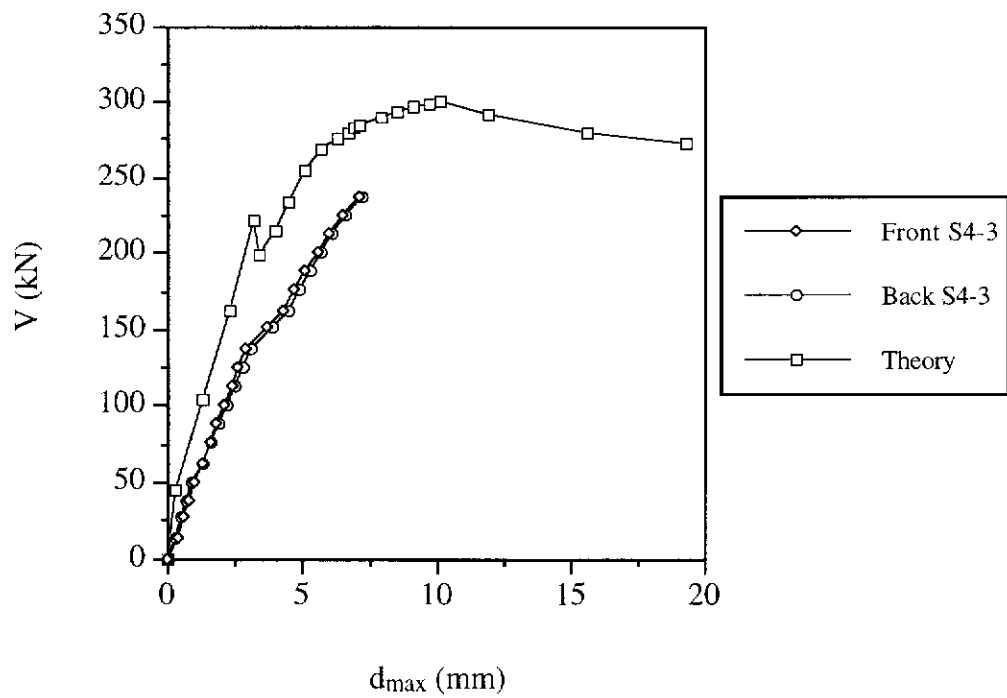
Figure C.21 Shear Force versus Midspan Deflection for Beam S4-3
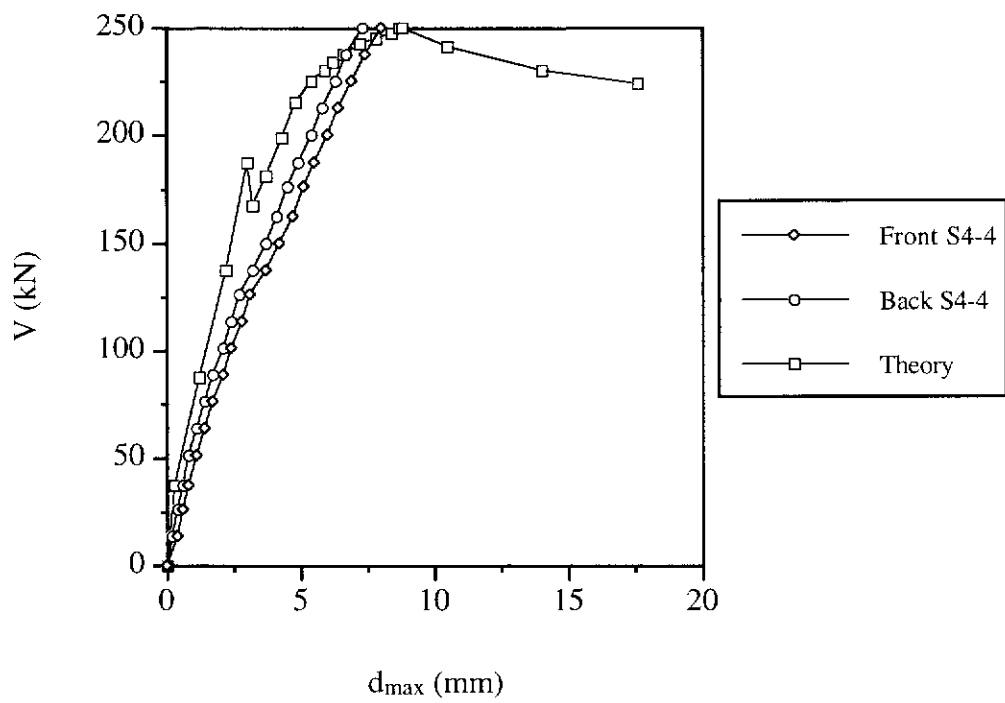
Figure C.22 Shear Force versus Midspan Deflection for Beam S4-4
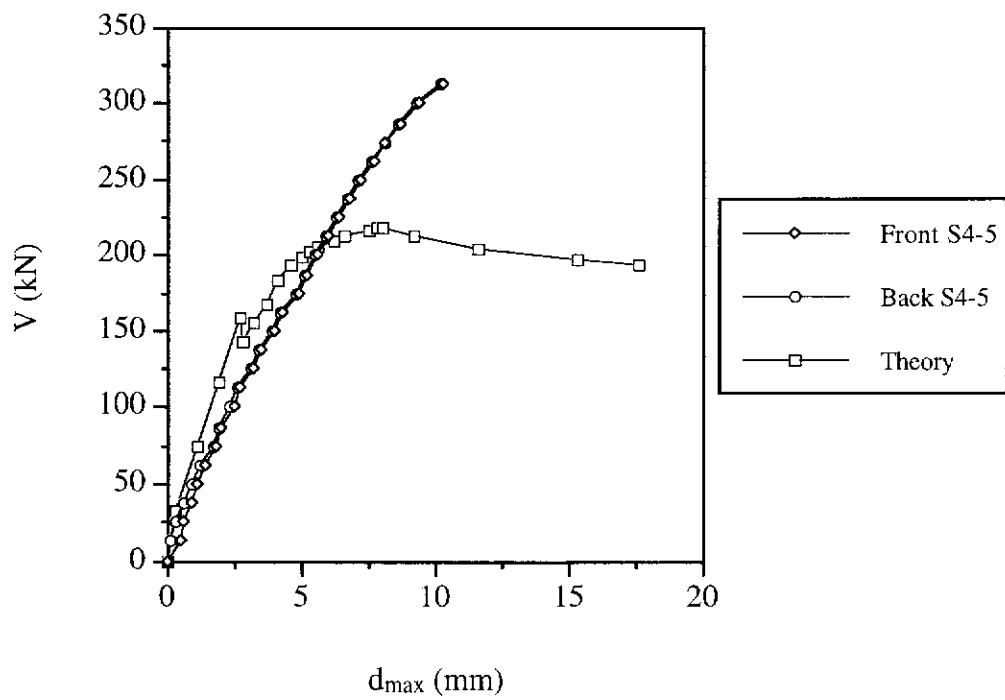
Figure C.23 Shear Force versus Midspan Deflection for Beam S4-5
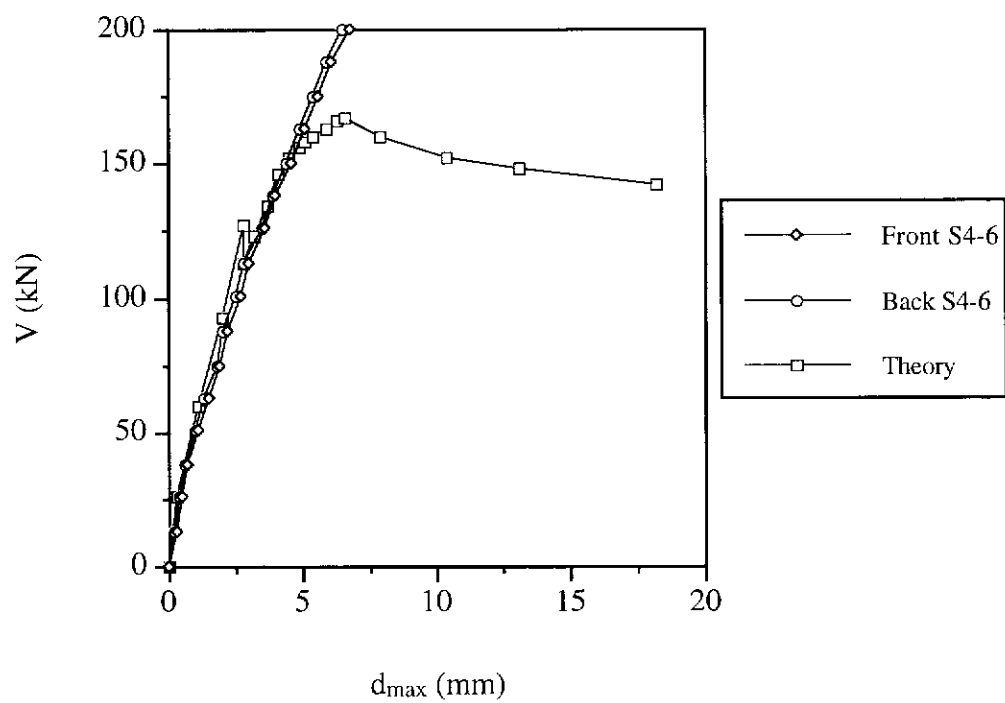
Figure C.24 Shear Force versus Midspan Deflection for Beam S4-6
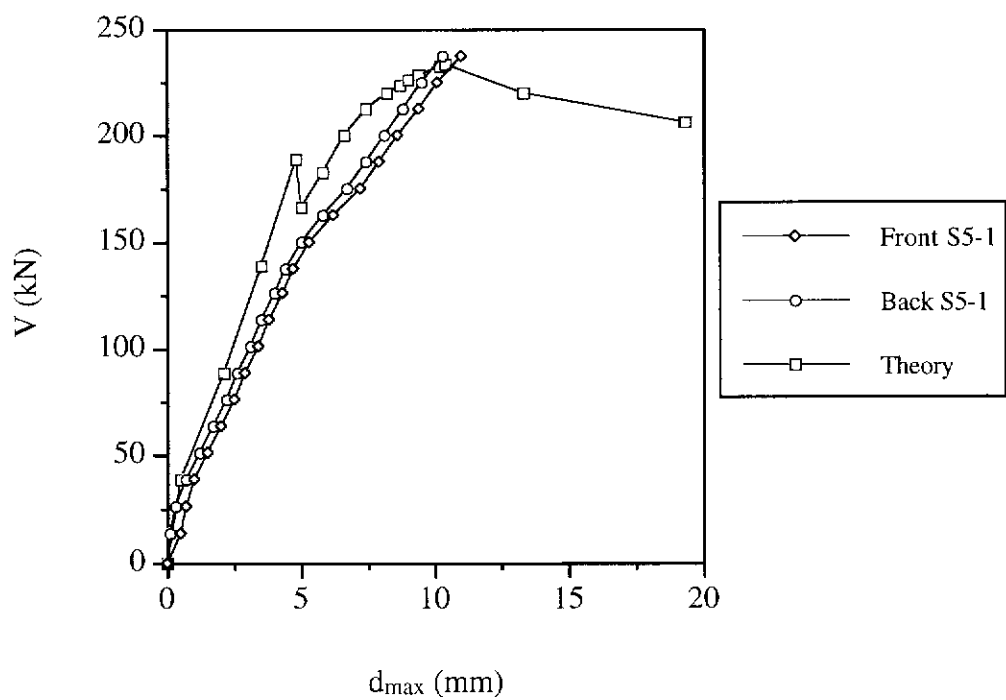
Figure C.25 Shear Force versus Midspan Deflection for Beam S5-1
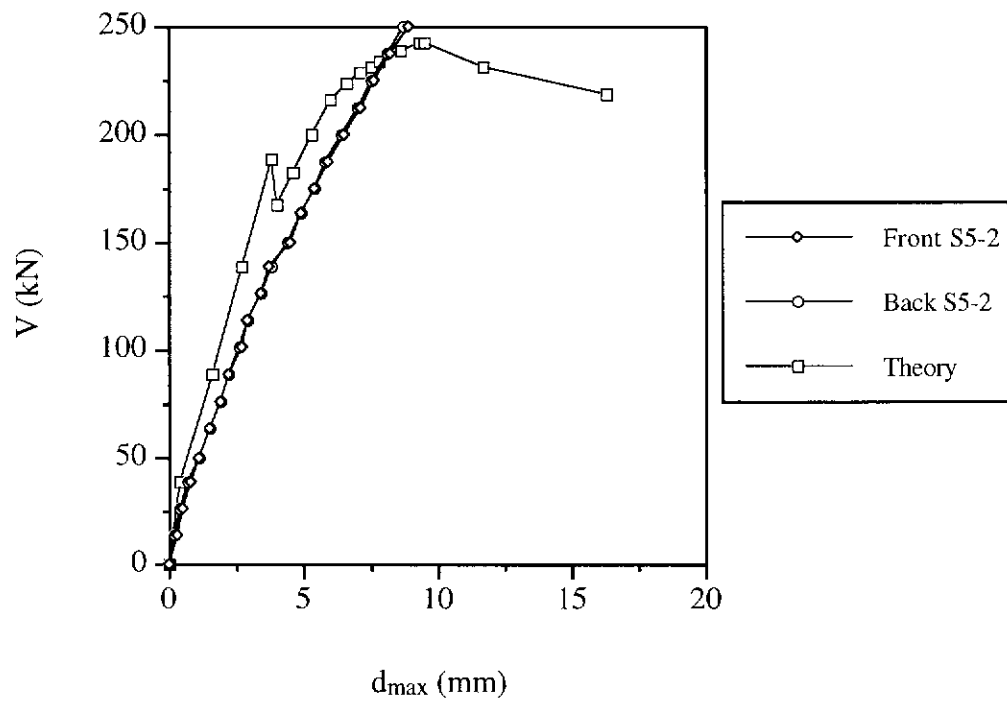
Figure C.26 Shear Force versus Midspan Deflection for Beam S5-2
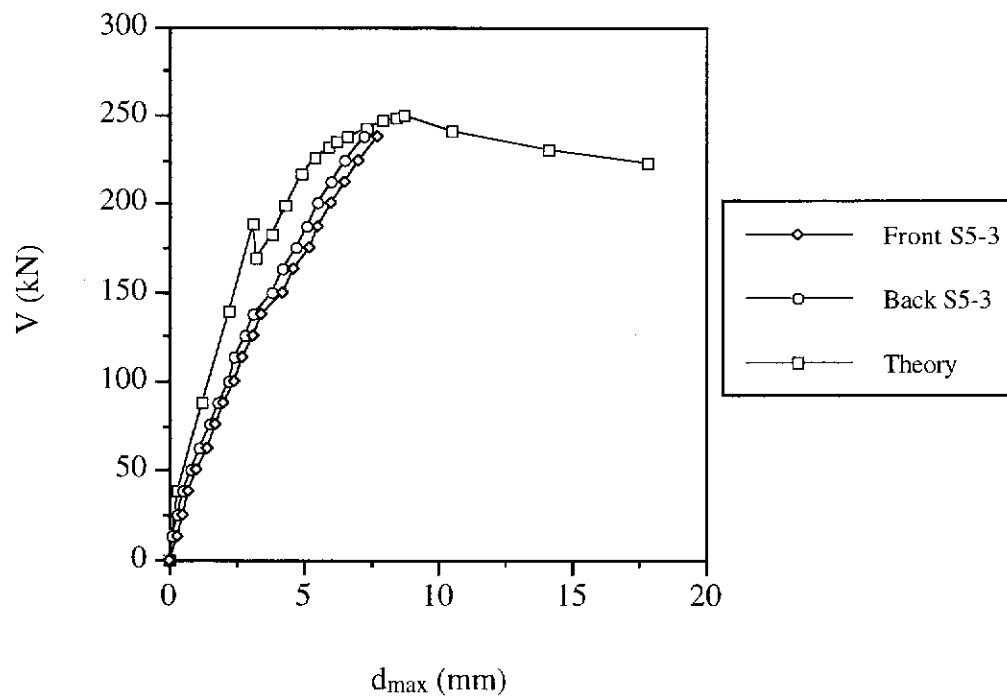
Figure C.27 Shear Force versus Midspan Deflection for Beam S5-3
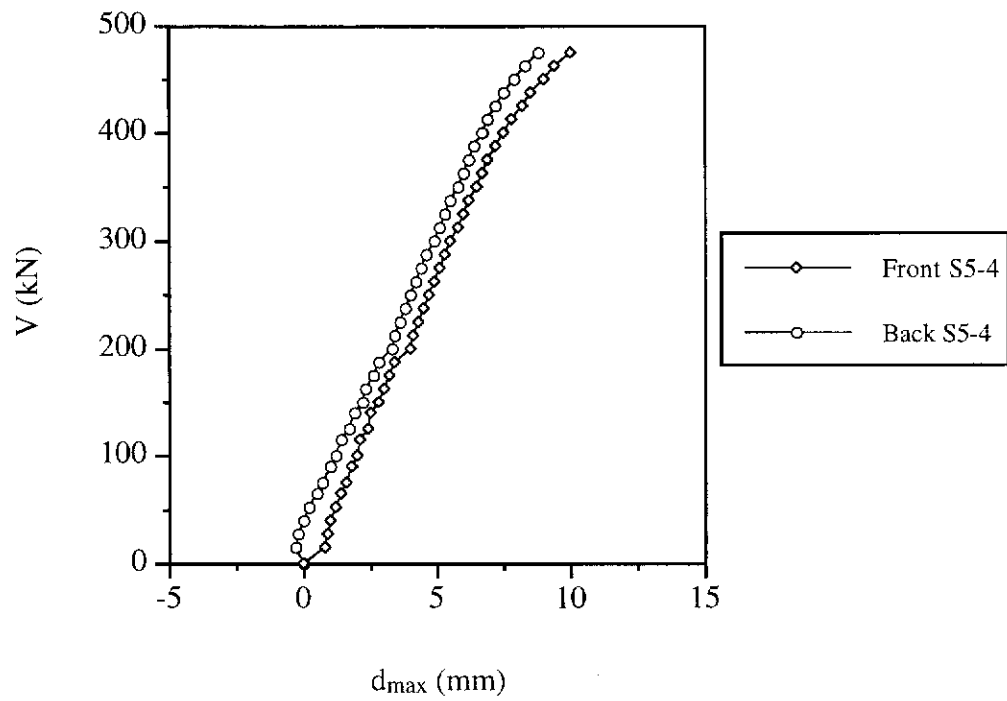
Figure C.28 Shear Force versus Midspan Deflection for Beam S5-4
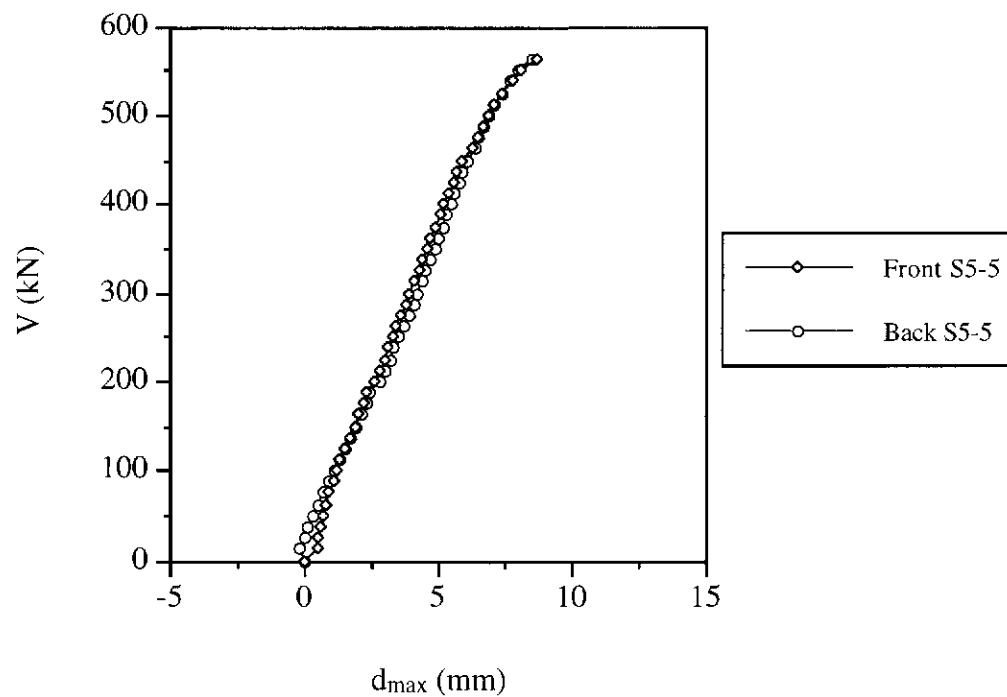
Figure C.29 Shear Force versus Midspan Deflection for Beam S5-5
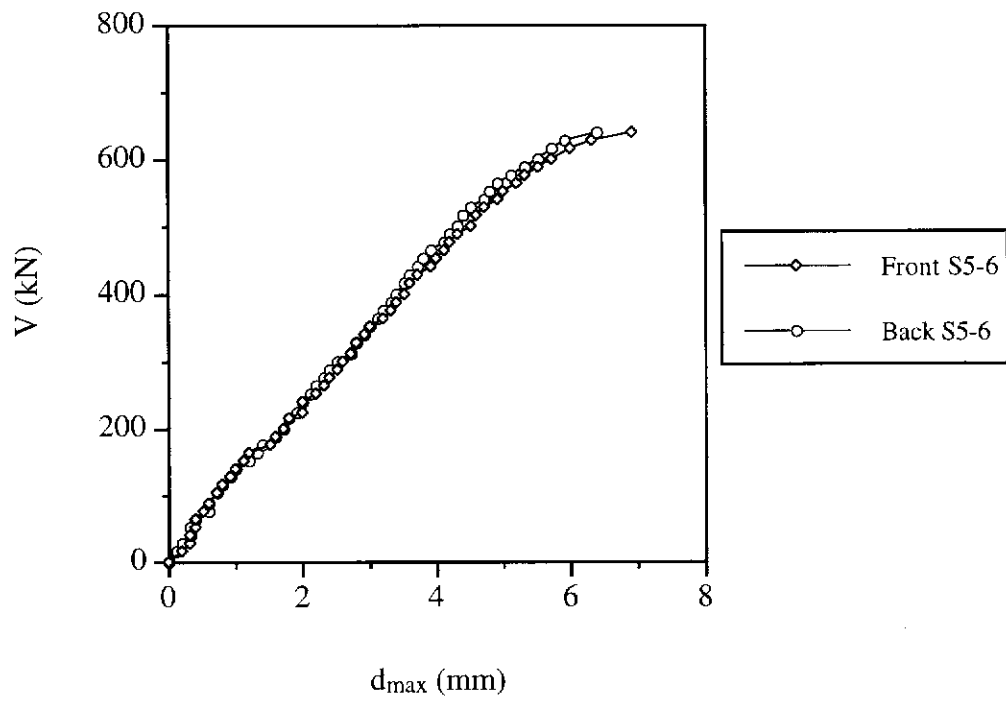
Figure C.30 Shear Force versus Midspan Deflection for Beam S5-6
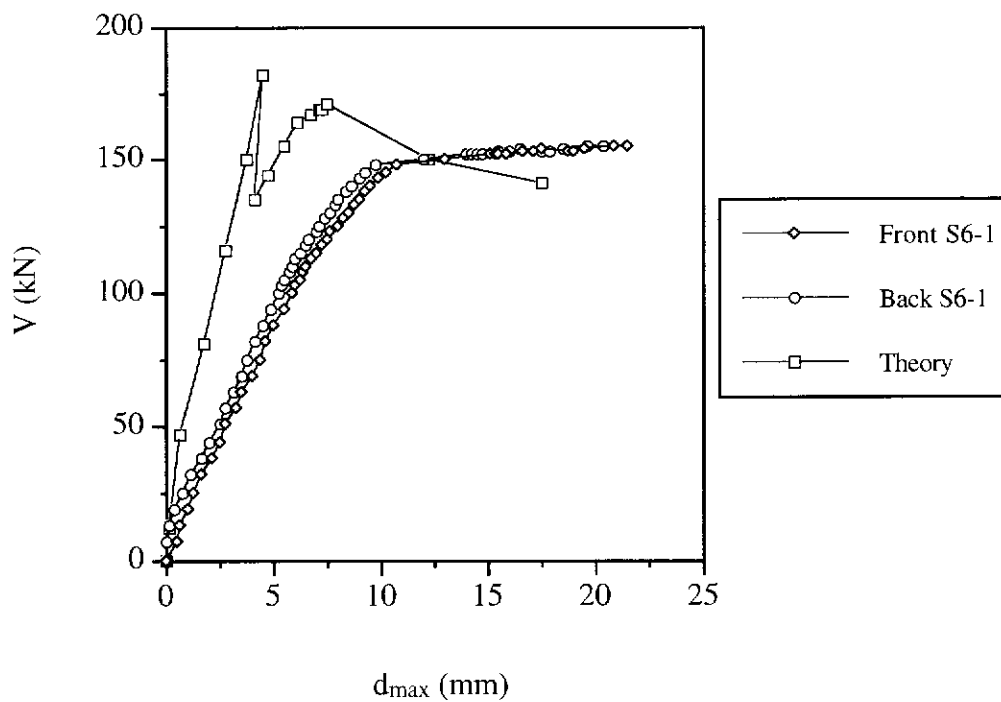
Figure C.31 Shear Force versus Midspan Deflection for Beam S6-1
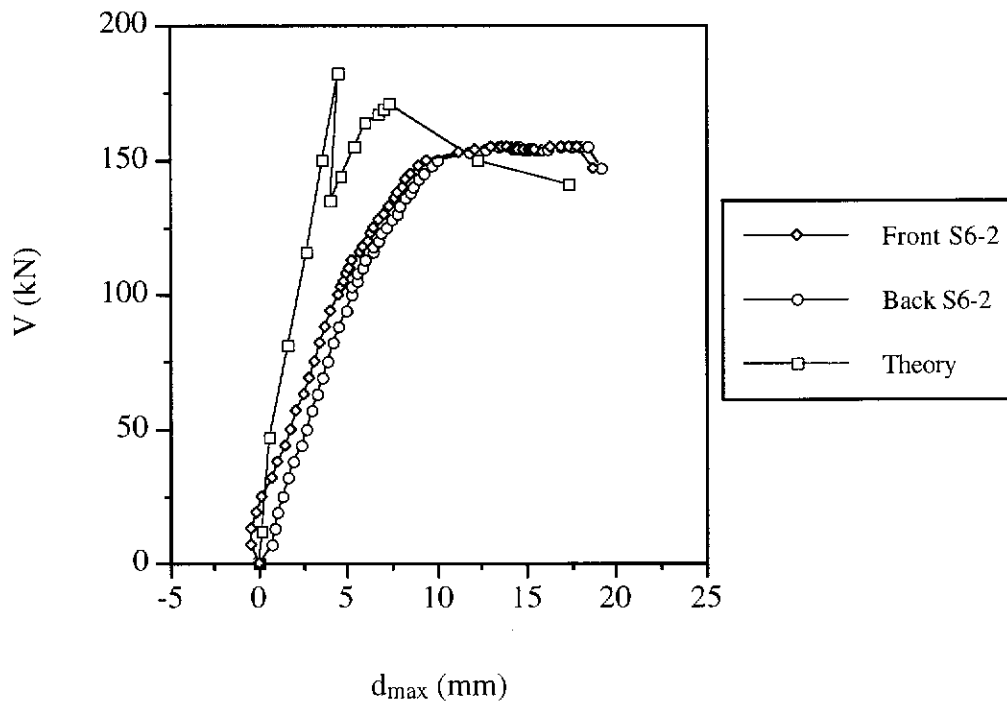
Figure C.32 Shear Force versus Midspan Deflection for Beam S6-2
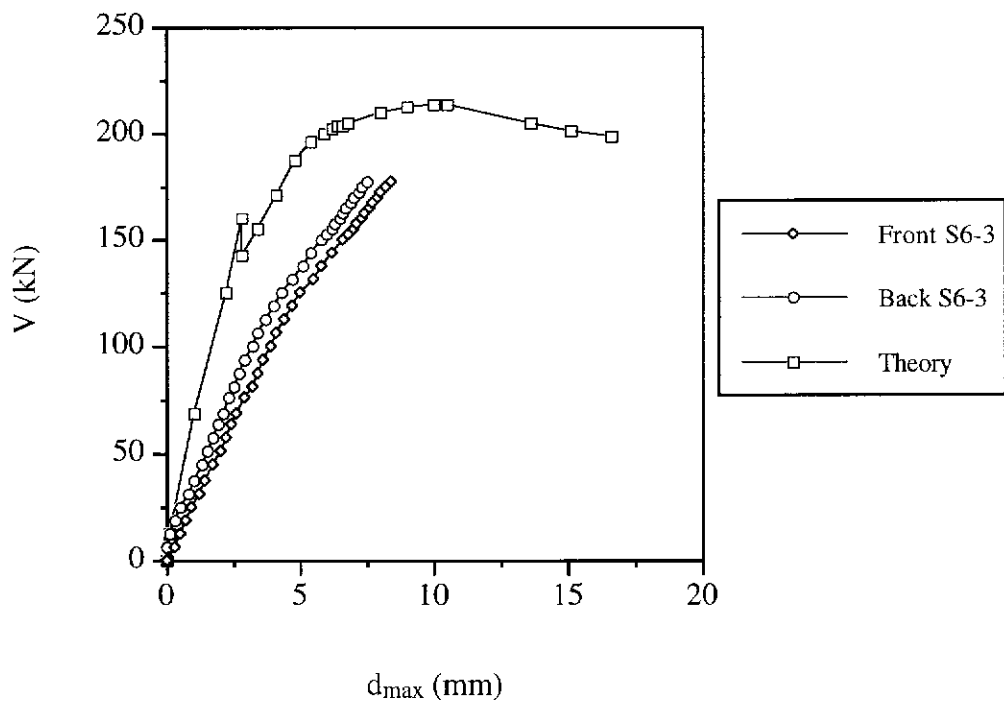
Figure C.33 Shear Force versus Midspan Deflection for Beam S6-3
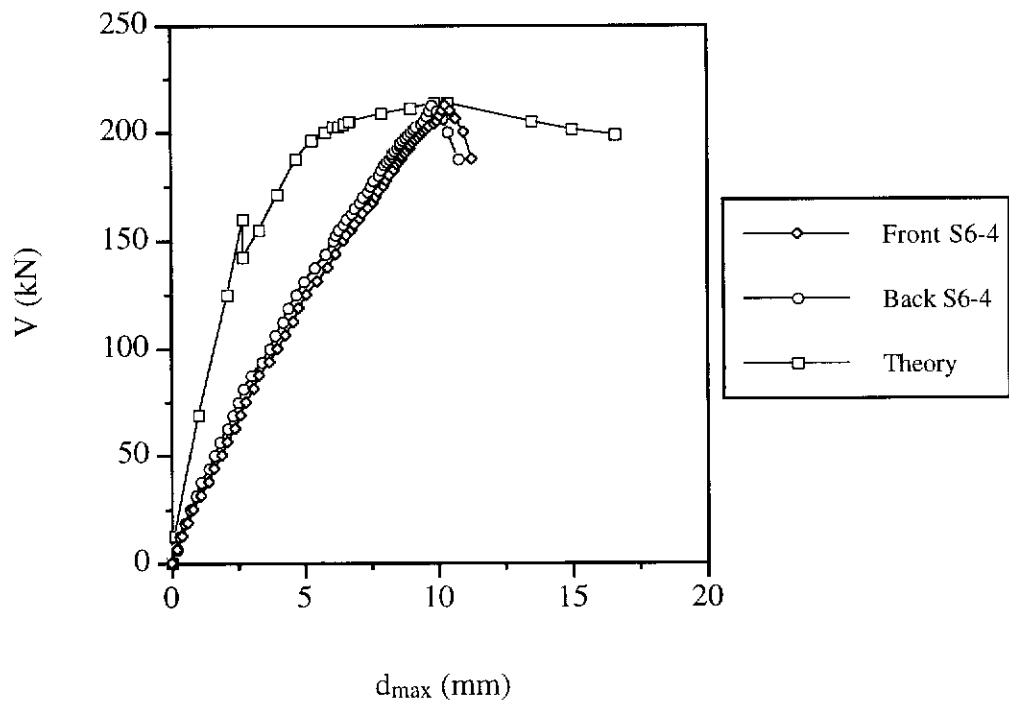
Figure C.34 Shear Force versus Midspan Deflection for Beam S6-4
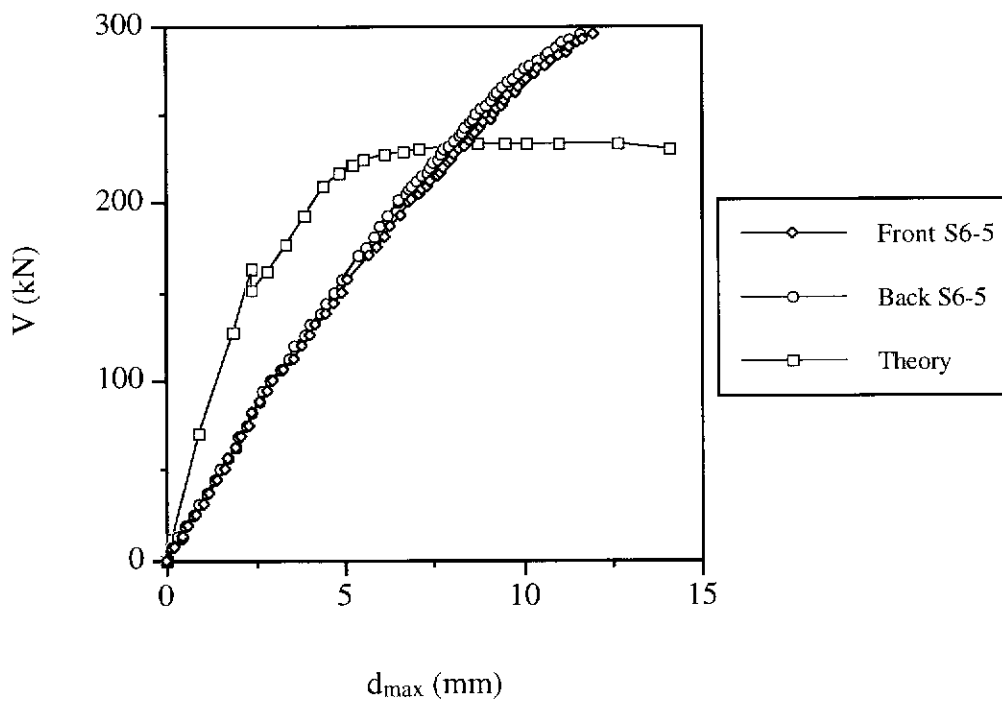
Figure C.35 Shear Force versus Midspan Deflection for Beam S6-5
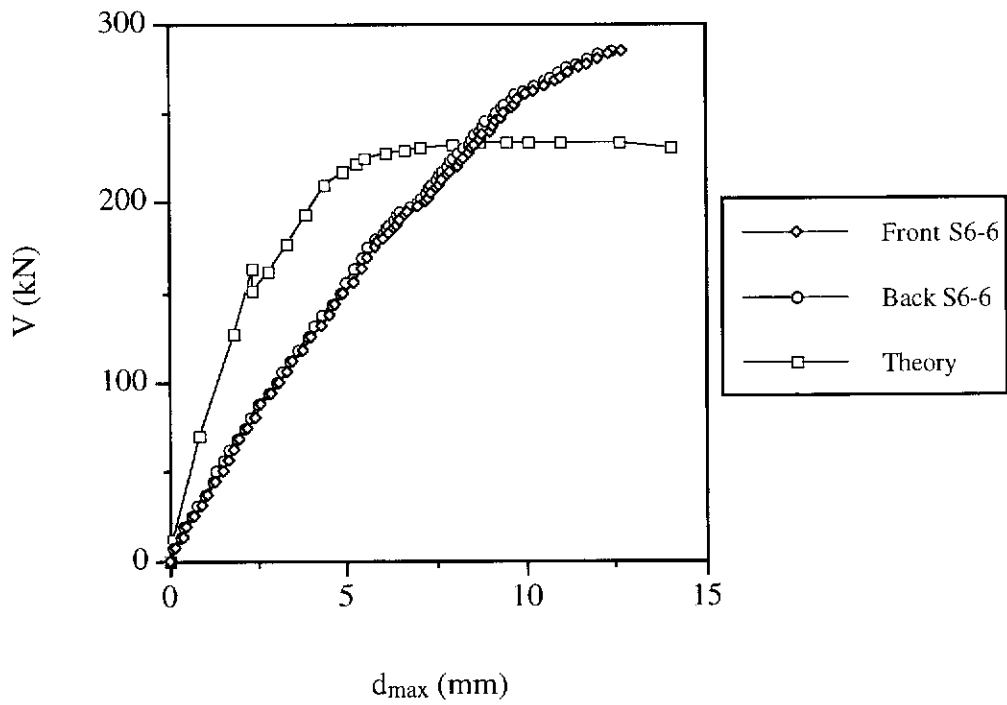
Figure C.36 Shear Force versus Midspan Deflection for Beam S6-6
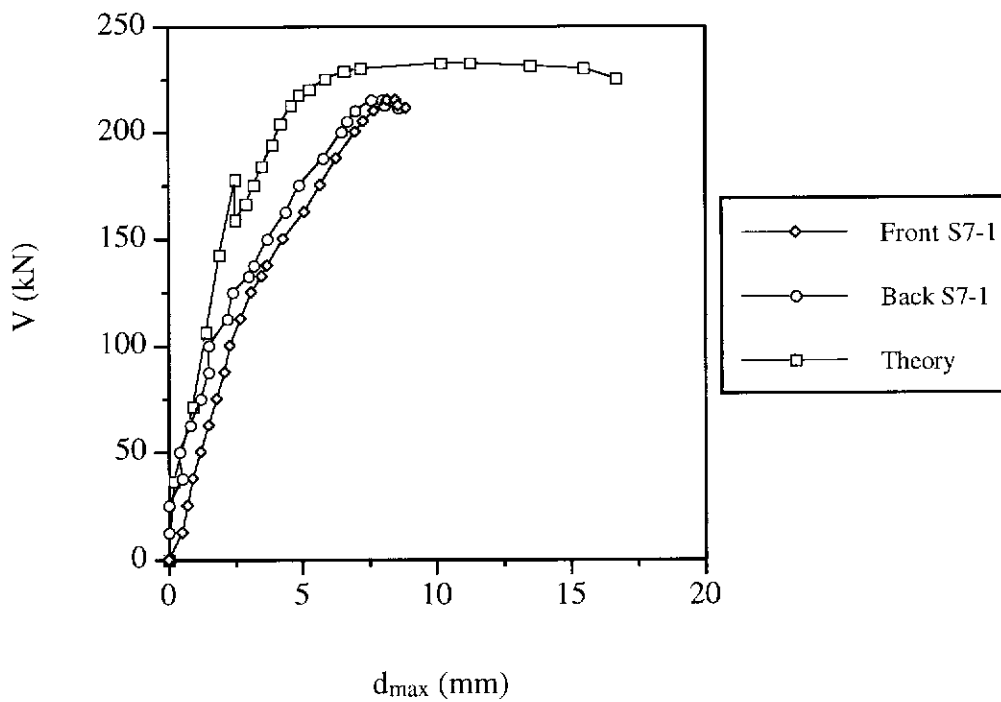
Figure C.37 Shear Force versus Midspan Deflection for Beam S7-1
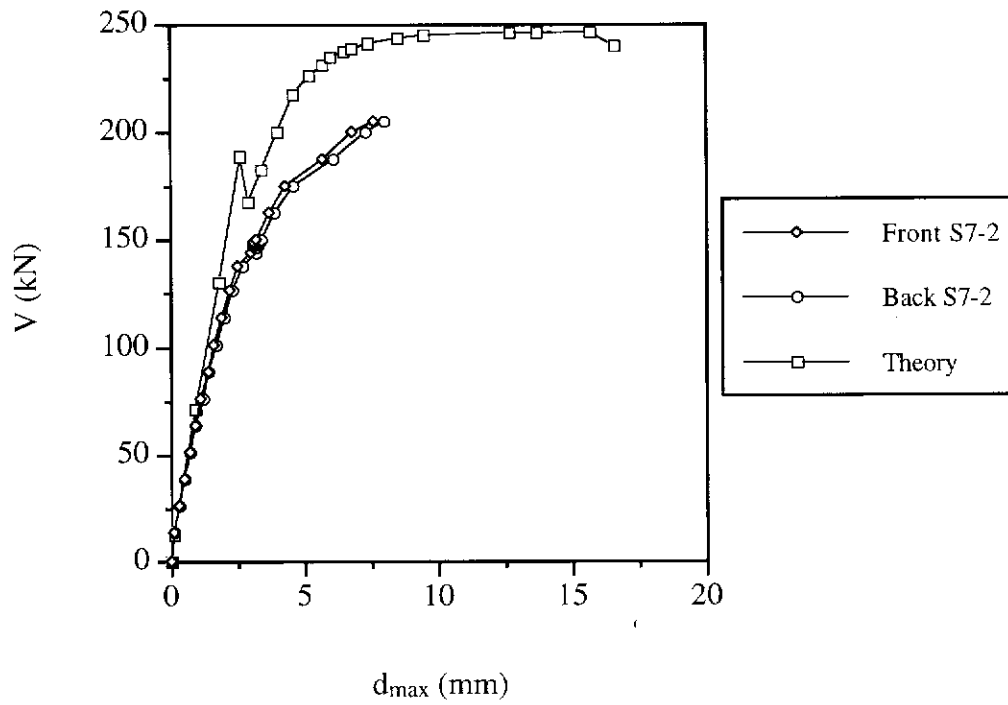
Figure C.38 Shear Force versus Midspan Deflection for Beam S7-2
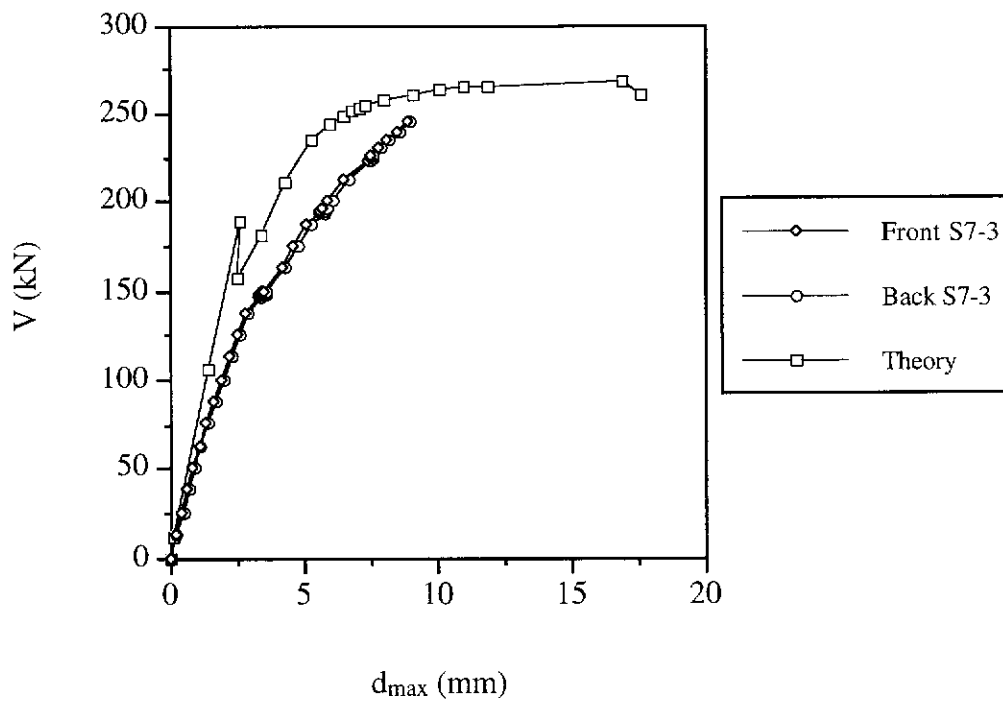
Figure C.39 Shear Force versus Midspan Deflection for Beam S7-3
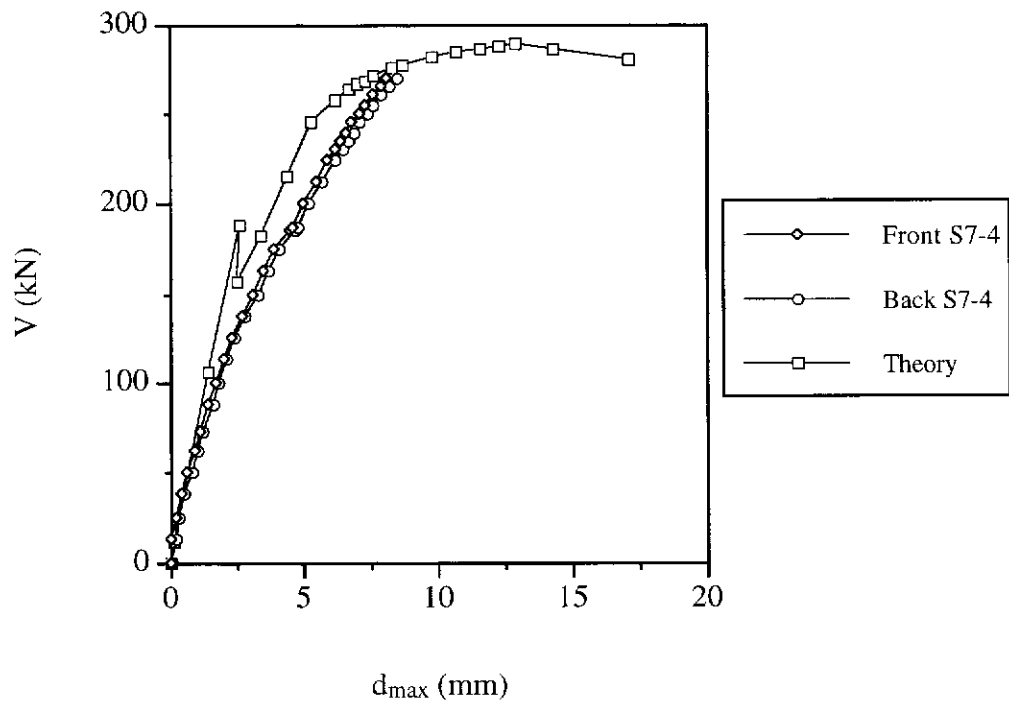
Figure C.40 Shear Force versus Midspan Deflection for Beam S7-4
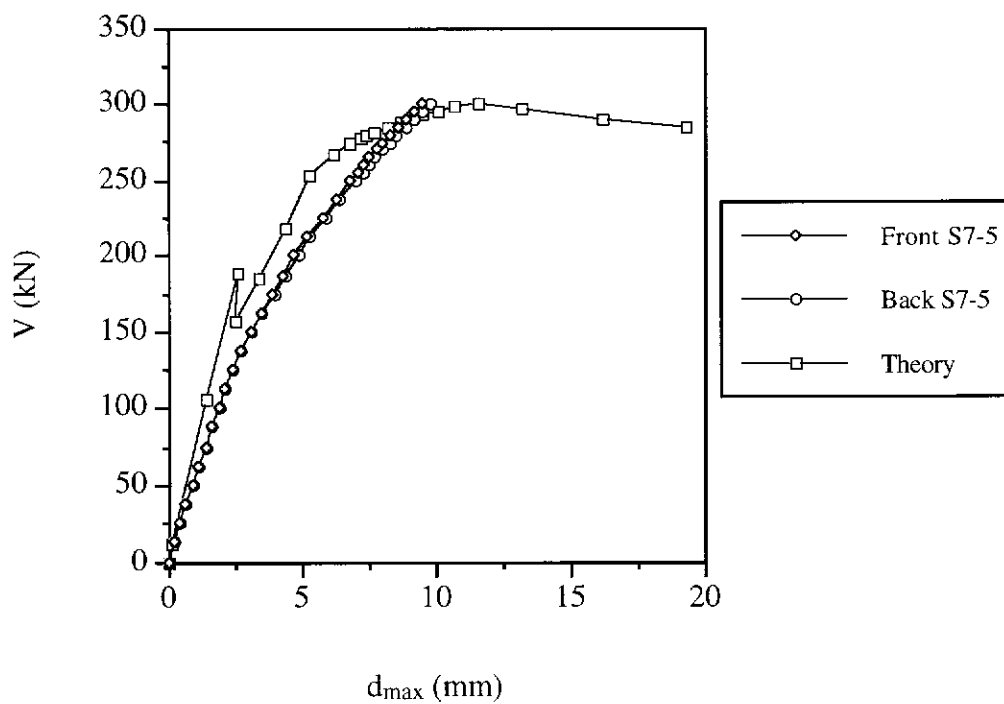
Figure C.41 Shear Force versus Midspan Deflection for Beam S7-5
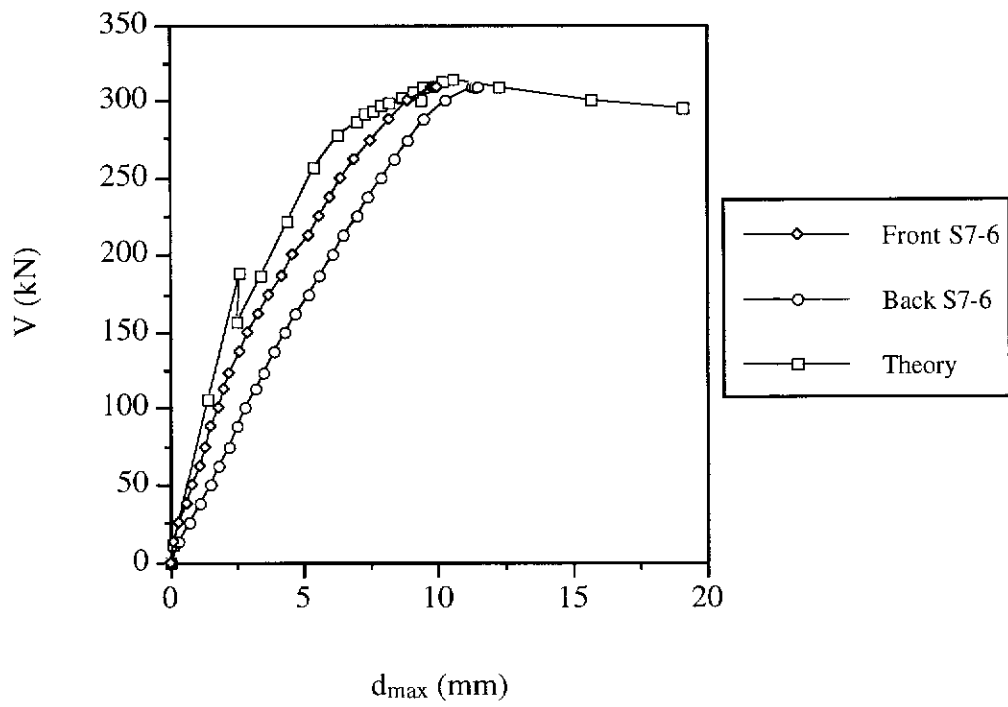
Figure C.42 Shear Force versus Midspan Deflection for Beam S7-6
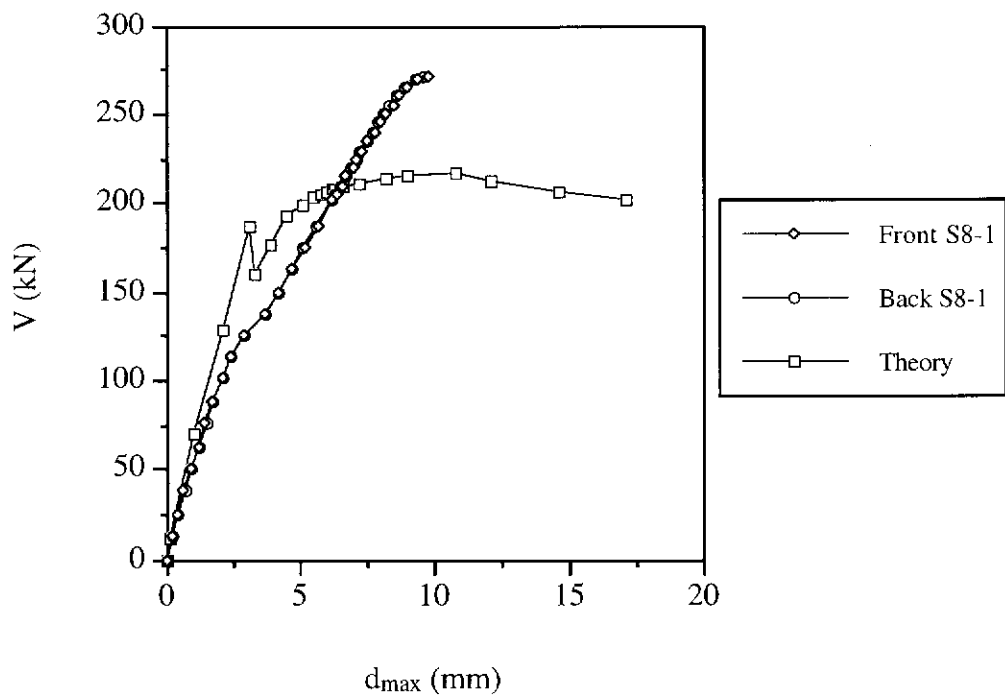
Figure C.43 Shear Force versus Midspan Deflection for Beam S8-1
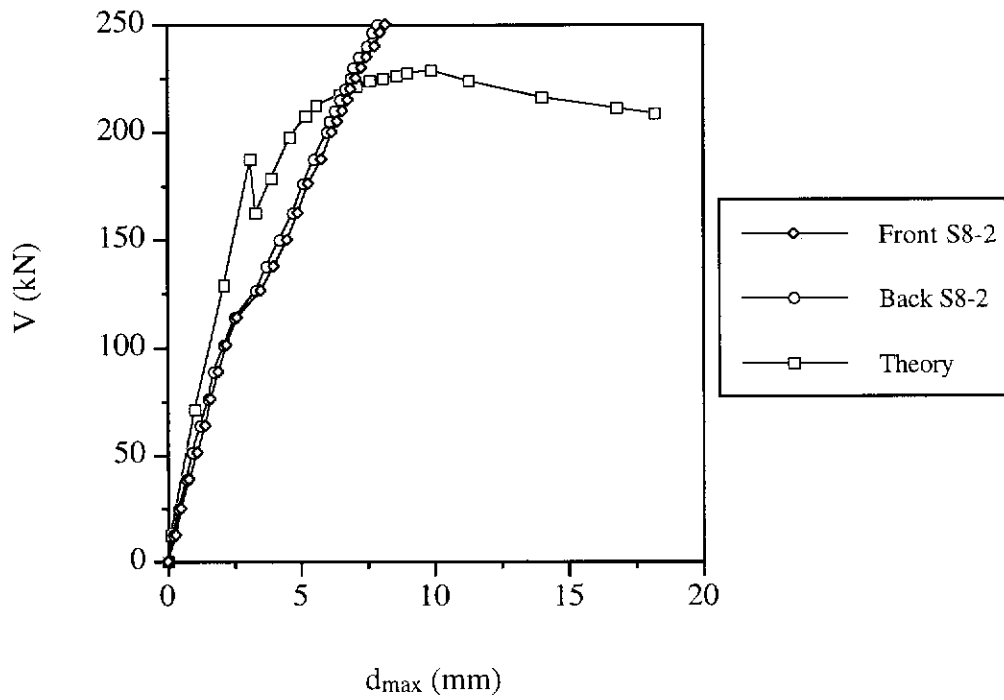
Figure C.44 Shear Force versus Midspan Deflection for Beam S8-2
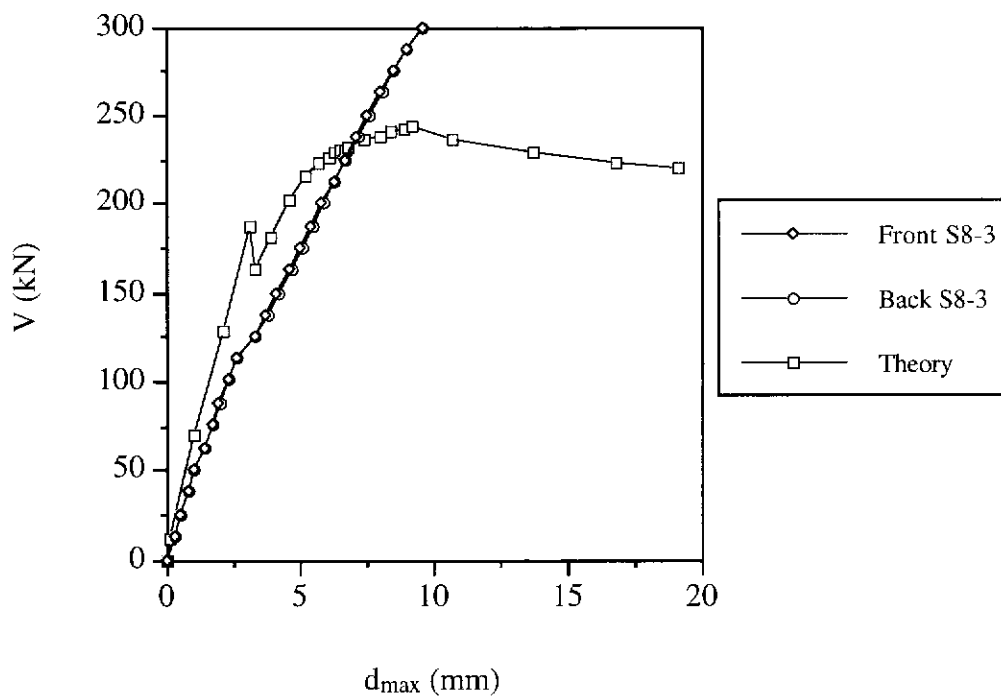
Figure C.45 Shear Force versus Midspan Deflection for Beam S8-3
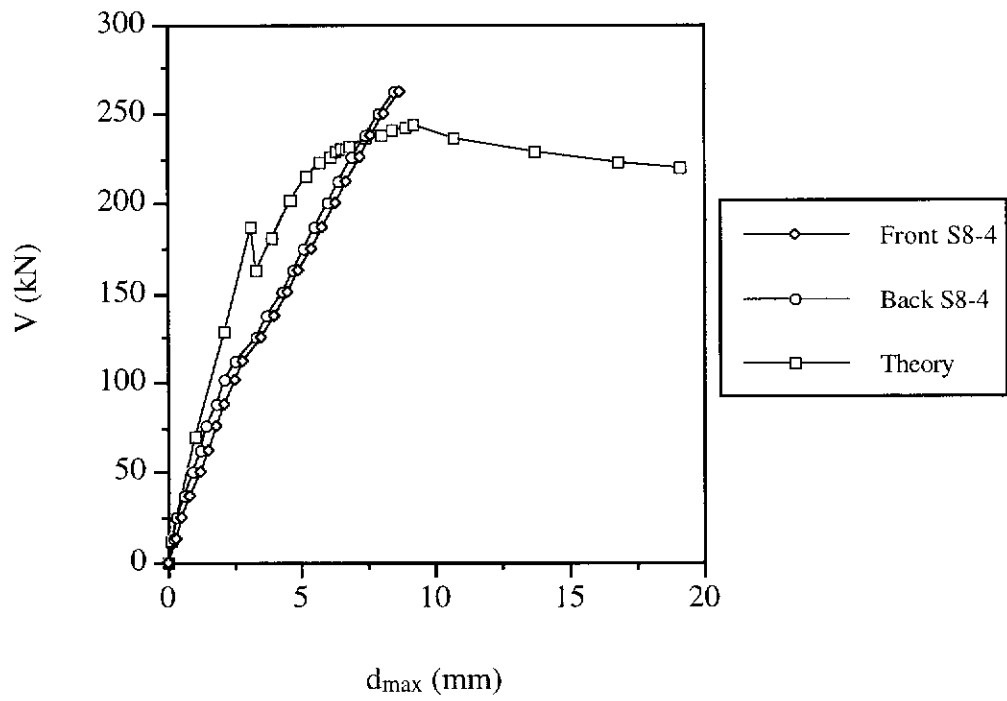
Figure C.46 Shear Force versus Midspan Deflection for Beam S8-4
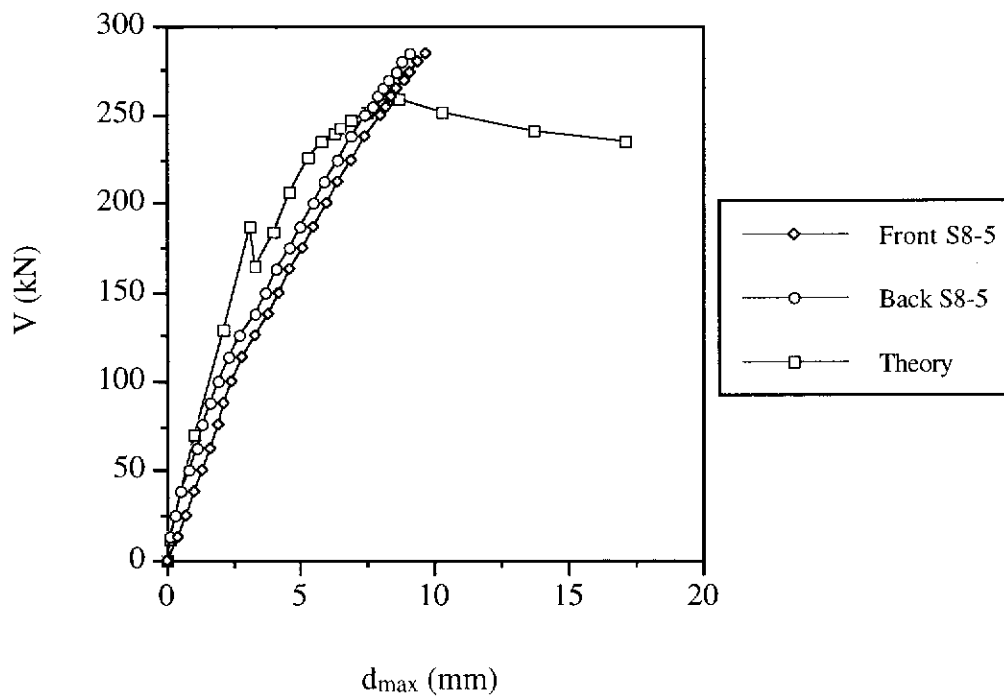
Figure C.47 Shear Force versus Midspan Deflection for Beam S8-5
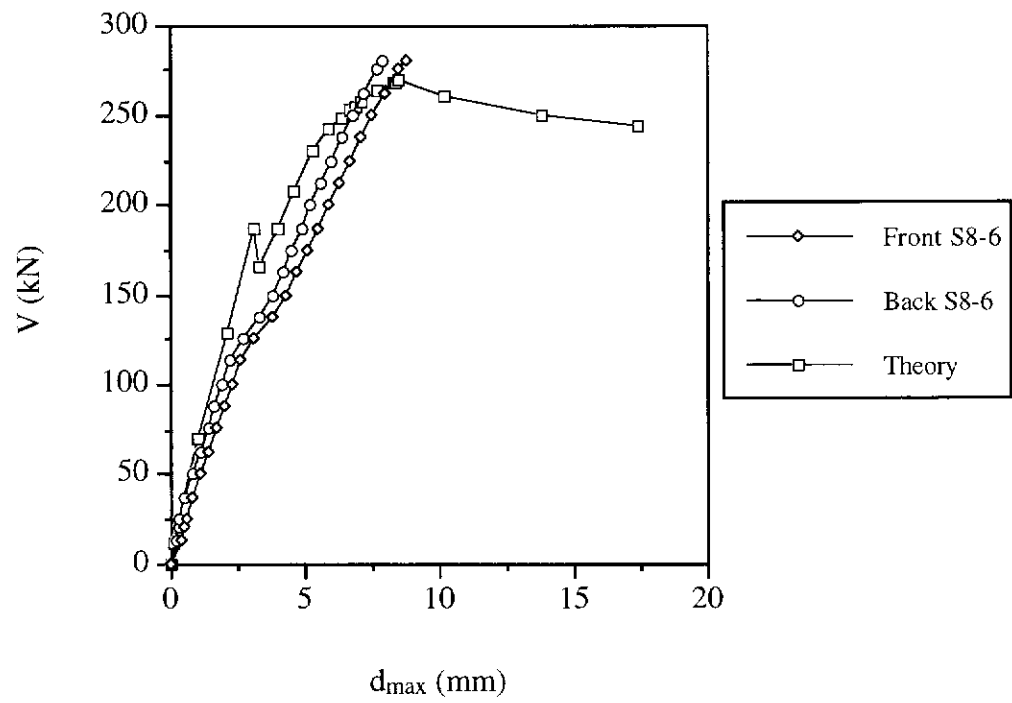
Figure C.48 Shear Force versus Midspan Deflection for Beam S8-6

Curvature Of Test Beams

The following are shear force versus curvature curves for test beams of the present study.
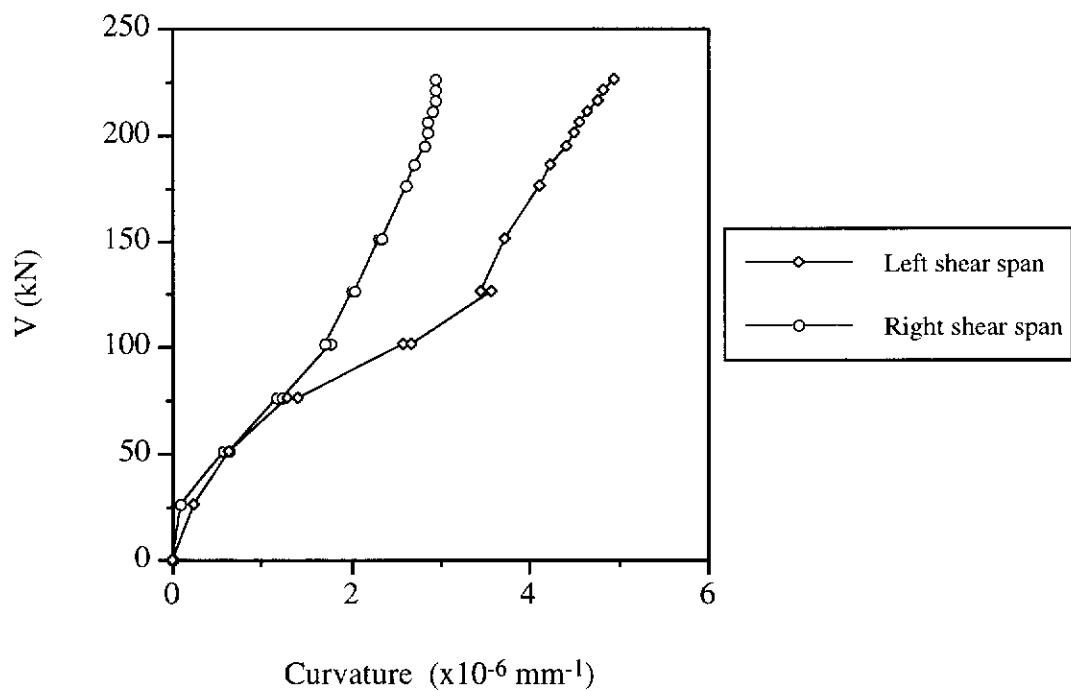
Figure D.1 Shear Force versus Curvature for Beam S1-1
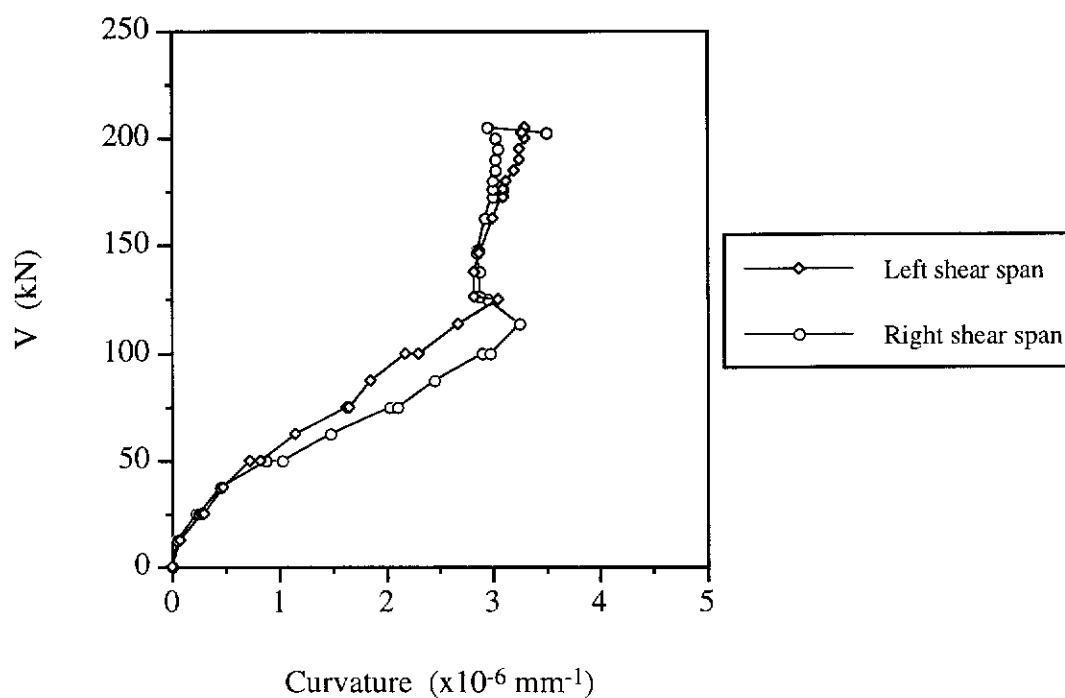
Figure D.2 Shear Force versus Curvature for Beam S1-2
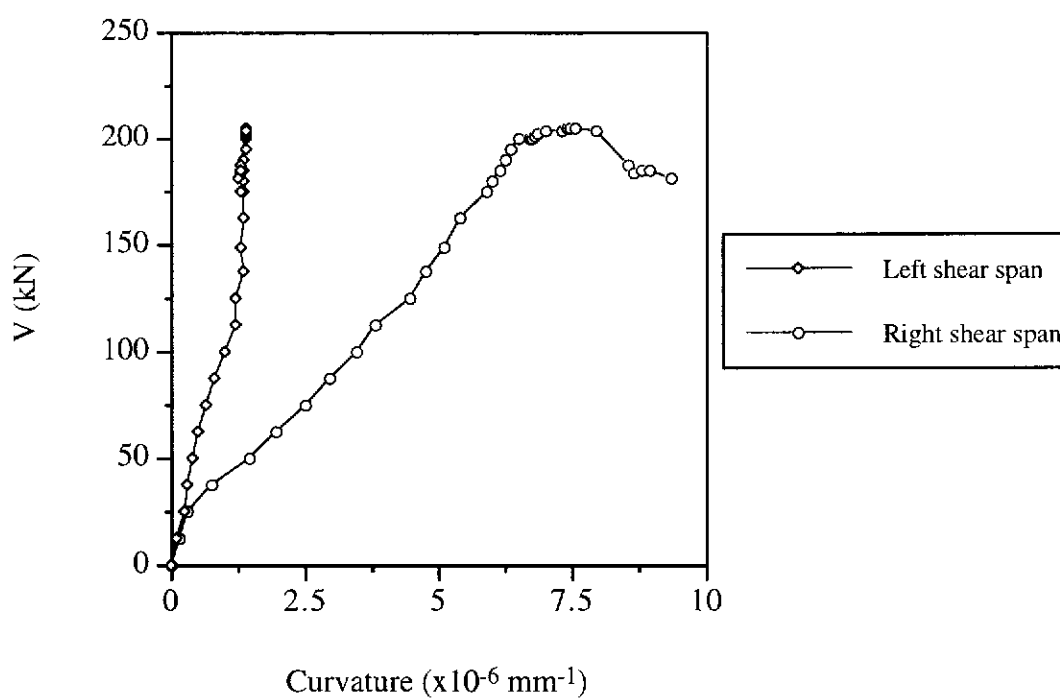
Figure D.3 Shear Force versus Curvature for Beam S1-3
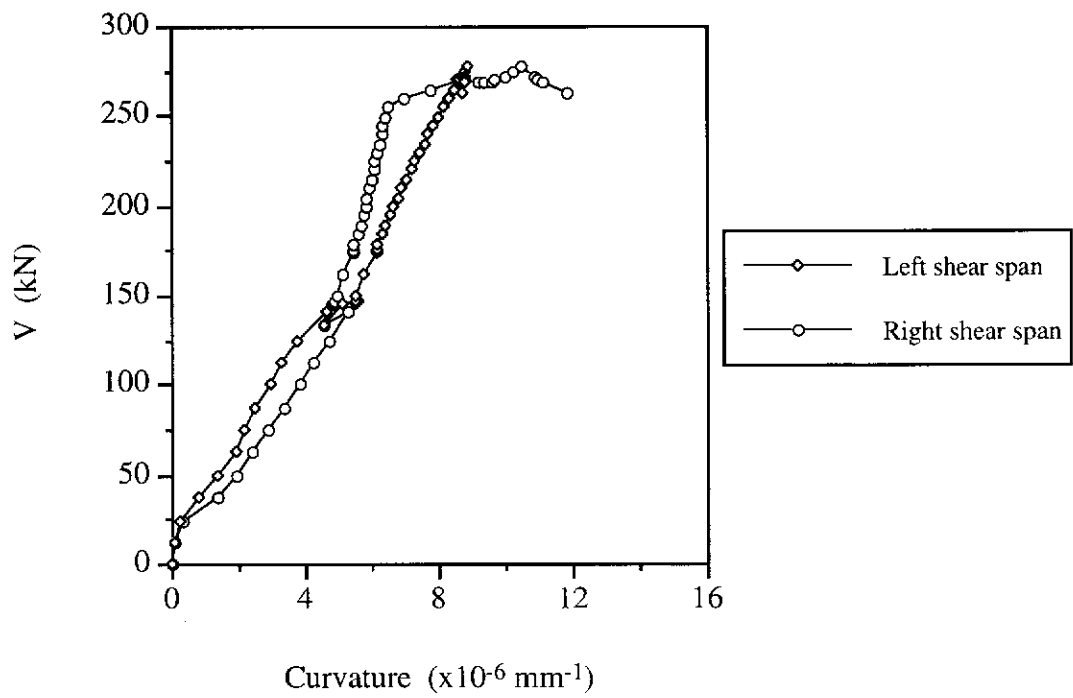
Figure D.4 Shear Force versus Curvature for Beam S1-4
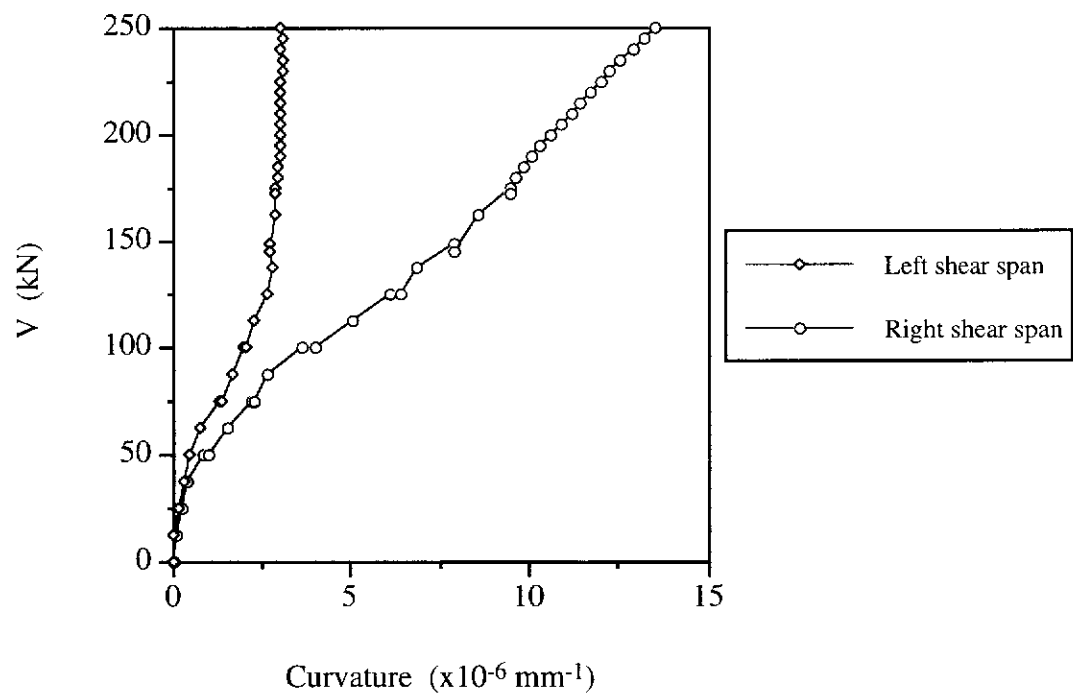
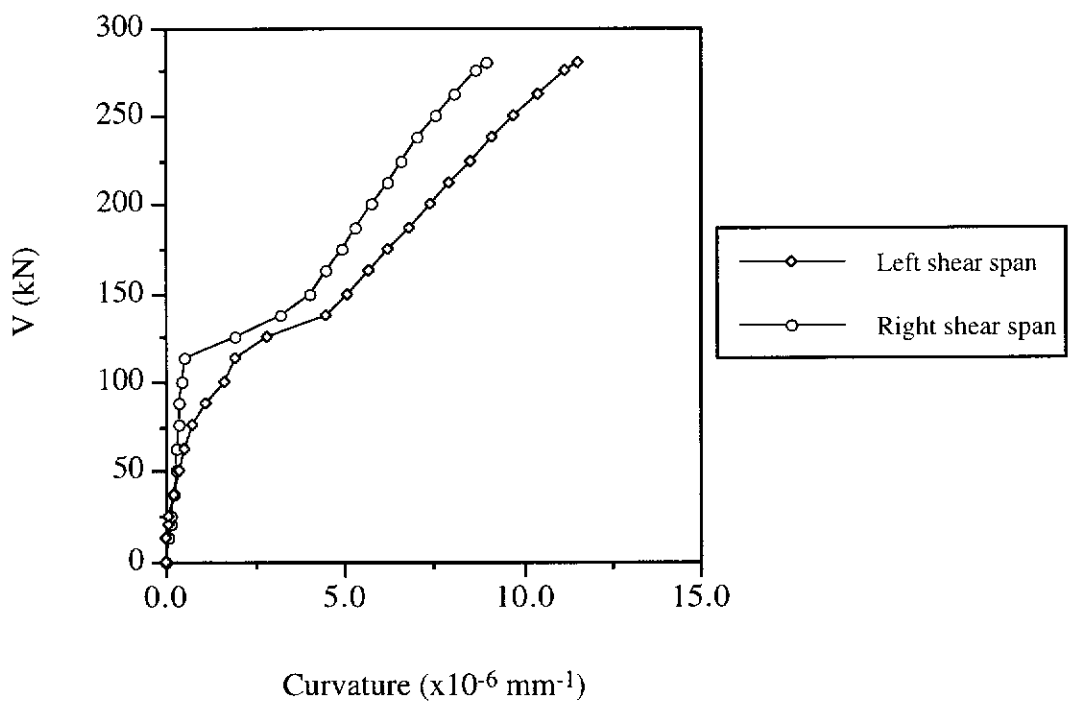**Figure D.5 Shear Force versus Curvature for Beam S1-5**
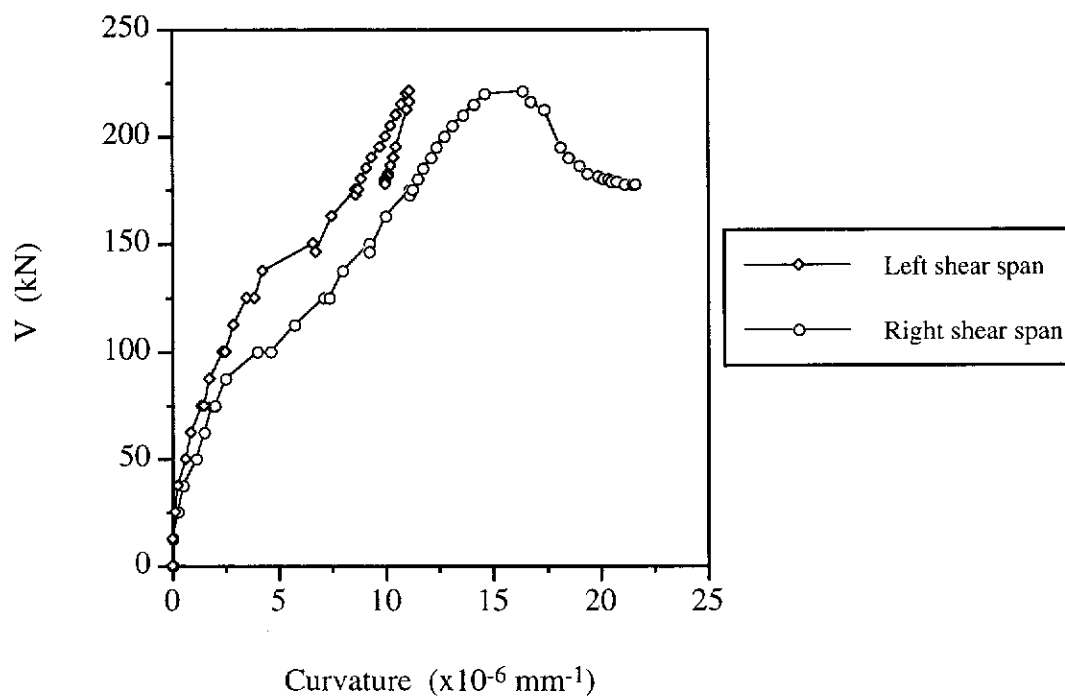
Figure D.6 Shear Force versus Curvature for Beam S1-6
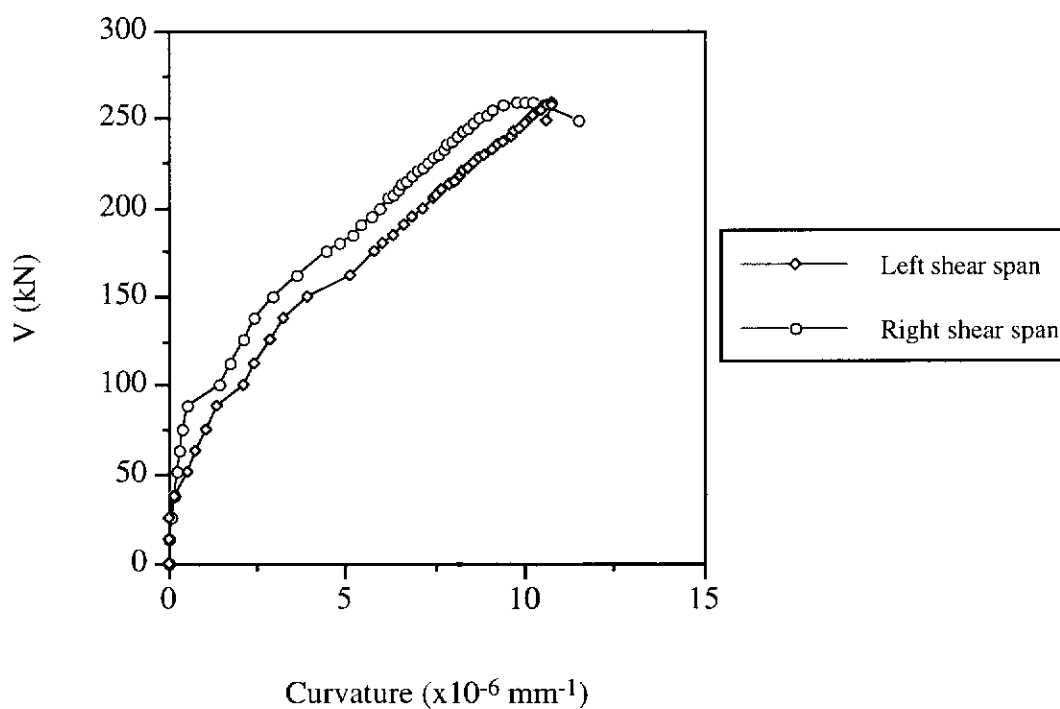
Figure D.7 Shear Force versus Curvature for Beam S2-1
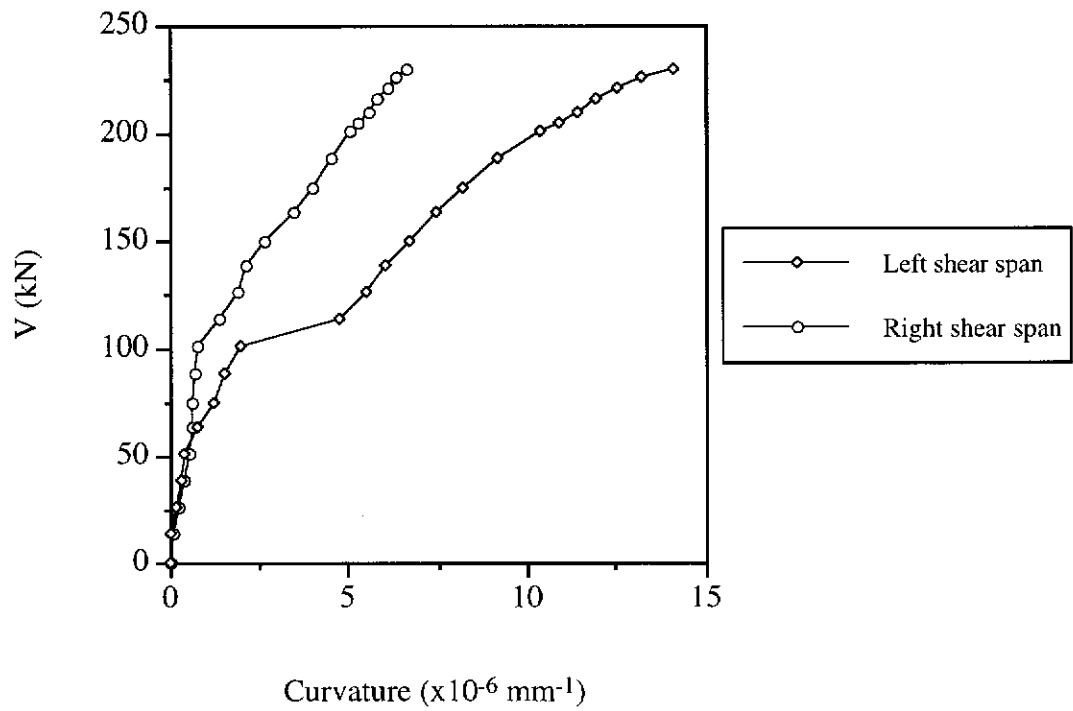
Figure D.8 Shear Force versus Curvature for Beam S2-2
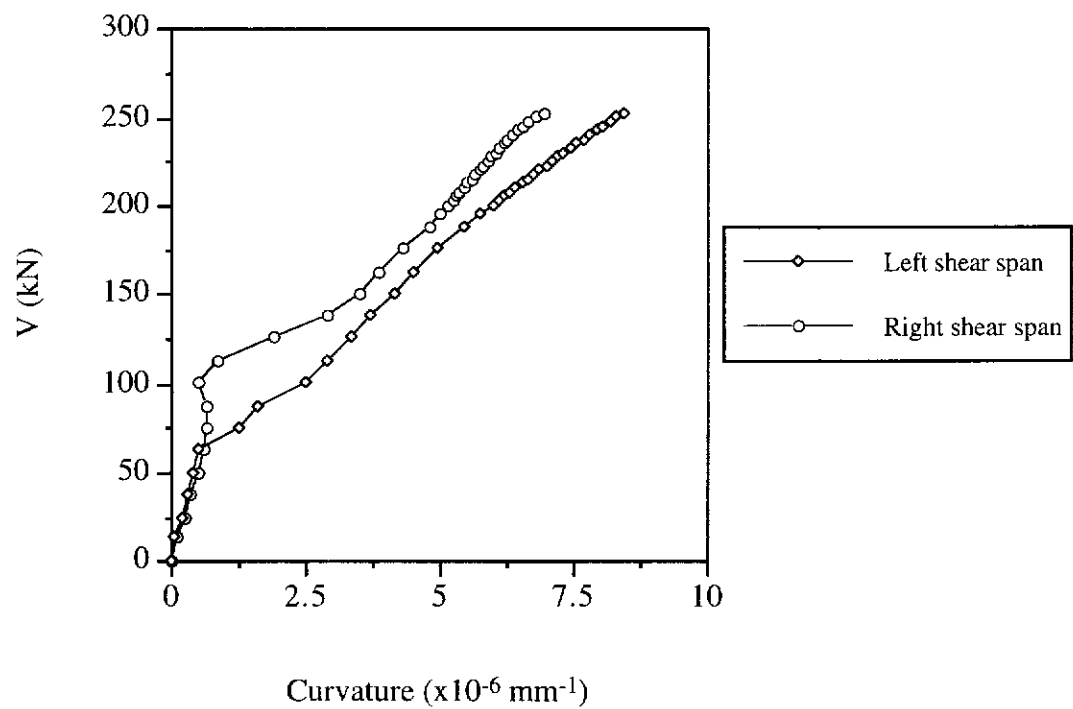
Figure D.9 Shear Force versus Curvature for Beam S2-3
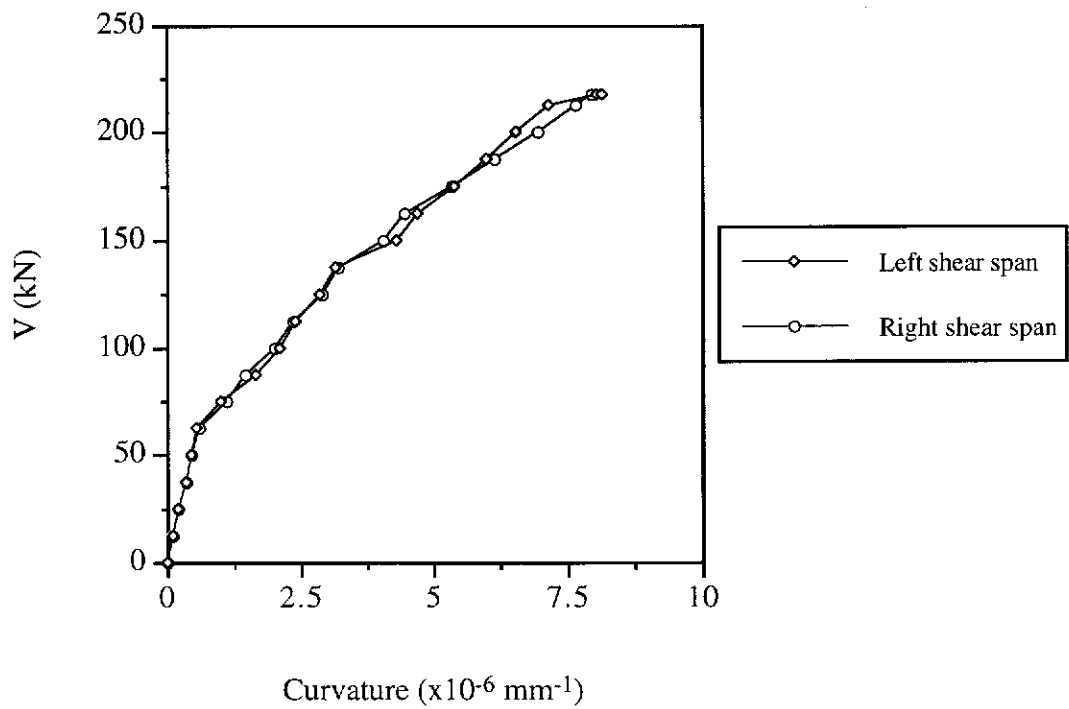
Figure D.10 Shear Force versus Curvature for Beam S2-4
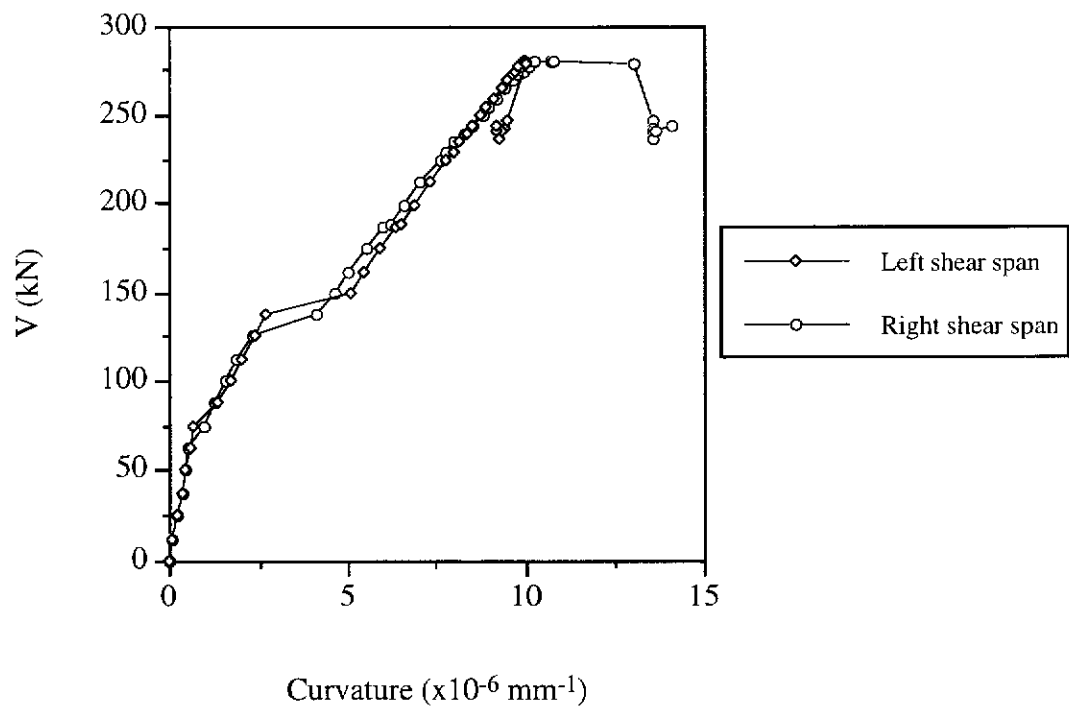
Figure D.11 Shear Force versus Curvature for Beam S2-5
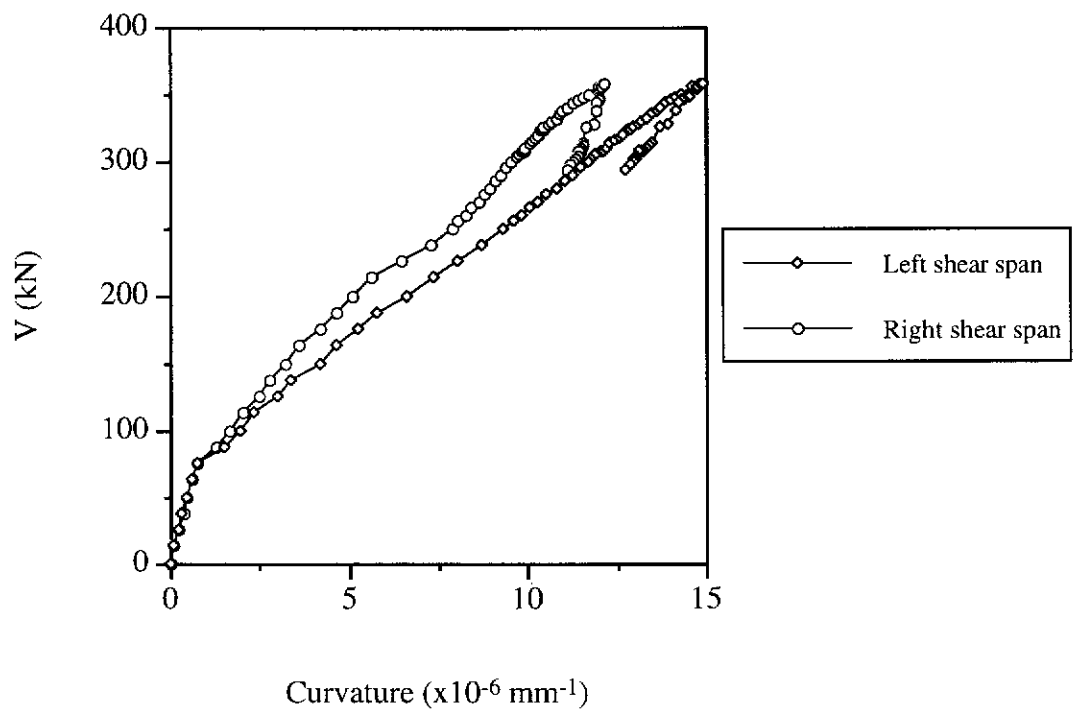
Figure D.12 Shear Force versus Curvature for Beam S2-6
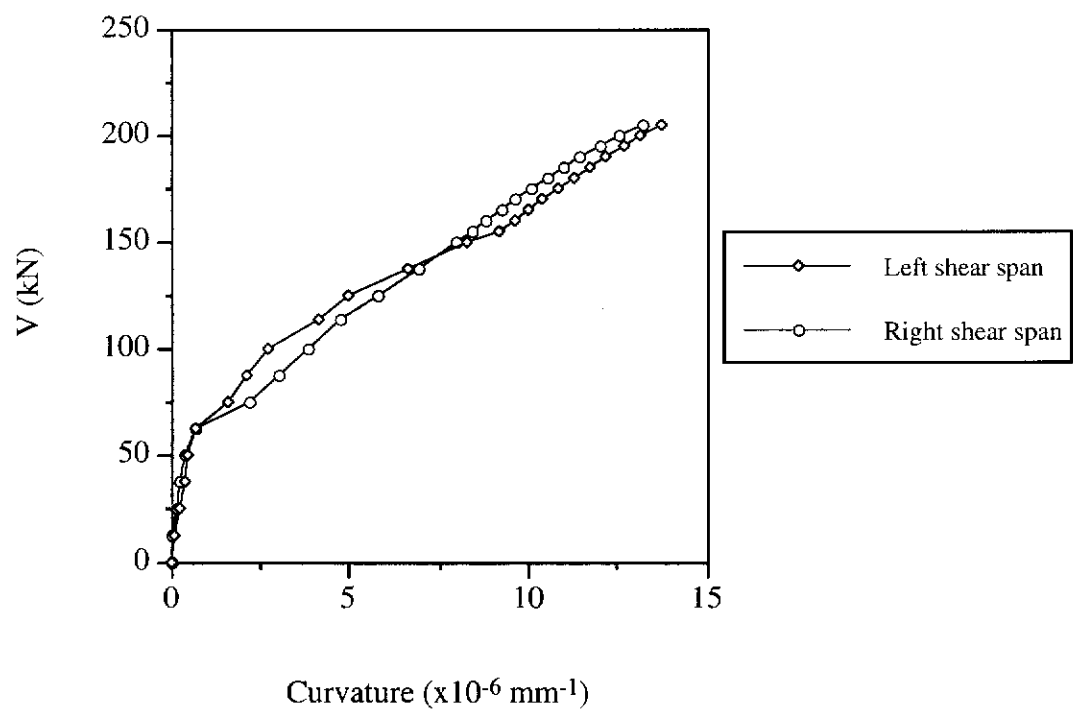
Figure D.13 Shear Force versus Curvature for Beam S3-1

D.7
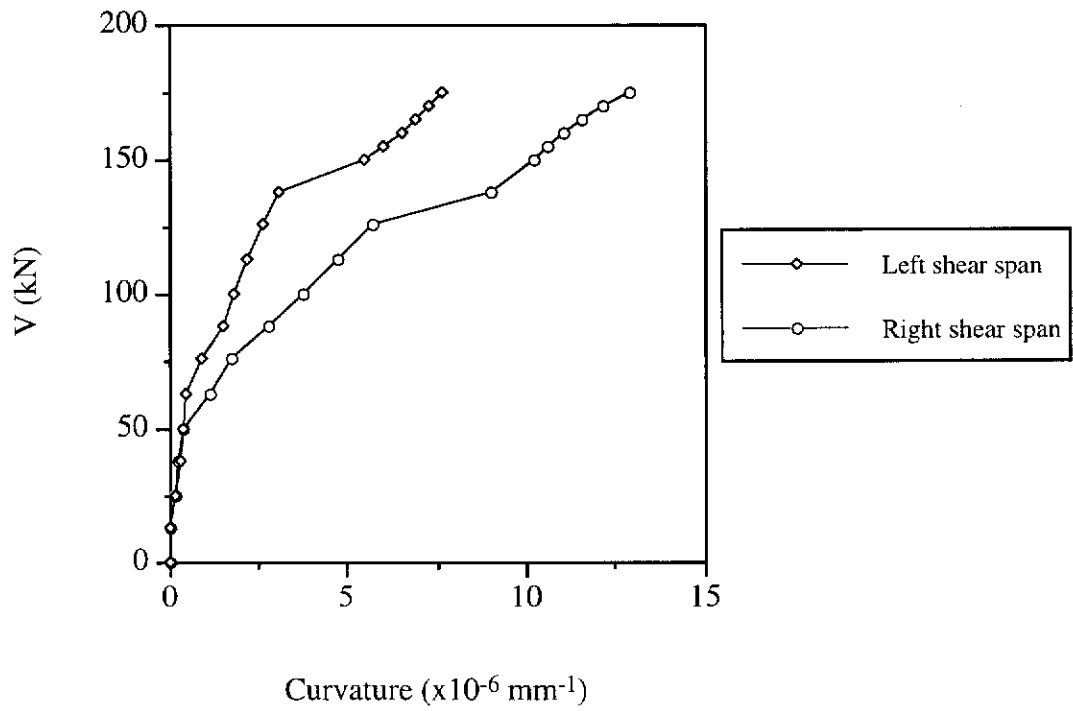
Figure D.14 Shear Force versus Curvature for Beam S3-2
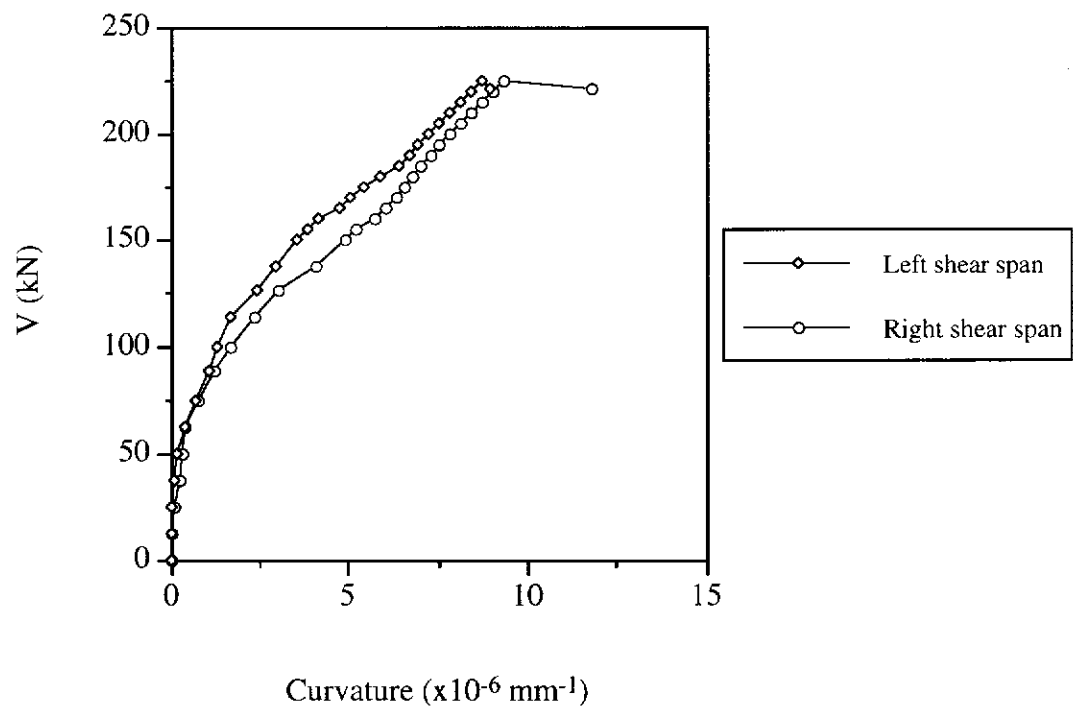
Figure D.15 Shear Force versus Curvature for Beam S3-3
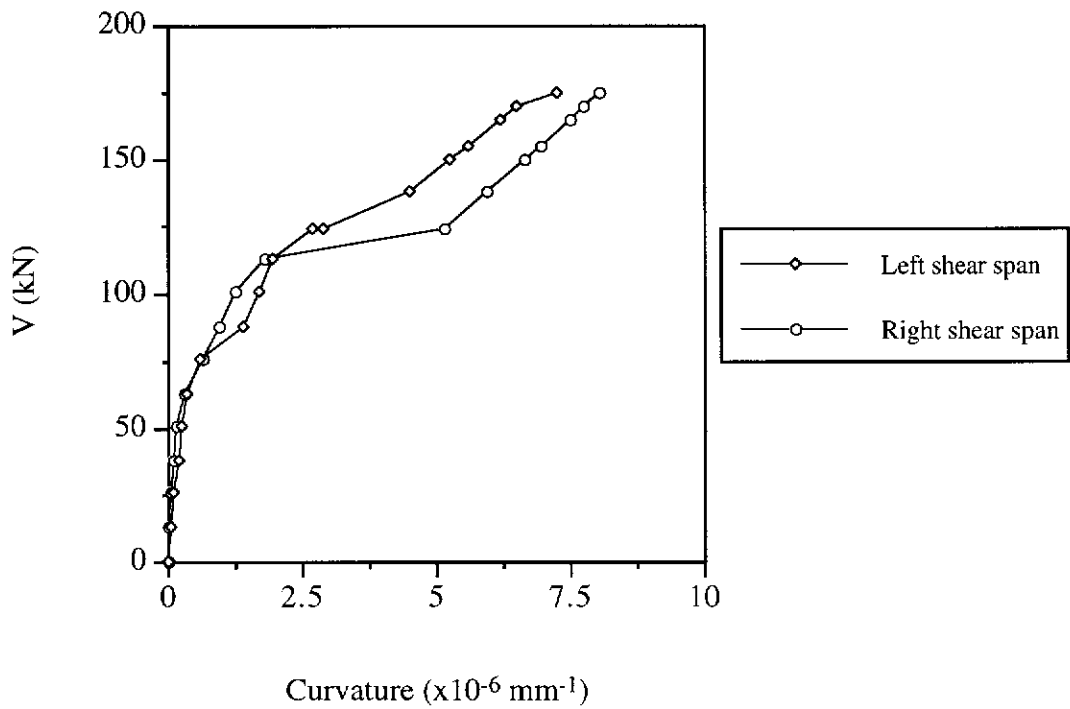
Figure D.16 Shear Force versus Curvature for Beam S3-4
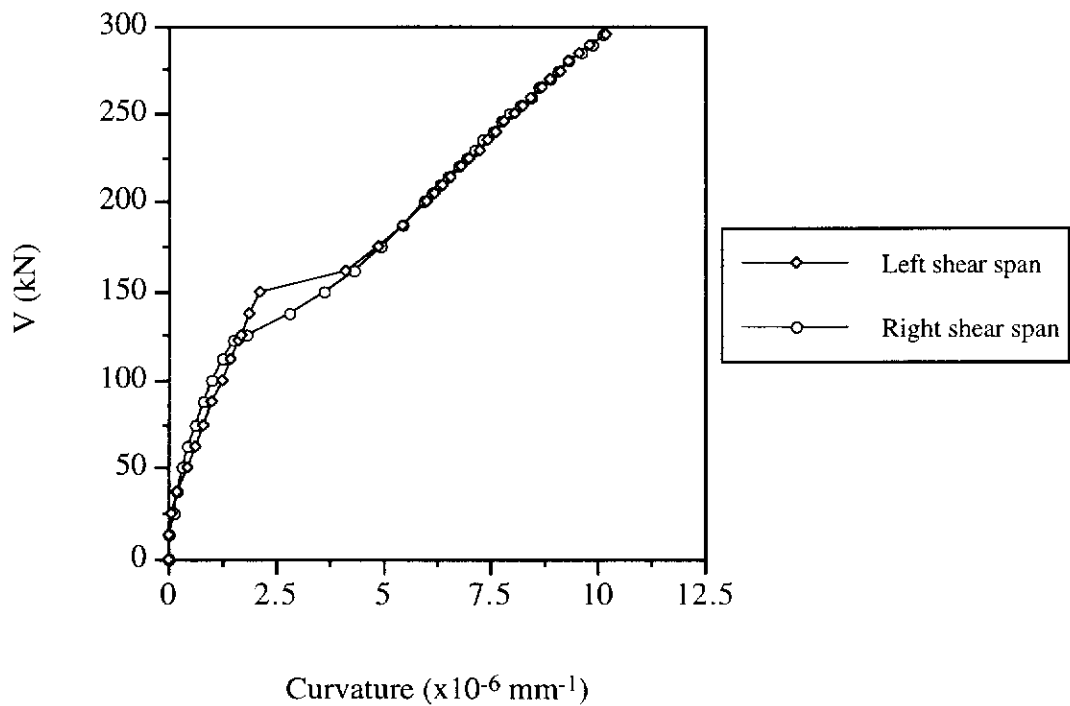
Figure D.17 Shear Force versus Curvature for Beam S3-5
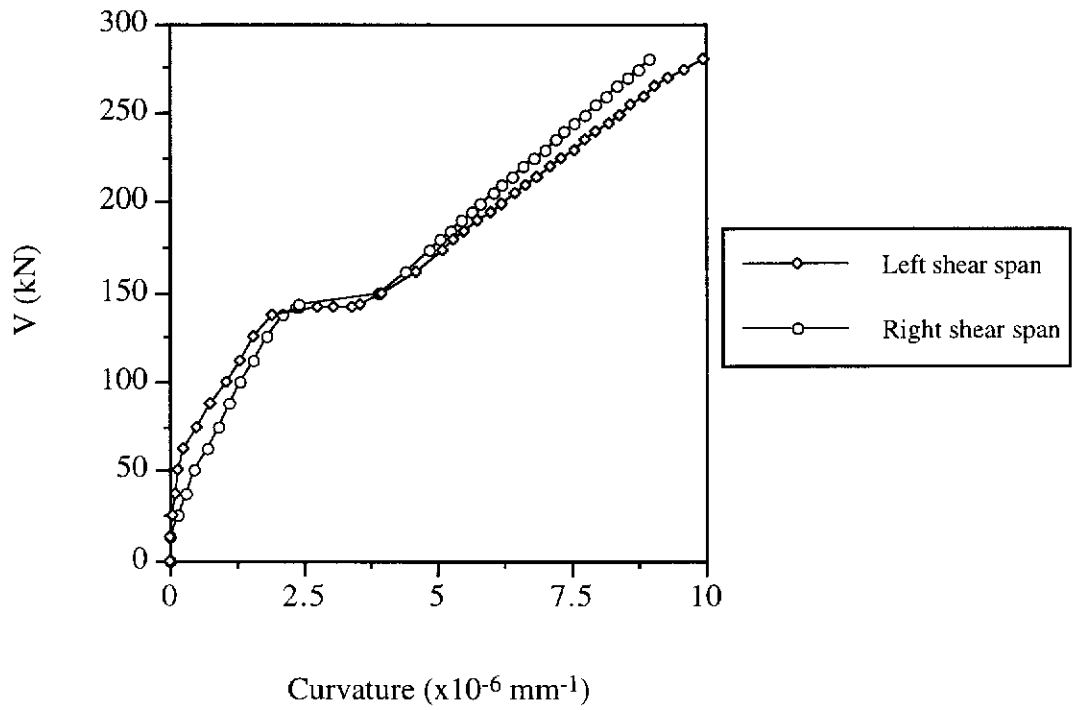
Figure D.18 Shear Force versus Curvature for Beam S3-6
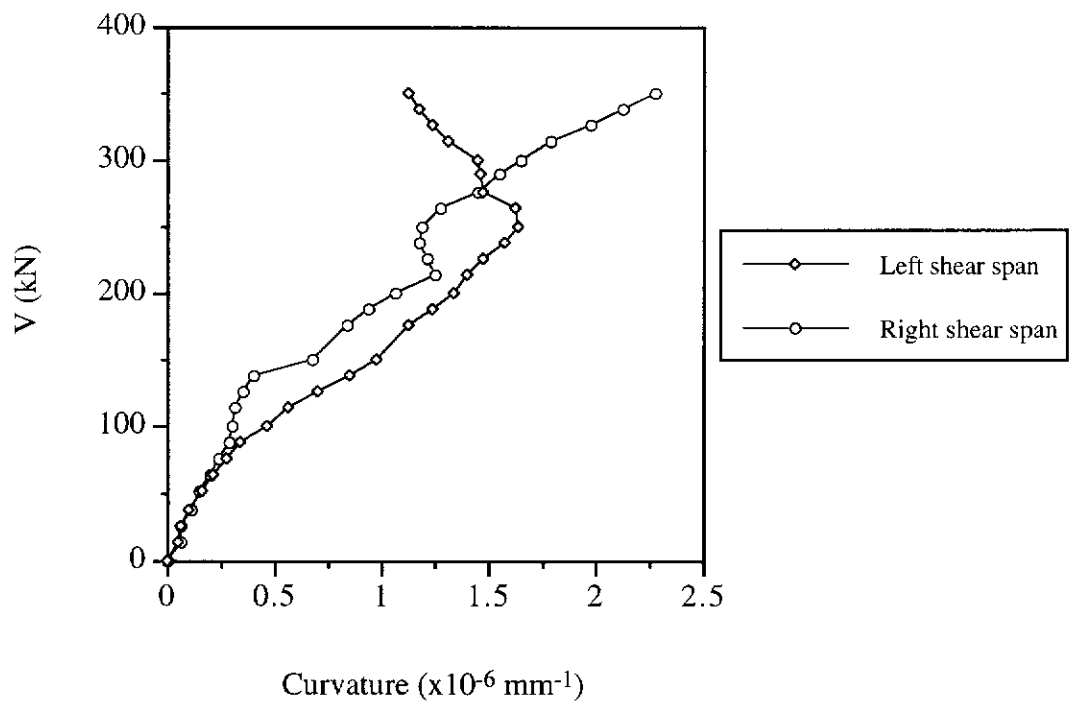
Figure D.19 Shear Force versus Curvature for Beam S4-1
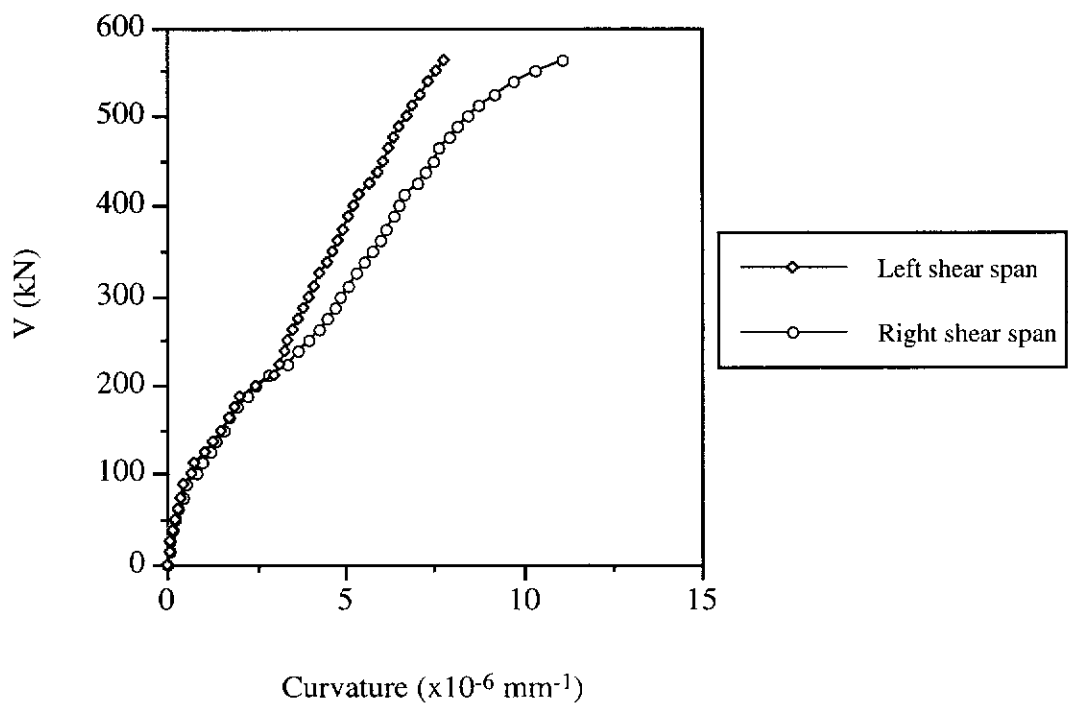
Figure D.20 Shear Force versus Curvature for Beam S4-2
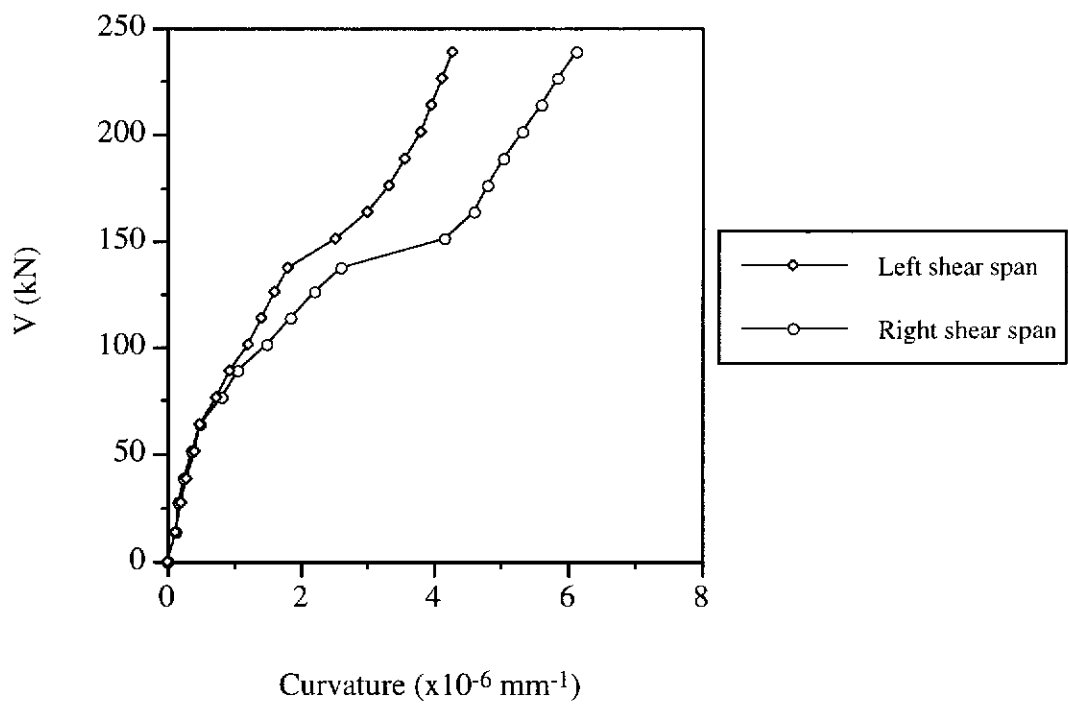
Figure D.21 Shear Force versus Curvature for Beam S4-3
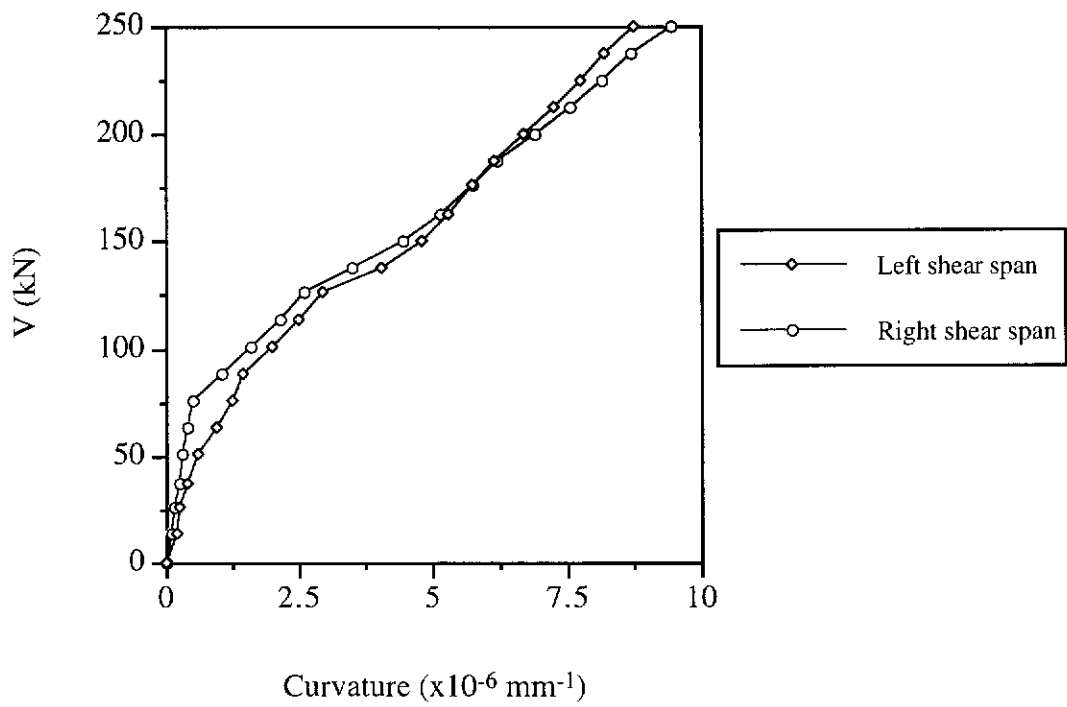
Figure D.22 Shear Force versus Curvature for Beam S4-4
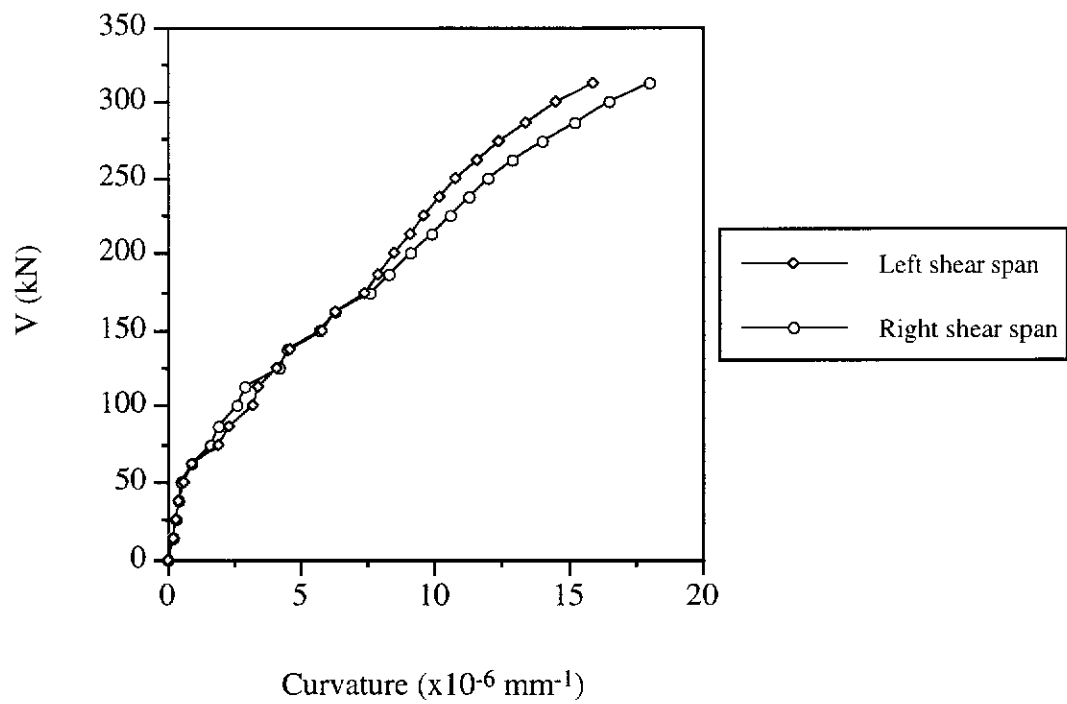
Figure D.23 Shear Force versus Curvature for Beam S4-5
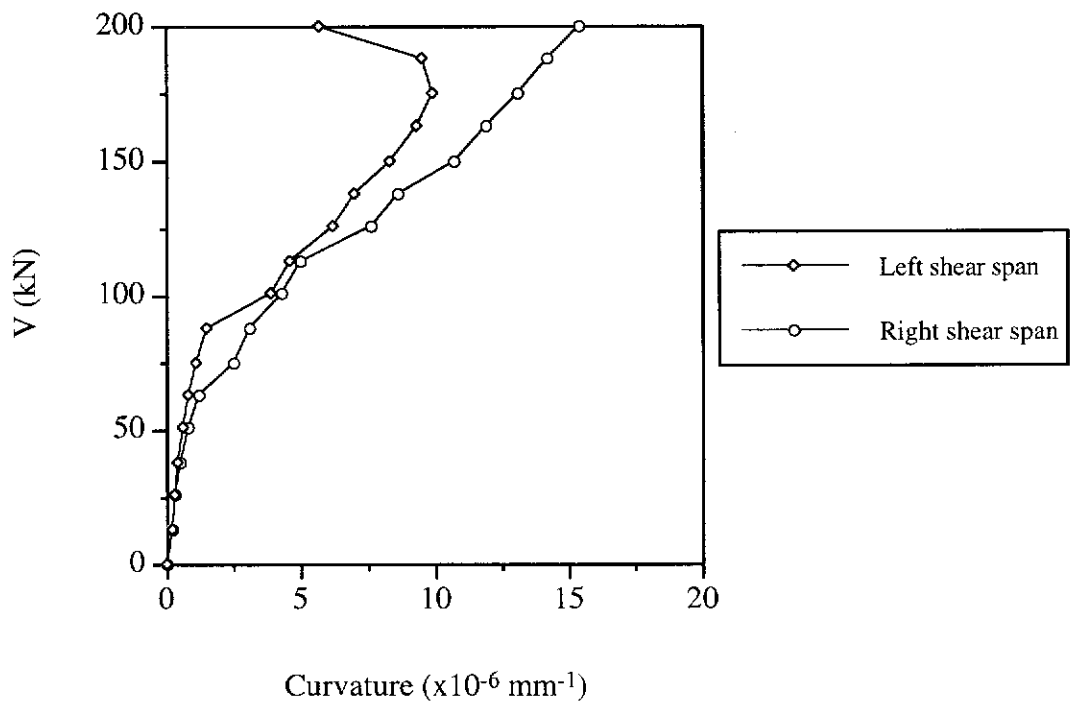
Figure D.24 Shear Force versus Curvature for Beam S4-6
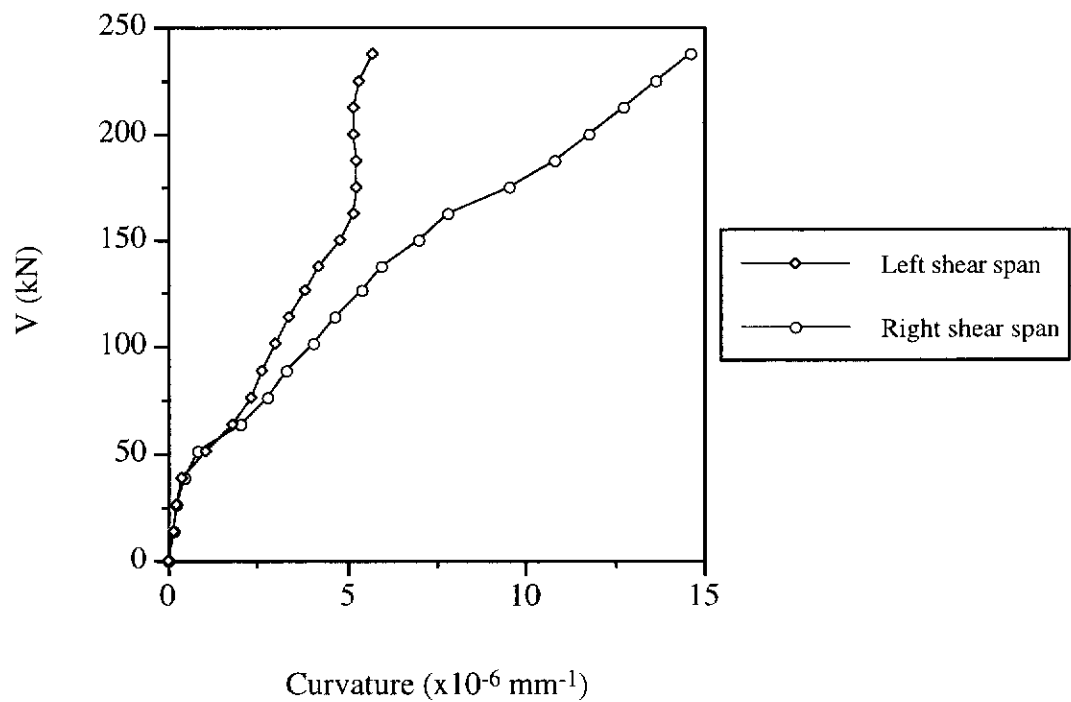
Figure D.25 Shear Force versus Curvature for Beam S5-1
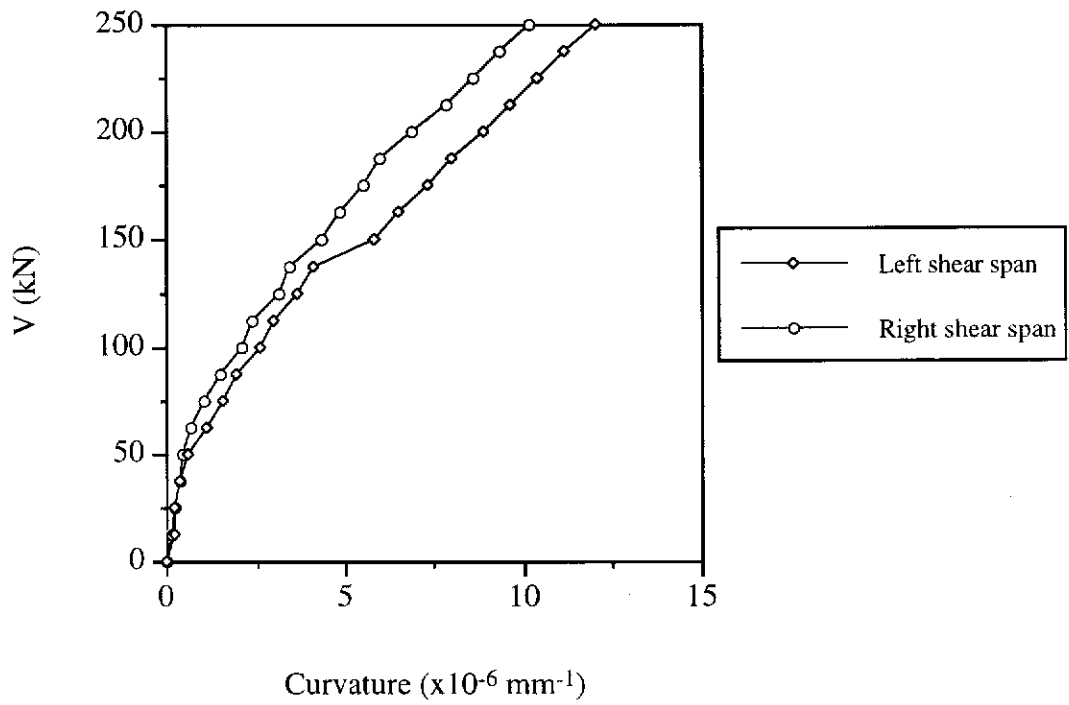
Figure D.26 Shear Force versus Curvature for Beam S5-2
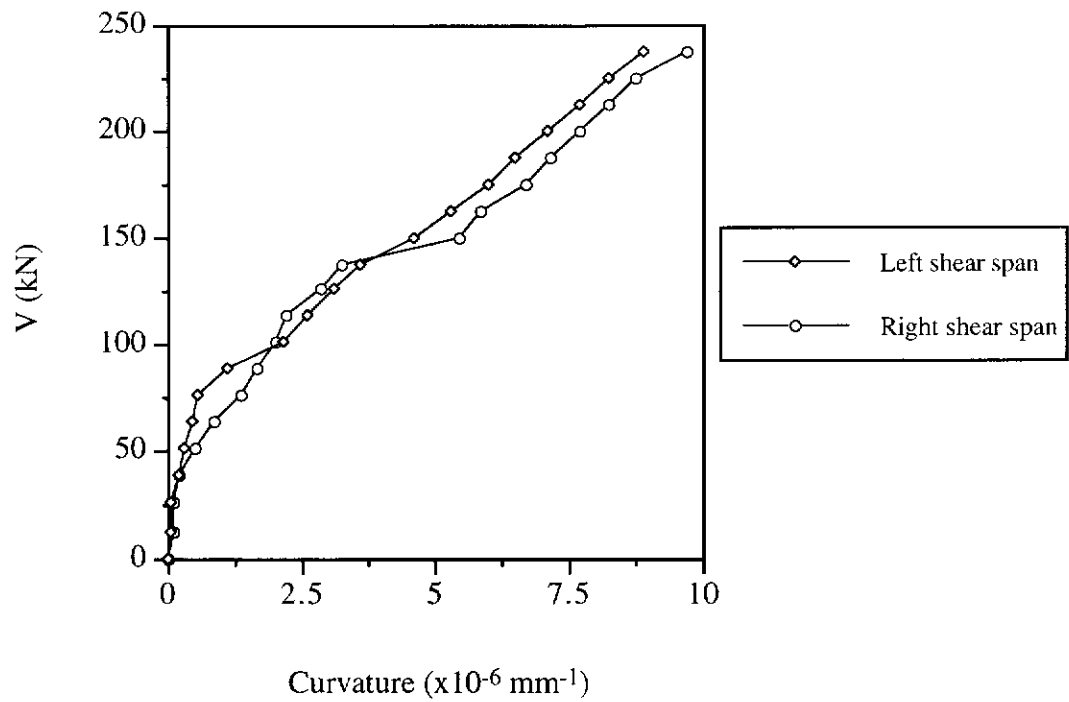
Figure D.27 Shear Force versus Curvature for Beam S5-3

D.14
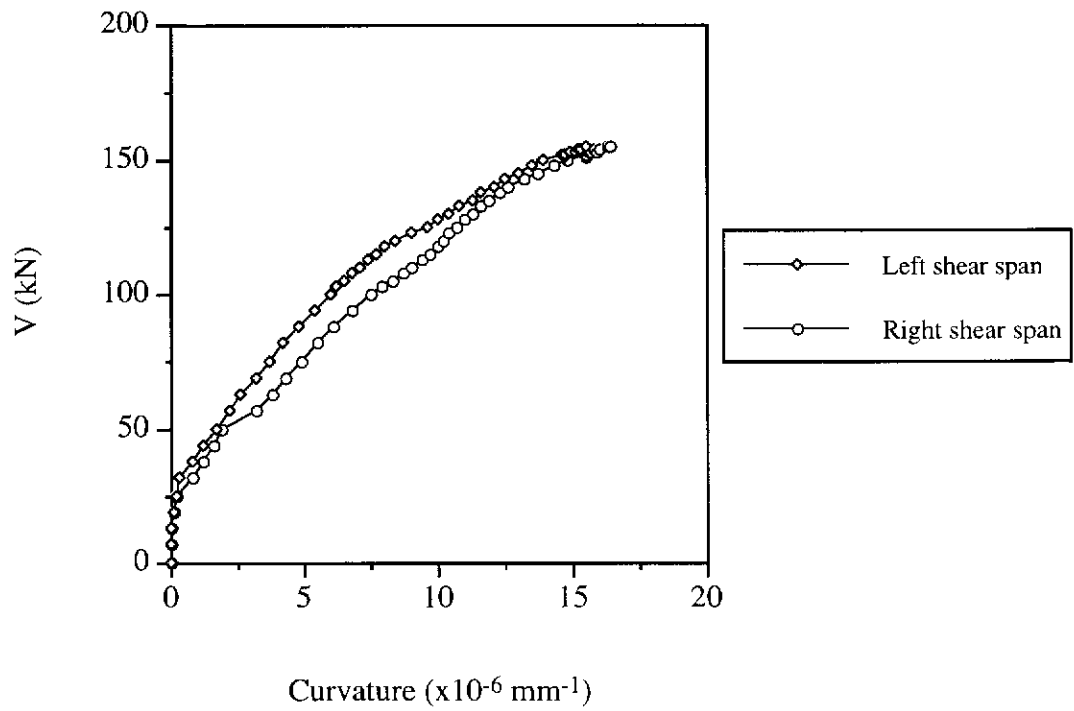
Figure D.28 Shear Force versus Curvature for Beam S6-1
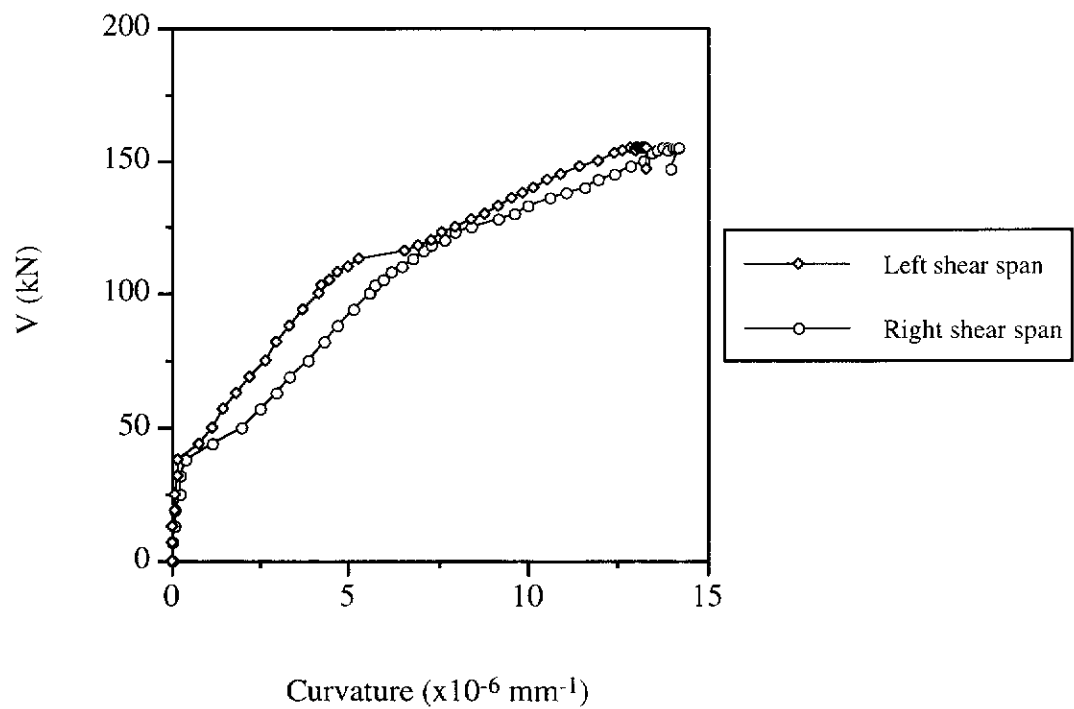
Figure D.29 Shear Force versus Curvature for Beam S6-2
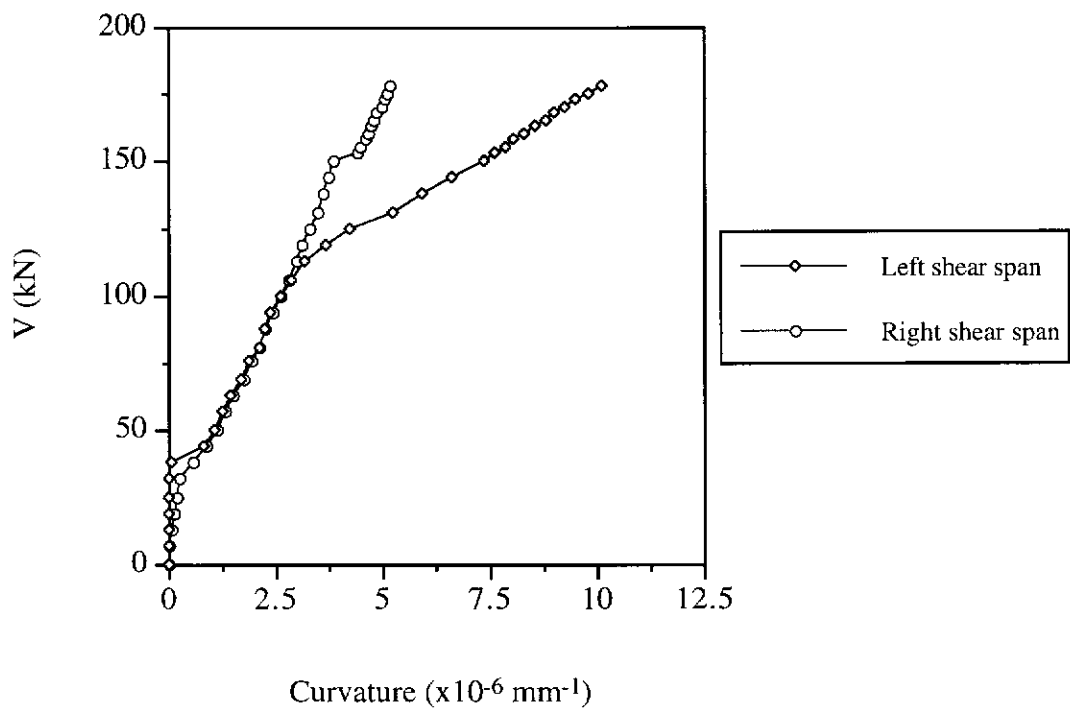
Figure D.30 Shear Force versus Curvature for Beam S6-3
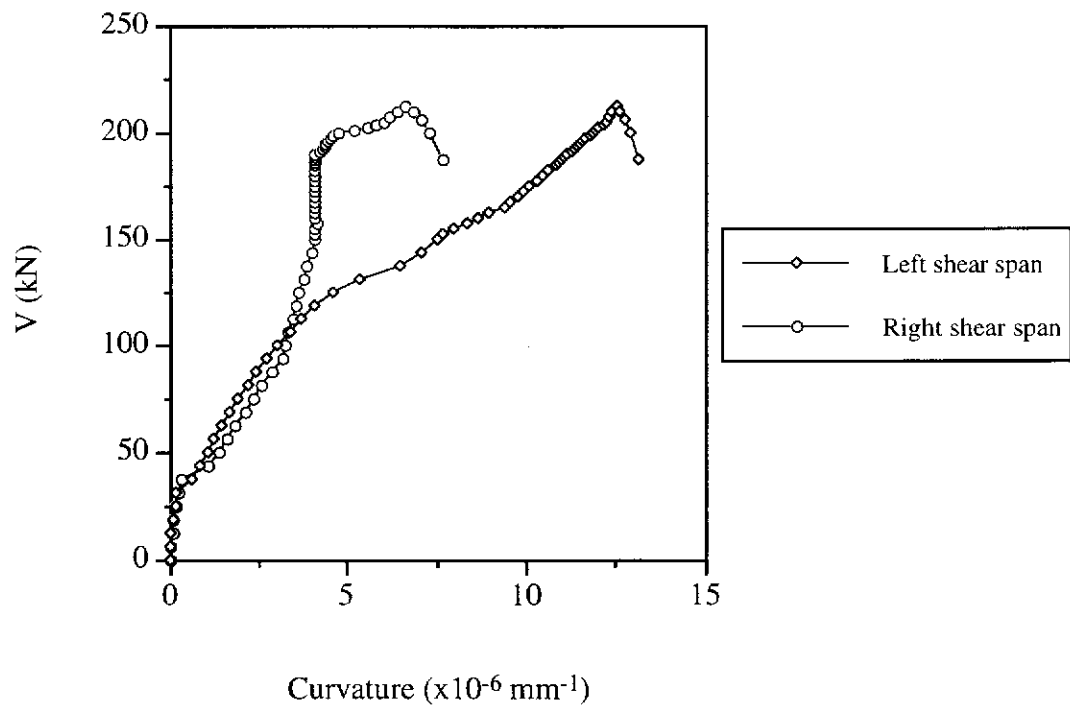
Figure D.31 Shear Force versus Curvature for Beam S6-4
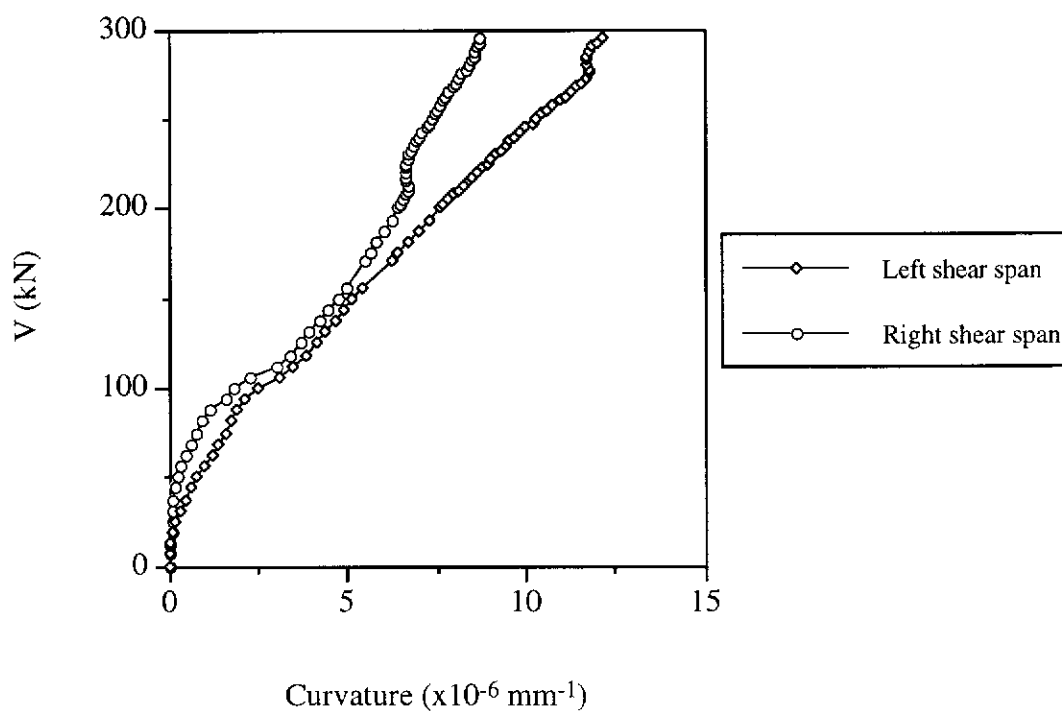
Figure D.32 Shear Force versus Curvature for Beam S6-5
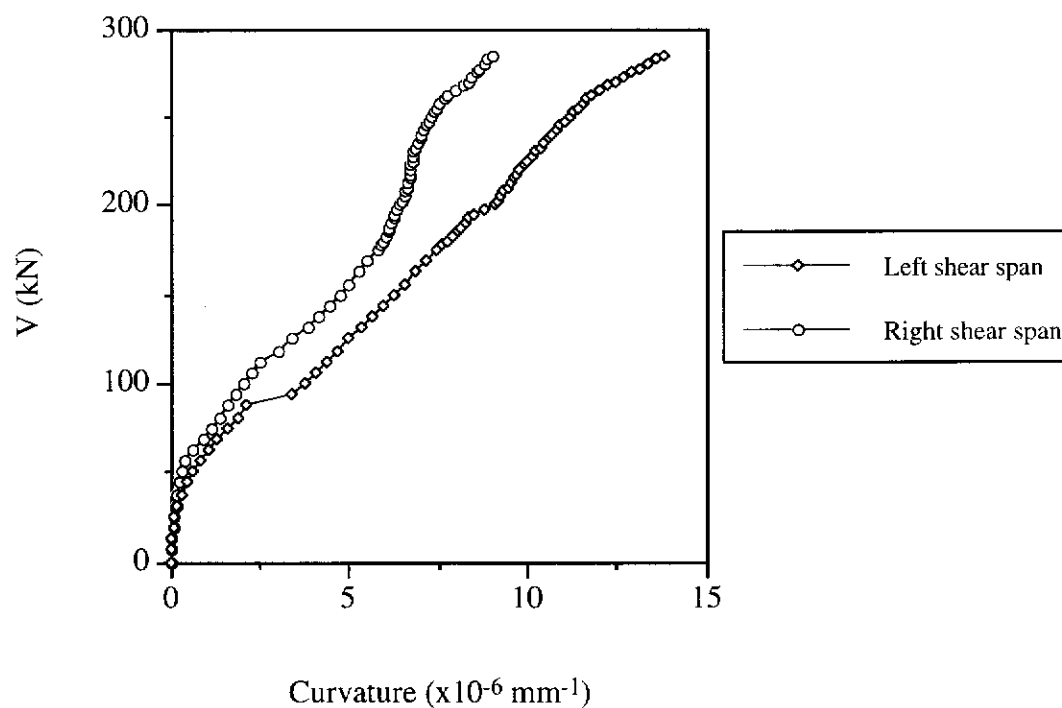
Figure D.33 Shear Force versus Curvature for Beam S6-6
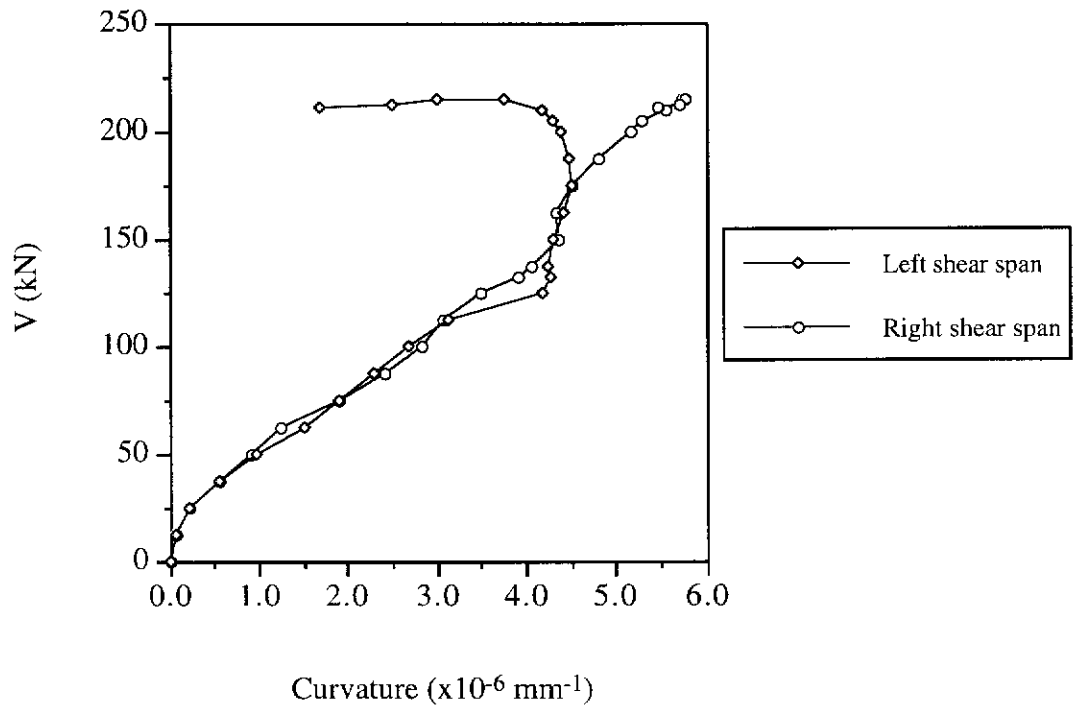
Figure D.34 Shear Force versus Curvature for Beam S7-1
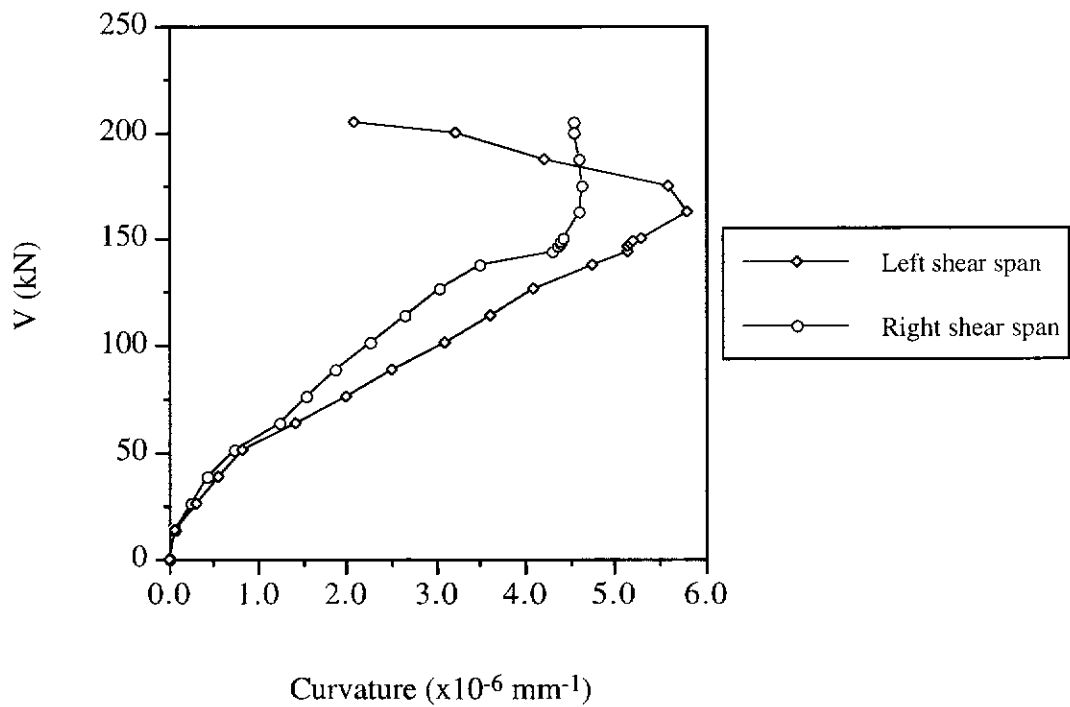
Figure D.35 Shear Force versus Curvature for Beam S7-2
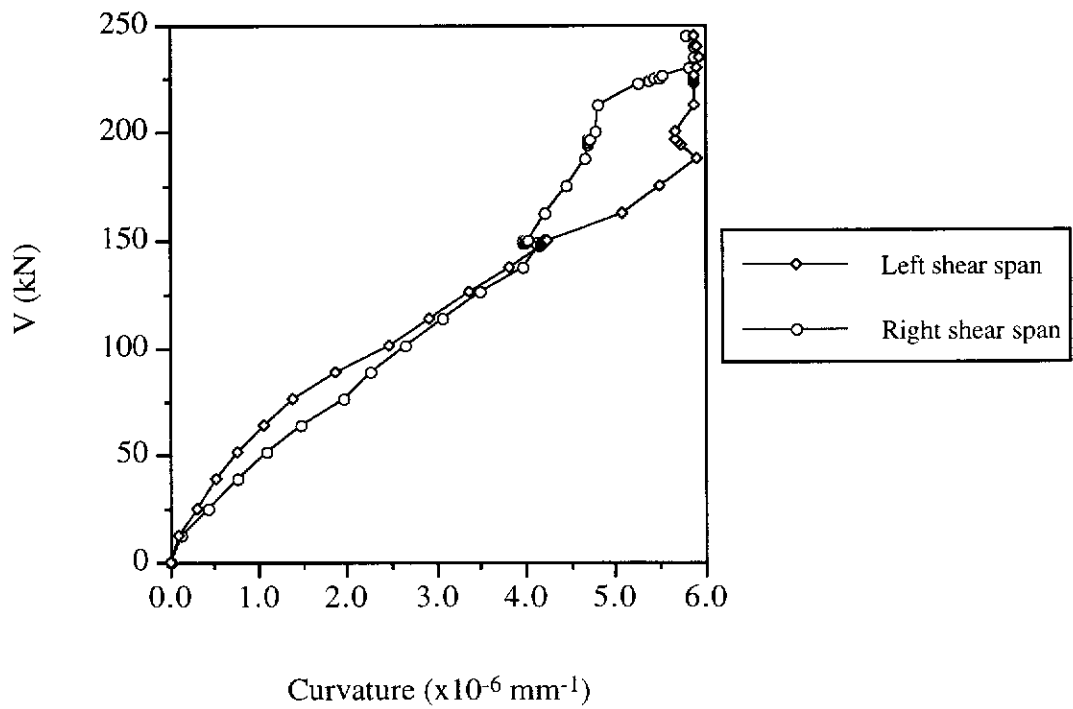
Figure D.36 Shear Force versus Curvature for Beam S7-3
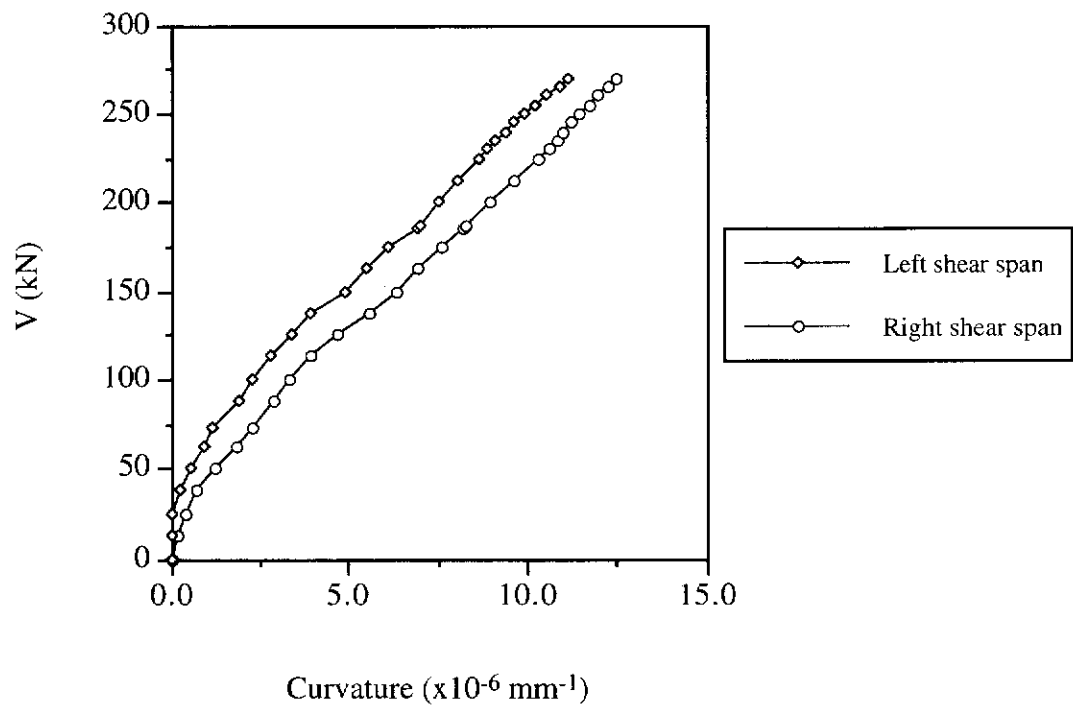
Figure D.37 Shear Force versus Curvature for Beam S7-4
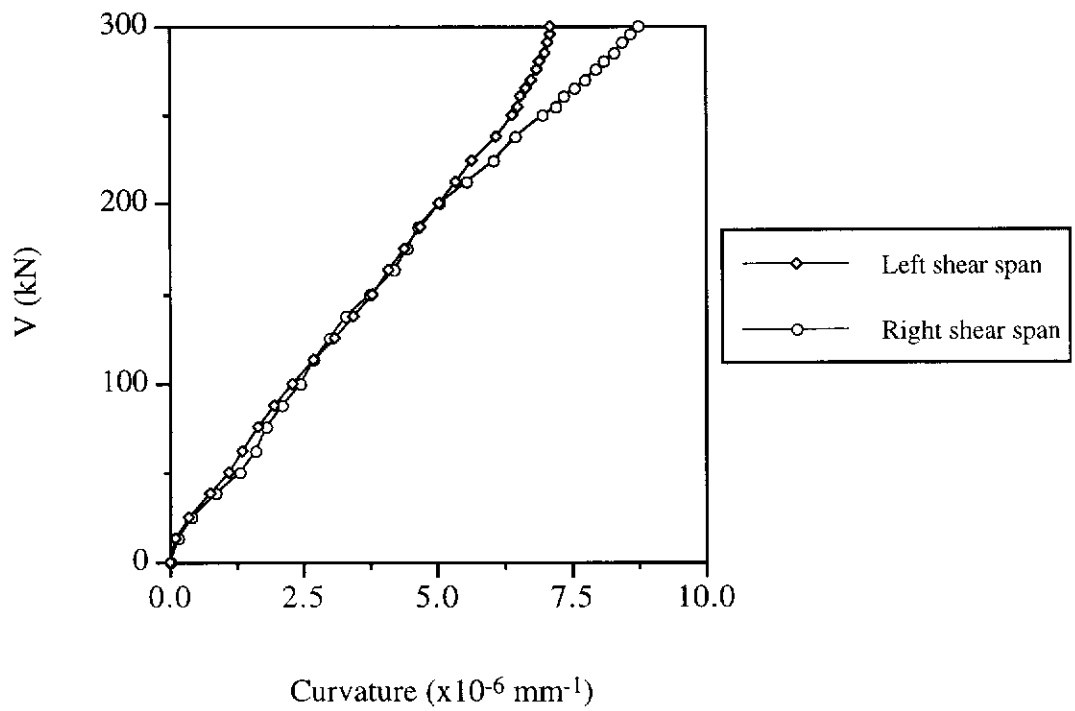
Figure D.38 Shear Force versus Curvature for Beam S7-5
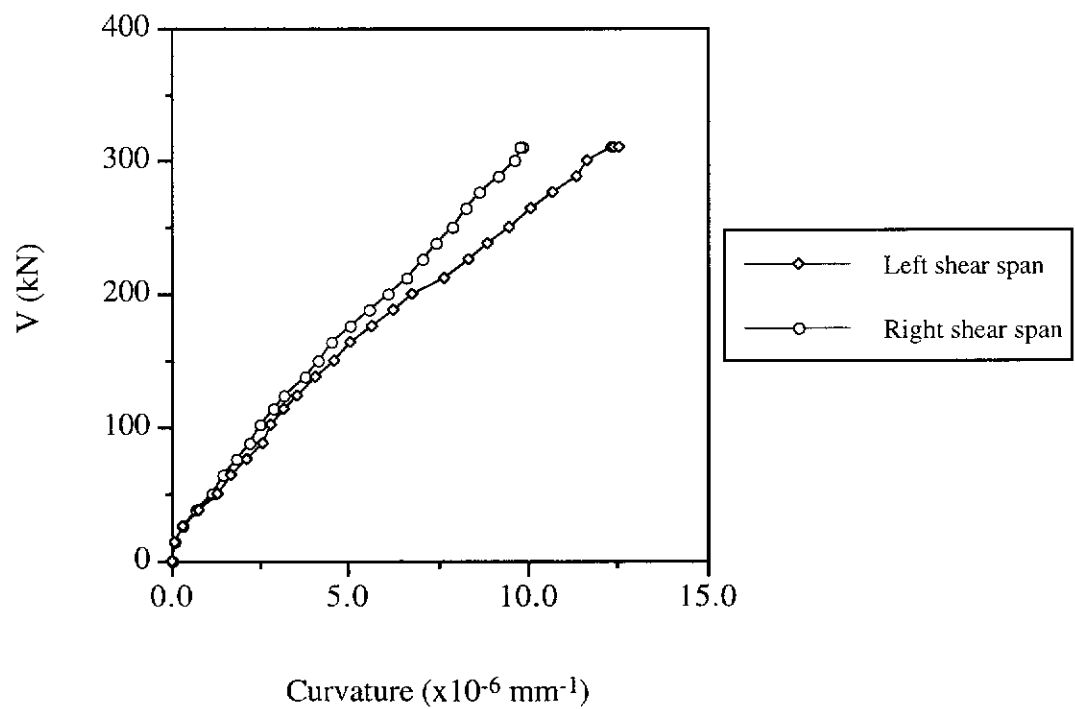
Figure D.39 Shear Force versus Curvature for Beam S7-6
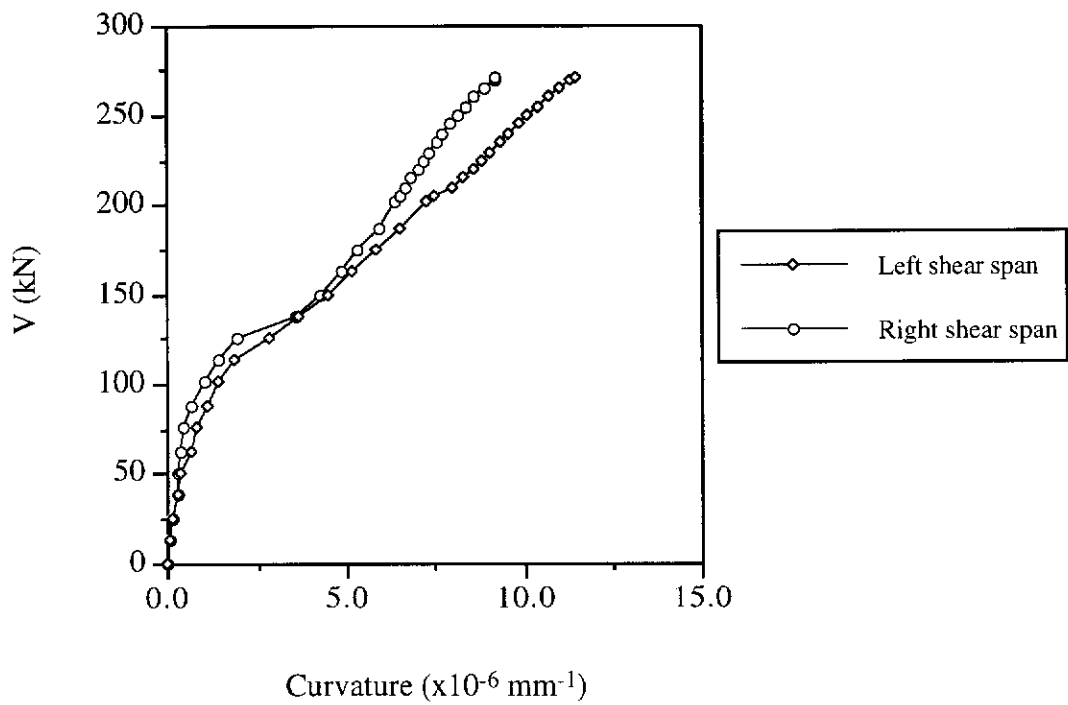
Figure D.40 Shear Force versus Curvature for Beam S8-1
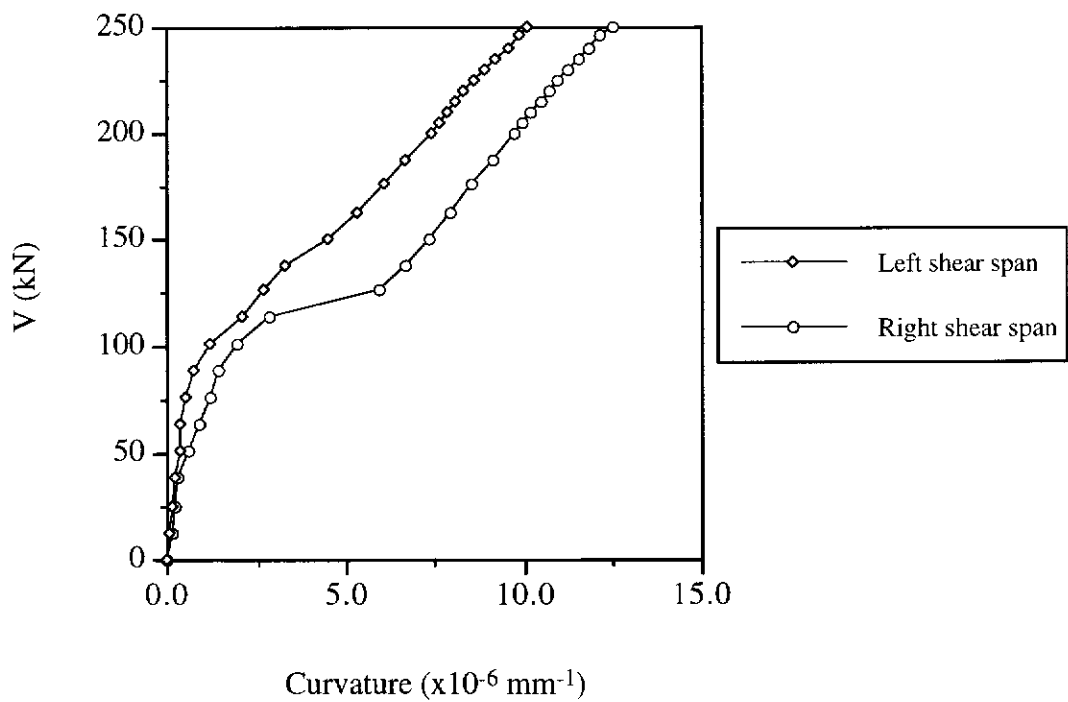
Figure D.41 Shear Force versus Curvature for Beam S8-2
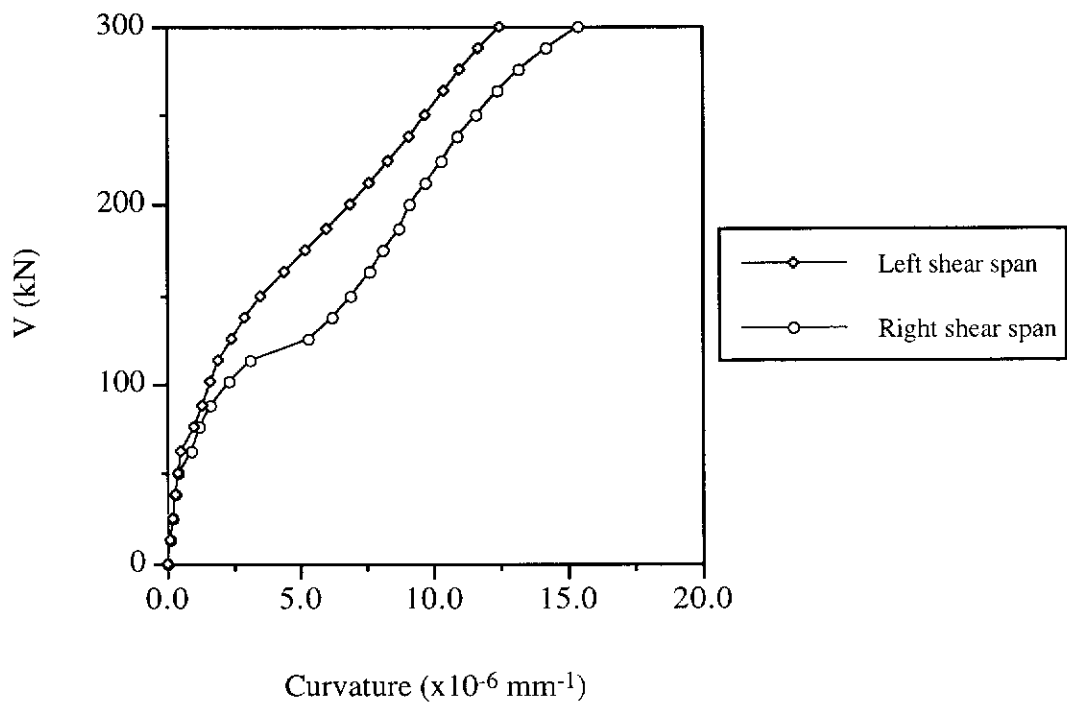
Figure D.42 Shear Force versus Curvature for Beam S8-3
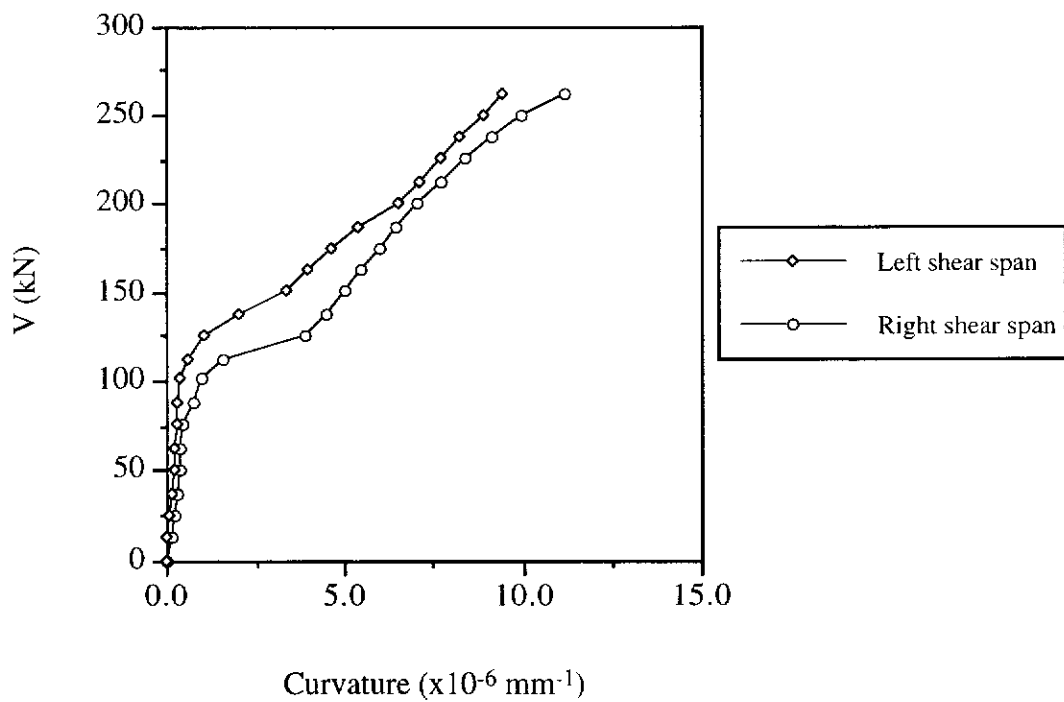
Figure D.43 Shear Force versus Curvature for Beam S8-4
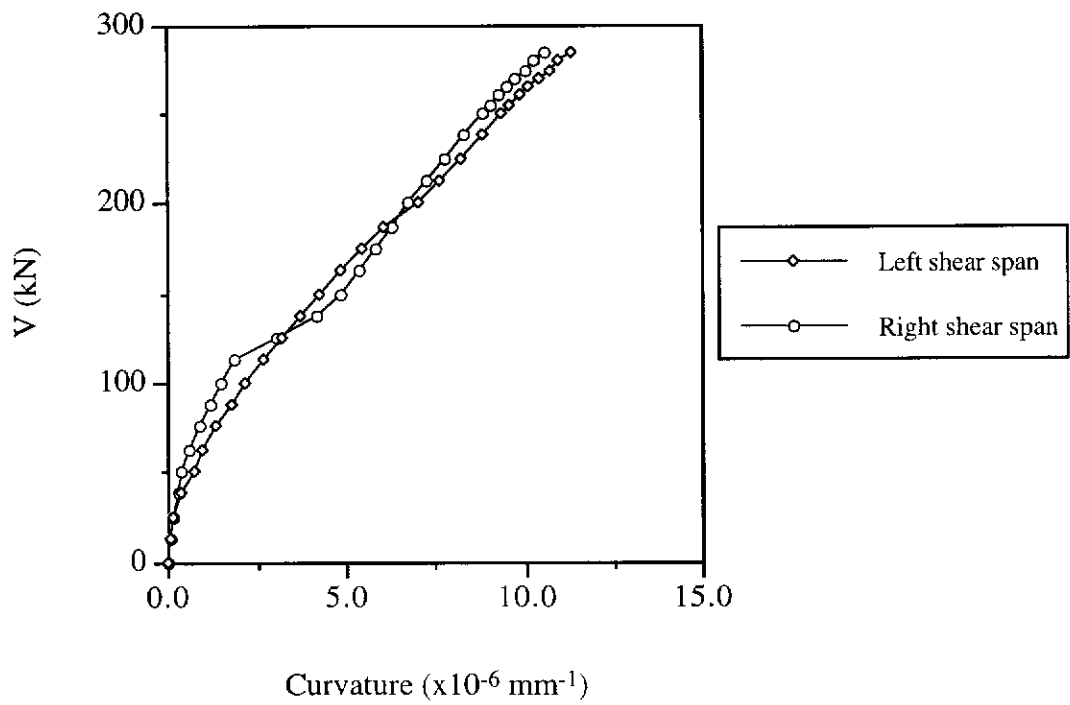
Figure D.44 Shear Force versus Curvature for Beam S8-5

Figure D.45 Shear Force versus Curvature for Beam S8-6

Strains In Longitudinal Tensile Steel Bars

The following are shear force versus tensile steel strain curves for test beams of the present study.
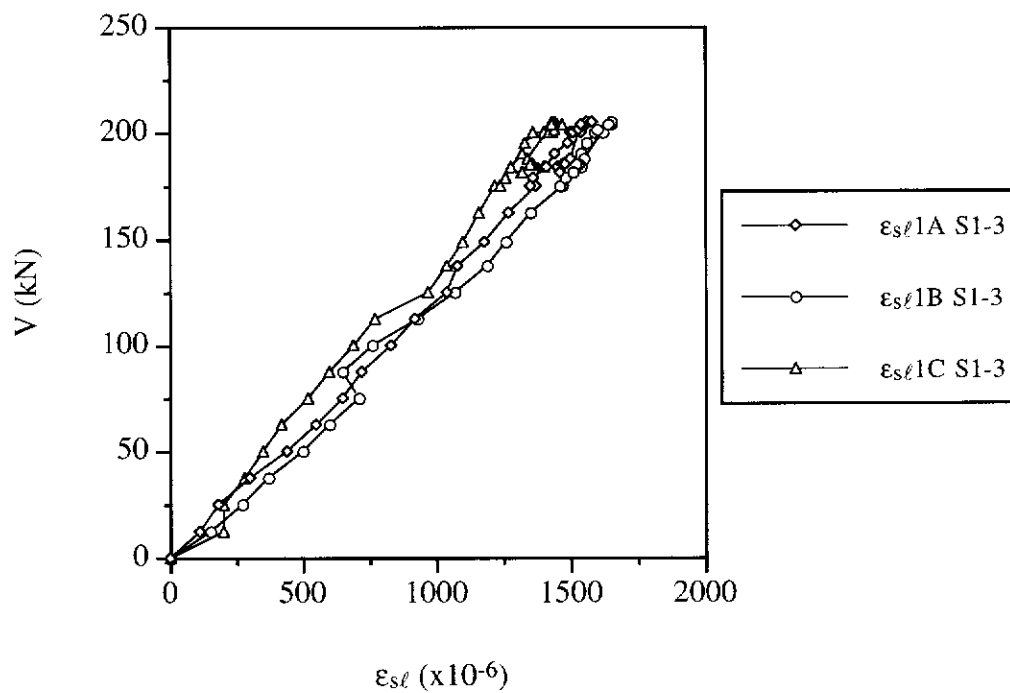
Figure E.1 Shear Force versus Tensile Steel Strains for Beam S1-3
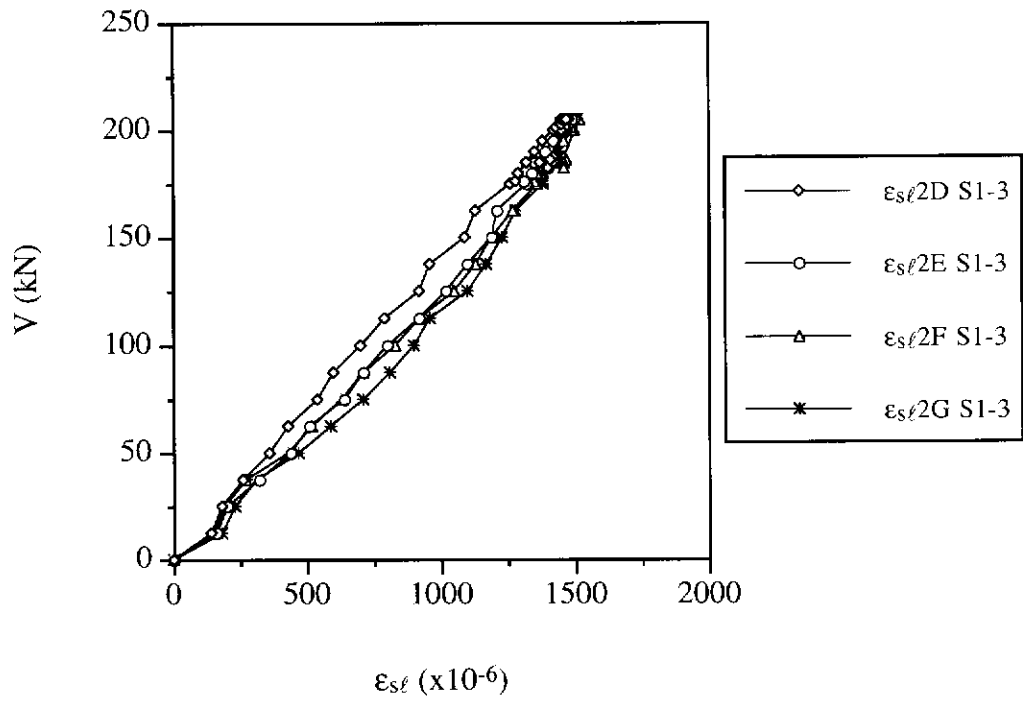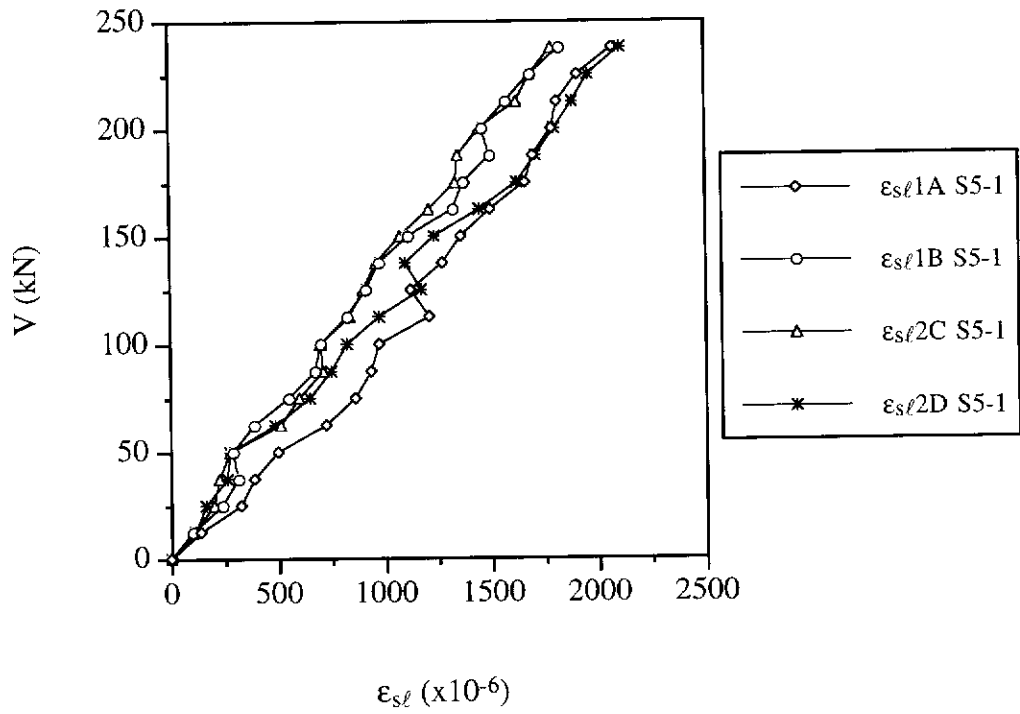
Figure E.2 Shear Force versus Tensile Steel Strains for Beam S1-3
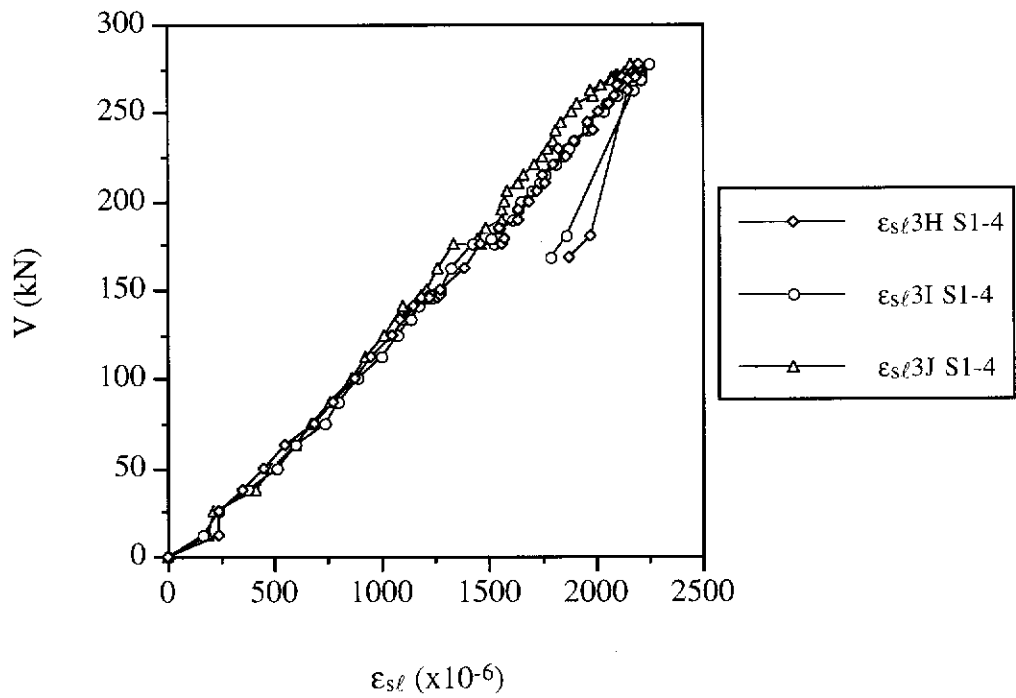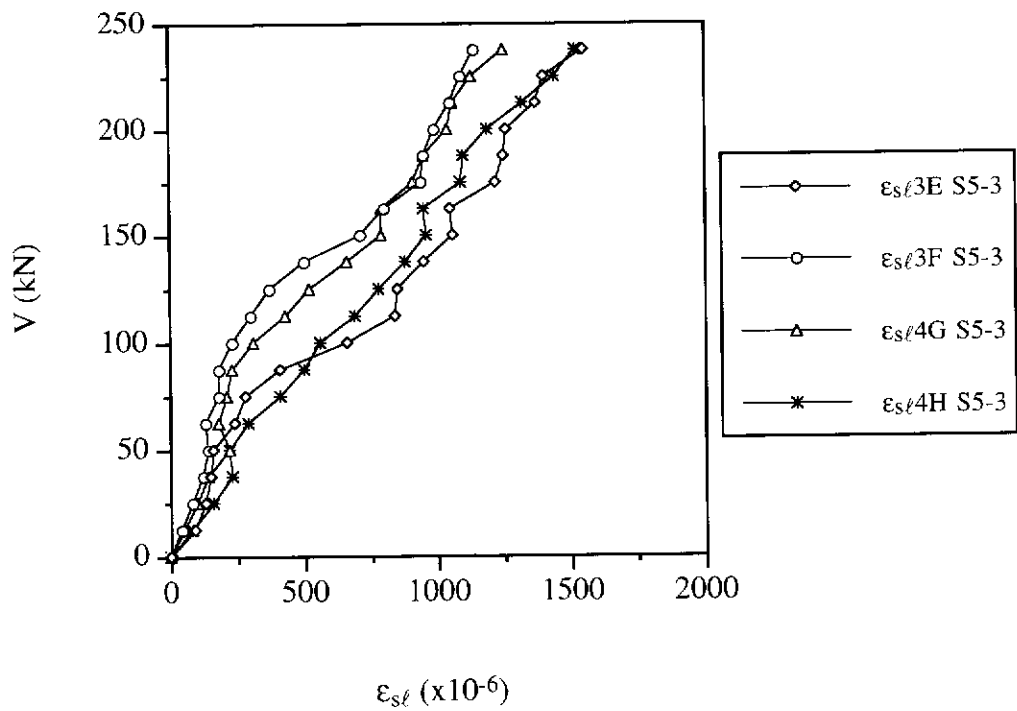

Figure E.3 Shear Force versus Tensile Steel Strains for Beam S1-4
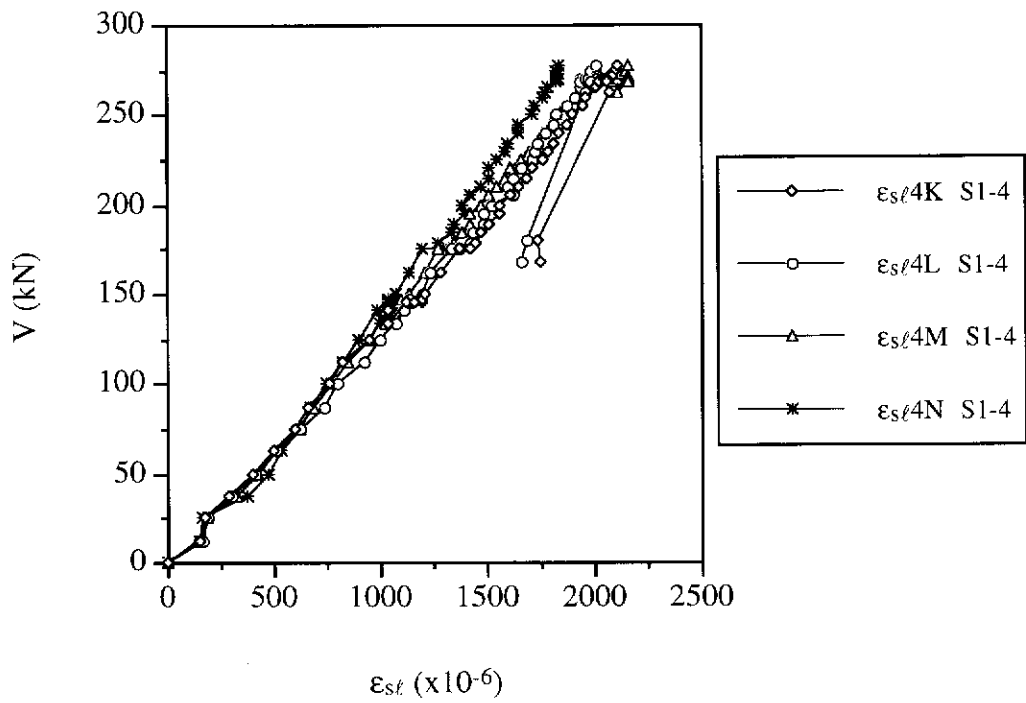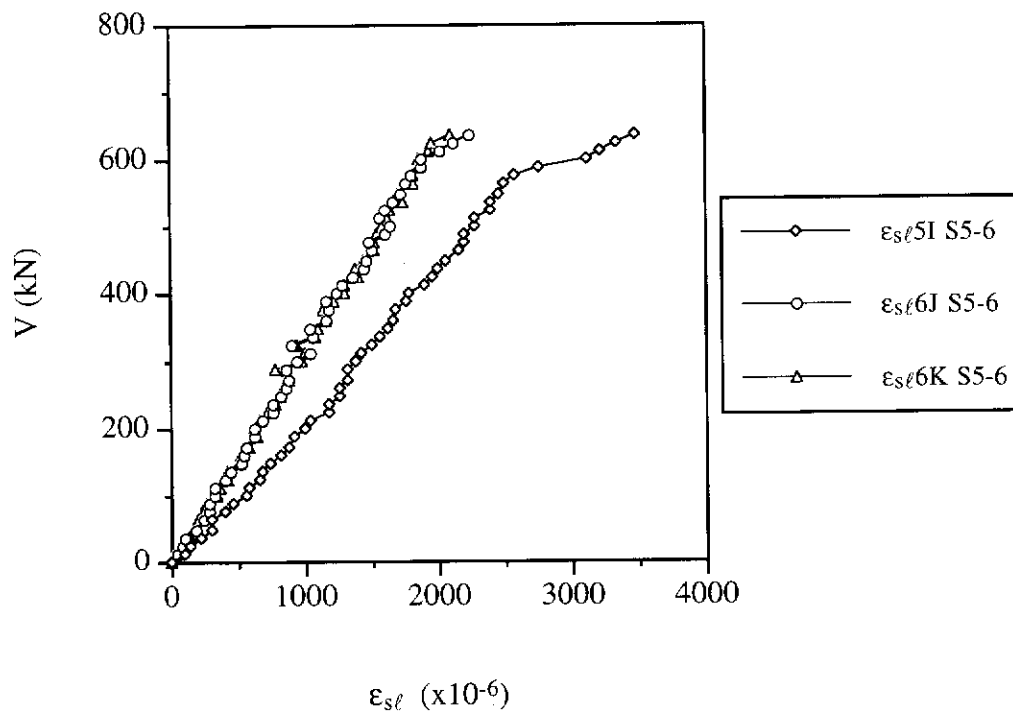
Figure E.4 Shear Force versus Tensile Steel Strains for Beam S1-4
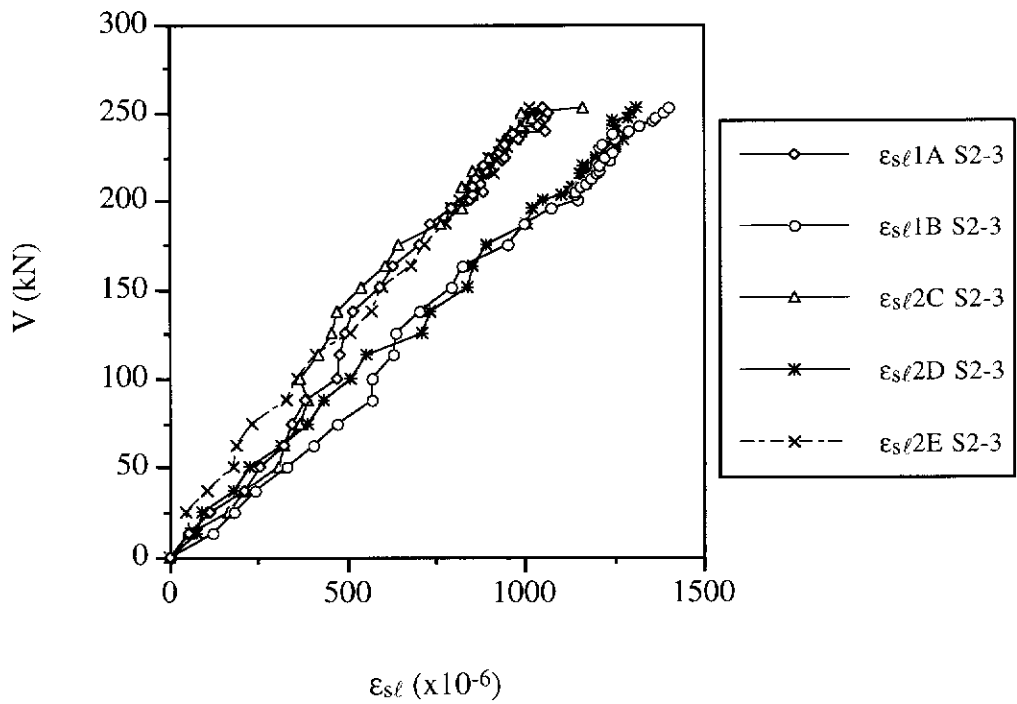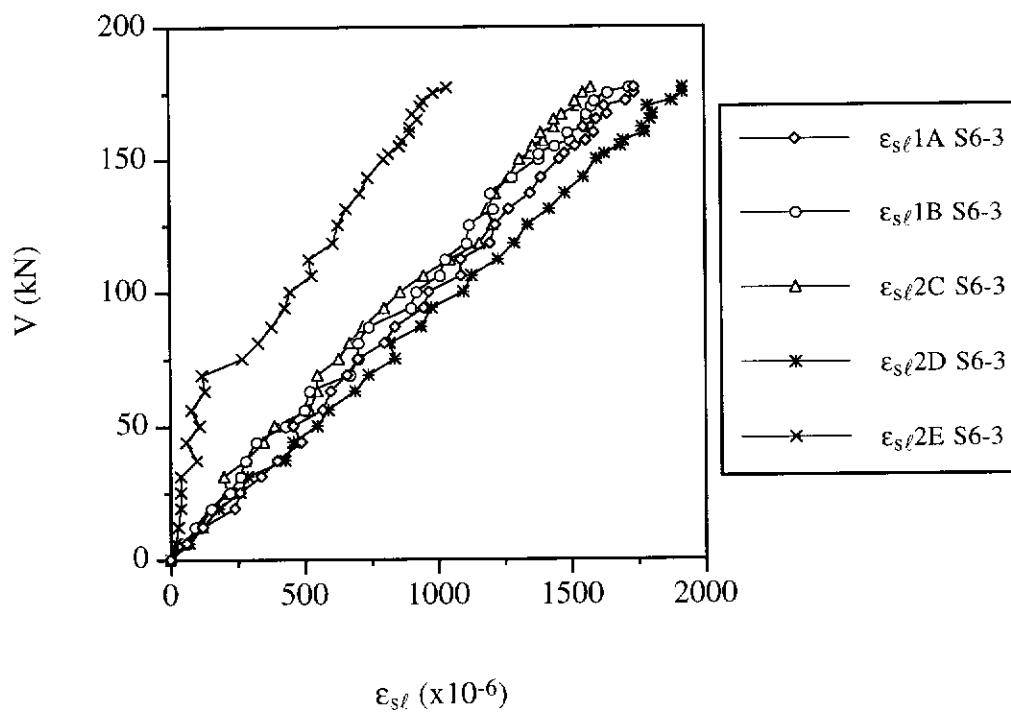

Figure E.5 Shear Force versus Tensile Steel Strains for Beam S2-3
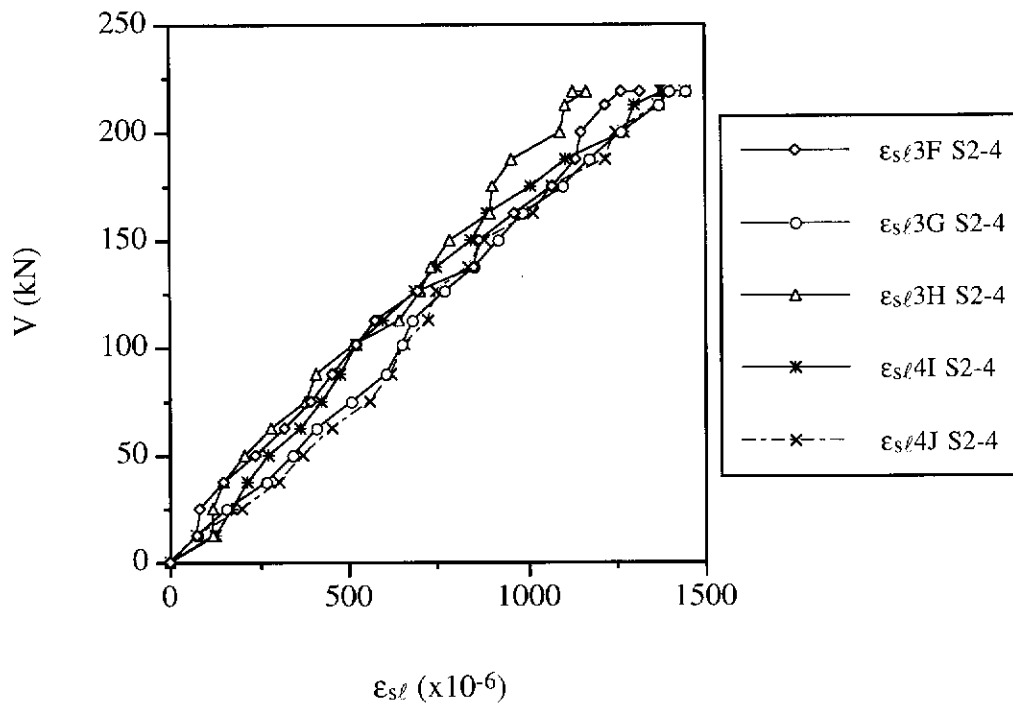
Figure E.6 Shear Force versus Tensile Steel Strains for Beam S2-4
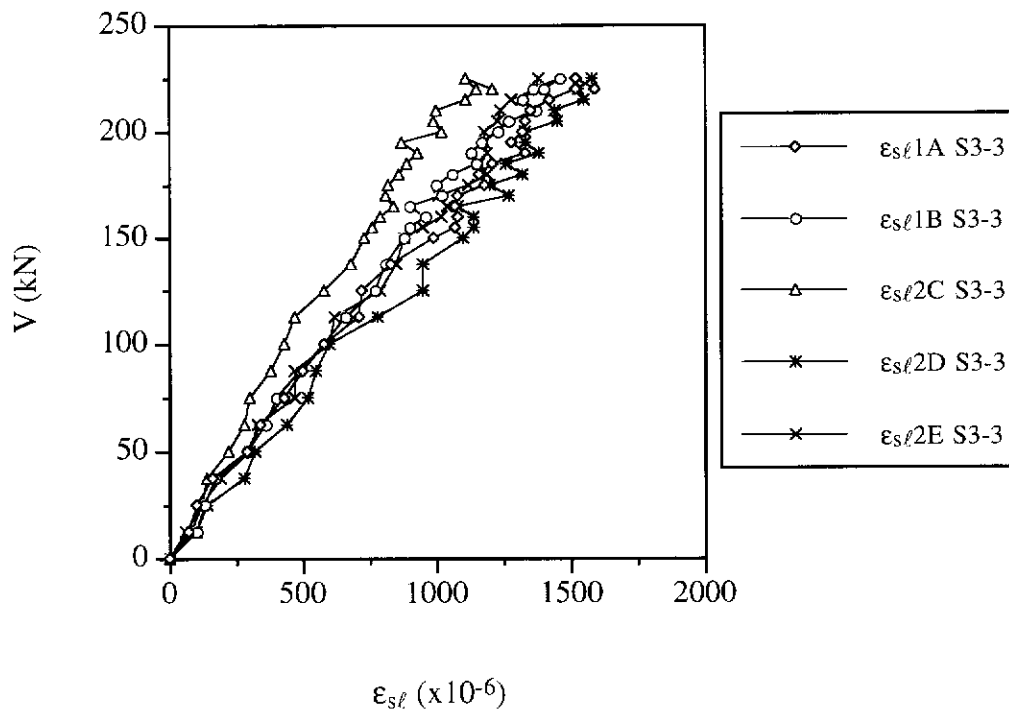
Figure E.7 Shear Force versus Tensile Steel Strains for Beam S3-3

E.4
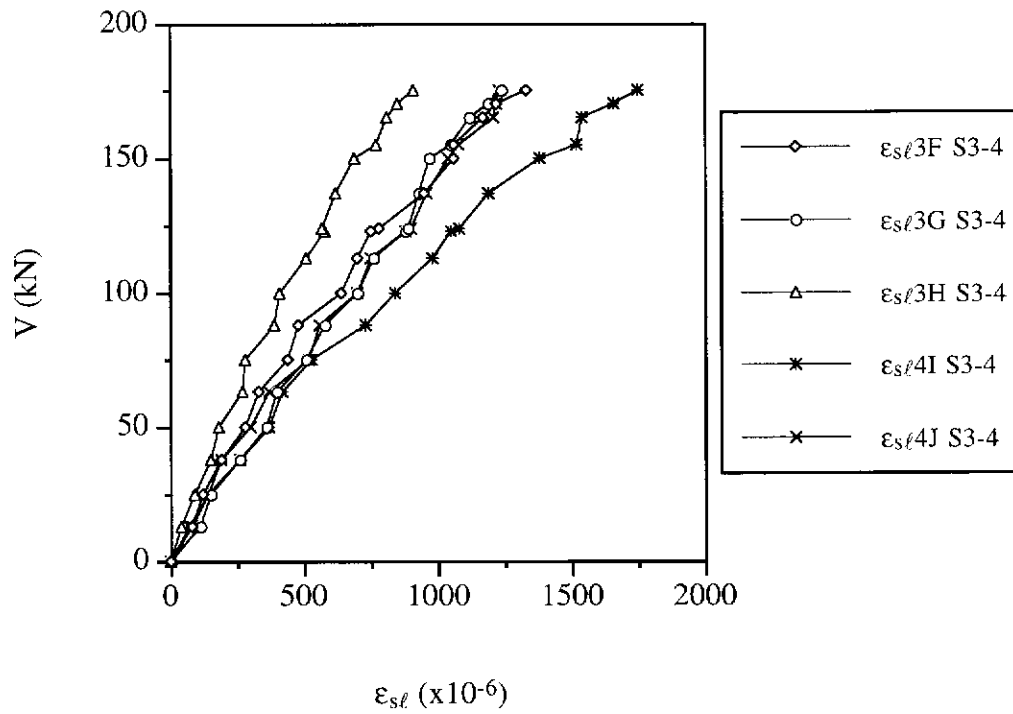
Figure E.8 Shear Force versus Tensile Steel Strains for Beam S3-4
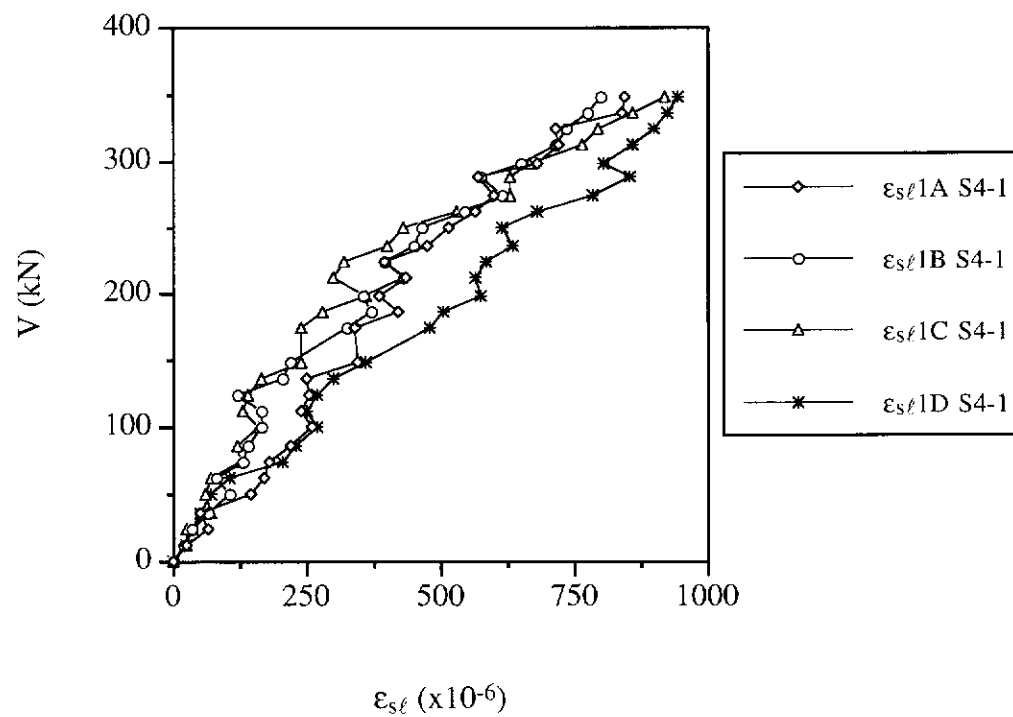
Figure E.9 Shear Force versus Tensile Steel Strains for Beam S4-1
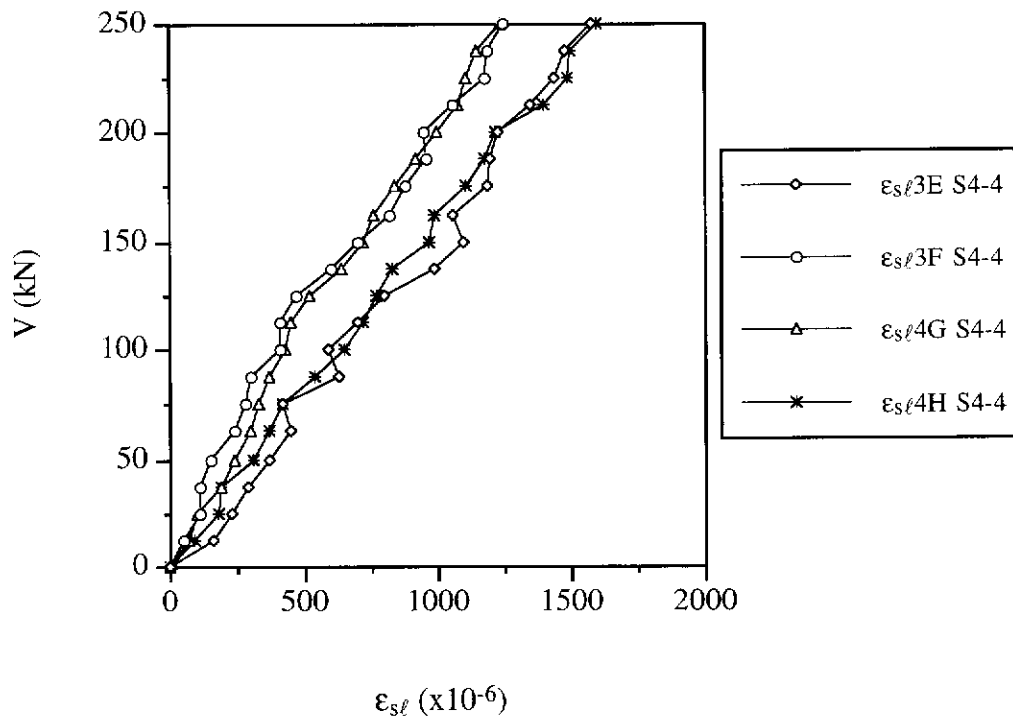
Figure E.10 Shear Force versus Tensile Steel Strains for Beam S4-4
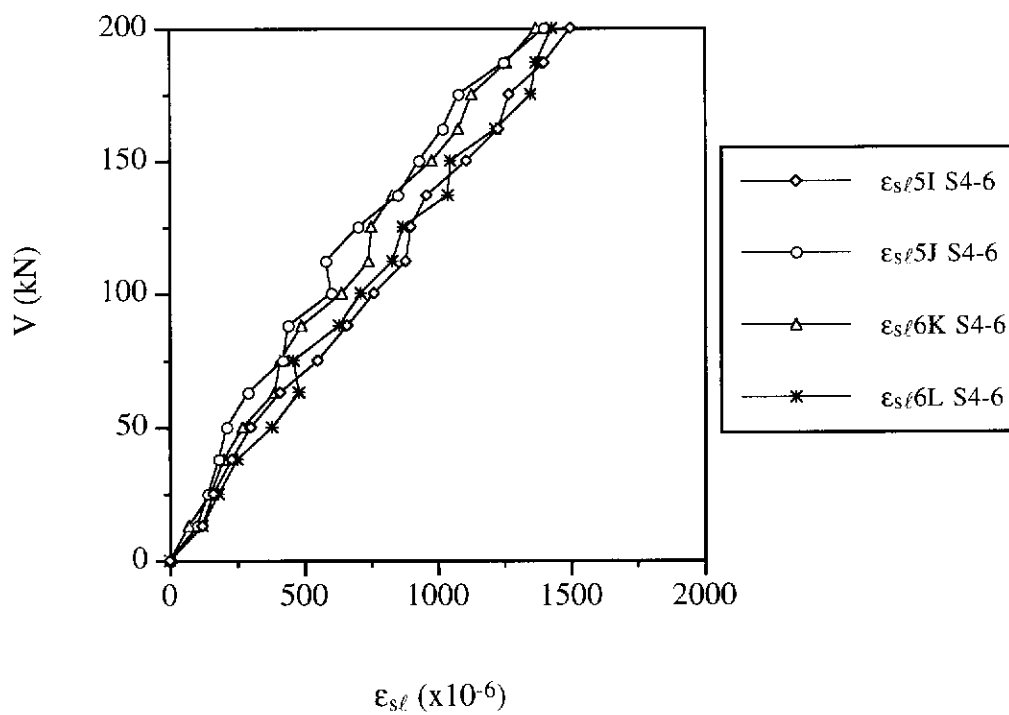
Figure E.11 Shear Force versus Tensile Steel Strains for Beam S4-6

Figure E.12 Shear Force versus Tensile Steel Strains for Beam S5-1

Figure E.13 Shear Force versus Tensile Steel Strains for Beam S5-3

Figure E.14 Shear Force versus Tensile Steel Strains for Beam S5-6

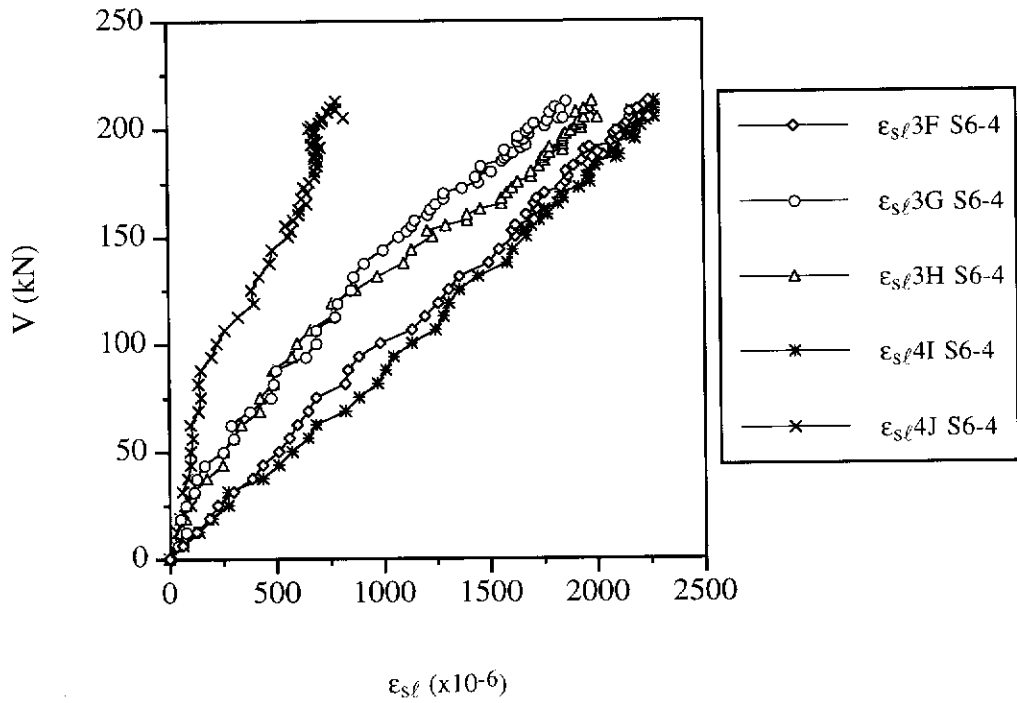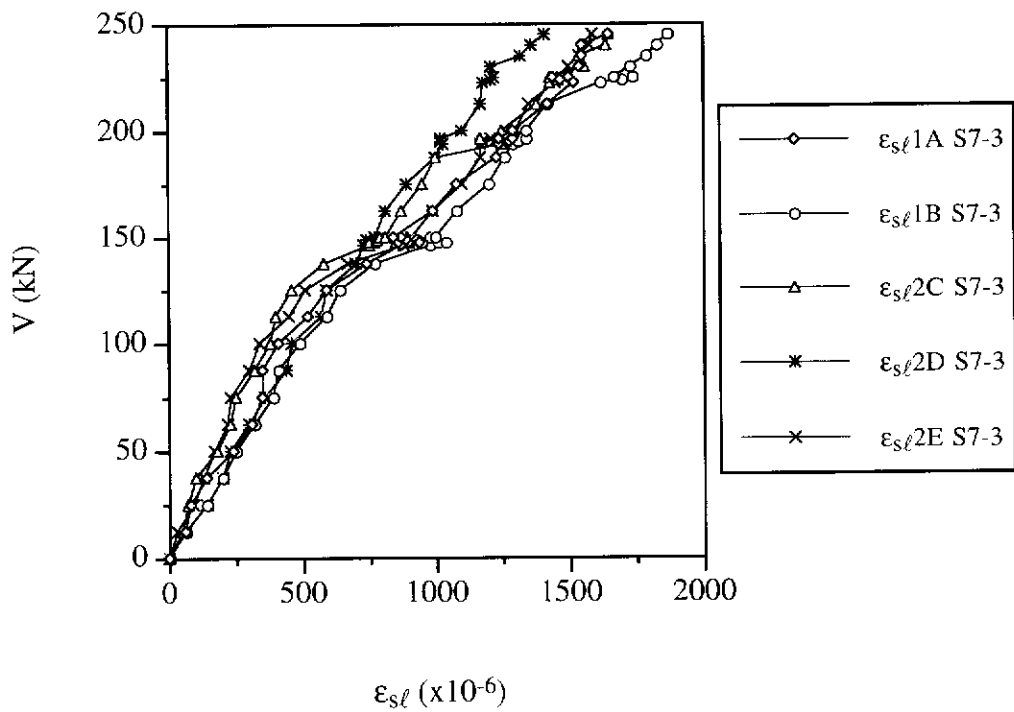**Figure E.15 Shear Force versus Tensile Steel Strains for Beam S6-3**

Figure E.16 Shear Force versus Tensile Steel Strains for Beam S6-4

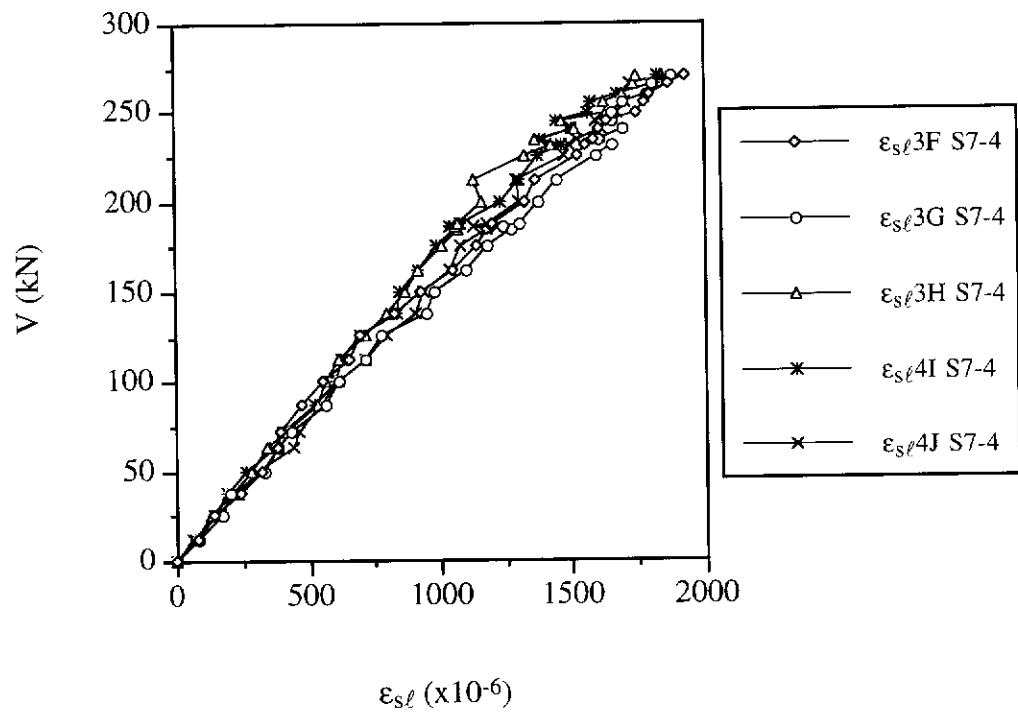**Figure E.17 Shear Force versus Tensile Steel Strains for Beam S7-3**

Figure E.18 Shear Force versus Tensile Steel Strains for Beam S7-4